NATIONAL CENTER FOR EARTHQUAKE ENGINEERING RESEARCH

ISSN 1088-3800

Seismic Performance of a Model Reinforced Concrete Bridge Pier Before and After Retrofit

by

J.B. Mander, J.H. Kim and C.A. Ligozio

Technical Report NCEER-96-0009

May 31, 1996

This research was conducted at the University at Buffalo, State University of New York and was supported by the Federal Highway Administration under contract number DTFH61-92-C-00106.

NOTICE

This report was prepared by the University at Buffalo, State University of New York as a result of research sponsored by the National Center for Earthquake Engineering Research (NCEER) through a contract from the Federal Highway Administration. Neither NCEER, associates of NCEER, its sponsors, the University at Buffalo, State University of New York nor any person acting on their behalf:

a. makes any warranty, express or implied, with respect to the use of any information, apparatus, method, or process disclosed in this report or that such use may not infringe upon privately owned rights; or

b. assumes any liabilities of whatsoever kind with respect to the use of, or the damage resulting from the use of, any information, apparatus, method, or process disclosed in this report.

Any opinions, findings, and conclusions or recommendations expressed in this publication are those of the author(s) and do not necessarily reflect the views of NCEER or the Federal Highway Administration.

NATIONAL CENTER FOR EARTHQUAKE ENGINEERING RESEARCH
Headquartered at the State University of New York at Buffalo

Seismic Performance of a Model Reinforced Concrete Bridge Pier Before and After Retrofit

by

J.B. Mander[1], J.H. Kim[2] and C.A. Ligozio[3]

Publication Date: May 31, 1996
Submittal Date: September 29, 1995

Technical Report NCEER-96-0009

NCEER Task Number 106-E-5.2

FHWA Contract Number DTFH61-92-C-00106

1 Associate Professor, Department of Civil Engineering, State University of New York at Buffalo
2 Research Associate, Department of Civil Engineering, State University of New York at Buffalo
3 Structural Engineer, Erdman Anthony and Associates; former Graduate Research Assistant, Department of Civil Engineering, State University of New York at Buffalo

NATIONAL CENTER FOR EARTHQUAKE ENGINEERING RESEARCH
State University of New York at Buffalo
Red Jacket Quadrangle, Buffalo, NY 14261

PREFACE

The National Center for Earthquake Engineering Research (NCEER) was established in 1986 to develop and disseminate new knowledge about earthquakes, earthquake-resistant design and seismic hazard mitigation procedures to minimize loss of life and property. The emphasis of the Center is on eastern and central United States *structures*, and *lifelines* throughout the country that may be exposed to any level of earthquake hazard.

NCEER's research is conducted under one of four Projects: the Building Project, the Nonstructural Components Project, and the Lifelines Project, all three of which are principally supported by the National Science Foundation, and the Highway Project which is primarily sponsored by the Federal Highway Administration.

The research and implementation plan in years six through ten (1991-1996) for the Building, Nonstructural Components, and Lifelines Projects comprises four interdependent elements, as shown in the figure below. Element I, Basic Research, is carried out to support projects in the Applied Research area. Element II, Applied Research, is the major focus of work for years six through ten for these three projects. Demonstration Projects under Element III have been planned to support the Applied Research projects and include individual case studies and regional studies. Element IV, Implementation, will result from activity in the Applied Research projects, and from Demonstration Projects.

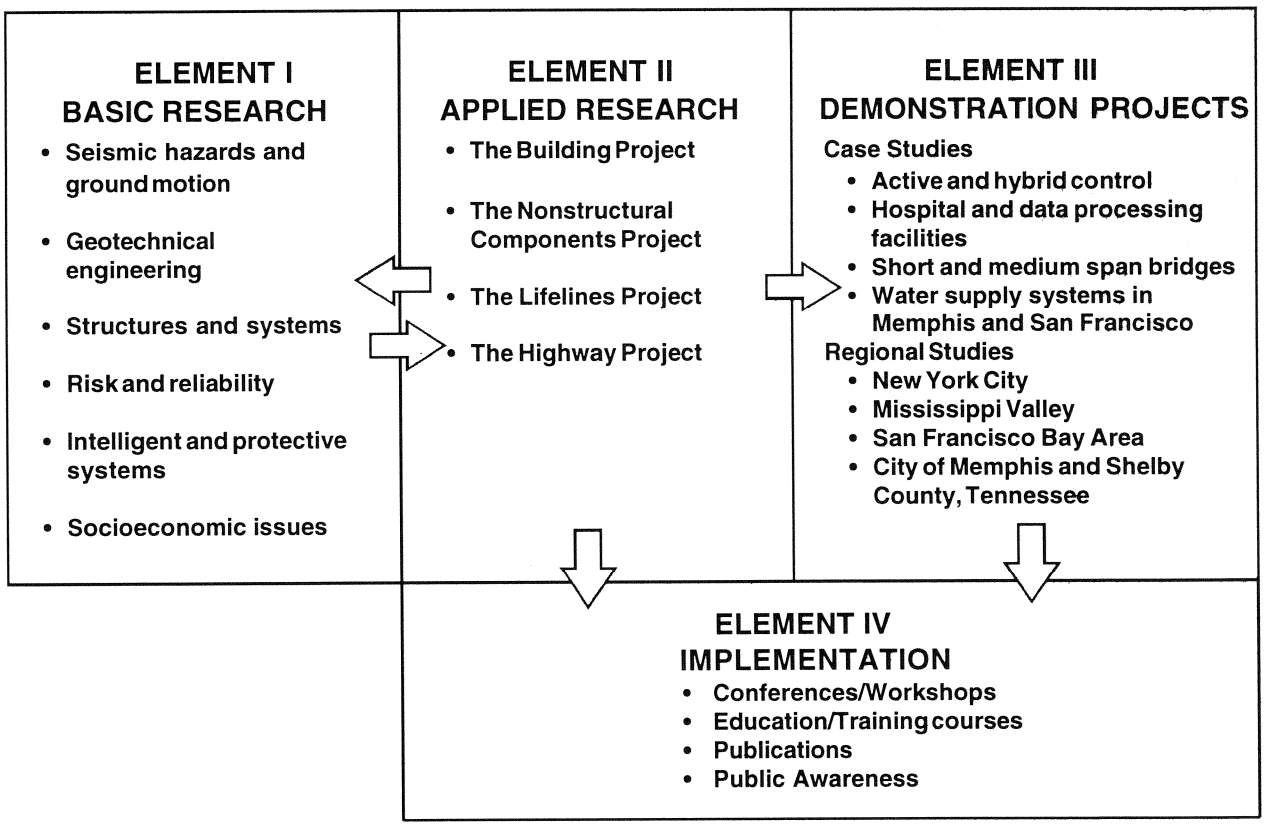

Research under the **Highway Project** develops retrofit and evaluation methodologies for existing bridges and other highway structures (including tunnels, retaining structures, slopes, culverts, and pavements), and develops improved seismic design criteria and procedures for bridges and other highway structures. Specifically, tasks are being conducted to: (1) assess the vulnerability of highway systems and structures; (2) develop concepts for retrofitting vulnerable highway structures and components; (3) develop improved design and analysis methodologies for bridges, tunnels, and retaining structures, with particular emphasis on soil-structure interaction mechanisms and their influence on structural response; and (4) review and improve seismic design and performance criteria for new highway systems and structures.

Highway Project research focuses on one of two distinct areas: the development of improved design criteria and philosophies for new or future highway construction, and the development of improved analysis and retrofitting methodologies for existing highway systems and structures. The research discussed in this report is a result of work conducted under the existing highway construction project, and was performed within Task 106-E-5.2, "Dependable Strength and Ductility of Eastern U.S. Bridge Columns" of the project as shown in the flowchart.

The overall objective of this task is to develop analytical procedures verified by experimental testing to determine the flexure-shear force-deformation behavior of bridge columns. This report presents the results from a series of experimental and analytical studies performed on a 1/3 scale model pier before and after retrofit. A seismic retrofit philosophy, capacity analysis and redesign, is introduced and implemented to retrofit the damaged model pier. Following extensive experimental testing, the ATC 6-2 capacity/demand ratio method and the equivalent lateral strength method were used to evaluate the model pier before and after retrofit.

SEISMIC VULNERABILITY OF EXISTING HIGHWAY CONSTRUCTION
FHWA Contract DTFH61-92-C-00106

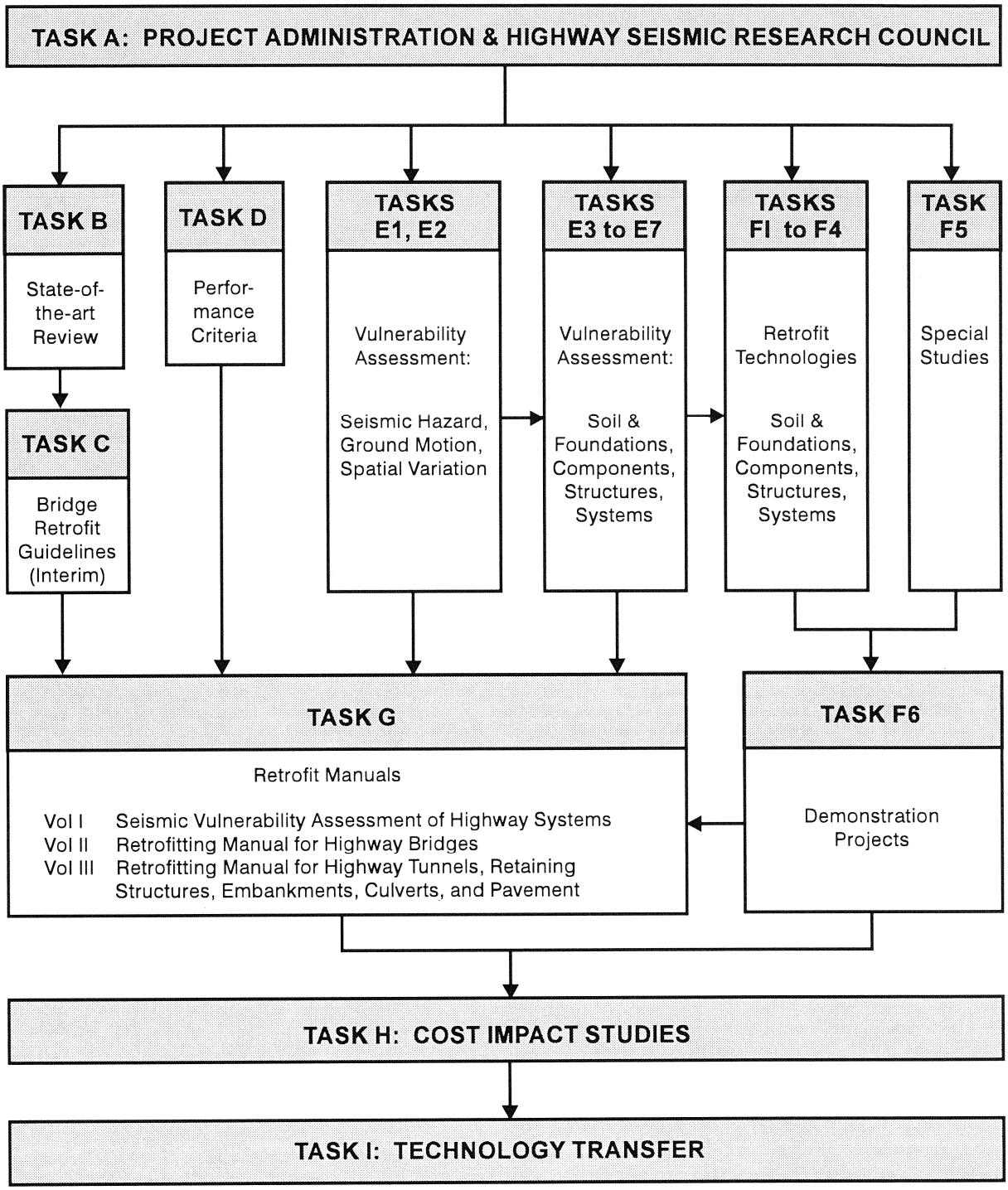

ABSTRACT

A series of experimental and analytical studies was performed on a 1/3 scale model pier before and after retrofit. The scale model represented a typical eastern U.S. non-seismically designed concrete bridge pier.

The pre-retrofitted model pier was tested under quasi-static inelastic loading and was governed by flexure at moderate drift levels, but ultimately limited by the cap beam-column joint shear capacity and a subsequent loss of bond strength in improperly anchored column longitudinal reinforcement. A seismic retrofit philosophy - "capacity analysis and redesign" was introduced and implemented to retrofit the damaged model pier resulting in a seismically strengthened and stiffened structure. The experimental behavior of the retrofitted model pier demonstrated that the failure due to joint shear and bond/anchorage could be avoided. However, the reduced clear column height due to retrofitting the pier cap beam and foundation beam led to an increase in mechanism strength which subsequently resulted in a premature semi-ductile column shear failure. Comparison with the experimental and analytical study on the companion prototype pier subassemblage before and after retrofit showed the failure mode to be similar to that of the scaled model. The model pier before and after retrofit was evaluated by the two existing methods advocated by the FHWA Retrofitting Manual for Highway Bridges - that is the Capacity/Demand method and the Equivalent Lateral Strength method.

ACKNOWLEDGEMENTS

The present study has been performed as part of the NCEER Highway Project granted under Federal Highway Administration (FHWA) contract DTFH61-92-C-00106. The financial support of FHWA via NCEER is gratefully acknowledged. The generous donation of special concrete materials from Master Builders™ is also acknowledged. Finally, the authors acknowledge the assistance provided by the technical staff of the seismic laboratory at the State University of New York at Buffalo.

TABLE OF CONTENTS

TABLE OF CONTENTS (cont'd)

TABLE OF CONTENTS (cont'd)

TABLE OF CONTENTS (cont'd)

TABLE OF CONTENTS (cont'd)

LIST OF FIGURES

LIST OF FIGURES (cont'd)

LIST OF FIGURES (cont'd)

LIST OF TABLES

SECTION 1
INTRODUCTION

1.1 Background

The design philosophy underlying modern seismic building and bridge codes can be summarized by the following three objectives: (i) A structure should resist minor ground motions with no damage; (ii) It should resist moderate motions with no significant structural damage; and (iii) It should survive a major ground motion without collapse *(Mayes and Sharpe, 1981; SEAOC, 1988; AASHTO, 1992)*. The primary seismic design goal is to ensure life-safety. To achieve this at reasonable cost, modern codes specify that structures should be designed to resist moderate ground motions, or a fraction of the maximum probable ground motion, in the elastic range, while providing sufficient ductility to dissipate the energy of a major ground motion in the inelastic range. This requires that structural strength be proportioned to ensure the formation of a desirable failure mechanism. For a reinforced concrete structure, ductility and strength proportioning can be achieved quite easily and inexpensively by providing adequate reinforcement, along with proper detailing.

There were a number of failures in the 1971 San Fernando earthquake that demonstrated the need for ductile design of bridge systems *(Buckle, et al., 1987)*. The collapse of many new bridge structures resulted in a reevaluation of Caltrans design codes, and eventually led to upgrades in the American Association of State Highway and Transportation Officials (AASHTO) seismic design code *(AASHTO, 1992)*. Prior to this time, bridges in the eastern and central United States were generally designed predominantly for gravity loads. Although the AASHTO code includes wind, centrifugal, and hydrodynamic loads, these are generally small when compared to earthquake lateral loads, and the design philosophies used to provide lateral strength for these loads is inherently different from the ductile inelastic strength principles associated with seismic design.

The principles of strength proportioning form the basis of modern Ultimate Strength

Design (USD) and Load and Resistance Factor Design (LRFD) by providing extra protection against undesirable failure modes (such as shear, compression, anchorage, etc.) in the form of partial load factors and under-capacity (resistance) factors. USD/LRFD provides a more rational approach, requiring an understanding of structural behavior and the likely failure modes. Historically, structures were designed using allowable Working Stress Design (WSD) based on unfactored service loads, with little consideration of post-elastic strength. Although USD was introduced in the United States as early as 1956 in the ACI building code *(Nickerson, 1969)*, it was not adopted by AASHTO until the 1970's, and even today is offered as an alternative to working stress design *(AASHTO, 1992 and 1994)*. A comparison of the ACI working and ultimate stress design principles by Nickerson *(1969)* has shown that the low $P/f'_c A_g$ ratios resulting from WSD often lead to columns with high inherent ductility. Conversely, USD can lead to smaller, more highly stressed columns requiring proper detailing to ensure sufficient ductility.

The failure of portions of the Cypress Viaduct and associated loss of life caused by the 1989 Loma Prieta earthquake in the San Francisco Bay Area have emphasized the need to reevaluate both the strength and ductility of existing reinforced concrete structures which were designed elastically using WSD with little consideration of seismic loads *(Housner, 1990)*. The research presented herein is part of an ongoing program to investigate the vulnerability of existing bridges in the eastern and central United States. This program is sponsored by the National Center for Earthquake Engineering Research (NCEER) via a contract with the Federal Highway Administration (FHWA). The pier investigated is a 30-year-old three-column-bent pier designed elastically using WSD, typical to highway crossings constructed between 1950 and 1970.

1.2 Description of the Prototype Bridge

The prototype bridge for this study was a two span, simply supported structure which carried two lanes of traffic over an unused portion of the Robert Moses Parkway onto Main Street in Niagara Falls, New York. The bridge was constructed in the early 1960's, owned by the New York State Parks Commission and maintained by the New York State DOT. Demolition of

the bridge was prompted by a park-land reclamation project which included a realignment of the parkway.

Figure 1-1 shows the prototype bridge in plan, elevation and section. The concrete deck was 10.5 m wide, consisting of two 3.7 m traffic lanes, 1.3 m and 1.8 m wide sidewalks. Bridge span lengths were 16.5 m in the north span, and 14.4 m in the south span, with a slight skew (5^{o} average skew). The deck was 191 mm thick and supported on five 762 mm deep rolled steel girders and had 1:24 super-elevation in the transverse direction. The as-built reinforcement plan for the single pier is reproduced in figure 1-2. The footing was cast on rock, and covered by 1.5 to 1.8 m layer of cohesionless backfill soil.

1.3 Scope of Present Study

In order to properly evaluate the existing bridge capacity before and after retrofit, a 1/3 scale reinforced concrete model pier of the Niagara Parkway bridge was constructed. The scale model was first tested under the quasi-static cyclic lateral loading (Section 2). The damaged model pier was retrofitted according to a methodology developed herein called *Capacity Analysis and Redesign* resulting in achievement of *Seismic Strengthening and Stiffening* (Section 3). The retrofitted model pier was tested again under the same experimental conditions and displacement path as previously tested prior to retrofitting (Section 4). Section 5 describes a comparative evaluation of the experimental results of the model pier and prototype cap beam-column subassemblage before and after retrofit. In Section 6, the performance of the model pier before and after retrofit is analyzed using two existing methodologies (the ATC 6-2 approach, and Equivalent Lateral Strength method). Finally, conclusions and recommendations for future research are presented in Section 7.

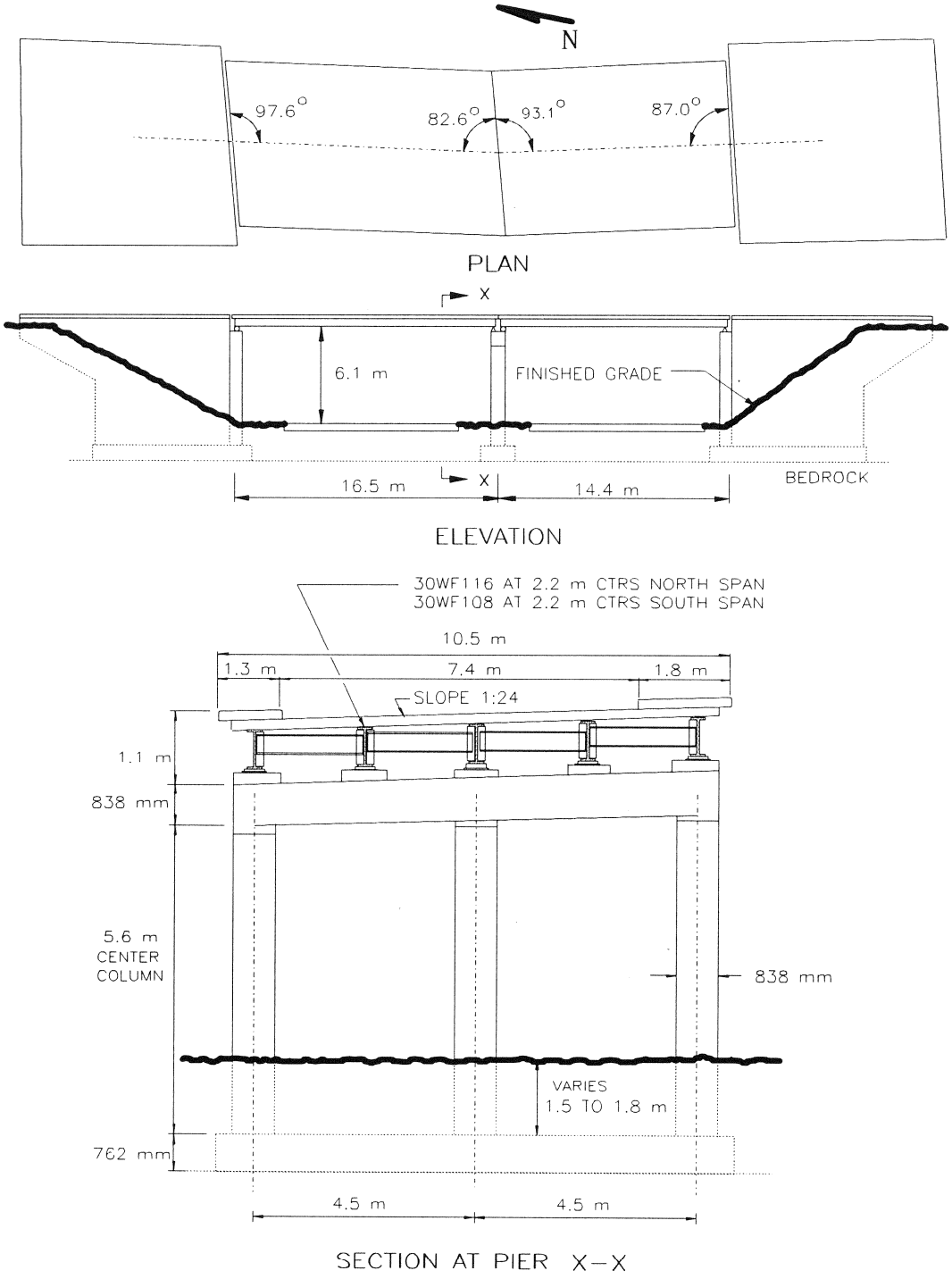

Figure 1-1. Configuration of Niagara Parkway Bridge.

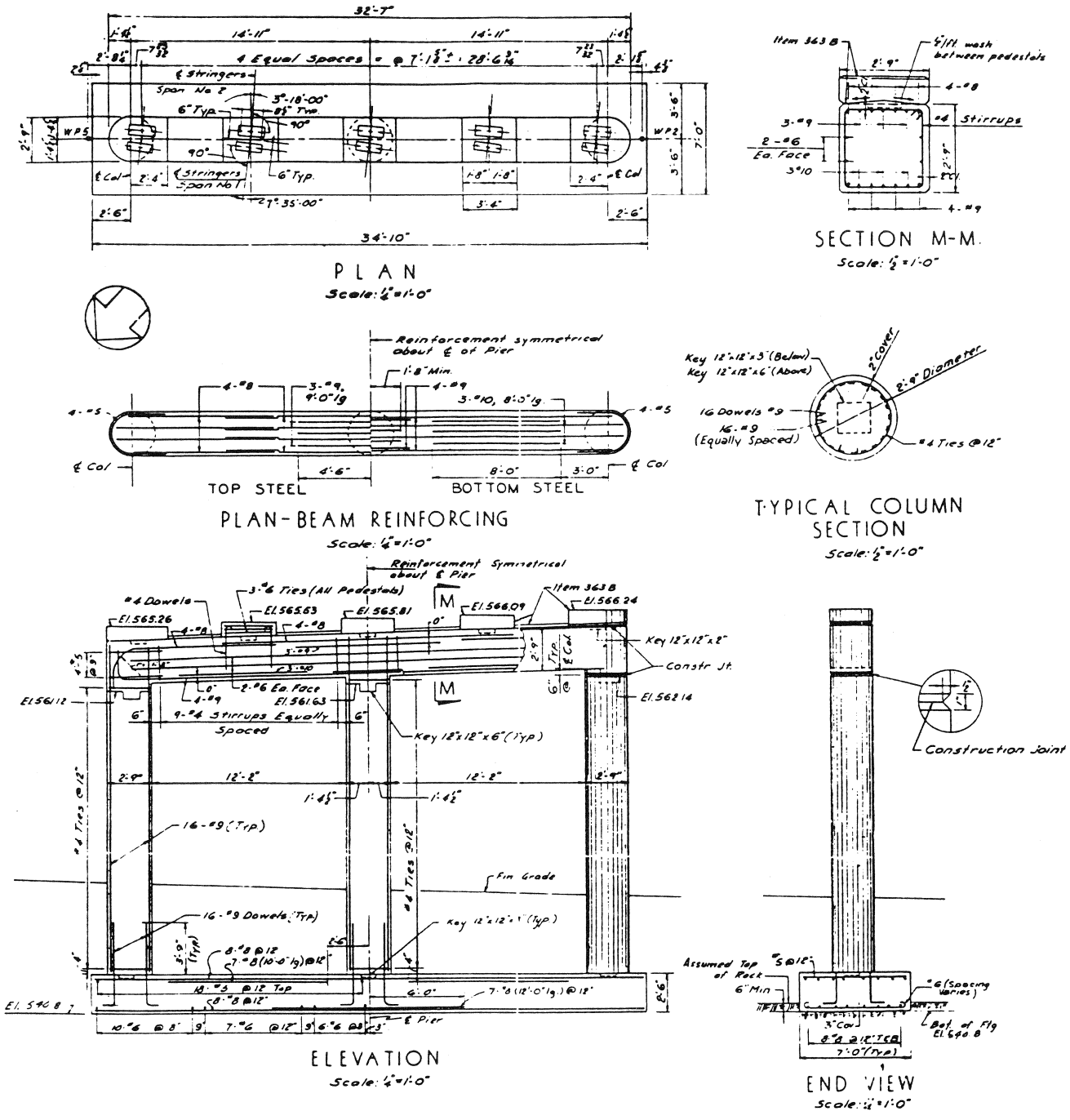

Figure 1-2. Prototype pier bent as-built plan.

SECTION 2
EXPERIMENTAL STUDY ON A NON-DUCTILE 1/3 SCALE MODEL PIER

2.1 Modeling Considerations

The destructive testing of reduced scale physical models using quasi-static cyclic loading is a common method for investigating the behavior of complex structures subjected to earthquake loading. Development of true model similitude relationships is well established in the literature *(ACI, 1970 and 1982)* and summarized in table 2-1. For ultimate strength similitude, one must ensure that the model materials have not only similar stress-strain behavior but also similar reinforcement bond characteristics. Satisfying these requirements leads to the concept of stress and strain similitude, thus,

$$S_\sigma = \frac{\sigma_p}{\sigma_m} = S_\epsilon = \frac{\epsilon_p}{\epsilon_m} = 1 \qquad \textbf{(2-1)}$$

in which S_σ = stress scale factor, σ_P = prototype stress, σ_m = model stress, S_ϵ = strain scale factor, ϵ_P = prototype strain, and ϵ_m = model strain.

A geometric scale factor was chosen on the basis of reliably modeling the #9 (28 mm diameter) longitudinal bars in the prototype column, using the smallest commercially available rebar with a similar deformation pattern. Thus using a #3 (10 mm nominal diameter) leads to a geometric scale factor of

$$S_\ell = \frac{\ell_{prototype}}{\ell_{model}} = \frac{3}{1} \qquad \textbf{(2-2)}$$

It was considered that the bond and material property (stress-strain) concerns often associated with model reinforcement would be minimized when using the #3 rebars. Additionally, a one third model was the largest that could be handled and tested due to size, weight, and force limitations of the laboratory test equipment. For a large scale model such as the one used in this study, regular concrete with 13 mm and smaller aggregate fulfills model material requirements,

and as shown in table 2-1, all scale factors can be derived from the geometric scale factor.

Table 2-1. Similitude requirements.

Quantity	Dimensions	Strain Similitude	Stress Similitude	This Study
Concrete Stress, σ_c	FL^{-2}	S_σ	1	1
Concrete Strain, ε_c	--	1	1	1
Concrete Modulus, E_c	FL^{-2}	S_σ	1	1
Poisson's Ratio, ν	--	1	1	1
Specific Weight, γ	FL^{-3}	S_σ/S_ℓ	$1/S_\ell$	1/3
Reinforcement Stress, σ_s	FL^{-2}	S_σ	1	1
Reinforcement Strain, ε_s	--	1	1	1
Linear Dimension, ℓ	L	S_ℓ	S_ℓ	3
Area	L^2	S_ℓ^2	S_ℓ^2	9
Structural Displacement, δ	L	S_ℓ	S_ℓ	3
Angular Displacement	--	1	1	1
Moment	FL	$S_\sigma S_\ell^3$	S_ℓ^3	27
Concentrated Load	F	$S_\sigma S_\ell^2$	S_ℓ^2	9
Line Load	FL^{-1}	$S_\sigma S_\ell$	S_ℓ	3

2.2 Model Design

Several simplifications were made in construction of the model, including the removal of the cap beam slope and pedestals. The model foundation width was reduced from 711 mm to 610 mm due to a limitation of the testing rig. This width reduction was offset by increasing the depth of the foundation from 254 mm to 279 mm, to maintain the moment of inertia of the section. Early development of an instrumentation plan also played a role in the pier design, including strain gauging of longitudinal column reinforcement in the plastic hinge zones, incorporation of multi-channel load cells to measure member forces at the column mid-heights, and the use of transverse threaded bars cast through the columns to measure section rotations. The load cells were designed to have similar flexural and axial stiffness as the reinforced concrete columns and were placed at mid-height in an attempt to minimize their influence on the overall behavior of the model pier specimen.

2.2.1 Strength Modeling

Although the dimensions of all members were determined by the geometric scale factor, it was not possible to simply scale bar sizes, as it is not always possible to obtain small diameter reinforcement with the required material properties. While a #9 bar scales correctly to a #3 bar, a convenient reduced model rebar for a prototype #8 or #10 rebar does not exist. Although it is possible to use deformed wire model reinforcement, this is often cold worked and must be annealed to obtain properties similar to mild steel.

An alternative to modeling individual bars with deformed model reinforcement is to model the strength of a set of bars. A target yield force for a set of bars can be obtained based on specified prototype reinforcement strengths such that:

$$\frac{(A_s f_y)_{prototype}}{(A_s f_y)_{model}} \cong 9 \qquad \textbf{(2-3)}$$

By considering typical reinforcement over-strengths a range of acceptable strength ratios can be determined as follows:

$$\left[\frac{(A_s f_y)_p}{(A_s f_y)_m}\right]_{\min} = \frac{(A_s)_p\,[414\ \text{MPa}]}{(A_s)_m\,[483\ \text{MPa}]} = 9 \times \frac{414}{483} = 7.7, \quad \text{and}$$

$$\left[\frac{(A_s f_y)_p}{(A_s f_y)_m}\right]_{\max} = \frac{(A_s)_p\,[483\ \text{MPa}]}{(A_s)_m\,[414\ \text{MPa}]} = 9 \times \frac{483}{414} = 10.5$$

For this model, the flexural reinforcement in the foundation and cap beam was modeled with #3 bars, based on the strength of the flexural steel in the prototype as shown in table 2-2 which presents the strength relationships between prototype and model reinforcement. The same methodology was used for the transverse steel in the top and bottom foundation mats.

Table 2-2. Reinforcement modeling.

Steel Location	Prototype		Model		Strength Ratio
	Designation	$A_s f_y$ (kN)	Designation	$A_s f_y$ (kN)	
Column Longitudinal	16 #9	4272	16 #3	470	9.09
Ties and Stirrups	#4	53	Soft Wire	5	10.43
Foundation Full Length Flexure	8 #8	1687	6 #3	176	9.58
Foundation Additional Flexural	7 #8	1477	5 #3	147	10.05
Bottom Foundation Transverse	10 #6	1174	10 D4	125	9.43
Foundation Top Transverse	35 #5	2897	27 D4	322	9.00
Cap Bottom Flexural	4 #9	1068	4 #3	118	9.09
Cap Bottom Additional Flexural	3 #10	1017	3 #3	88	11.54
Cap Top Flexural	4 #8	844	4#3	118	7.18
Cap Top Additional Flexural	3 #9	801	3 #3	88	9.09
Cap Beam Face	2 #6	235	2 D4	25	9.42
Cap Beam End	4 #5	331	4 D4	50	6.64

Unfortunately, the same group strength method could not be used for the transverse ties in the column because bar spacing is as important as overall strength when confinement and anti-buckling (bar stability) is being considered. To properly capture the confinement capacity of the #4 ties in the prototype column hinge regions, the model required ties with the proper scaled strength and spacing. More specifically, such scaled ties would require a section with a tension yield strength equal to 1/9 that of a #4 bar, and a stress-strain curve of the same shape as Grade 60 mild steel. A suitable soft wire was established by testing several wire specimens obtained from a local supplier. The 4.8 mm dia soft wire with Grade 1022 was selected. Stress-strain curves for the soft wire and #3 deformed bars used for the scale model along with #4 and #9 deformed bars used for the prototype are shown in figure 2-1. The as-built reinforcement plan is shown in figure 2-2.

2.2.2 Foundation Support Modeling

Positive foundation tie down was required to prevent overturning of the model prior to a structural failure. If analysis of the prototype foundation had shown its strength to exceed the strength of the columns, it would have been possible to simply strengthen the model to

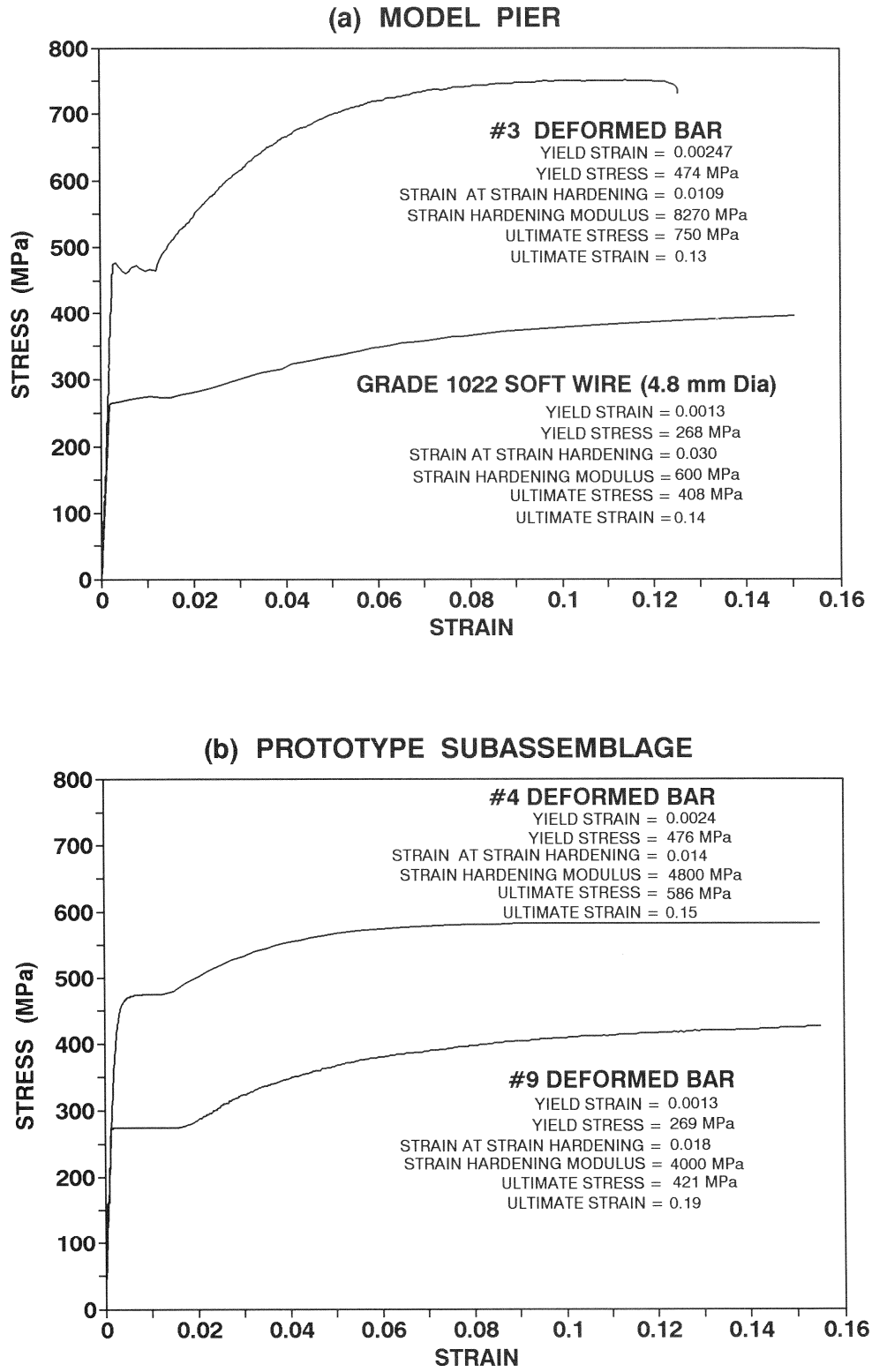

Figure 2-1. Reinforcement properties for model and prototype.

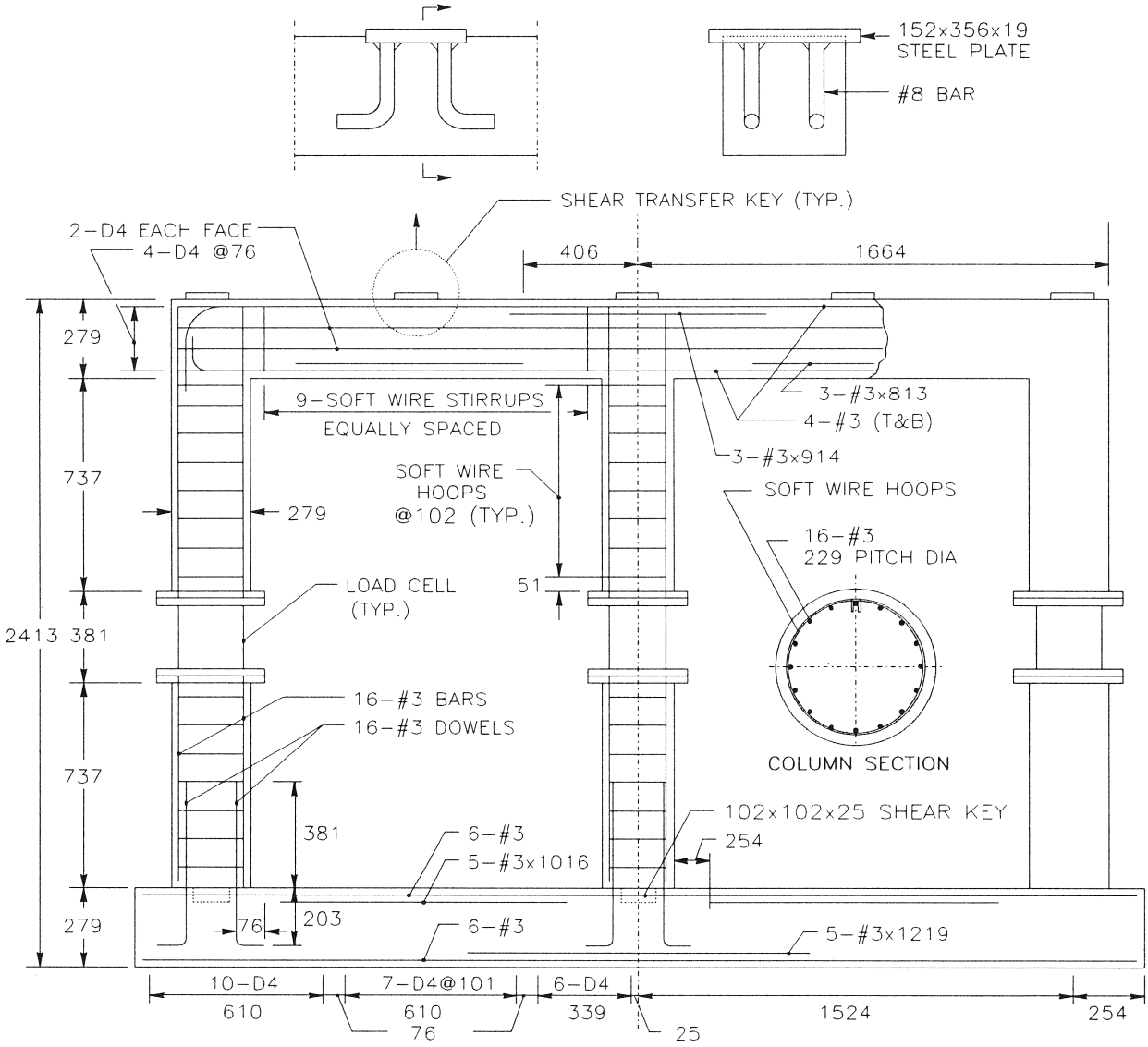

Figure 2-2. Model pier bent construction plan.

accommodate a typical strong floor tie down scheme, thereby enforcing a column hinge mechanism. However, this was not the case as demonstrated in figure 2-3, which shows the moment capacity and the bending moment diagram for the foundation at the formation of a column hinge mechanism. Note that the moment required exceeds the capacity just inside the compression column, demonstrating the development of a potential plastic hinge in the foundation prior to the formation of a column hinging mechanism. For this reason, it was considered necessary to accurately model both the strength and support conditions for the model foundation, to simulate the uplift restraint of soil overburden, and to create the proper distribution of bending moments in the foundation beam.

Figure 2-4 shows the foundation support for the model. Model uplift restraint was simulated using threaded tie down bars, prestressed through the strong floor to produce a downward foundation pressure similar to that provided by the prototype overburden. This force was distributed along the length of the footing by transverse foundation cross beams supported on 152 mm square wooden beams parallel to the footing. The bearing area of the cross beams on the timbers was designed to crush the wood at 117 kN, a value modeled from prototype soil uplift failure.

Compression in the footing, produced through end bearing, was important to maintain the shear strength of the concrete as there was no shear reinforcement in the foundation. During a pull test cycle, bearing was provided directly through a W8x31 strut connected to a 113 kN actuator at the base level. During a push cycle, the foundation reacted against an end bearing plate which was tied off to the base actuator with longitudinal tie bars placed through ducts cast in the footing.

2.2.3 Model Loading

The vertical load applied to the model was based on the gravity load of the prototype deck and girders and kept constant throughout the test. A total superstructure dead load of 2270 kN was calculated for the prototype. Half of this weight, 1135 kN, was distributed to the pier due

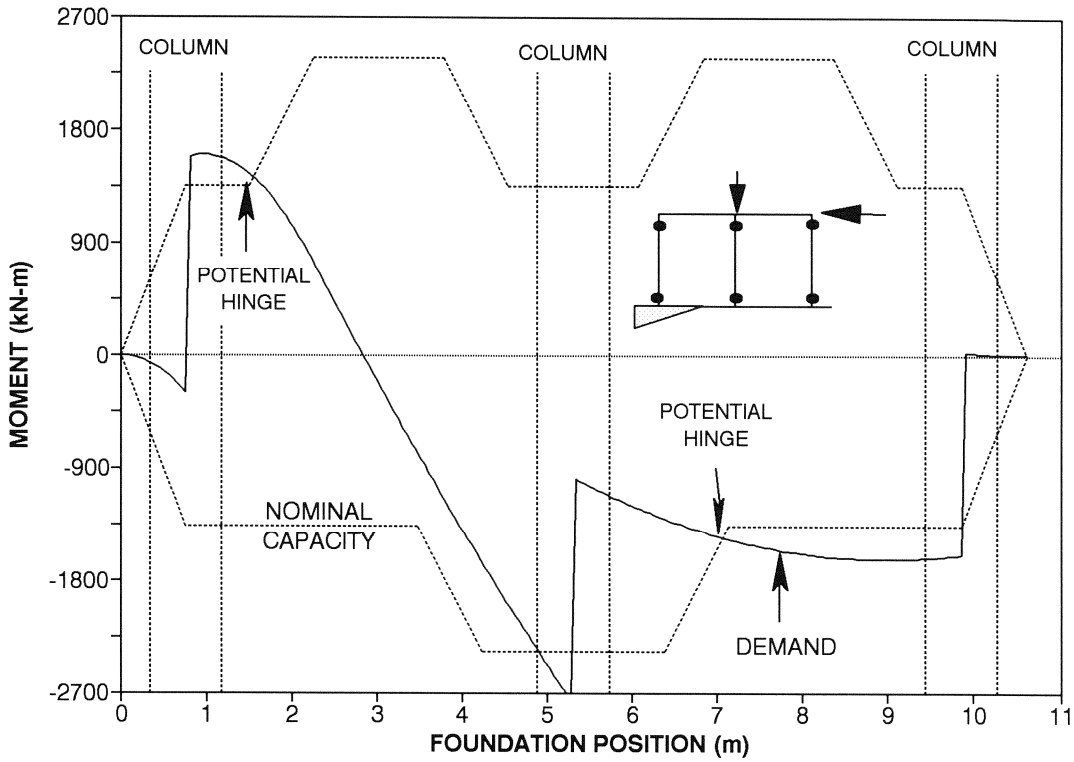

Figure 2-3. Prototype pier foundation moment capacity and demand.

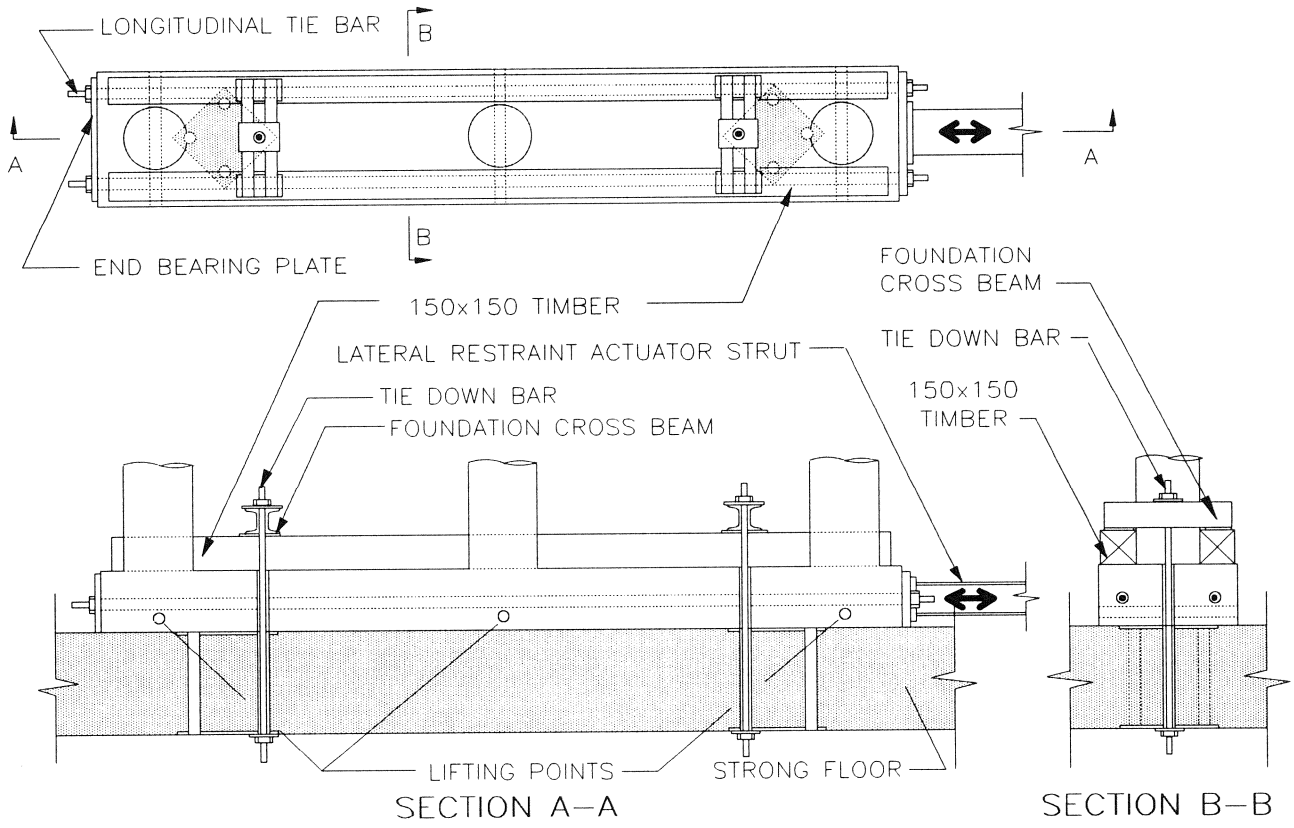

Figure 2-4. Foundation support detail for model pier.
(All dimensions in mm)

to the simply-supported configuration of the bridge. Using the stress equivalence modeling relationship

$$\frac{DL_{prototype}}{DL_{model}} = S_l^2 = 9 \qquad \textbf{(2-4)}$$

the model vertical load requirement can be calculated as 126 kN.

The overburden force used to determine the uplift restraint for the model was based on an assumed cohesionless soil with a unit weight of 15.7 kN/m^3 and a failure wedge with a 2:1 slope, approximating a friction angle of 27°. The volume of soil in the wedge was calculated using a prototype embedment depth of 1.8 m, resulting in a total uplift restraint of 1032 kN for the prototype, and 115 kN for the model.

Lateral load was applied to the pier under displacement control, but it was necessary to determine the approximate lateral load capacity of the model to size the lateral load actuator. A column sidesway mechanism was used to determine an upper bound flexural capacity of 200 kN for the model pier.

2.3 Model Construction

Model Construction was completed in four steps: the foundation, the lower half-columns to the load cell's lower connection plates, the upper half-columns above the top connection plate, and the cap beam. Both ready-mixed concrete and materials used to mix concrete in the lab were obtained from a local materials supplier. Water : cement : aggregate mix proportions by weight for the concrete were:

0.27 : 1 : 5.65 (1.70 sand + 3.95 stone) for the lower half-columns, and
0.35 : 1 : 5.65 (1.70 sand + 3.95 stone) for the rest of the model.

Cylinder test results are presented in table 2-3 for each stage of construction. The grade 60 #3 deformed reinforcement used for the model was purchased from a local steel supplier. From table

2-3 it is evident that the 28 day strength is reasonably substantial. It was the intention of this project to produce concrete strengths typical of what may be observed in the field for bridge structures in the order of 25 to 35 years of age *(Mander, et al., 1993, 1996)*.

Table 2-3. Concrete cylinder strength test results.

Pour	Average Cylinder Strength (MPa)				
	3-Day	7-Day	14-Day	21-Day	28-Day
Foundation	42	59	54	--	57
Lower Columns	--	34	32	37	59
Upper Columns (1st Lift)[1]	39	48	49	68	68
Upper Columns (2nd Lift)[1]	23	32	35	45	43
Cap Beam	50	59	52	59	73

[1]Two lifts, approximately 381 mm of column height each.

2.3.1 Foundation Construction

Forms for the foundation were built from 19 mm plywood sheathing supported by 50 mm x 100 mm framing, all built on a 19 mm plywood floor. The bottom reinforcement mat, consisting of #3 longitudinal bars and transverse D4 deformed wire, was tied and seated on chairs to maintain 19 mm bottom cover. Before the top mat was placed, pipes (to provide lifting points and ducts for foundation tie down and longitudinal restraint bars) were positioned and sealed to prevent concrete intrusion. The top mat was similar to the bottom, except that it was supported on wire brackets attached to the sides of the forms. Figure 2-5(a) shows the foundation form with the top and bottom reinforcement mats in place along with the ducts for the longitudinal foundation tie bars (white PVC in photograph), the lifting point bars (transverse black mild steel), and the foundation tie down bars (vertical black mild steel).

Column dowel bars were cut, bent, and positioned with hooks radiating outward and 203 mm of foundation embedment, in a 229 mm cage diameter. The extreme north and south dowels in each column had their deformations ground off for strain gauge mounting just above the top

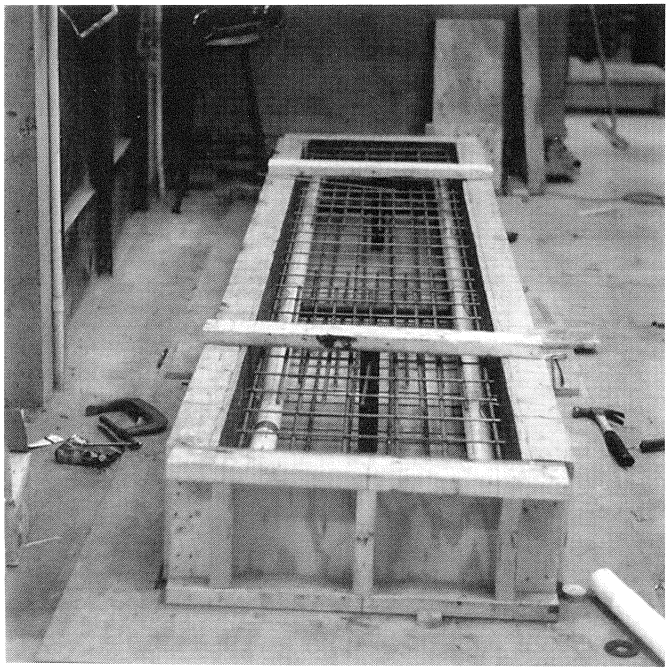

(a) Formwork with reinforcement

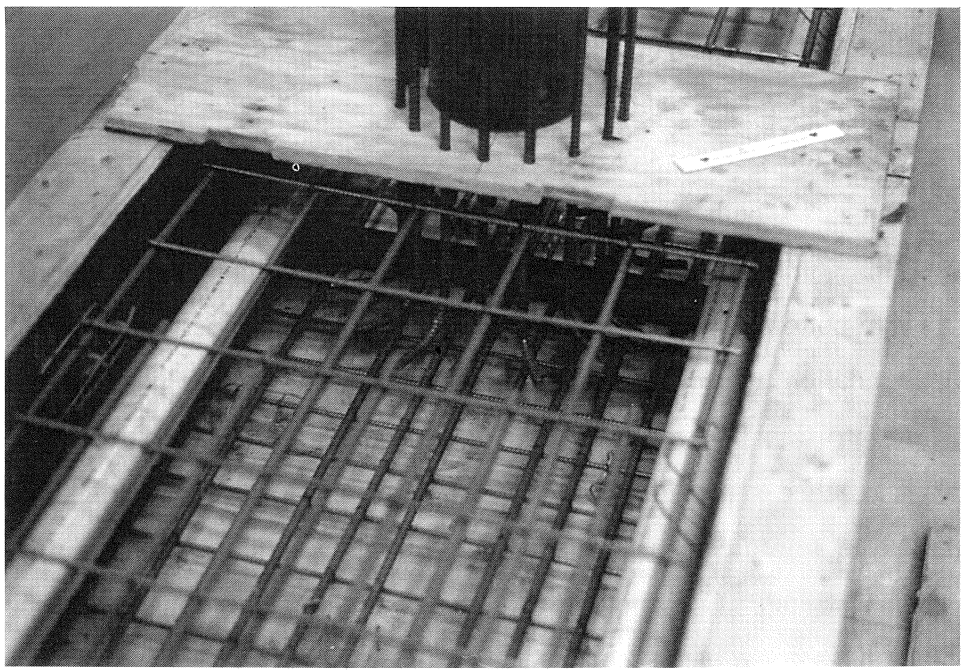

(b) Column dowel bar detail

Figure 2-5. Foundation construction photographs.

of the foundation. Strain gauges were placed after the foundation was cast to measure the bar force transmitted across the lap splice. The dowels were held in place by wood templates spanning across the top of the foundation forms which also formed the shear key at each column. Figure 2-5(b) shows a close-up photograph of the middle column dowel hooks held in place by the plywood template. A typical foundation-column joint is shown in figure 2-2. Ready-mixed concrete was placed in the foundation.

2.3.2 Column Construction

Formwork for the columns below the load cells was constructed from schedule 80 PVC pipe with an 287 mm inside diameter, and a 17 mm wall thickness. Three sets of forms, 737 mm long were constructed and used for both the top and bottom column sections. The PVC pipe was split longitudinally into two halves to allow easy removal. Four threaded bars were used to tie the half-forms together through the column. These bars were located so they could eventually be instrumented to measure section rotations.

The 16 #3 longitudinal reinforcement bars were tied beside the dowel bars with the same 229 mm center line cage diameter. The top of each of these bars was threaded and anchored with nuts above and below the lower load cell connection plate as shown in figure 2-6. This bolt configuration allowed the connection plates to be leveled both individually and as a group to ensure proper load cell alignment. Each plate had a 127 mm diameter access hole to permit placement of concrete. Figure 2-7(b) shows a photograph of the lower column cage, load cell connection plate, and column forms in position but not secured. The extreme north and south longitudinal bars were strain gauged just above the top of the lap splice, in a manner similar to the dowel bars, to measure bar force developed at the top of the lap splice. Individual circular wire hoops provided transverse reinforcement at 102 mm center to center spacing. Due to the small volume involved, concrete for both the lower and upper half-columns was mixed in the laboratory using the aggregate and proportions similar to the ready mix concrete used in the foundation.

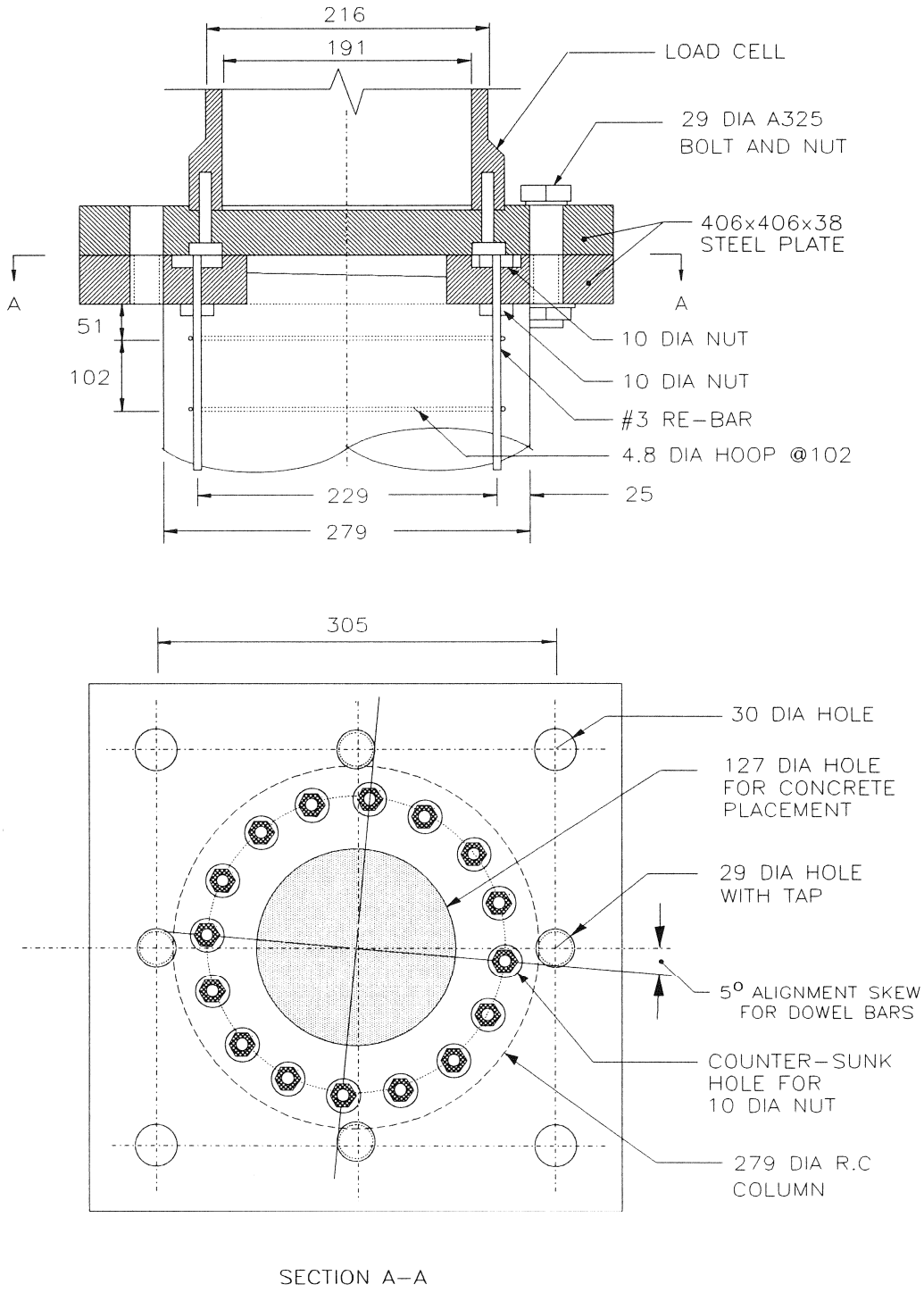

Figure 2-6. Column load cell connection detail.
(All dimensions in mm)

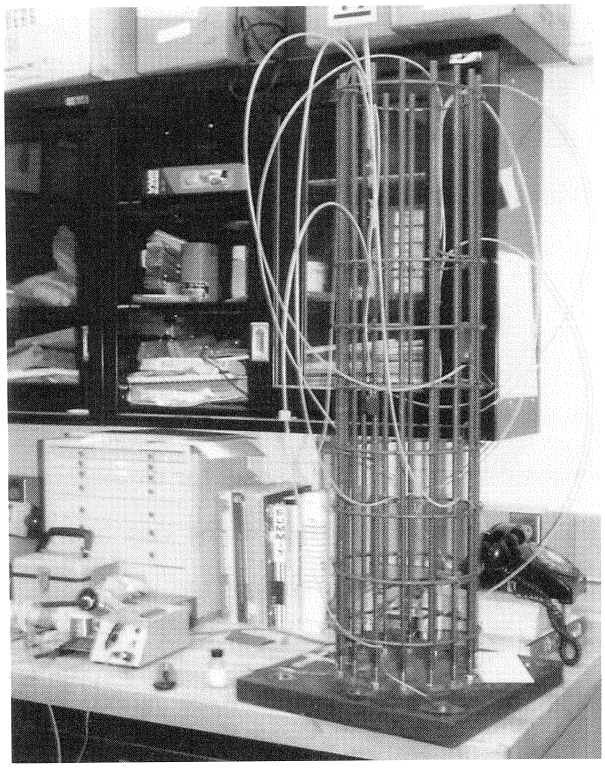

(a) Top half-column reinforcement

(b) Bottom half-column reinforcement with forms

Figure 2-7. Column construction photographs.

The upper half-columns were constructed directly on top of the lower half-column load cell connection plates, without the load cells in place. The longitudinal reinforcement was anchored to the upper load cell connection plates at the base of the upper half-columns. The upper and lower load cell plates were bolted together to ensure they would be parallel and aligned when the load cells were inserted. Formwork from the lower half-columns was reused for casting the upper half.

Upper column reinforcement was also similar to the lower columns, except that the longitudinal steel extended beyond the top of the forms for eventual cap beam connection and was strain gauged in five positions above and below the cap beam soffit to help determine curvature profiles in the joint and yield penetration into the cap beam. Figure 2-7(a) shows an upper half-column cage mounted to the upper column load cell connection plate with strain gauges and strain gauge wiring in place. Load cells were placed in the column halves after construction was completed, just before testing.

2.3.3 Cap Beam Construction

Formwork for the sides and soffit of the cap beam was of a wood construction similar to the foundation. The rounded ends were formed using a short section of the PVC pipe used for the columns. This was split longitudinally and anchored at both ends of the form to a pair of the transverse bars cast in the column. The remaining formwork was supported by 50 mm x 100 mm posts anchored to the foundation forms. The formwork was installed after the cage was completed.

The cage was assembled in place by tying the flexural steel to the longitudinal bars projecting above the column tops, and then wiring the stirrups in place to provide rigidity to the cage. The end and face steel was added after the stirrups were secured. At the interior column-cap beam joint, the column longitudinal steel and the cap beam bottom flexural steel was very congested, and the cap beam cage size had to be reduced, increasing concrete cover in this area. Figure 2-8 shows photographs of the cap beam cage at the north column joint, with and without

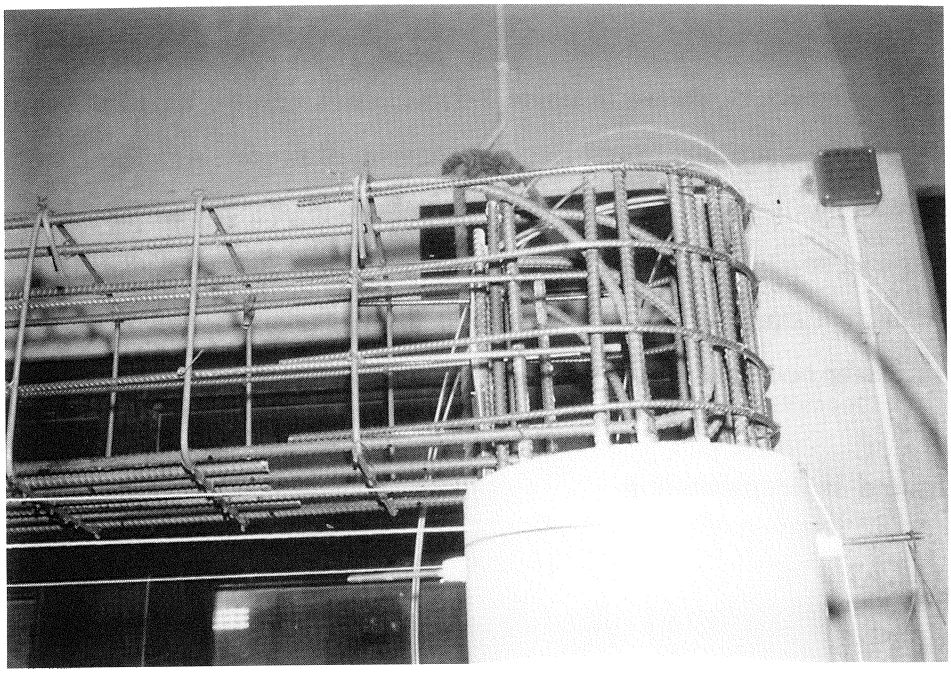

(a) Cap beam reinforcement

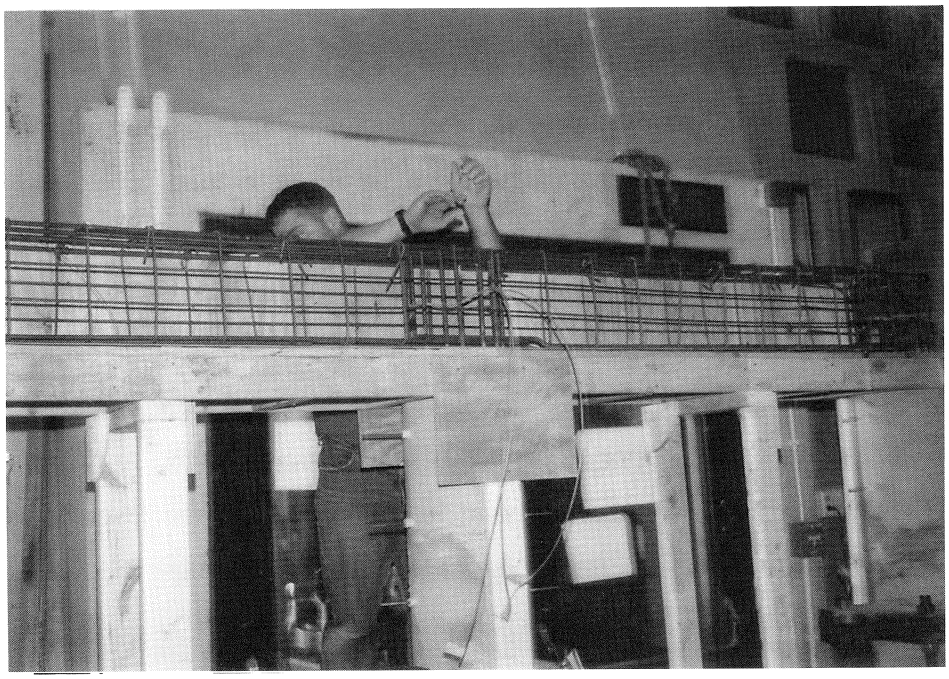

(b) Cap beam reinforcement with forms

Figure 2-8. Cap beam construction photographs.

forms in place.

Five shear connectors, shown in figure 2-2, were cast into the top of the cap beam at the pedestal locations to link it to the lateral force mechanism of the test rig. These connectors were constructed by welding four hooked #8 bars to the underside of a 152 mm x 356 mm x 19 mm plate which was cast nearly flush with the top of the cap beam. This plate was drilled and tapped to accept 19 mm high strength bolts, connecting it to the bottom flange of the W14x257 steel beam used to transfer both lateral and dead load to the model during the test.

2.4 Test Rig and Instrumentation

2.4.1 Test Rig

The test rig employed for this test is shown in figure 2-9. The model was anchored to the laboratory strong floor to provide restraint against uplift only. Lateral load was provided by a 1000 kN MTS hydraulic actuator, anchored to a rigid reaction frame, and connected to the model through a W14x257 beam bolted on top of the cap beam. Lateral restraint was supplied by a 1100 kN hydraulic actuator braced to the reaction frame at ground level, and tied to the longitudinal restraint bars in the model foundation. The base actuator was operated in force control, so the lateral resistance was equal and opposite to the lateral load in the top actuator.

Axial load to simulate the weight of the deck was provided by a 100 kN MTS actuator through a W10x77 lever beam supported on the W14x257 beam bolted to the cap beam. The W14x257, being quite stiff, distributed the point load produced by the lever beam. The lever beam was 3658 mm long with its fulcrum in the center, thereby doubling the load ability of the 100 kN actuator.

2.4.2 Instrumentation

A total of four types of measurements were made during the test, using four types of

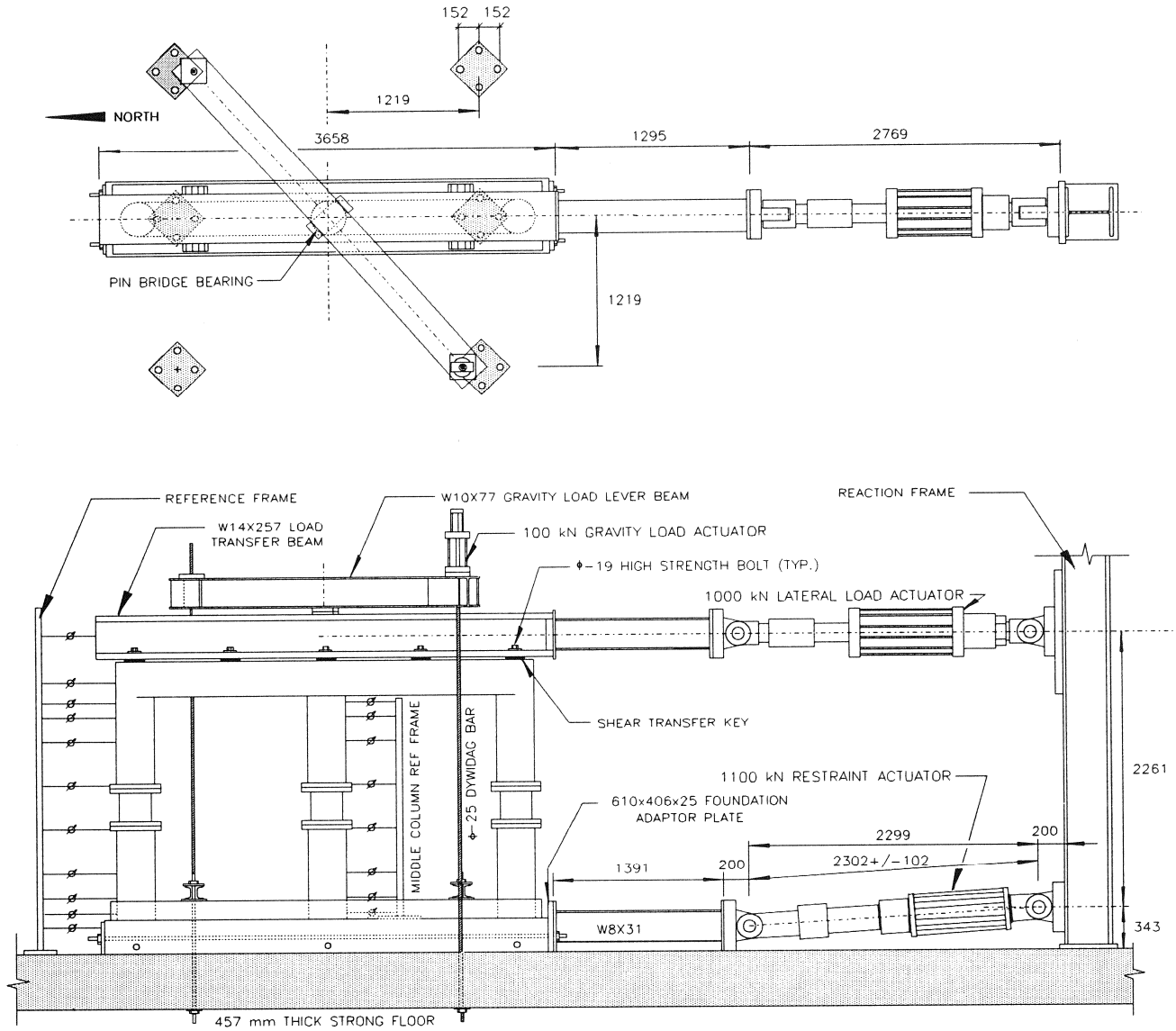

Figure 2-9. Test rig for pre-retrofitted model pier bent.
(All dimensions in mm)

instruments, including sonic transducers, linear resistance potentiometers, multi-channel load cells, and reinforcement strain gauges.

2.4.2.1 Displacements

Sonic transducers were mounted to a reference frame, north of the specimen, to monitor transverse structural displacements relative to the strong floor for the foundation (instrument TF), several heights along the north column (instruments T1 to T8), the cap beam (TCB), and the W14x257 bolted to the cap beam (TRB) as shown in figure 2-10. A drift angle θ based on the relative displacement between cap beam and foundation displacement was used to control the lateral load actuator. Thus,

$$\theta_{drift} = \frac{\Delta_c - \Delta_f}{L_c} \qquad \textbf{(2-5)}$$

in which θ_{drift} = column drift angle, Δ_c = cap beam displacement, Δ_f = foundation displacement, and L_c = distance between cap beam (TCB) and foundation (TF) transducer.

Total displacements for the middle column were also measured with sonic transducers. However, these were mounted on a frame bolted to the model foundation and recorded displacements relative to the foundation. Like the north column, the middle column was instrumented at 8 levels corresponding to the locations of the transversely cast column threadbars used to measure section curvatures.

2.4.2.2 Rotations

Section rotations for the north and middle column were measured with linear resistance potentiometers, mounted in pairs parallel to the columns as shown in figure 2-10. These instrument pairs measured the change in distance between the ends of the threadbars cast transversely to the columns. Mounting the gauges to bars cast through the columns permitted reliable measurements even after spalling of the cover. Gauge lengths were shortened at the top and bottom of the columns to provide higher resolution in the hinge zones where larger rotations

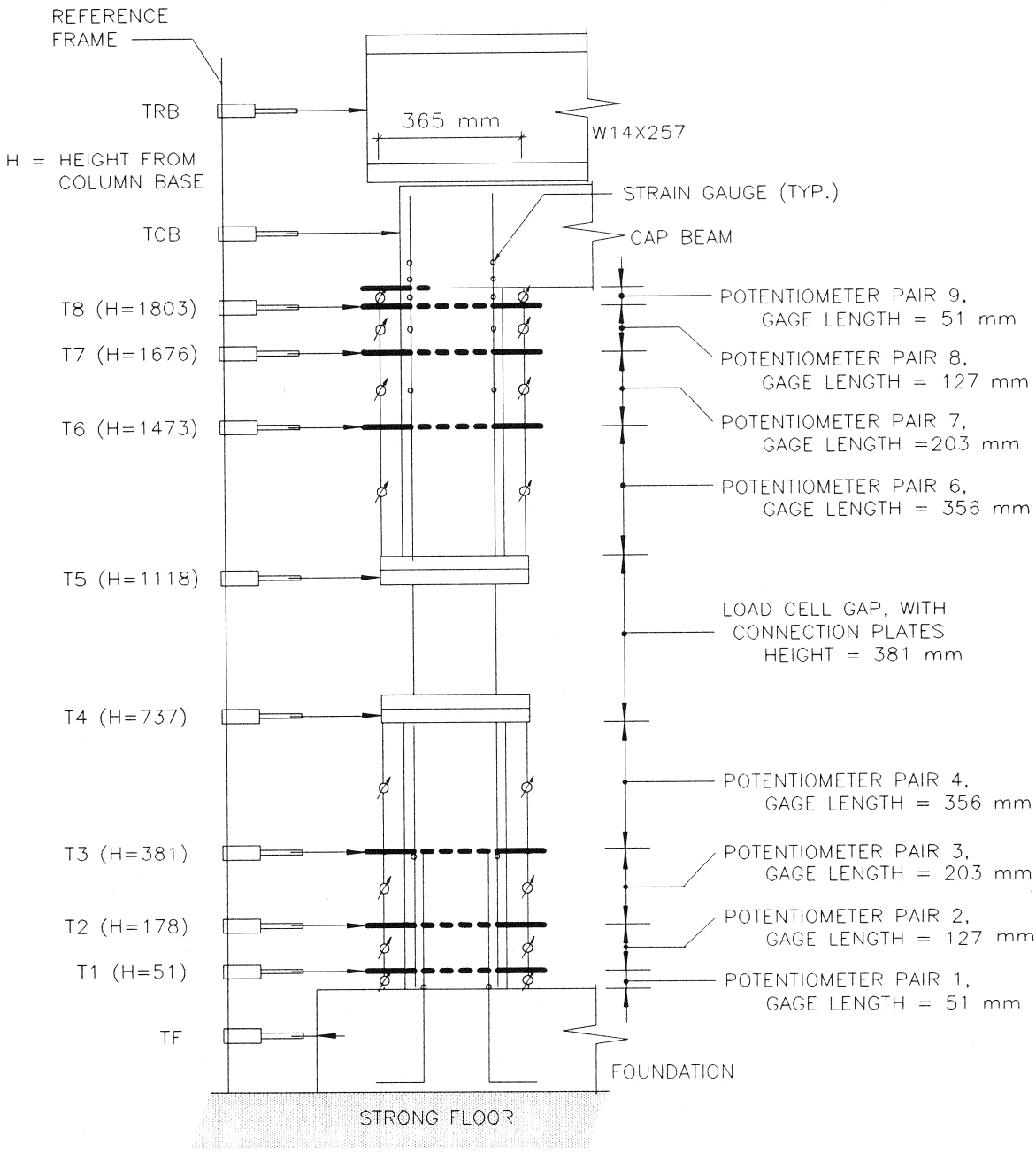

Figure 2-10. Instrumentation for pre-retrofitted model pier test.

were expected.

Average curvatures were calculated for each instrument pair based on the measured average rotation and the gauge length. Inferred flexural displacements were determined by applying moment-area theorems to the experimentally observed curvatures.

2.4.2.3 Column Loads

Bending moment along with axial and shear forces were measured at the mid height of all three columns using multi-channel load cells designed, built, and calibrated for this model. The load cells were bolted to connection plates cast at the middle of the columns and bolted to the longitudinal column reinforcement. The model was built without load cells in place by bolting the top connection plate to the bottom plate. Before testing the model was split by lifting the cap beam and upper columns to allow installation of the load cells. Unfortunately, the load cells were not zeroed and monitored as the model was reassembled to determine the column loads at the start of the test. Therefore, it was necessary to assess the initial values by analytical modeling. However, the initial assessments were corroborated by the final readings taken as the test rig was disassembled.

Forces were also measured in all three actuators and the foundation tie-down bars, which were instrumented so they could be pretensioned. The total actuator lateral load was compared with the sum of the shears measured in the column load cells as an initial check of the test rig setup.

2.4.2.4 Reinforcement Strain Gauges

The north and south extreme longitudinal reinforcement in all three columns was strain gauged at seven locations each, including the dowel bars just above the foundation, the longitudinal bars above the splice, and at the top of the columns at 279 mm, 127 mm, and 25 mm below the cap beam soffit and 25 mm and 76 mm above in the cap beam as shown in figure

2-10.

A 6.4 mm wide flat was provided by removing the deformations from the reinforcement at each gauge position. Gauges were glued in place before the bars were wired into the cage. A general purpose gauge with a narrow width, Micro-Measurements CEA-125-UN, was used to minimize the required width of the mounting flats. A two layered protection system was used for the gauges. The first was a latex sealant used to provide moisture protection, and the second was a stiff rubber pad to provide mechanical protection. The gauges were wired using a two-wire lead conveyed through the concrete in water-tight plastic ducts forming a quarter bridge with a signal conditioner. The gauge end of the plastic wire duct was sealed with the gauge to provide moisture protection for the lead. Leads and ducts were gathered together and taken out the side of the column near the load cell connection plates. Before testing, strain gauges were shunt calibrated to a maximum strain of 0.02.

2.5 Test Program

All model tests were conducted using a sinusoidal wave form with a frequency of one cycle per minute. The test frequency was limited by the actuator velocity limit, a result of the actuator servo-valve flow rate. Data collection was performed at 3 Hz to limit the size of the 116 channel data files. For all tests, the 100 kN vertical actuator was set in load control, at 53 kN, to produce a vertical load of 126 kN at the pier. During testing, data was collected and saved in an ASCII format using an Optim Megadac 5533A Data Acquisition System.

Model testing was carried out in three phases: (i) a low level pretest; (ii) variable drift testing; and (iii) a constant high amplitude drift. A low level force-control pretest was used to check the operation of all instruments. This was a one cycle test with a maximum lateral load of ±56 kips, or approximately 30% of the ultimate strength. This value was selected to keep the response in the elastic range, thereby checking the test setup without producing any damage.

The majority of test data were collected during the variable drift test segment. The pier

was tested in drift control with three cycles at ±0.25% drift and two cycles each for remaining drift levels of ±0.5%, ±1%, ±2%, ±3%, ±4%, and ±5%. The first 3% drift amplitude test experienced a system shutdown caused by an incorrectly set actuator stroke limit. Data collected before the shutdown was saved, and the test rerun. Unfortunately, some damage occurred, and much of the data shows a discontinuity at the 3% drift level. The test also aborted prematurely after the first cycle and a half at 5% drift as the mounting for the sonic transducer controlling the lateral load actuator broke free of the specimen due to spalling of cover concrete.

The final test segment consisted of a series of twenty cycles at a 5% drift amplitude. This segment was conducted with limited instrumentation to determine the overall force-displacement and energy dissipation in each loading cycle.

2.6 Visual Observations

Figure 2-11 shows photographs of the damaged model pier resulting from the cyclic loading test. It is evident that damage is most prevalent in cap beam-column joint regions. A full description of the condition of the model at the end of testing is presented in figure 2-12.

The first visible damage, flexural cracking of the upper columns, was observed at the 1% drift level and was more prevalent in the south column. This flexural cracking was accompanied by some minor shear cracks in the cap beam, over the exterior columns. Damage, in the form of flexural column cracks and compression cracks in the face of the foundation at the ends, spread to the base of the pier at the 2% drift level, along with further upper column and cap beam cracking. This early foundation damage may be attributed to stress concentrations resulting from the flexibility of the end bearing plates coupled with crack propagation caused by the ends of the longitudinal tie bar ducts. The column damage was fairly well distributed over the column height indicating general flexural cracking-not hinge formation which is characterized by concentrated damage in the end hinge regions.

The 3% drift level marked the beginning of significant inelastic deformation, and it is

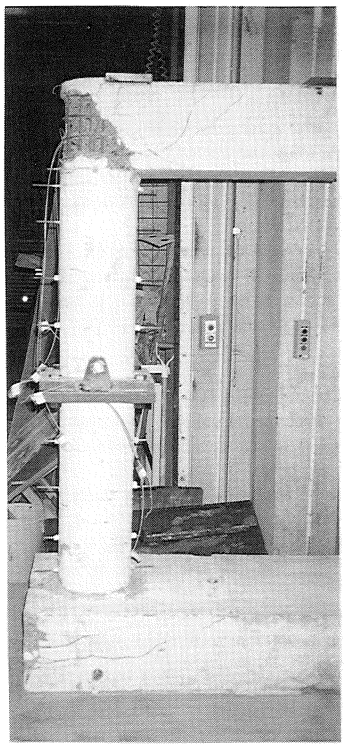

(a) North column

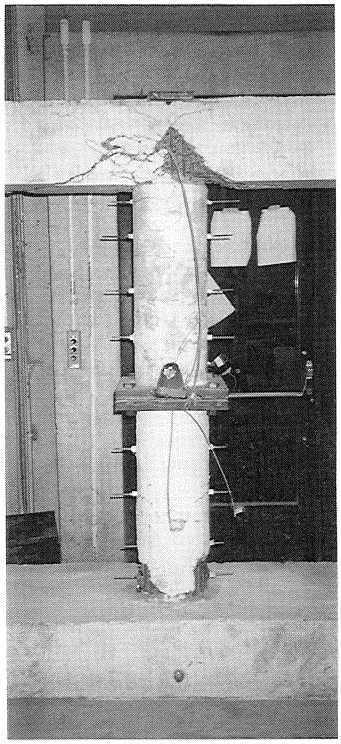

(b) Middle Column

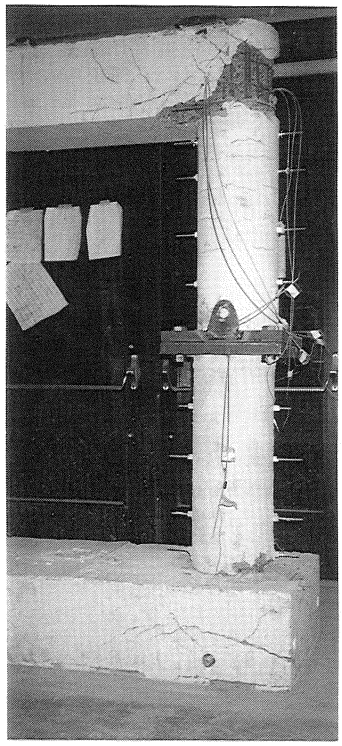

(c) South column

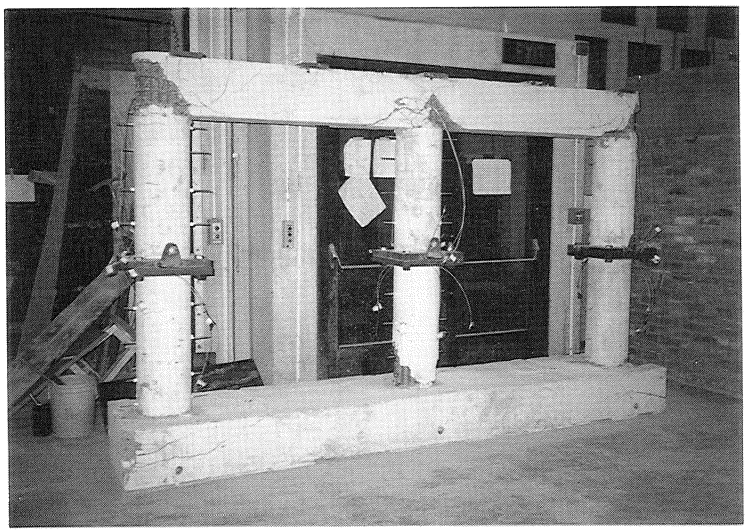

(d) Overall pier

Figure 2-11. Post-test views of the damaged model pier resulting from cyclic loading.

Joint 1: Foundation to North Column
- Longitudinal cracks at the mid-height of both foundation faces, extending from the end of the foundation to just beyond the column.
- Moderate to heavy damage in the foundation top from just south of the column to the North foundation tie down duct.
- Light column damage at base.

Joint 2: Foundation to Middle Column
- Moderate to heavy spalling on both sides of column, above the foundation.
- Some buckling of longitudinal dowel bars. No buckling evident for column bars.
- Limited diagonal cracking on the east face, and a minor crack on the top of the foundation, north of the column.

Joint 3: Foundation to South Column
- Light column cracking at base. Initiation of spall on the south side.
- Some foundation concrete crushing along top and faces at bearing plate.
- Possible flexural and/or shear cracks in the west face of the foundation at column center line.

Joint 4: North Column to Cap Beam
- Heavy damage to cap beam; Diagonal shear cracks extending from soffit just south of column upwards and to the south to top of cap beam. End cap beam concrete cover spalled and missing.
- Flexure cracks in cap beam soffit south of the column.
- Construction joint appears de-bonded.
- Light column damage, including some spalling of the south face cover underneath the cap beam.

Joint 5: Middle Column to Cap Beam
- Light column damage, including flexural cracks, and the initiation of cover spall on both sides of column.
- Heavy diagonal shear cracking in cap beam.
- Large open transverse crack in cap beam soffit approximately 250 mm north of the column extending up both faces to the center of the cap beam above the column.
- Loss of soffit cover just south of column at the end of the bottom cap beam flexural steel splice, and first stirrup in the south span. Diagonal shear crack continues up both faces into cap beam.

Joint 6: South Column to Cap Beam
- Moderate cracking in column, including the initiation of cover spall on the north column face below the cap beam.
- Heavy shear cracking in cap beam, including spall of south end concrete cover.
- Transverse Cracks in the cap beam soffit north of the column, due to either flexure, or cover spall.
- Light diagonal shear cracking in cap beam face approximately 250 mm north of column.

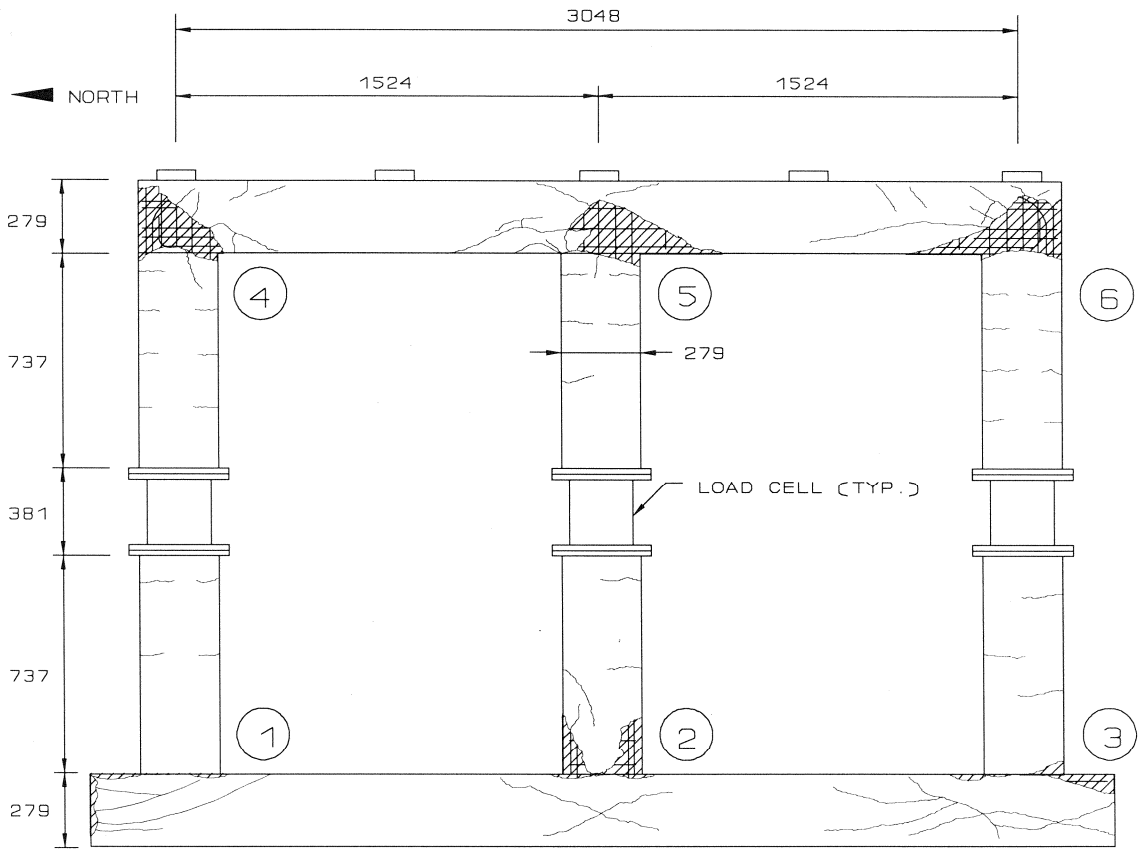

Figure 2-12. Description of damaged connections in which hatched parts denote spalled concrete.

unfortunate that the first test at this level experienced a shut down in the first push half cycle at 2.6% drift. During this short test segment cracking progressed at the ends of the foundation, and more significantly, initiated at the base of the columns, along the construction joint, indicating the commencement of hinging at the base of the columns. Fortunately, data for this aborted test was recorded, and is plotted, where appropriate, along with the other data from the variable drift tests.

Shear cracks propagated across the cap beam-column joints in the cap beam at both the inside and outside columns during the full 3% drift test. Although the ends of the cap beam were significantly damaged, there was no spalling of loose concrete at this stage. The flexural cracks in the middle region of the lower half-columns showed little further propagation, as damage concentrated at the base of the columns. The force displacement plots for 3% drift in figure 2-13 show significant pinching due to longitudinal reinforcement yield. They also show strength degradation both between the two 3% cycles, and between the 2% and 3% drift tests due to the advance of shear, bond and anchorage damage in the joints. The maximum lateral load was achieved in the first 2% drift test, for both the forward and reverse loading cases.

Damage in the 4% drift test was similar to that at 3%, with an increase in the strength deterioration. Cracks at the base of the middle column opened to 3.2 mm gap, while damage at the base of the exterior columns spread into the foundation. A crack in the cap beam soffit opened just south of the middle column as an extension of the joint shear crack in the pull direction.

Spalling of concrete at the ends of the cap beam and at the base of the middle column in the lap splice zone was observed at 5% drift. The loss of cover concrete at the north end of the cap beam caused a loss of the cap beam sonic transducer mount, prompting termination of the test after the first one and one half cycles. The dowel bars, but not the spliced column bars, showed slight buckling at the base of the middle column, indicating that the lap splice was still functioning in compression, transferring steel force to the dowel bars at the base of the column. The first 5% drift test (1-1/2 cycles) marked the end of the variable drift test segment, as well

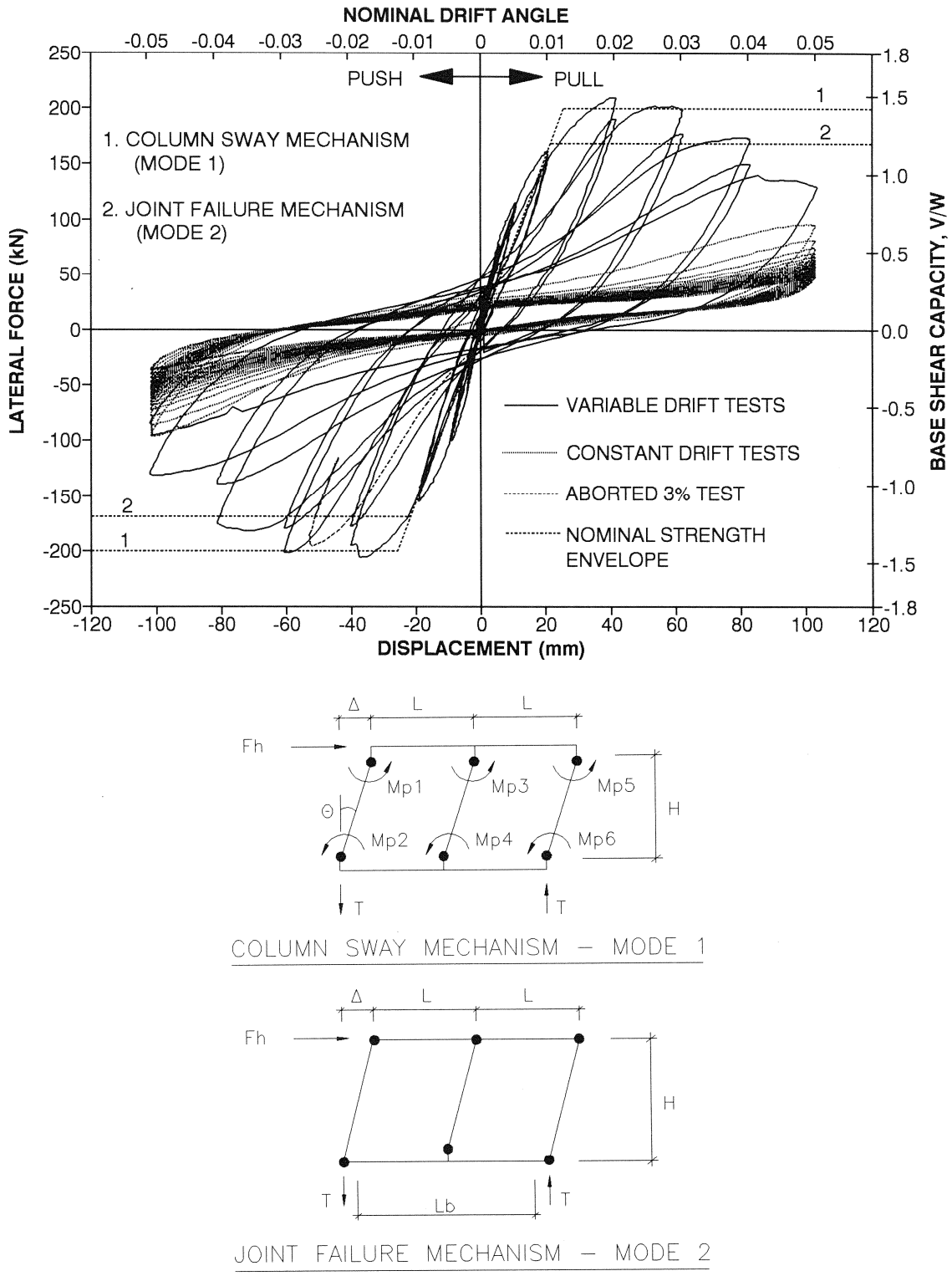

Figure 2-13. Force-displacement relationship of pre-retrofitted model pier.

as the end of the first day of model testing.

During the remaining 5% drift amplitude cycles, damage was concentrated in the joint regions. In the first five cycles, severe spalling in the cap beam above the columns along with spalling of the north face of the middle column to the end of the lap splice zone was observed. The lateral strength of the pier at this point had reduced to approximately 67 kN and was equal in both directions. Further damage to the top of the foundation just inside the north column occurred as the foundation hinge fully developed during cycles five to ten. By cycle 10, damage to the ends of the cap beam had developed full hinges with the cap beam simply rotating on the column tops at both ends. The column longitudinal and cap beam end steel provided almost all remaining stiffness and integrity for the cap beam column joints, with the majority of the joint concrete moving with the cap beam. Concrete at the central cap beam-column joint continued to spall and deteriorate.

Finally, at cycle 17, the extreme south longitudinal dowel bar in the base of the middle column fractured due to low cycle fatigue, indicating continued functioning of the lap splice. Lateral strength of the model had reduced to about 22 kN in both directions and was holding approximately steady due to the formation of a rocking mechanism.

2.7 Hysteretic Performance

2.7.1 Force-Displacement Relationship

Figure 2-13 presents a plot of total model lateral force versus column drift angle. Data from the variable drift tests is shown in solid lines, constant amplitude data in dotted lines, and the aborted 3% test in dashed lines. The normalized base shear capacity V/W shown on the right hand scale of the plot, is defined as applied lateral load divided by the applied vertical load plus half the pier weight (141 kN). The strength envelope shown as a dashed line in figure 2-13 is based on a flexural mechanism (mode 1) and a joint failure mechanism (mode 2). It was observed that the mode 1 mechanism occurred first. Then, the mode 2 mechanism became prevalent after

2% drift level tests due to the lack of reinforcement anchorage in the joints. The experimentally observed stiffness is defined as the secant stiffness measured at 75% of the nominal flexural strength. This corresponds to a pier stiffness with EI_{eff} taken at $0.6\,EI_g$. The corresponding yield drift θ_y is 0.0125 rad. The hysteretic plot shown in figure 2-13 has been corrected for an initial $P-\Delta$ moment offset that was originally present due to the eccentric weight of the horizontal actuator attached to the south end of the load transfer beam.

A common definition of the limit of useful ductility is the drift corresponding to a strength equal to a 20% to 30% drop in the nominal capacity *(Mander, Priestley and Park, 1984)*. This occurred after the first cycle at 3.8% drift levels, corresponding to a ductility factor $\mu = 3$. However, even following the heavy damage caused by the cycling at the 5% drift amplitude, the model continued to show moderate ductility and energy dissipation capacity.

2.7.2 Moment-Curvature Relationship

Figure 2-14 shows plots of moment-curvature relationship for the top and bottom gauge lengths of the north and middle columns. Section rotations and average curvatures were calculated for all nine north and middle column potentiometer pairs in the variable drift tests, thus:

$$\theta_i = \frac{P_{ni} - P_{si}}{L_p} \qquad \textbf{(2-6)}$$

and

$$\phi_i = \frac{\theta_i}{\ell_{gi}} = \frac{P_{ni} - P_{si}}{L_p \ell_{gi}} \qquad \textbf{(2-7)}$$

in which θ_i = net section rotation over the ith gauge length, ϕ_i = average curvature over the ith gauge length, P_{ni} = change in length across north potentiometer of pair i, P_{si} = change in length across south potentiometer of pair i, L_p = distance between north and south potentiometer = $365\ mm$, and ℓ_{gi} = gauge length of potentiometer pair i. Although the potentiometer mounts were solid throughout testing, damage in the cap beam and foundation at

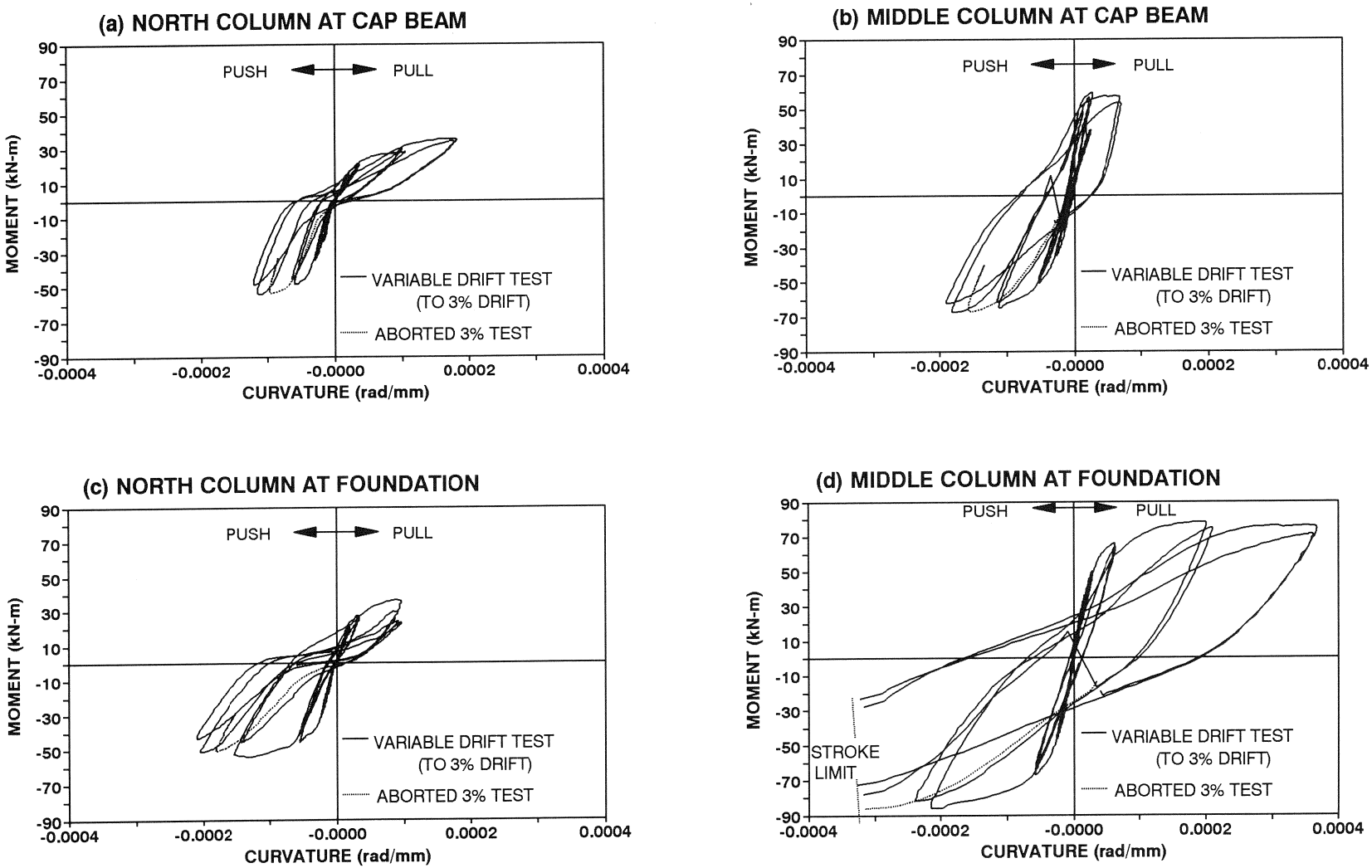

Figure 2-14. Column moment-curvature relationship of pre-retrofitted model pier.

the column ends limited the reliability of potentiometer readings beyond the 3% drift level.

Column bending moments were calculated for the center of the end gauge lengths directly from the column load cell data. The measured shear force was taken as the slope of the column moment, and although the location of the inflection point should be determined from the measured moment, the zero points for load cell moment were not set reliably. Therefore, the inflection point levels were determined using an analytical model.

The upper gauge length of the north column shows dual stiffnesses, being stiffer in the push direction when the effective axial load is increased. The low level of hysteresis shown in figure 2-14(a) for this gauge length is indicative of a joint shear failure in the cap beam-column joint, rather than the development of a flexural hinge in the column.

The lower gauge length of the north column also shows a higher stiffness and capacity in the push direction, especially for higher drift levels, when cracking is more extensive. Note also the flat region of the hysteretic curve just below the zero moment level indicating some slip along the rebar splice as it progresses from compression across the section in a push cycle, to tension in a pull cycle.

The upper gauge length of the middle column shows some energy dissipation in the 3% drift cycles, due to yielding of the longitudinal steel, before the degradation of concrete shear strength in the joint area. As the shear capacity of the concrete in the cap beam-column joint degrades, joint shear failure governs over the more ductile flexural hinge in the column. The energy dissipation is greater in the push direction due to the influence of initial shear cracking in the joint which was propagated from the cap beam soffit just south of the column. This crack was open in the pull direction decreasing joint concrete strength, and closed in the push direction, increasing joint strength beyond the moment capacity of the column at the point of first yield in the steel.

The greatest energy absorption occurred at the base of the middle column, where in spite

of the presence of a lap-splice, a flexural hinge developed in the column. Rotation in this gauge length exceeded the limit of the south potentiometer before reaching the 3% drift range, causing truncation of the hysteresis loops in the push direction.

2.7.3 Column Axial Load-Moment Interaction

Figure 2-15 presents the axial load-bending moment relationship plotted for all three columns based on the peak forward and reverse drift levels during the phase 2 (variable drift) tests. Also shown is the nominal P-M interaction curve for the column section, which was determined from the measured concrete and steel yield strengths, using ACI 318 procedures *(ACI 318, 1995)*. Note the low level of axial load in all three columns. This is a characteristic of bridge piers with aged concrete.

The slope of the points plotted for the north and south columns demonstrates the effect of frame action on columns. In the push direction the north column picks up axial load and the south column axial load decreases to react to the applied overturning moment. The axial load in the middle column should remain constant; however, the combination of low gravity axial load and high overturning moment produces a net uplift force at one end of the foundation which is resisted by tension in one of the foundation tie-down bolts. Under low applied lateral loads this uplift is transmitted by the reduction of axial load in the windward column, resulting in even a slight tension force across the column section. In the case of high lateral load, the tension capacity of the windward column is exceeded, and the middle column axial load must also decrease to maintain equilibrium with the applied overturning moment. This phenomenon accounts for the flattening of the slope for peaks of light cycles in the external columns when the net axial load is negative (tension) for the column and the decrease in the middle column axial load for cycles with high moment.

The data plotted outside of the nominal envelope for the top of the middle column is probably attributable to over-strength caused by strain hardening of the longitudinal steel. The yielding of this steel is evident in both the moment-curvature time history plots and the

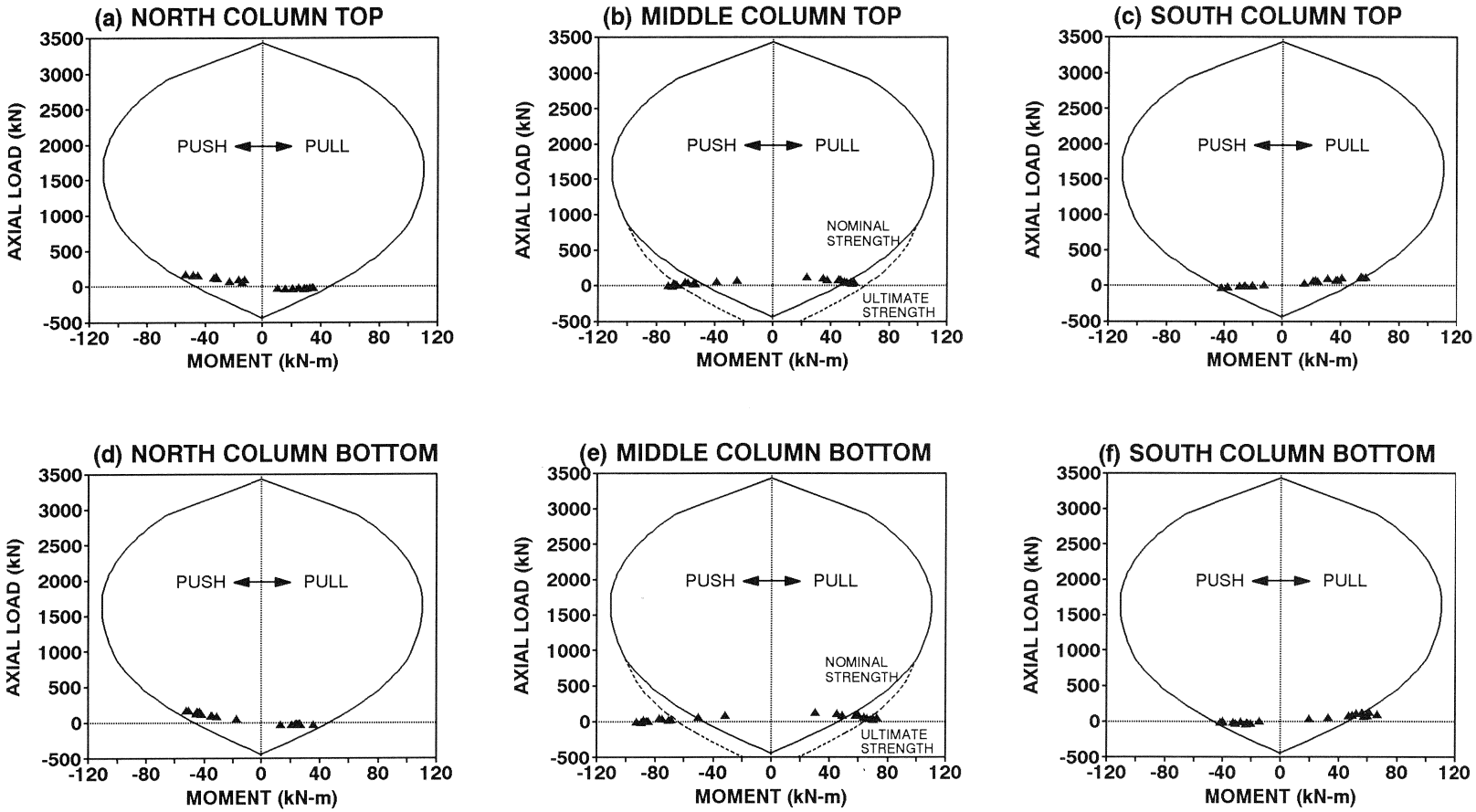

Figure 2-15. Column axial load-moment interaction diagrams for each column end of the model pier, showing experimentally observed peak values at each cycle.

reinforcement strain profiles presented in the following subsection. It is also clear from the stress strain characteristics of the #3 deformed bar in figure 2-1 that the levels of strain measured are well into the strain hardening region. Although the true ultimate interaction curve is dependent upon loading history, it has been approximated in figures 2-15(b) and 2-15(e) by plotting portions of an additional interaction curve using a steel ultimate strength of 750 MPa (see figure 2-1). Concrete strength beyond that assumed in the analysis has little effect on the nominal curve in a region of low axial load.

2.7.4 Response Profiles

2.7.4.1 Moment and Curvature

Figure 2-16 presents moment and average curvature profiles plotted for the first peak forward and reverse drift of the 0.25% to 3% drift levels in the variable drift tests. The average curvature calculated for each gauge length is plotted at the center height of the gauge length.

As expected, most of the curvature was concentrated at the column ends. For a homogenous material, the inelastic curvature between the column ends would be linear in proportion to the bending moment diagram. However, for a concrete column, localized flexural cracks can cause deviations from linearity in the curvature diagram such as shown for the middle column at a height of 559 mm.

Both profiles show the position of the column inflection point. As expected, this is just above the center height of the columns for elastic conditions, because the foundation stiffness is greater than the cap beam stiffness. Although it is not shown in these plots, as damage to the model progresses towards a full mechanism, the inflection point moves down the column towards the center height. The location of the inflection point calculated from the curvature measured in the center gauge lengths provided an independent verification of the analytical model used to determine the zero point for column bending moment.

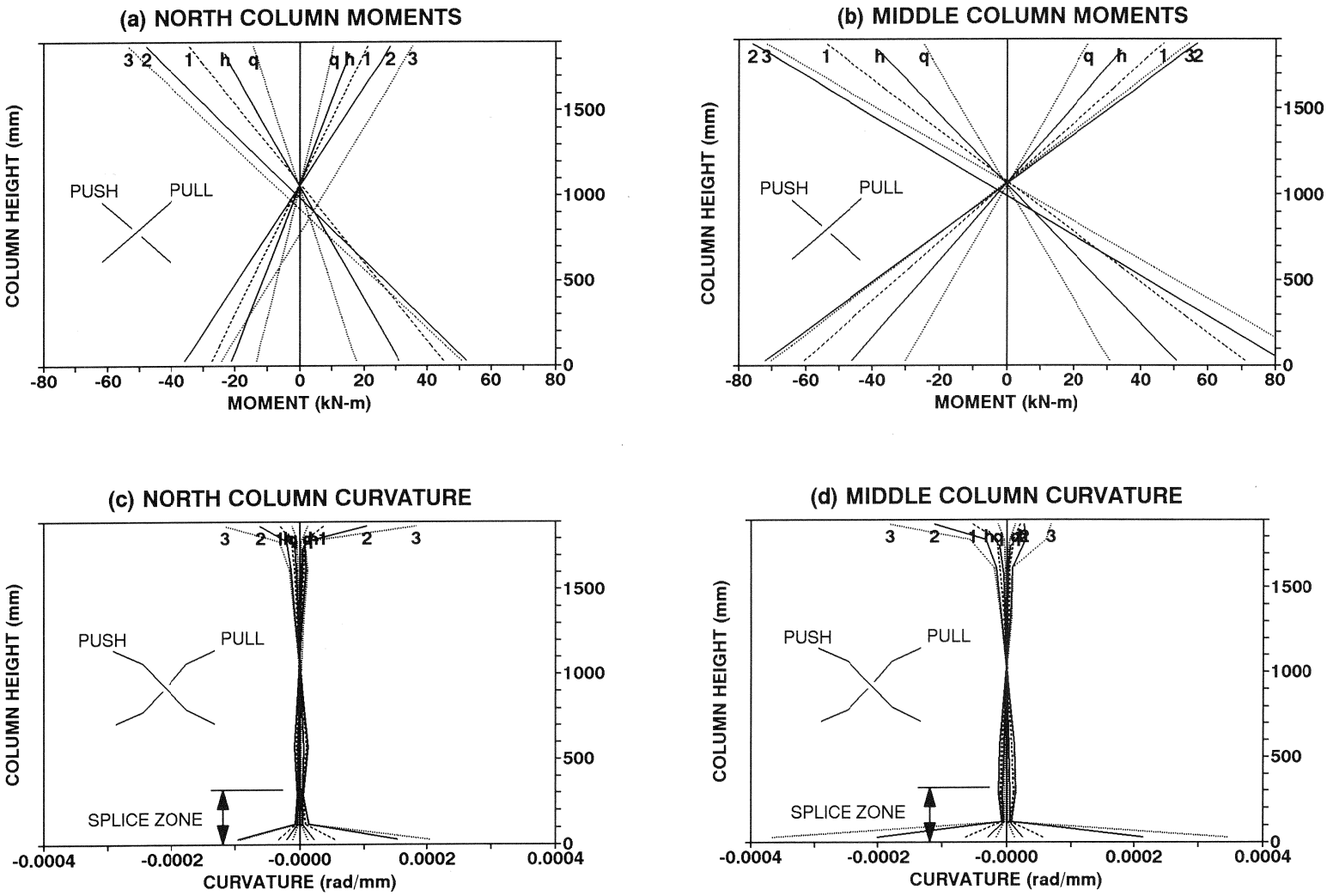

Figure 2-16. Column moment and curvature profiles of pre-retrofitted model pier.

The middle column curvature plot demonstrates the difference between the formation of a flexural hinge in the column and failure caused by shear degradation of a joint. Curvatures at the base of the middle column are quite high, indicating ductile behavior, with most of the curvature occurring in a flexural hinge. At the top, most of the deformation is occurring across shear cracks in the cap beam rather than rotation of a flexural column hinge. This shear crack deformation is more prevalent in the pull direction due to significant shear cracks that formed in the joint before 3% drift.

2.7.4.2 Column Displacement

Figure 2-17 shows total column displacement profiles and displacement components resulting from column flexure, shear, and rotation. Data is shown for the first forward and reverse half-cycles of the 0.25% to 3% drift levels for the variable drift test (phase 2), as in figure 2-16.

Total displacements were measured by the sonic transducers attached to the column at the same level as the potentiometers. Results for the north column were corrected for the measured foundation sliding, so there is zero displacement for either column at the base (H=0). The displacement plotted for both columns at H=1854 mm was measured at the cap beam, and neglecting axial flexibility of the cap beam, is roughly the same for both columns.

Flexural displacements were calculated from the curvatures plotted in figure 2-16 using the moment-area theorem, which is given by:

$$\Delta_{ab} = \int_a^b \phi_x x\,dx \qquad \textbf{(2-8)}$$

in which ϕ_x = curvature at position x calculated by equation (2-7) and Δ_{ab} = the deflection of a point b relative to the tangent of displacement at a point a.

For this case, point a was taken at the base, so that in theory, the tangent at a is vertical, and the displacement at the top of any potentiometer gauge length is given by the moment of the average curvature of all gauge lengths below the section being considered. However, some

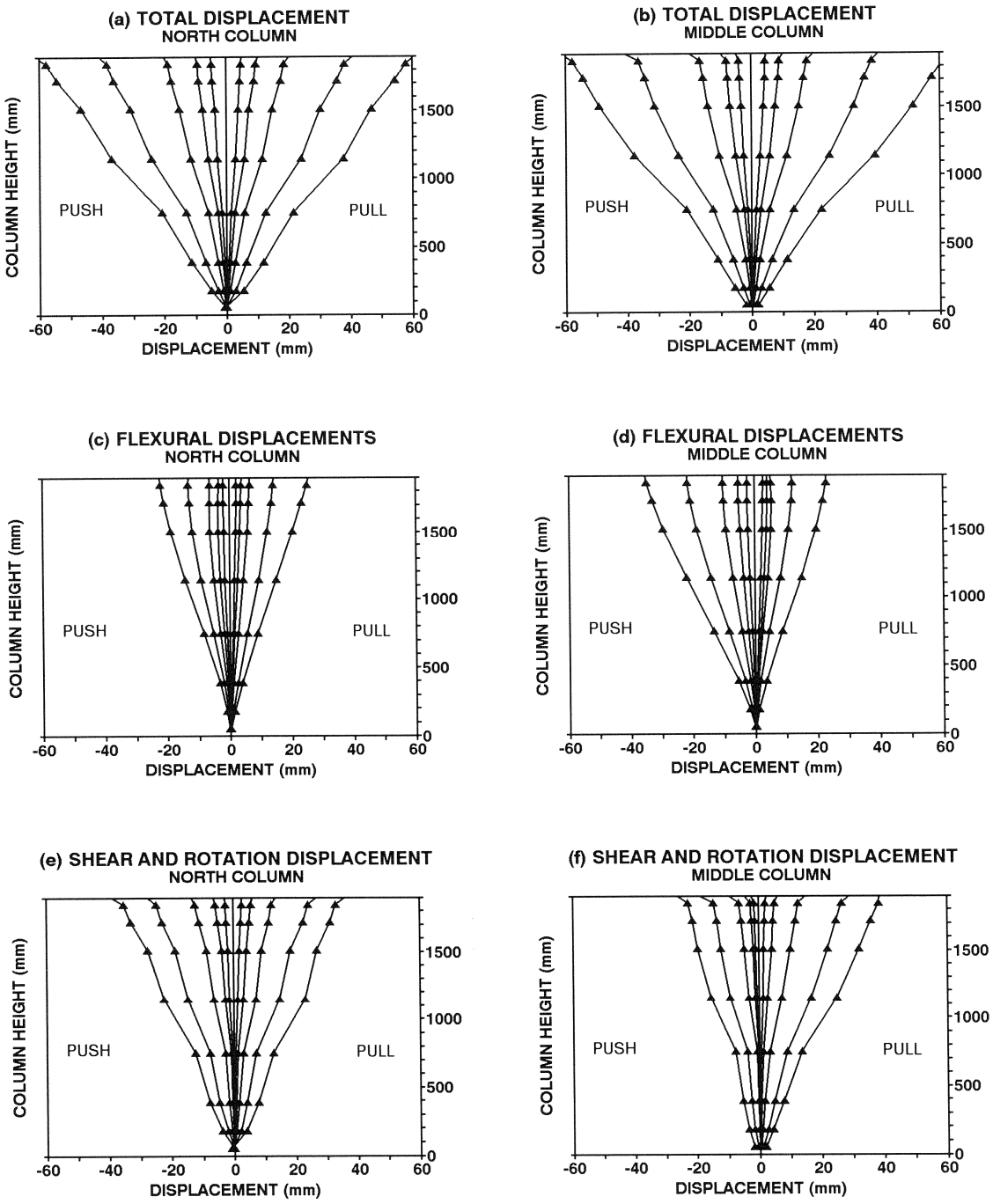

Figure 2-17. Column displacement profiles of pre-retrofitted model pier.

unmeasured column rotations occurred within the foundation and are not accounted for by the curvature calculations. Therefore, the difference between the observed total displacements and the calculated flexural displacements is a combination of column shear deformation and foundation flexibility effects that includes column-foundation joint rotation.

The slope of the shear and rotation profiles in the middle gauge lengths of the columns is approximately equal to the rotation occurring in the foundation. The increase in slope at the column ends is due to rotational displacements in the hinge zones, and the increase at the middle length is due to shear displacements and slip across the bolted load cell connections.

2.7.4.3 Reinforcement Strain

Figure 2-18 shows the column extreme longitudinal reinforcement strain profiles at cap beam-column joints. The peak forward and reverse drift for the first cycle at the 0.25% to 3% drift levels is shown in dotted lines and the second cycle peaks for 2% and 3% is plotted in solid lines. The plotted column heights are relative to the cap beam soffit. Gauge readings from the north bar in each column are plotted to the left, south to the right. Note that the sign convention for strain is tension positive. The yield strains of ±0.0024 were determined experimentally.

First yield occurs consistently in tension and is usually accompanied by bond slip, causing the gauge to remain in the positive strain region, even after the bar returns to a compression half-cycle. The highest strain levels are found at or just below the soffit, and die down quickly into the cap beam, indicating sufficient anchorage for these low levels of drift. However, the bond slip mentioned above is an early symptom of anchorage loss.

2.7.5 Energy Dissipation

Figure 2-19 shows the energy absorption capacity of the pier for loading cycles and cumulative drift amplitudes. The energy dissipated per cycle is defined as the work done on the pier by the applied lateral load, over a full forward and reverse drift cycle. The energy dissipated

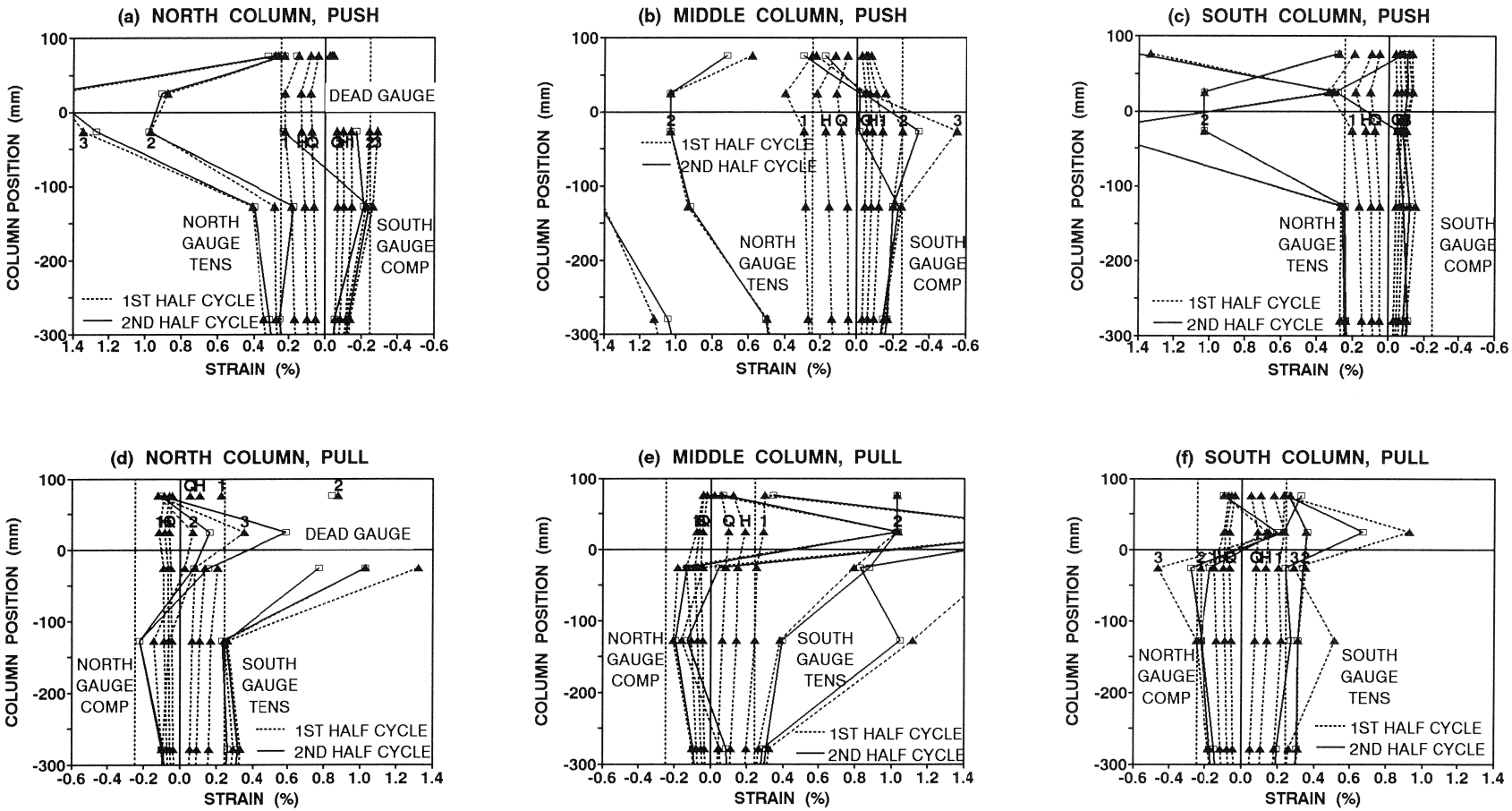

Figure 2-18. Column reinforcement strain profiles at cap beam before retrofit.

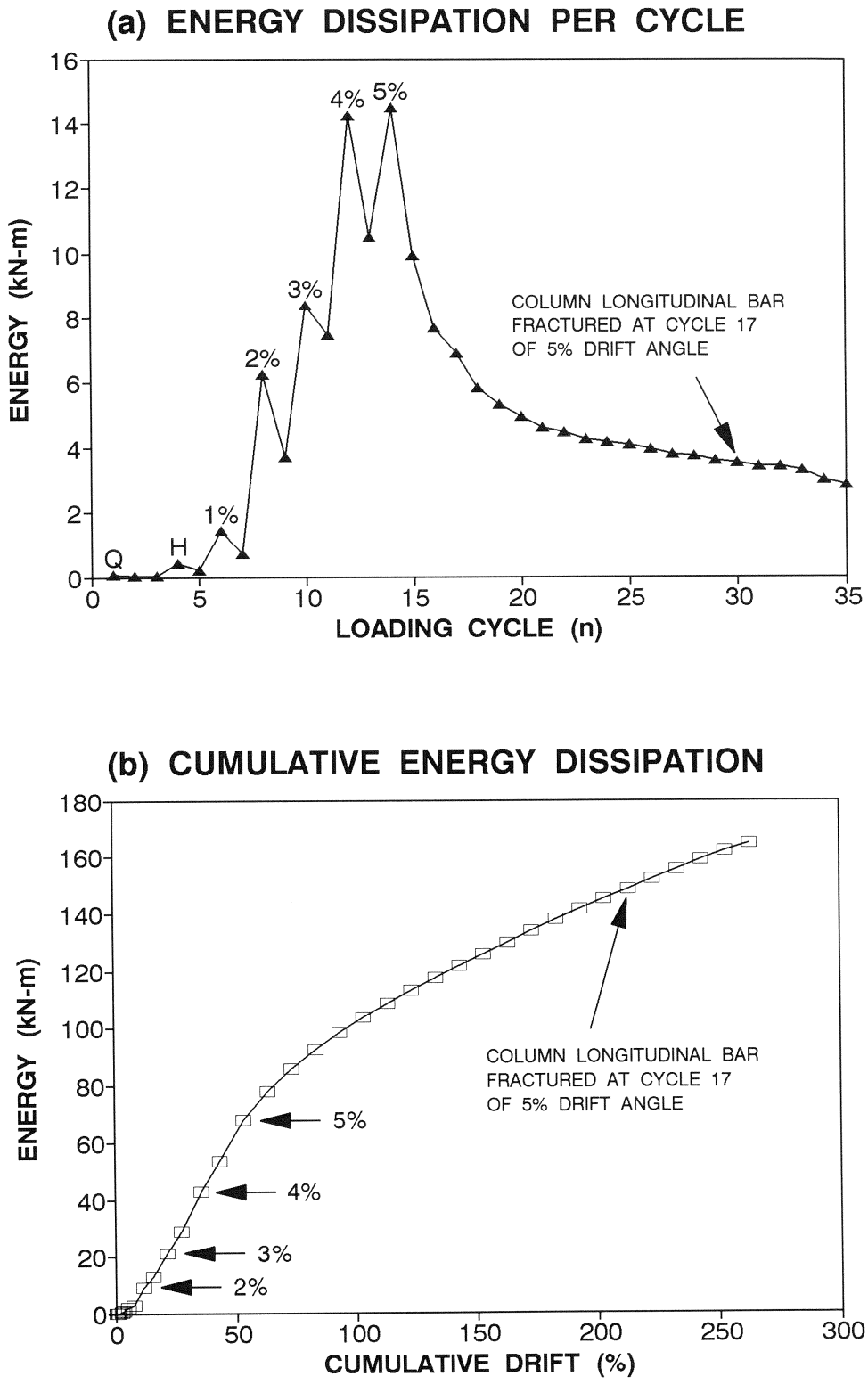

Figure 2-19. Energy absorption capacity of pre-retrofitted model pier.

per cycle can be determined quantitatively from the area enclosed by a force displacement loop. Thus,

$$E_{cycle} = \int_{cycle} F \cdot dx \tag{2-9}$$

Numerically integrating using the trapezoidal rule gives:

$$E_{cycle} = \sum_{i=1}^{n} \left(\frac{F_i + F_{i-1}}{2} \right) \cdot (x_i - x_{i-1}) \tag{2-10}$$

in which F_i = total lateral force at step i and x_i = cap beam displacement at step i.

Energy dissipation decreased for each successive cycle during the constant drift amplitude test, and approached an asymptote constant level near the end of the test. The model displayed good energy dissipation even in its highly damaged condition at the end of testing. However, it should be noted that longitudinal rebar fracture occurred very close to the end of the testing sequence, and the per cycle energy dissipation showed a visible drop following the fracture. It is expected that the rate of energy absorption would have decreased significantly under further load cycles following the fracture of additional column bars.

2.8 Summary

The model pier, which is attributed as a typical gravity-load-designed bridge pier, was governed by flexure at moderate drift levels, but ultimately by the limited bond and anchorage capacity of the cap beam-column joints subsequently led to joint shear failure. The observed fracture of longitudinal bars at the base of the middle column due to low cycle fatigue implies that well anchored splices may lead to premature fracture due to a very short effective plastic hinge length.

SECTION 3
SEISMIC RETROFIT: CAPACITY ANALYSIS AND REDESIGN

3.1 Background

Capacity design procedures for earthquake resistant detailing of structures are now part of a well established seismic design philosophy. Developed primarily in New Zealand in the 1970's, capacity design approaches have been used extensively for buildings as well as bridges *(Paulay and Priestley, 1992).*

The capacity design philosophy enables the designer to select a desirable hierarchy of failure mechanisms for framed structures. Regions not participating in the primary energy dissipating mechanism have a measure of capacity protection by providing overstrength to those regions. In principle, a plastic mechanism is chosen such that the necessary overall displacement ductility can be developed that leads to the smallest inelastic rotational demands in the plastic hinges. For building frames this generally leads to a beam sidesway mechanism with strong columns and weak beams. Thus, soft story mechanisms are avoided as the rotational demands on the columns are excessive. For bridges, however, it is generally not possible to avoid a column sidesway mechanism. Therefore, the plastic hinge regions within columns need to be carefully detailed to ensure ductile behavior.

Capacity design principles have been implemented in various ways in different countries including the United States. For example, the ACI 318 building code *(1995)* introduces capacity design implicitly in the form of the following equation:

$$\Sigma M_e \geq \frac{6}{5} \Sigma M_g \qquad \textbf{(3-1)}$$

where ΣM_e = sum of moments, at the center of the joint, corresponding to the design flexural strength of the columns framing into that joint and ΣM_g = sum of moments, at the center of the joint, corresponding to the design flexural strength of the girder framing into the joint in which an overstrength factor of 1.25 is applied. For bridges, the sum of the girder moment strengths

should not be less than 6/5 times the sum of the column moment strengths at a joint. AASHTO specifications for seismic design *(1992)* require the use of overstrength capacity of $1.25 f_y$ for longitudinal reinforcement for design of column connections. Shear design is then based on flexural overstrength using 1.25 times the nominal yield stress for reinforcing steel.

3.2 Capacity Analysis and Redesign of A Gravity Load Designed Bridge Pier

The capacity design philosophy can be adapted and applied to the seismic repair and/or retrofit of existing non-ductile (gravity load designed) bridge piers. The procedure will be referred to herein as *capacity analysis and redesign.*

The average gravity load inducing axial stress in non-seismically designed bridge pier bents existing in the eastern and central United States is generally quite low ($P_e < 0.1 f'_c A_g$). Moreover, ductility demands on columns arising from a column sidesway mechanism may not be excessive, particularly in zones of low to medium seismicity such as the central and eastern United States. Plastic hinge zones in such columns may have sufficient inherent ductility capacity to withstand the ductility demand. This means that in accordance with capacity design principles, those areas not participating in the primary energy dissipating mechanism should have a measure of capacity protection to ensure elastic behavior. This may require some retrofitting of those areas. Thus the primary principles in *capacity analysis and redesign* for existing gravity load designed bridge piers are threefold:

1. To enhance the shear strength capacity and bond strength of the longitudinal column bars at the cap beam-column joint.
2. To upgrade the ductility capacity of column hinges at ground level, particularly if a lap-splice is present, and improve the column-foundation joint.
3. To ensure that columns possess sufficient ductility capacity to withstand expected rotational demands.

The order shown above in principle reflects the order of importance. In case all upgrading

features cannot be implemented in the redesign stage, then it is suggested that the most important aspects be tackled first.

The above mentioned retrofitting strategies have emerged as a result of laboratory experimental observation on the 1/3 scale model pier behavior under inelastic lateral cyclic loading described in Section 2. Figures 2-11 and 2-12 show the damaged model pier. The pre-retrofitted model pier corresponding to the typical eastern and central U.S. highway bridge piers designed for gravity loads possesses the following weaknesses:

1. Cap beam and column joint connections are weaker than the columns under cyclic lateral loading, especially at the exterior joints.
2. Lap-splices in the potential plastic hinge zones at the foundation level may lack confinement reinforcement. However, if the lap length is sufficient to avoid bond deterioration, premature low cycle fatigue failure of the longitudinal rebars may occur as a result of the high plastic strain range due to the very short effective plastic hinge length at the base of the column.
3. Inappropriate anchorage of the longitudinal column steel is common in flexurally deficient cap and/or foundation beam.

The observed deficiencies in existing bridge piers designed for gravity loads only may be overcome by utilizing principles of *capacity analysis and redesign*. Thus, the corresponding retrofit process for the bent type pier is addressed as follows:

1. The pier cap beam is increased in section and prestressed longitudinally to enhance its strength and anchorage of column steel.
2. The foundation is extended up to the lap splice to remove the plastic hinge outside that zone.
3. The foundation is strengthened to ensure the plastic mechanism will occur in the column.

Providing that the axial load levels are low in the columns, then the columns remain as

they are prior to retrofitting. The decreased overall column height due to the increase of cap and foundation beam section will lead to a stiffer structure and a larger mechanism strength. The foundation should, therefore, be checked for possible rocking/overload.

3.3 Capacity Analysis of Columns

The first step in the procedure is to determine the flexural overstrength capacity of the columns in the bridge pier. This is then used as a basis of evaluating the weak links within the designed hierarchy of failure mechanisms.

The retrofit schemes presented herein assume that the existing columns, by virtue of their low axial load levels, possess sufficient ductility capacity to withstand the modest seismic demands imposed on them in low to moderate seismic risk zones such as the eastern and central United States *(Mander, et al., 1993)*. Furthermore, bridge pier columns usually satisfy the relation, $M/Vd > 2.5$, where M/V is the shear span and d the member depth. Thus, it is assumed that the columns are sufficiently slender so that the shear strength demand is smaller than the capacity *(Park and Paulay, 1975)*. In any case the strength and ductility capacity should be assessed. If insufficient, additional transverse reinforcement with a concrete jacket should be provided as per current code requirements. For a plastic column-elastic beam mechanism the column shear force is calculated as

$$V_c = \frac{2M_c}{l_c} \qquad \textbf{(3-2)}$$

where V_c = column design shear force, M_c = column moment capacity and l_c = column clear height.

3.4 Redesign of Cap Beam

3.4.1 Cap Beam Flexural Strength

According to principles of capacity design, the cap beam is redesigned to behave elastically based on the column overstrength moment capacity. Using a relatively conservative overstrength factor of 1.5 equation (3-1) can be rewritten for design as

$$M_p = 1.5\, M_n^{col} \tag{3-3}$$

where M_p= overstrength moment of column and M_n^{col} = nominal flexural strength of the column. Since the existing pier cap beam has sufficient strength to sustain gravity load, the capacity redesign process need only consider additional seismic force due to column overstrength. Two solutions are possible for cap beam redesign: ordinary reinforced concrete jacket; and prestressed concrete jacket. However, an ordinary reinforced concrete solution is expected to require a larger jacket size to avoid reinforcement congestion due to a large amount of reinforcement. Therefore, a prestressed concrete solution promises some advantage, not only from a constructability standpoint, but also for the enhancement of shear capacity.

In determination of proper level of prestress, it is helpful to consider stress blocks under combined axial and flexural stresses as shown in figure 3-1. The stress blocks for extreme fiber stresses can be expressed in the following form:

$$-\frac{P}{A_b} - \frac{M_p}{S_b} \geq -0.6 f'_c \tag{3-4a}$$

$$-\frac{P}{A_b} + \frac{M_p}{S_b} \leq 1.0\sqrt{f'_c\ (MPa)} \tag{3-4b}$$

where P= prestressing tendon force after losses, A_b= area of concrete at cap beam section considered, $S_b = A_b h_b / 6$= cap beam sectional modulus and h_b=overall depth of cap beam section. Equations (3-4a) and (3-4b) represent the limit of compressive and tensile stress at extreme fiber, respectively. The optimal prestressing force P, may be obtained by solving the

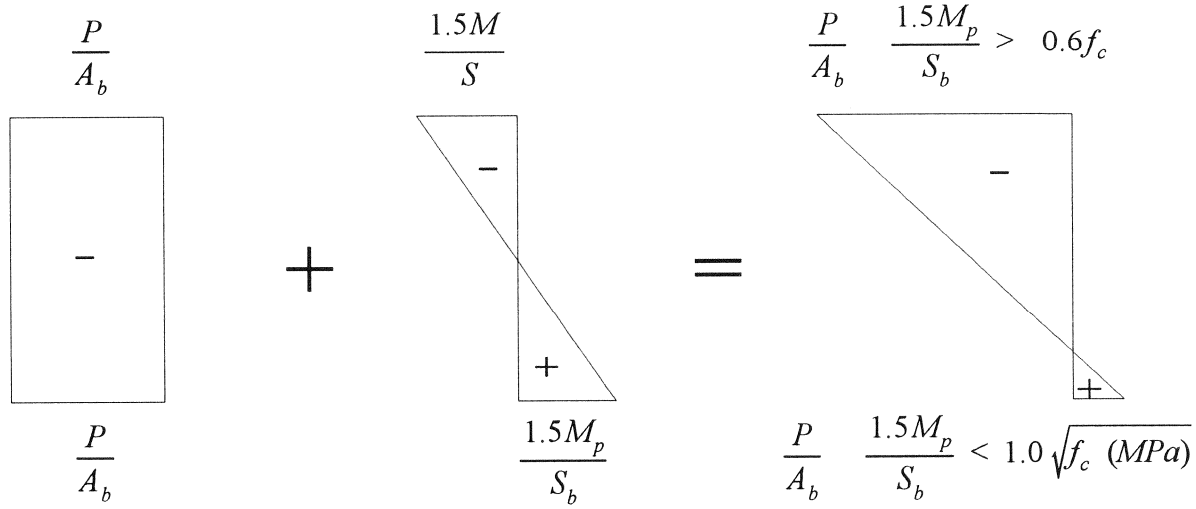

Figure 3-1. Combination of axial and flexural stress blocks.
(Note that tension stress is positive.)

equations simultaneously as follows

$$\frac{6M_p}{h_b} - 1.0\sqrt{f_c'\ (MPa)}\ bh_b \le P \le 0.6 f_c'\ bh_b - \frac{6M_p}{h_b} \qquad \textbf{(3-5)}$$

where b= width of cap beam. In application of the amount of prestress through the cap beam, code provisions for prestressed concrete should be checked.

3.4.2 Cap Beam Shear Strength

The shear force applied to the cap beam can be determined as follows from the plastic column — elastic beam mechanism shown in figure 3-2(a):

$$V_{bL} = (M_{P1} + 0.5M_{P2})\left(\frac{l_c + h_b}{l_b l_c}\right) \qquad \textbf{(3-6a)}$$

$$V_{bR} = (0.5M_{P2} + M_{P3})\left(\frac{l_c + h_b}{l_b l_c}\right) \qquad \textbf{(3-6b)}$$

where V_{bL}= beam shear in left span due to mechanism and gravity loads, V_{bR}= beam shear in right span due to mechanism and gravity loads, M_{P1}= windward column overstrength moment, M_{P2}= middle column overstrength moment, M_{P3}= leeward column overstrength moment, and l_b= cap beam span. If sufficient prestress is applied to the cap beam, then additional transverse reinforcement may not be needed. The uncracked shear capacity of the prestressed concrete cap beam may be assessed by the code equation $v_{cw} = 0.3\sqrt{f_c'\ (MPa)} + 0.3 f_{pc}$, where f_{pc}= resultant compressive stress at the section centroid due to prestress *(ACI, 1995)*. If this stress is exceeded under the load V_b^{max}, then the beam should be detailed in accordance with the principles of reinforced concrete design.

3.5 Capacity Redesign of Foundation

The flexural strength of foundation should be checked for the column overstrength moment and redesign should ensure that the plastic hinging form outside the footing.

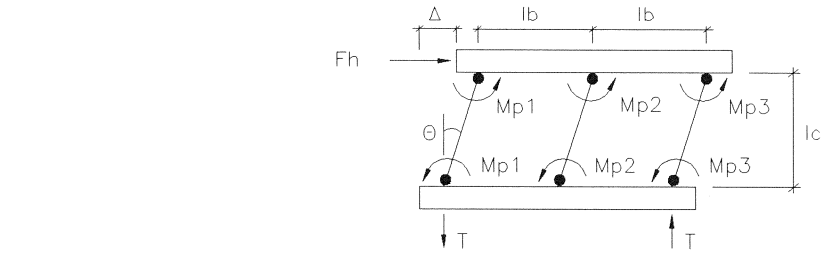

(a) Plastic Column – Elastic Beam Mechanism

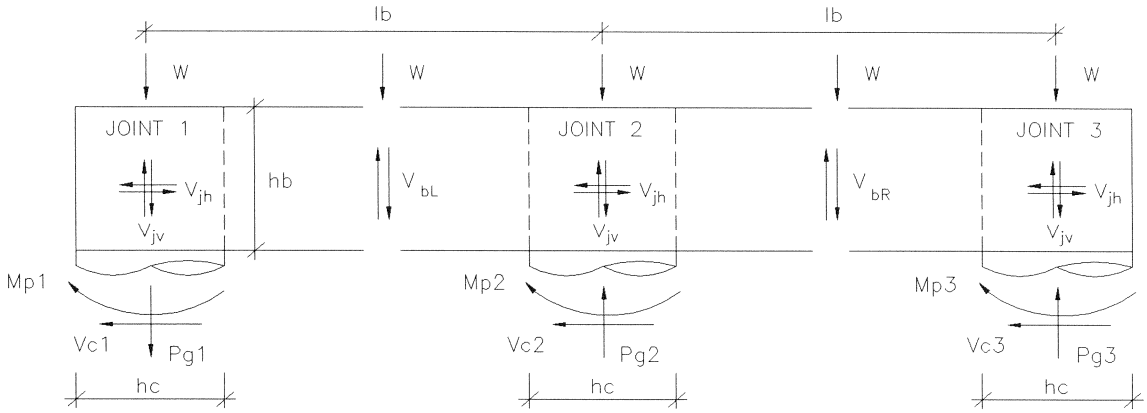

(b) Force Equilibrium at Joints

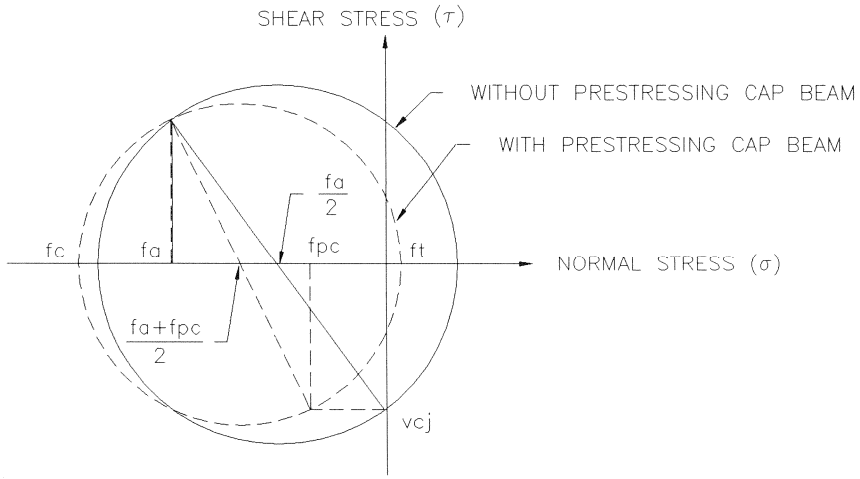

(c) Effect of Prestress on Principal Tension Stress

Figure 3-2. Force equilibrium at joints for post-retrofitted pier.

3.6 Shear Strength of Cap Beam-Column Joint

From the plastic column-elastic beam mechanism, bending moment and shear force for the cap beam and columns can be calculated. Then, using geometry and force equilibrium as shown in figure 3-2(b), the shear force demand at cap beam-column joints can be computed:

$$V_{jv} = \frac{M_{P1}}{jd} - \frac{\Sigma M_{Pi}}{4l_b} + \frac{P_{g1}}{2} \quad for\ joint\ 1 \tag{3-7a}$$

$$V_{jv} = \frac{M_{P2}}{jd} - (M_{P1} + 0.5M_{P2})\left(\frac{l_c + h_b}{l_b l_c}\right) + \frac{P_{g2}}{2} \quad for\ joint\ 2 \tag{3-7b}$$

$$V_{jv} = \frac{M_{P3}}{jd} + \frac{\Sigma M_{pi}}{4l_b} - (0.5M_{P2} + M_{P3})\left(\frac{l_c + h_b}{l_b l_c}\right) + \frac{P_{g3}}{2} \quad for\ joint\ 3 \tag{3-7c}$$

where V_{jv}= vertical component of joint shear force demand due to plastic column-elastic beam mechanism, jd= internal moment arm in column section= $d\text{-}d' \approx 0.8h_c$, h_c= column overall depth diameter, ΣM_{Pi}= sum of column overstrength moments of the mechanism, P_{g1}= gravity and overturning moment induced axial load on the windward column, P_{g2}= gravity induced axial load on the middle column, and P_{g3}= gravity and overturning moment induced axial load on the leeward column. This approach for calculating the vertical component of joint shear demand based on the plastic column-elastic beam mechanism is demonstrated for the prototype pier of the Niagara Parkway Bridge in figure 3-3. The corresponding horizontal component of joint shear force is calculated using the theory of elasticity in which shear stresses applied horizontally and vertically on a plane stress element in a joint are the same in magnitude, thus,

$$V_{jh} = \left(\frac{h_c}{h_b}\right)V_{jv} \tag{3-8}$$

where V_{jh}= horizontal component of joint shear force demand.

The principal tension stress demand with prestressing at a joint due to the joint shear force is determined constructing Mohr's circle as shown in figure 3-2(c):

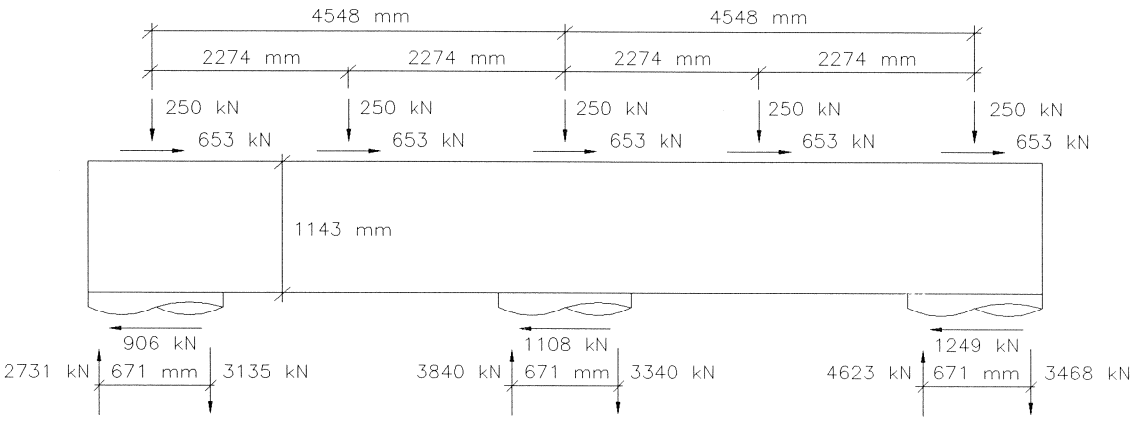

(a) Plastic Column Actions on the Cap Beam

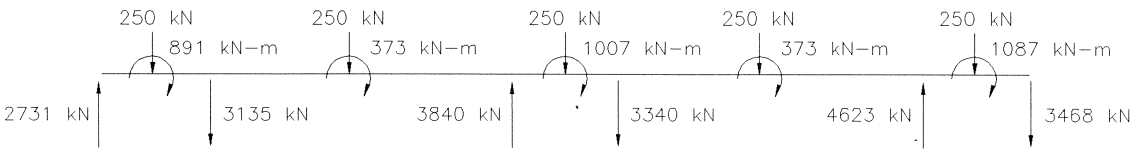

(b) Forces Acting along The Centerline of Cap Beam

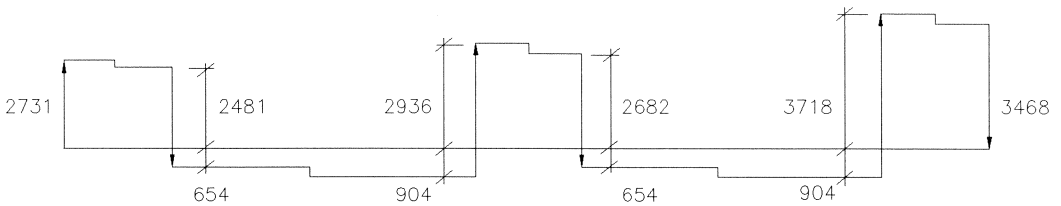

(c) Resultant Shear Force Diagram of Cap Beam (kN)

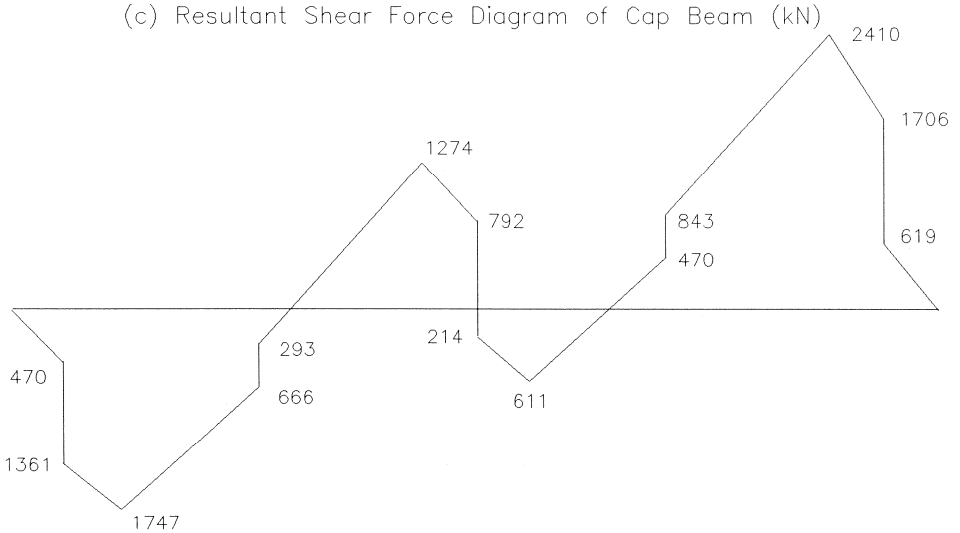

(d) Resultant Moment Diagram of Cap Beam (kN−m)

Figure 3-3. Example of joint force equilibrium for post-retrofitted prototype pier.

$$f_t = \sqrt{\left(\frac{f_a - f_{pc}}{2}\right)^2 + (v_{cj})^2} - \left(\frac{f_a + f_{pc}}{2}\right) \quad \textbf{(3-9)}$$

where f_t= principal tension stress demand, f_a= column axial stress due to gravity load and mechanism induced overturning moment, v_{cj}= joint shear stress= $V_{jv} / bh_b = V_{jh} / bh_c$. The calculated principal tension stress demand f_t may be resisted by the concrete if f_t is not greater than the tensile strength of concrete, that is, $f_t \leq \frac{1}{3}\sqrt{f_c'}$ (MPa). If the principal tension stress exceeds the capacity, the joint is liable to crack. The joint should then be designed as a conventional reinforced concrete system. Cracked reinforced concrete joint shear forces are then resisted by two mechanisms: concrete strut; and steel truss mechanisms. That is,

$$V_{jh} = V_{ch} + V_{sh} \quad \textbf{(3-10a)}$$

$$V_{jv} = V_{cv} + V_{sv} \quad \textbf{(3-10b)}$$

where subscripts c and s refer to the contribution of the concrete strut and the steel truss mechanism, respectively. The capacity design of such reinforced concrete joints for shear may be found in Paulay and Priestley *(1992)*.

3.7 Anchorage of Flexural Reinforcement

3.7.1 Lap Splice Zone

Experimental work performed by Paulay *(1982)* has shown that lap splices can sustain large plastic hinge rotations if sufficient transverse reinforcement is provided to properly clamp the spliced bars together. A retrofit may use this technique. However, removal of existing concrete cover to enable the new hoops to be placed tightly around the longitudinal steel is a difficult task. Alternatively, steel jacketing may be used in the lap splice region. This method has been used extensively in California and is described by Chai, Priestley and Seible *(1991)*. However, the use of steel casings in the northeastern and midwestern U.S. should be applied with caution owing to the severe corrosion problems associated with deicing salts.

It is therefore advocated that the lap splice zone be eliminated by casting a new foundation beam around the existing column splice starter bars. This also strengthens the weak spread footing.

3.7.2 Cap Beam Anchorage of Column Reinforcement

In most of the gravity load designed columns of existing highway bridge construction the longitudinal column bars are anchored into the cap beam with a relatively short straight anchorage. Under reverse cyclic loading during earthquake ground motions yielding of those bars in the column penetrates into the anchorage zone. Pull-out may result after a number of cycles of loading. It is, therefore, generally necessary to enhance the anchorage of these bars. The development length may be enhanced by providing a fillet between the column and cap beam. Additional longitudinal cap beam prestress may be applied to enhance the pull-out resistance of the bars. Theoretical conditions pertaining to the amount of prestress and fillet size is presented in what follows.

It is well known that the bond phenomenon is provided by a combination of chemical adhesion of the concrete to the steel reinforcement bars, mechanical resistance from the deformation lugs, and frictional resistance. The frictional resistance which becomes effective at the final stage is somewhat similar to, and can be idealized as, a Mohr-Coulomb failure criteria. Initially resistance is mobilized by chemical adhesion. This is soon destroyed when the bond stress increases resulting in bond slip particularly under cyclic loading. Mechanical bearing of the lugs then plays a major role in resisting the applied bar forces until the concrete between successive lugs begins to fail in sliding shear. Following this stage, bond resistance is provided by friction between the ribs and the surrounding concrete. The frictional resistance is due to the existence of either passive or active confinement.

Figure 3-4 shows the commonly accepted idealization for bond stress-slip relationship. The average bond stress resisting the ultimate load can be expressed in terms of the sum of passive and active confinement pressures:

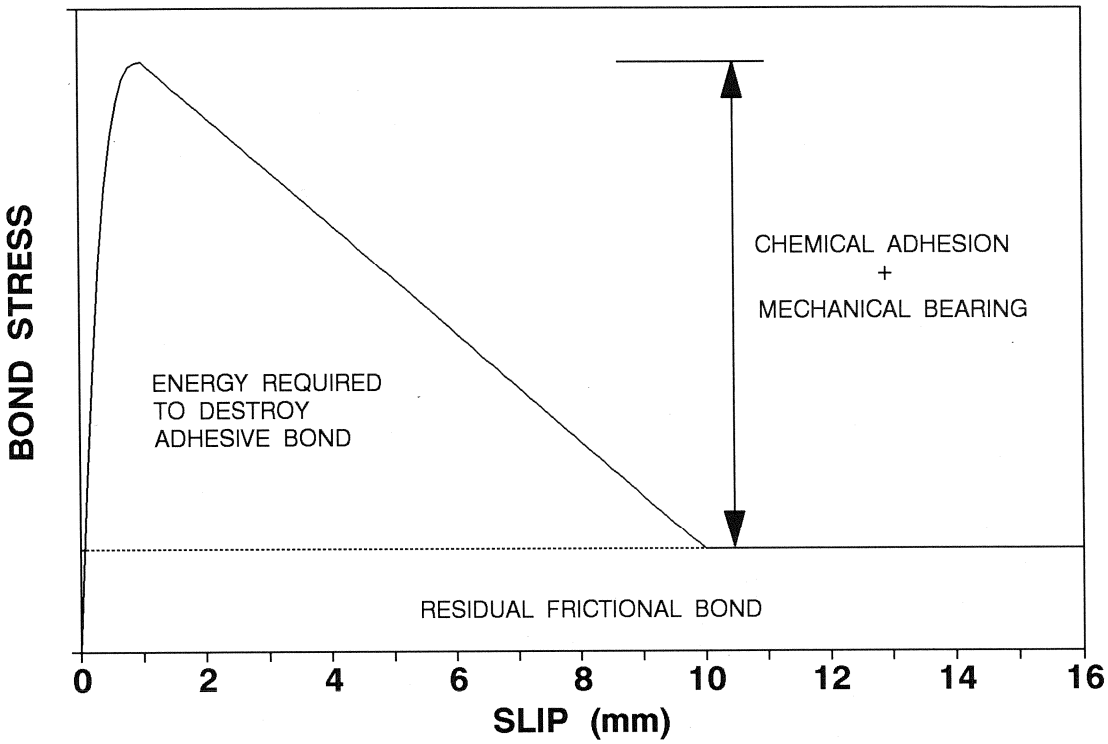

Figure 3-4. Typical bond-slip relationship with confinement.

$$u_b = (f_{fr})_p + (f_{fr})_a \qquad \textbf{(3-11)}$$

where u_b= the total bond strength of an anchored reinforcing bar, $(f_{fr})_p$= frictional resistance due to passive confinement (i.e., residual frictional resistance) and $(f_{fr})_a$=frictional resistance due to active confinement.

In quantifying the parameters in equation (3-11) for seismic design, it is necessary to review other researchers' experimental work. Previous researchers have performed extensive experimental work on bond resistance of concrete under lateral confining pressure. However, much of the data is scattered through a wide range and a careful interpretation for seismic design purposes is required.

Hungspreug *(1981)* studied the effect of confining lateral pressure on maximum bond strength under monotonic and cyclic loading. Maximum bond force was linearly increased with transverse confining pressure up to about 2.8 MPa but dropped markedly at the pressure above 2.8 MPa caused by longitudinal tensile stress of concrete due to Poisson's effect. An empirical equation for maximum bond strength in terms of confining pressure was suggested. However, both experimental results and the equation values showed far higher in maximum bond strengths as well as frictional resistances than the other researchers' values cited in this section.

Eligehausen, Popov and Bertero *(1983)* systematically performed bond resistance tests for various parameters influencing bond stress-slip relationship under monotonic and cyclic loading. Frictional bond resistance was not influenced greatly by different bar diameters, lug spacing or rib area. It was also found that frictional bond resistance during cycling was dependent upon the value of the peak slip and the number of cycles. Frictional and maximum bond resistance were increased by transverse confining pressure. For example, the maximum bond resistance was increased by about 25% for a pressure increase of 13.5 MPa. However, the ratio between the added bond resistance and confining pressure decreased significantly with increasing pressure. Experimental results confirm the widely accepted assumption on proportionality between bond resistance and $\sqrt{f'_c}$.

Malvar *(1992)* studied the effect of confining pressure on bond strength by a series of monotonic loading tests. Bond was completely lost in a very early stage without confinement. The maximum bond stress was increased by up to 200% by increasing the confinement pressure from 3.4 to 31 MPa but the effect of confinement in bond behavior became less for the higher confining stresses.

According to the report of ACI Committee 408 *(1991 and 1992)*, the straight anchorage terminating in external beam-column joints subjected to large load reversals may be given by

$$l_d = \frac{f_y d_b}{2.08\sqrt{f'_c(MPa)}} \quad (mm) \qquad \textbf{(3-12)}$$

where l_d=development (embedment) length of the bar and d_b=bar diameter. The residual (passive) bond strength back-calculated from equation (3-12) is

$$u_o = 0.52\sqrt{f'_c} \quad (MPa) \qquad \textbf{(3-13)}$$

where u_o=residual (passive) bond stress. The Committee suggested that a damage threshold of the bond strength for design consideration at large slip is 2.8 MPa.

Due to the nature of the beam-column joint where a reasonable confinement can be expected, the bond strength at the stage of strain hardening caused by earthquake motion can be represented assuming that a Mohr-Coulomb failure criteria applies, that is,

$$u_b = u_o + \mu f_{pc} \qquad \textbf{(3-14)}$$

where u_b= bond strength at ultimate stage, u_o=residual (passive) frictional resistance, μ = frictional coefficient, and f_{pc} = externally applied normal pressure/prestress. Using the value of residual bond strength recommended by ACI 408 and estimated value of active frictional coefficient from the work of Eligehausen, Popov and Bertero *(1983)*, the parameters in equation (3-14) are $u_o = 0.52\sqrt{f'_c}$ **(MPa)** of equation (3-13) and $\mu = 0.25$. The estimated values of residual (passive) and active frictional bond strengths based on those researchers' experimental results (by Eligehausen, et al. and Malvar) are compared with equation (3-14) in figure 3-5. The

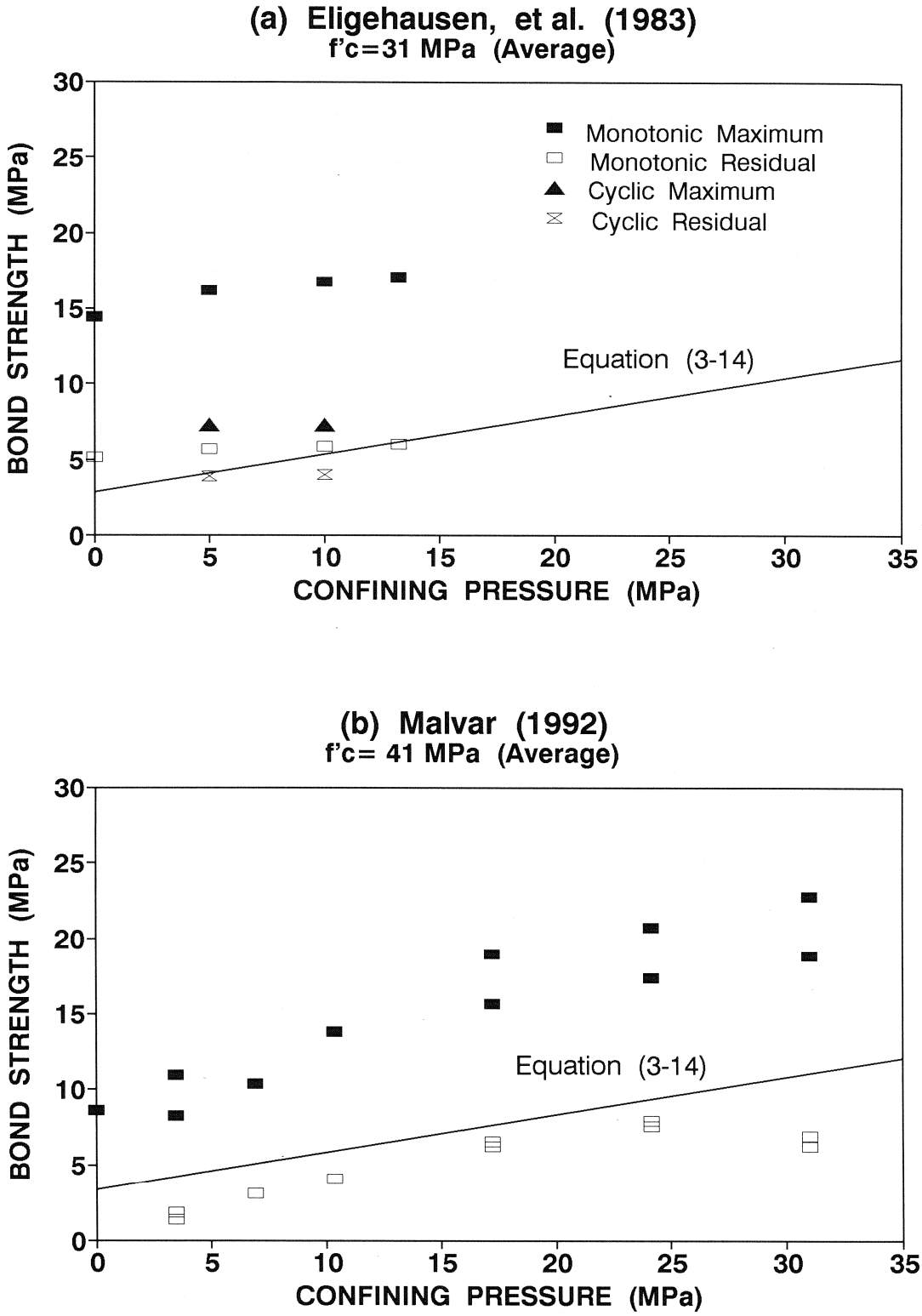

Figure 3-5. Experimental results of bond strength with confinement.

dependable pull-out bar stress f_b of a deformed bar is therefore computed from:

$$f_b = (4u_o + 2.55\mu f_{pc})\frac{l_{em}}{d_b} \qquad \textbf{(3-15)}$$

where l_{em}= provided embedment length of the bar.

Using the aforementioned parameters for u_o and μ in equation (3-15) gives a design relationship:

$$f_b = \left(2.08\sqrt{f_c'} + 0.64 f_{pc}\right)\left(\frac{l_{em}}{d_b}\right) \geq 1.25 f_y \quad (MPa) \qquad \textbf{(3-16)}$$

The dependable pull-out capacity is thus provided by choosing appropriate values of f_{pc} and l_{em}.

3.8 Summary of the Redesign Processes

The *capacity analysis and redesign* procedure is summarized and compared to the capacity design procedure in the next page. Both procedures are based on the assumed plastic column - elastic beam mechanism.

CAPACITY ANALYSIS AND REDESIGN	**CAPACITY DESIGN PROCEDURE**
Step 1: Column Flexural Strength	
R.1 *The flexural capacity of the existing columns is assessed at overstrength. This then forms the basis of the capacity redesign process.*	**D.1** Columns are designed for code-specified gravity and static lateral loads. Column plastic hinges are generally located at the cap beam and foundation faces and adequately detailed for ductility.
Step 2: Column Transverse Reinforcement	
R.2.1 *If shear strength of columns outside plastic hinge zones is not sufficient, additional shear reinforcement should be provided by a concrete jacket.*	**D.2.1** Shear design of columns outside plastic hinge zones is achieved by providing shear strength through the entire column corresponding to the flexural overstrength at the plastic hinges of the column.
R.2.2 *If $P_e < 0.1 f_c' A_g$, confinement is not usually a problem even in the plastic hinge zones. In that case, shear strength and bar stability only need be checked.*	**D.2.2** For the plastic hinge zones, proper confinement, shear strength and bar stability (anti-buckling) should be considered when designing column transverse reinforcement.
Step 3: Cap Beam Flexural Strength	
R.3 *The existing cap beam is considered strong enough to sustain the gravity load induced moments. Thus the required flexural strength based on column overstrength moments is achieved by the provision of a partially prestressed concrete jacket.*	**D.3** The flexural strength of cap beam required for the elastic behavior through the seismic response is calculated based on column overstrength moments and the gravity load applied directly to the cap beam.
Step 4: Foundation Strength	
R.4 *The strength of the existing foundation is enhanced by providing a new composite foundation beam to resist the overstrength moment and shear driven from the regional columns.*	**D.4** Flexural and shear strength of the foundation is calculated based on column overstrength moment and the gravity load applied through the columns.
Step 5: Cap Beam And Cap Beam-Column Joint Shear Strength	
R.5 *The prestress applied through the entire length of the cap beam can significantly reduce or eliminate the diagonal tensile principal stress that develop due to joint shear force. No additional transverse reinforcement is usually needed. In case that the diagonal principal tensile stress exceeds the concrete tensile strength, diagonal cracks are expected to result. In such cases the joint is designed as a conventional reinforced concrete joint with the axial prestress in the beam taken as the axial load in the design shear strength equations.*	**D.5.1** From the most adverse combination of internal forces at the beam-column joint the maximum design shear force in the cap beam is calculated. Transverse shear reinforcement is provided over the entire length of cap beam. **D.5.2** The beam-column joint is usually considered as a poor source of energy dissipation and thus needs to be detailed to resist the high shear input from the beam and column actions. In this step the designer should attempt to keep the joint elastic by reducing if not eliminating any inelastic deformation due to the joint shear forces and bond deterioration.
Step 6: Anchorage and Lap Splice Zone	
R.6.1 *Existing bars anchored with insufficient development length may have their pull-out capacity enhanced by a combination of: (a) providing a joint fillet and thus increasing the anchorage length, (b) post-tensioning the cap beam to enhance frictional resistance of anchored bars.*	**D.6.1** Column steel is normally anchored in deep pile caps and pier cap beams.
R.6.2 *Lap splice zone in column is clamped with well-detailed reinforcing bars and may be finally eliminated by the casting a new composite foundation beam.*	**D.6.2** Lap splice zone should be moved outside the potential plastic hinge region.

SECTION 4
EXPERIMENTAL STUDY OF A RETROFITTED 1/3 SCALE MODEL PIER

4.1 Retrofit Construction

This section describes the construction as per the retrofit concept introduced in Section 3 and presents the experimental results of the quasi-static cyclic load testing on the retrofitted 1/3 scale model pier bent.

4.1.1 Material Properties

Measured material properties for repairing and retrofitting the damaged model pier are presented in tables 4-1 and 4-2. A series of the split cylinder and the modulus of three point beam rupture tests were performed to measure the uniaxial tensile strength of a proprietary high strength concrete material for cap beam-column joint retrofit by prestressing. These tests were performed in accordance with ASTM C78 *(1984)* and C496 *(1990)*, respectively.

The split cylinder test was performed on three 76 mm x 152 mm cylindrical specimens with the average maximum force of $P = 67\ kN$. The splitting tensile strength is calculated by the

Table 4-1. Measured properties of concrete specimens for retrofit.

Test Unit	Cap Beam[1]	Foundation Pad[2]	Foundation Beam[2]
f'_c[3] at 28 Day (MPa)	61	39	30
Days at Test	92	--	--
f'_c[3] at Test (MPa)	61	--	--
f'_t[4] at Test (MPa)	13	--	--

[1]Sulfate and chloride-resistant one cement-based repair mortar with high strength.
[2]Ordinary Portland cement concrete.
[3]Average compression strength of three 76 mm x 152 mm cylinders.
[4]Average modulus of rupture of two specimens.

Table 4-2. Measured properties of reinforcement for retrofit.

Test Unit	#3 Rebar	D4 Deformed Wire[1]	ϕ-12.7 mm Threadbar[2]
ASTM Grade	60		B7
Yield Strength, f_y (MPa)	474	455	755
Yield Strain, ε_y	0.0024	0.0023	0.0038
Ultimate Strength, f_u (MPa)	750	503	905
Strain at Hardening, ε_{sh}	0.0109	0.0261	0.007

[1] d_b= 5.72 mm and A_b= 25.8 mm^2.
[2] Used for prestressing the cap beam (effective diameter: 10.8 mm).

equation, $T = 2P/\pi Ld$. The calculated split tensile strength in relation to the compressive cylinder strength f_c' is $T = 0.47\sqrt{f_c'}$ (MPa). The modulus of rupture test was performed on two 78 x 75 x 224 mm (average) specimens with measured average maximum force of $P = 26\,kN$. The modulus of rupture is calculated by the equation, $R = PL/bd^2$. The calculated modulus of rupture in relation to the compressive cylinder strength is $R = 1.7\sqrt{f'_c}$ (MPa) which is considerably higher than the specified values in ACI 318 *(1995)*.

Monotonic tensile tests on 12.7 mm diameter threadbar specimens used for prestressing the cap beam were performed with strain rate of 0.0005/s, and the results are presented in table 4-2. The yield stress was taken as equal to the stress producing an extension of 0.7% as usual for those steel bars for which yield stresses are not well defined *(Nilson, 1987)*.

4.1.2 Retrofit Construction Procedure

The retrofit construction on the damaged model pier was performed as per the retrofit plan shown in figure 4-1 prepared in accordance with the *capacity analysis and redesign* procedure described in Section 3. The photographs of construction practice for retrofitting of lap splice zones and cap beam-column joints are presented in figure 4-2.

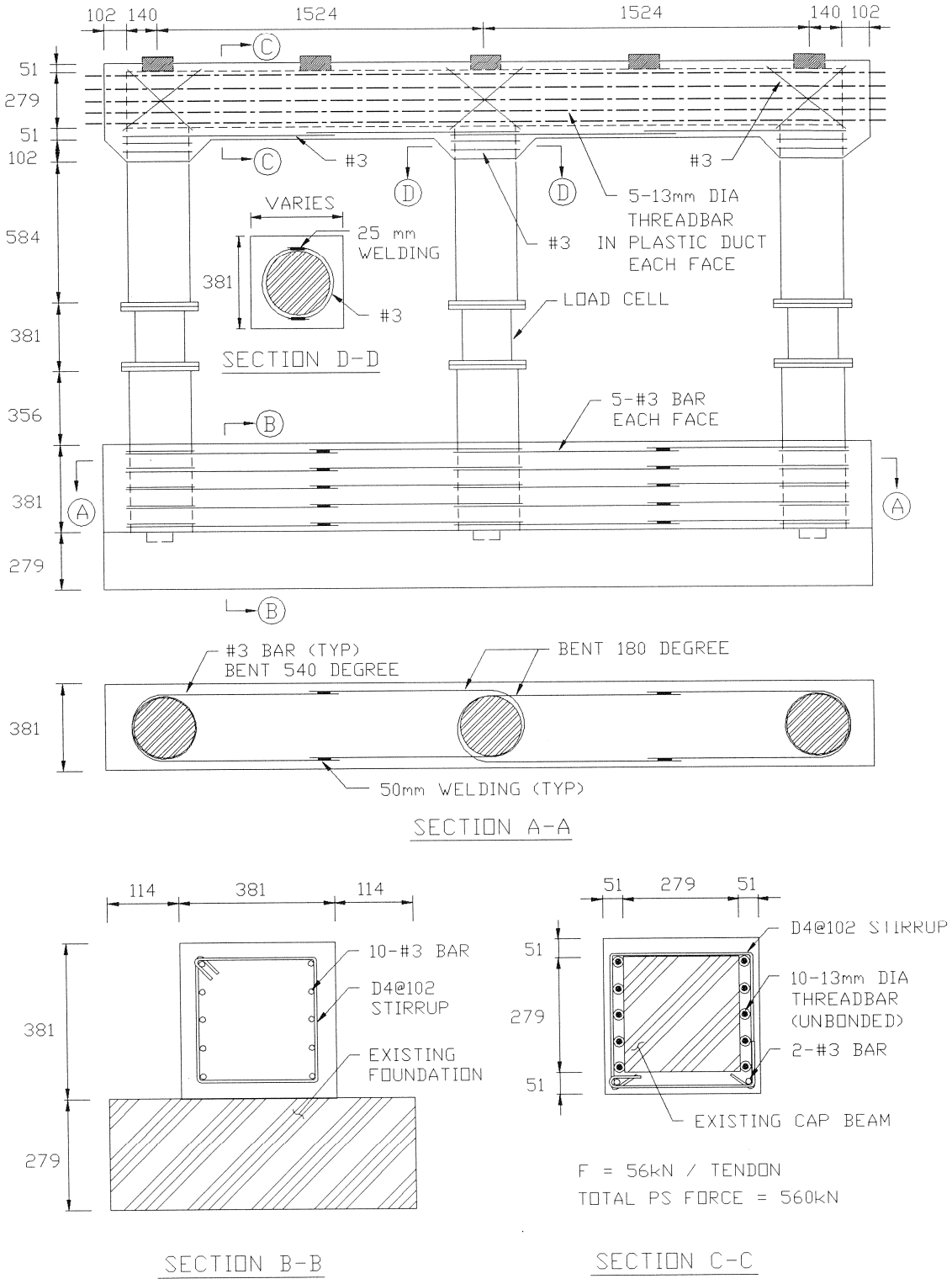

Figure 4-1. Retrofit construction plan for model pier.

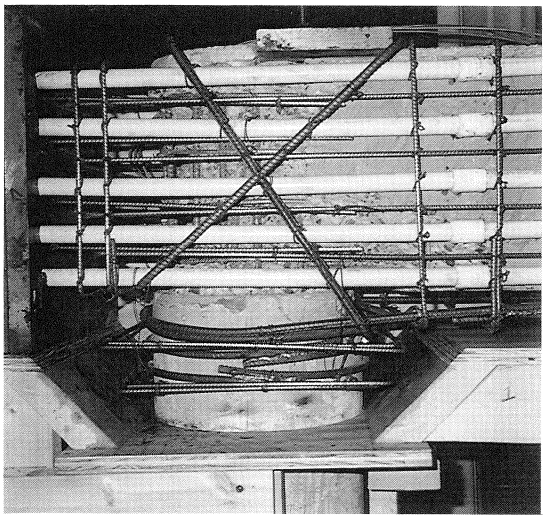

(a) Cap beam at exterior column

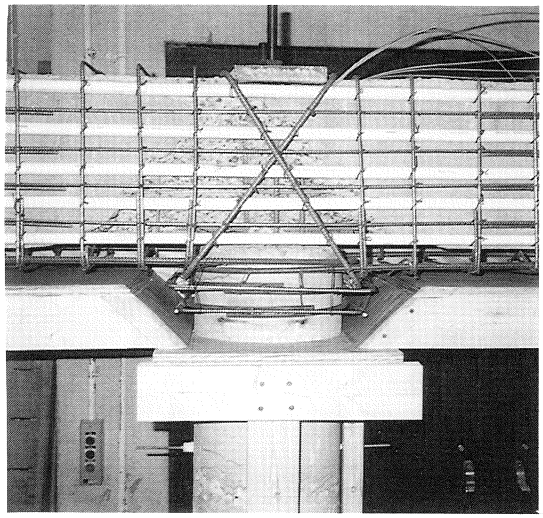

(b) Cap beam at middle column

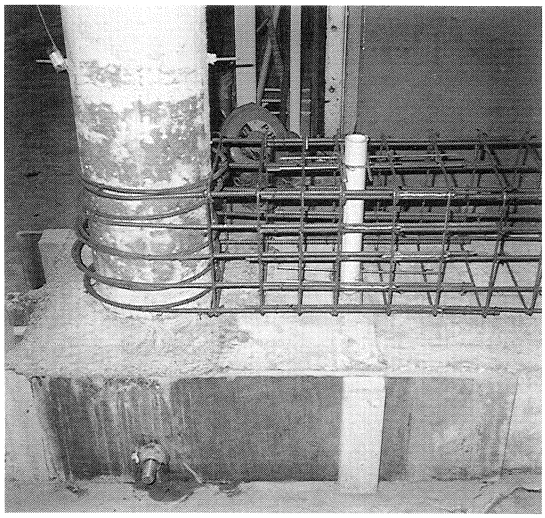

(c) Foundation at exterior column

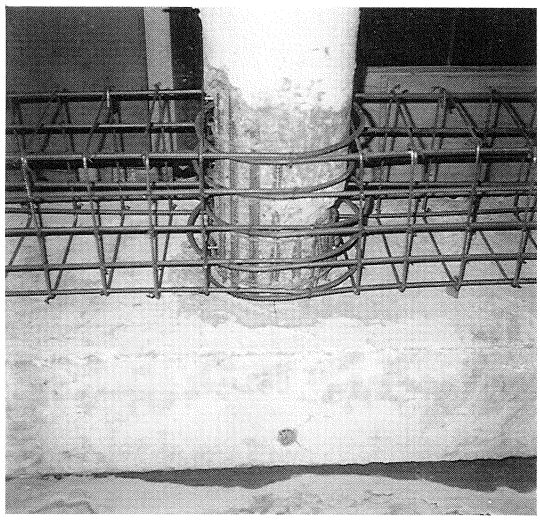

(d) Foundation at middle column

Figure 4-2. Retrofit of cap beam and foundation for model pier.

Foundation

1. All the severely damaged concrete was chipped away and new laboratory-mixed concrete was placed in the chipped-out part.
2. After the damaged foundation was repaired, five evenly-spaced layers of #3 confining reinforcement were bent around the columns and spliced midway along the foundation beam by lap welding. Thus, in addition to column confinement these bars also provided flexural strengthening of the existing damaged foundation.
3. The new additional foundation beam included D4 stirrups at 102 mm centers for the model thus providing a strong measure of shear resistance.
4. Ready-mixed concrete was poured into plywood formwork.

Cap Beam

1. All severely damaged and cracked concrete was jack-hammered out.
2. In a fashion similar to (2) above, one layer of #3 confining/flexural reinforcement was placed at the soffit of the cap beam.
3. D4 stirrups at 102 mm centers were placed to hold the plastic prestressing ducts in position and to help any control differential strains between old and new concrete.
4. Five evenly-spaced layers of ϕ-18 mm plastic ducts were anchored along each side of existing cap beam.
5. A 381 x 381 x 25 mm steel plate for anchoring the prestressing bars was placed at each end of the cap beam.
6. A proprietary-high strength concrete was mixed in the laboratory, and placed and vibrated within plywood formwork. This highly fluid sulphate and chloride resistant concrete was able to penetrate the cracks in the existing concrete.
7. The cap beam was prestressed after the new concrete jacket cured. A 267 kN capacity hydraulic jack with a center hole was used to apply 56 kN prestressing force to each of the ten 12.7 mm diameter threadbar tendons for the cap beam in the longitudinal direction. Thus the total force of 560 kN resulted in a 3.86 MPa prestress, with each tendon being stressed to 70% of its ultimate stress.

4.2 Test Setup

After the retrofitted model pier was put in the place, it was anchored down to the 457 mm thick strong-floor with two 25 mm diameter prestressing threadbars. A prestressing force of 236 kN was applied to each of these anchors. The same test setup was used as for the pre-retrofit study, but several changes were made as follows and are shown in figure 4-3. A 1100 kN capacity actuator was used instead of the previous 1000 kN capacity MTS actuator. To provide an improved vertical load balance, the location for the top actuator and extension beam previously attached to the end of W14x257 load transfer beam were switched. For the same purpose, counter weights were also used consisting of 64 lead bricks weighing 116 N each. These weights were placed on the opposite end of the load transfer beam to ensure the center of mass of that beam was above the center column of the pier specimen.

4.3 Instrumentation

Figure 4-4 presents the instrumentation scheme adopted for the retrofit pier test. This consisted of: (a) 11 sonic transducers (T1 to T11); (b) 18 linear potentiometers (PN1 to PN6, PC1 to PC6, and PS1 to PS6 for north exterior, middle, and south exterior columns, respectively); (c) three multi-channel load cells for axial, shear and moment at each column; and (d) 18 strain gauges (six for each column) attached to the column longitudinal reinforcement were used for the measurement of deformations and forces on the retrofitted model pier. Sonic transducers T9 and T10 were used to detect any possible rocking motion of the strong pier model.

When compared with the previous instrumentation plan for the pre-retrofitted model pier in figure 2-10, it will be noted that the number of linear potentiometers and sonic transducers along a column is reduced. This is because certain threadbars used for mounting potentiometers were embedded in the newly poured retrofit concrete. Also, some strain gauges were found inactive as a result of the previous testing and could not be used in the retrofit experiment.

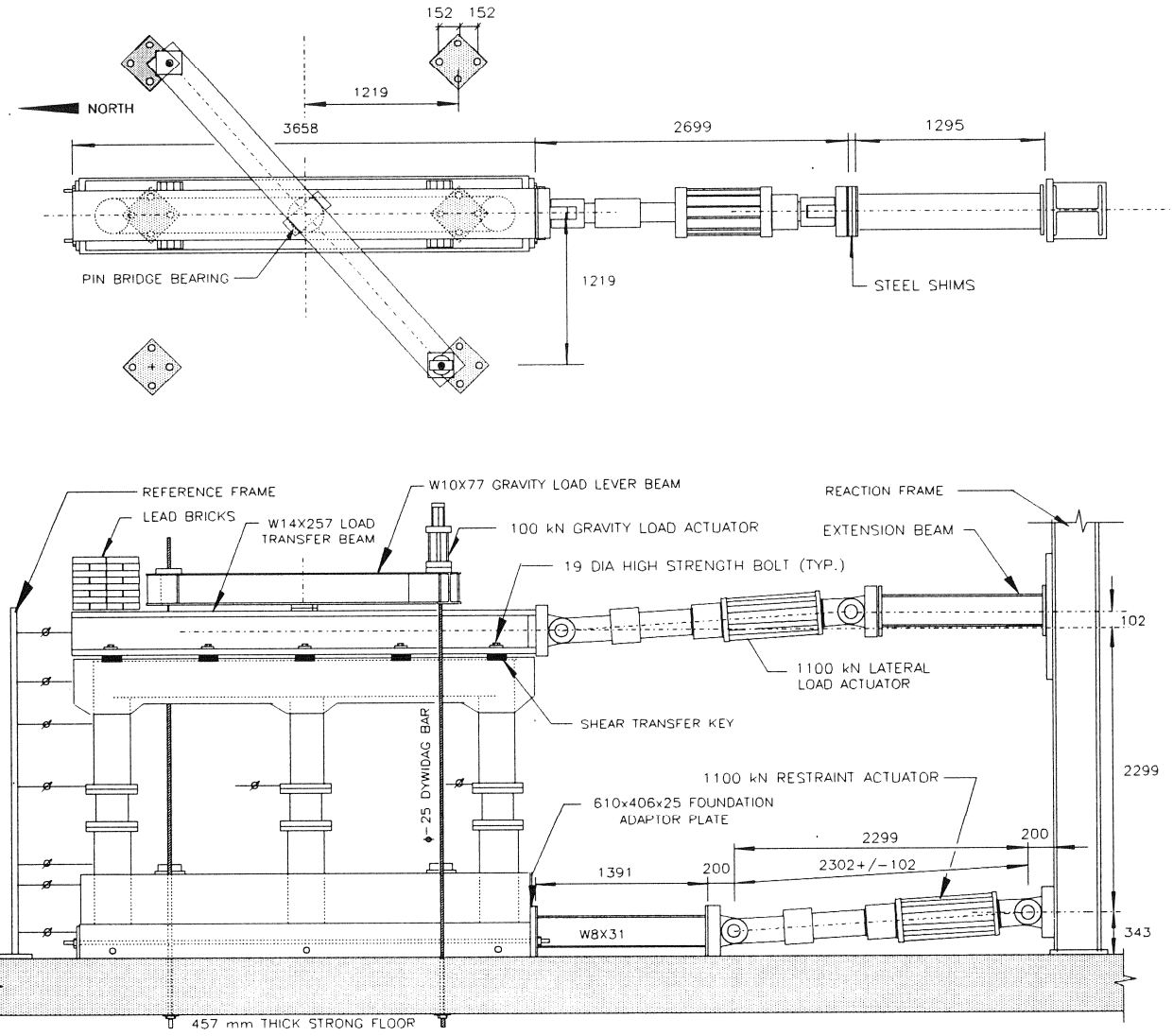

Figure 4-3. Test rig for post-retrofitted model pier.
(All dimensions in mm).

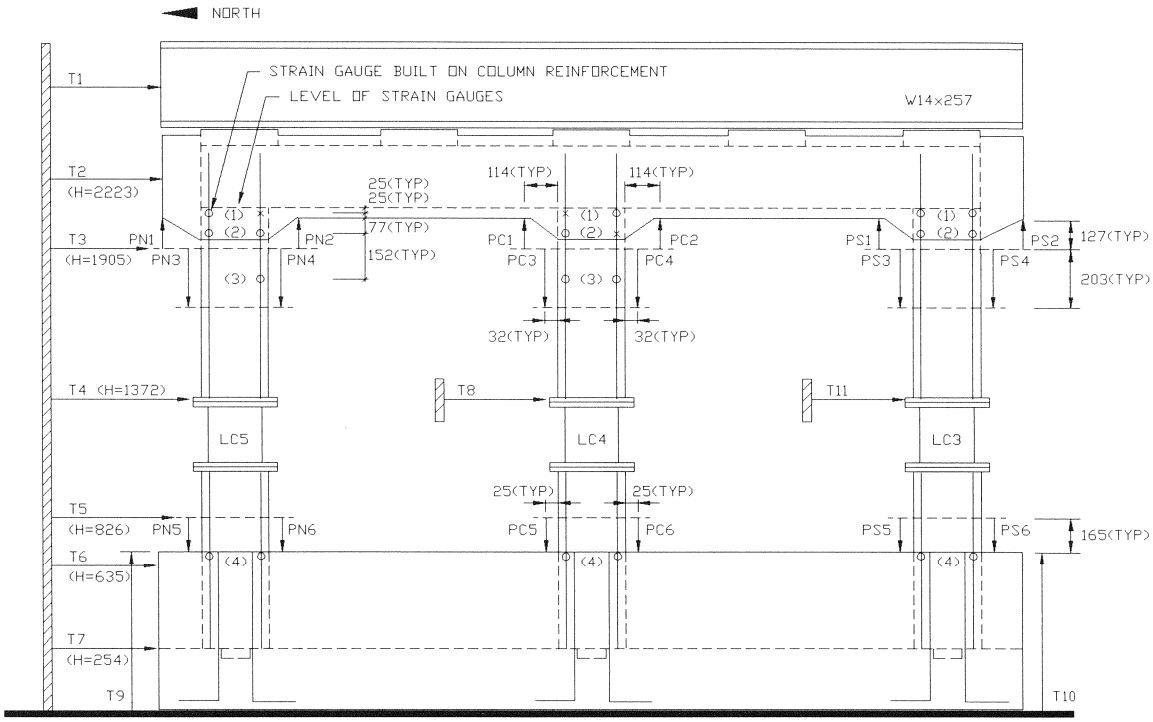

Figure 4-4. Instrumentation for post-retrofitted model pier.

4.4 Experimental Procedures

The experimental procedures adopted for testing the retrofitted specimen were similar to those of the pre-retrofit tests. The same displacement history was adhered to for both tests. Displacement-controlled quasi-static lateral force was applied using the top actuator through the W14x257 load transfer beam to the cap beam in a series of sinusoidal wave forms with a frequency of one cycle per minute (0.0167 Hz). The 100 kN vertical actuator was set at 53 kN to produce the scaled gravity load of 126 kN at the level of pier cap beam and 176 kN at the level of column mid-height including the upper half pier weight. The measured column axial loads through the load cells at the beginning of the test with scaled gravity load were 51 kN, 59 kN, and 66 kN for north exterior, middle, and south exterior columns, respectively. Differences in these initial load cell axial loads are considered to be due to lack-of-fit indeterminacy when fitting the upper and lower halves of the specimen.

The data acquisition rate was 3 Hz (each channel was scanned three times per second) using the Optim Megadac 5533A data acquisition system for data collection. The retrofitted model pier was tested by performing a series of small displacement elastic pretests followed by large displacement tests. Both force-controlled and displacement-controlled pretests were performed to check the loading system and instrumentation. Among the pretests, one cycle of force-controlled test with maximum of ± 67 kN lateral load which is 23% of the nominal ultimate strength of column sway mechanism produced an initial stiffness of 24 kN/mm which is 14% of gross section based stiffness (175 kN/mm). This low initial stiffness is due to pre-cracked column section during the previous test on the model pier before retrofitting.

The large displacement tests consisted of two completely reversed cycles of lateral loading at displacement of ± 21 mm, ± 42 mm, and ± 63 mm with the exception of ± 21 mm displacement amplitude which was applied for three complete cycles. The corresponding drift amplitudes were ± 1.6%, ± 3.1%, and ± 4.7%. It should be emphasized that these displacement amplitudes were the same as the original pre-retrofit test history with nominal specimen drifts of ± 1%, ±2%, and ± 3%, respectively. It should also be noted that the column drift amplitude

for the post-retrofit condition is based on a clear column height of l_c= 1321 mm, where the distance between the center of the cap beam and foundation beams (2057 mm) is taken in the definition of nominal drift prior to retrofitting.

Figure 4-5 presents the displacement and corresponding force history applied to the test specimen. The difference between the applied lateral displacements at the top actuator and drift (sonic transducers T2 - T6) is due to slippage of W14x257 load transfer beam, bolted to the shear connectors on top of the cap beam, traveling within the clearance gap between bolts and bolt holes.

4.5 Experimental Results

4.5.1 Visual Observations

During the initial series of elastic pretests, no visible cracking or damage was evident. However, during the 1.6% drift amplitude test segment, cracking commenced. Radial flexural cracks occurred around the circumference of the column ends adjacent to the top surface of the new foundation beam, as well as the soffit of the cap beam fillet. A diagonal flexure-shear crack also opened in the upper part of the middle column.

During the 3.1% drift test segment, corner-to-corner diagonal cracks developed in both the upper and lower parts of the columns as shown in the photographs (a) and (b) of figure 4-6. There was further development of cracks at cap beam fillets of all columns.

During the final two cycles of loading at the 4.7% drift amplitude, the above-mentioned diagonal shear cracks widened considerably and precipitated the failure of the specimen as a whole. Photographs (c), (d) and (h) in figure 4-6 show the extent of damage at the end of testing. It will be noted that the upper part of the north exterior column, the upper part of the middle column, and the lower part of the south exterior column were most severely damaged, with a large portion of crushed concrete, which followed from fracture of several transverse hoops. The

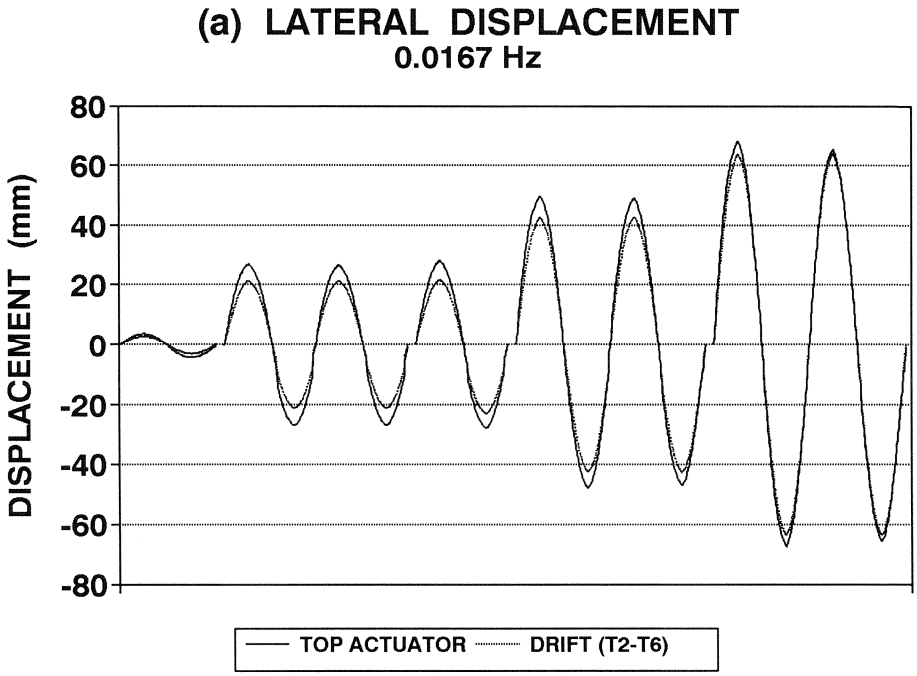

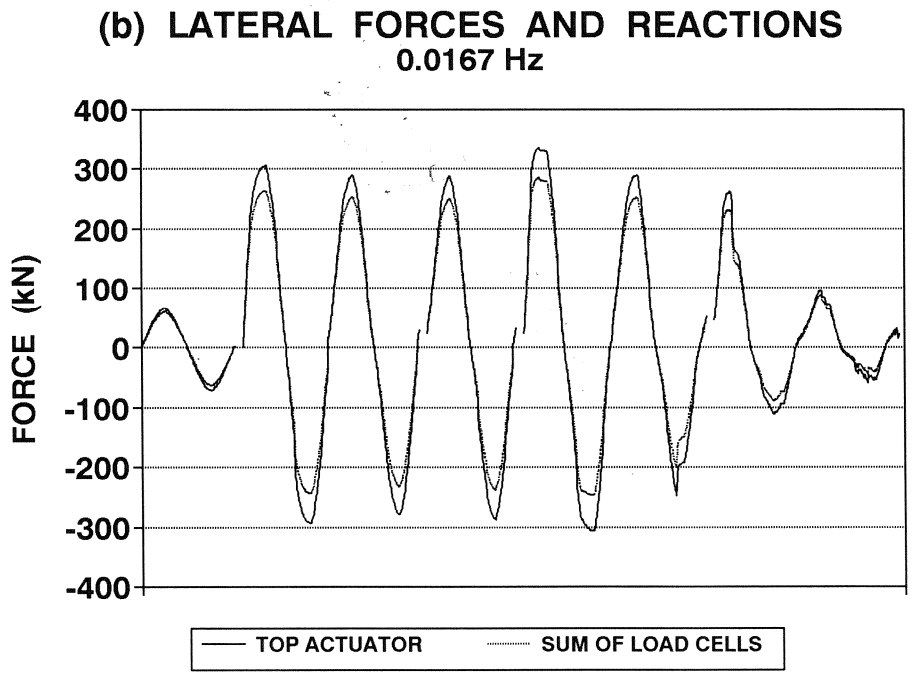

Figure 4-5. Applied displacement and force history for retrofitted model pier.

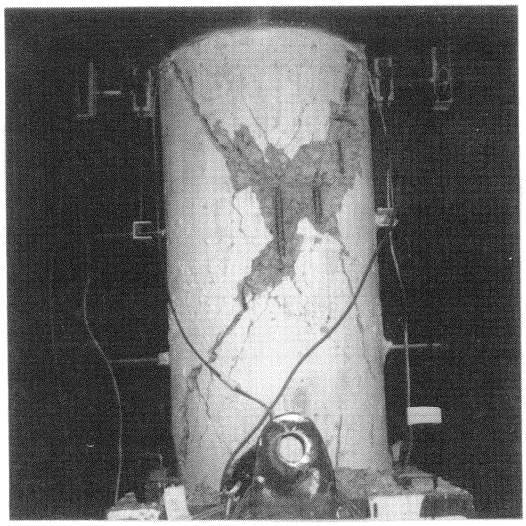

(a) Middle upper column (3.1%)

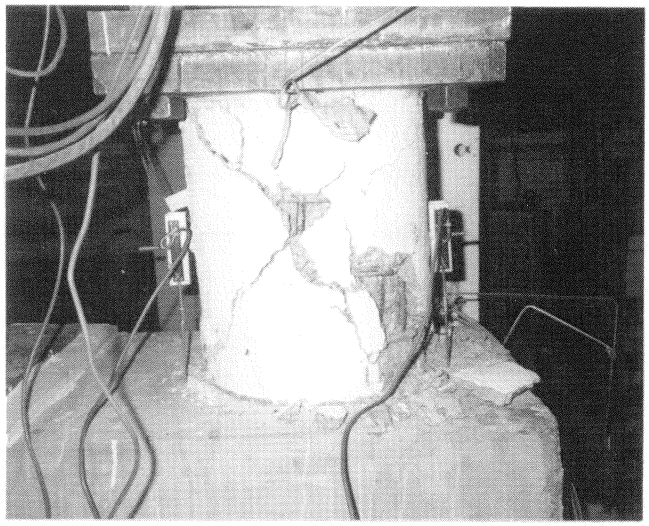

(b) South lower column (3.1%)

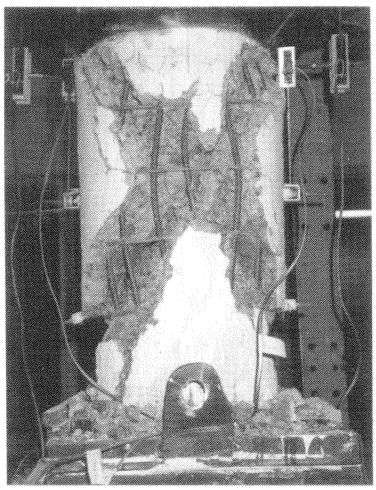

(c) North upper column (4.7%)

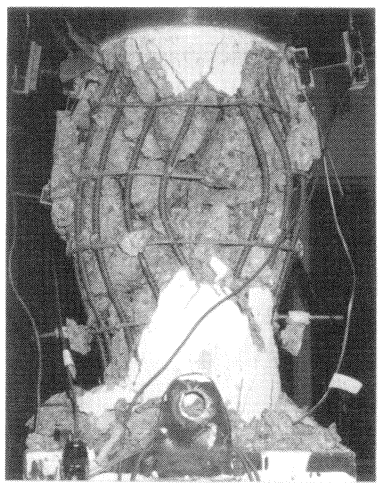

(d) Middle upper column (4.7%)

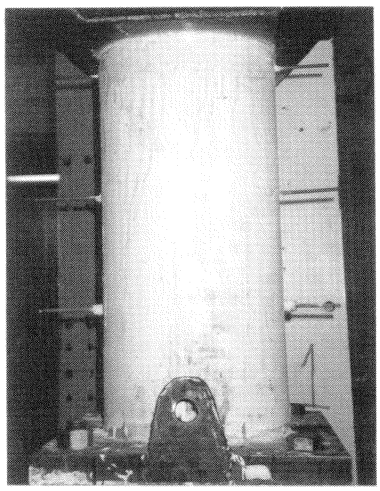

(e) South upper column (4.7%)

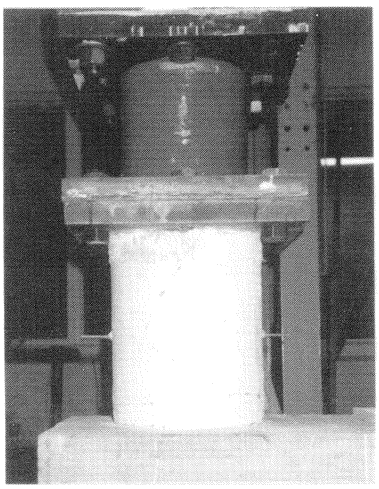

(f) North lower column (4.7%)

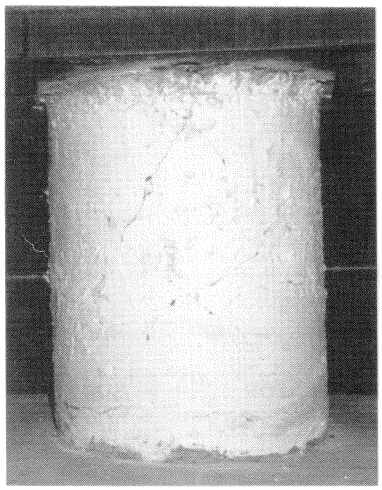

(g) Middle lower column (4.7%)

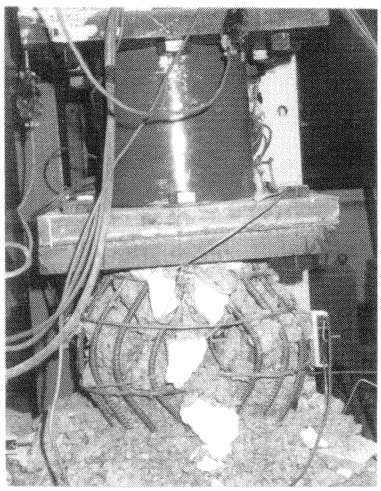

(h) South lower column (4.7%)

Figure 4-6. Damage on the retrofitted model pier resulting from cyclic loading test.

other halves of the damaged columns sustained only a moderate amount of cracking as shown in photographs (e), (f) and (g) of figure 4-6.

4.5.2 Force-Displacement Response

Figure 4-7 presents the force-displacement response of the retrofitted model bridge pier under the same reverse cyclic loading path that was used previously prior to retrofit. It should be noted that this force-displacement response has been corrected for accidental eccentricity noted previously in Section 4.4. This accidental eccentricity is ascribed to the differences in the column axial forces which imply that the centroid of the axial forces in the three columns has shifted south by 135 mm. Also plotted on figure 4-7 is the envelope of the nominal ultimate strength based on a column sidesway mechanism by the pier bent, and it can be seen that the actual strength exceeded the nominal strength by some 10% at a column drift angle of 3%. This level of overstrength is normal for such columns with relatively low levels of axial load and is principally due to strain hardening of the longitudinal reinforcement.

On the second cycle approaching the + 3% drift amplitude, there is a sudden drop in the lateral force resistance. This is due to the first crack that occurred in the south lower column. In spite of this apparent sudden loss of strength of the south column, it appears that it was the interior (middle) column in which the strength loss, due to premature shear failure, first commenced. This can be seen in figure 4-8 which plots the column shear forces measured by the individual load cells against actual drift for each of the three columns. It will be noted that the first apparent drop in strength occurs at - 2.9% and + 2.2% under forward and reverse loading, respectively. These strength drops are relatively gradual compared to the south column.

Figure 4-9 shows the force displacement behavior of each of the half-column portions for the pier bent. The displacement is measured at the inflection point for each of the columns. These inflection points were generally in the neighborhood of the load cell as determined from the column end moments, as shown in figure 4-10.

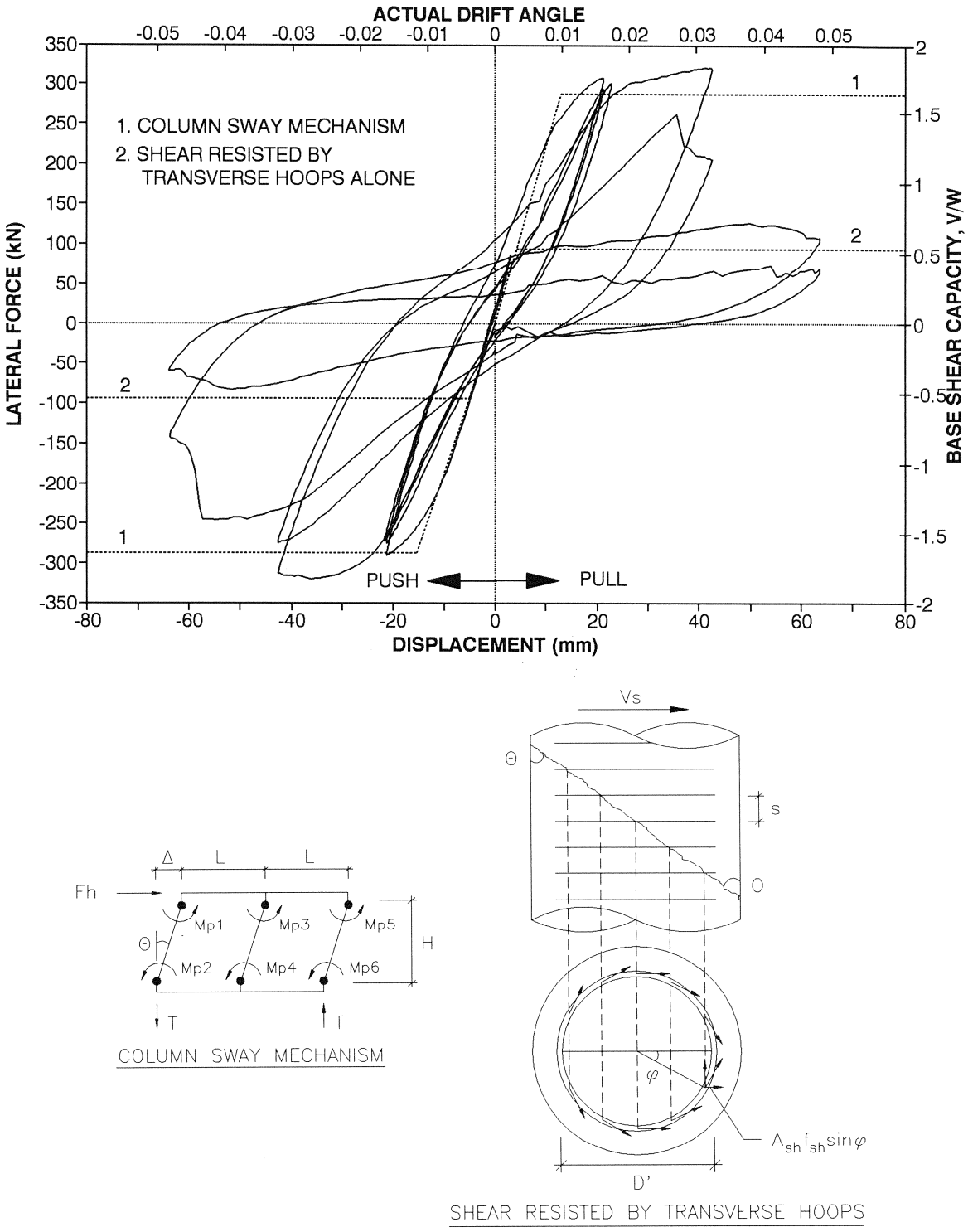

Figure 4-7. Force-displacement relationship of retrofitted model pier.

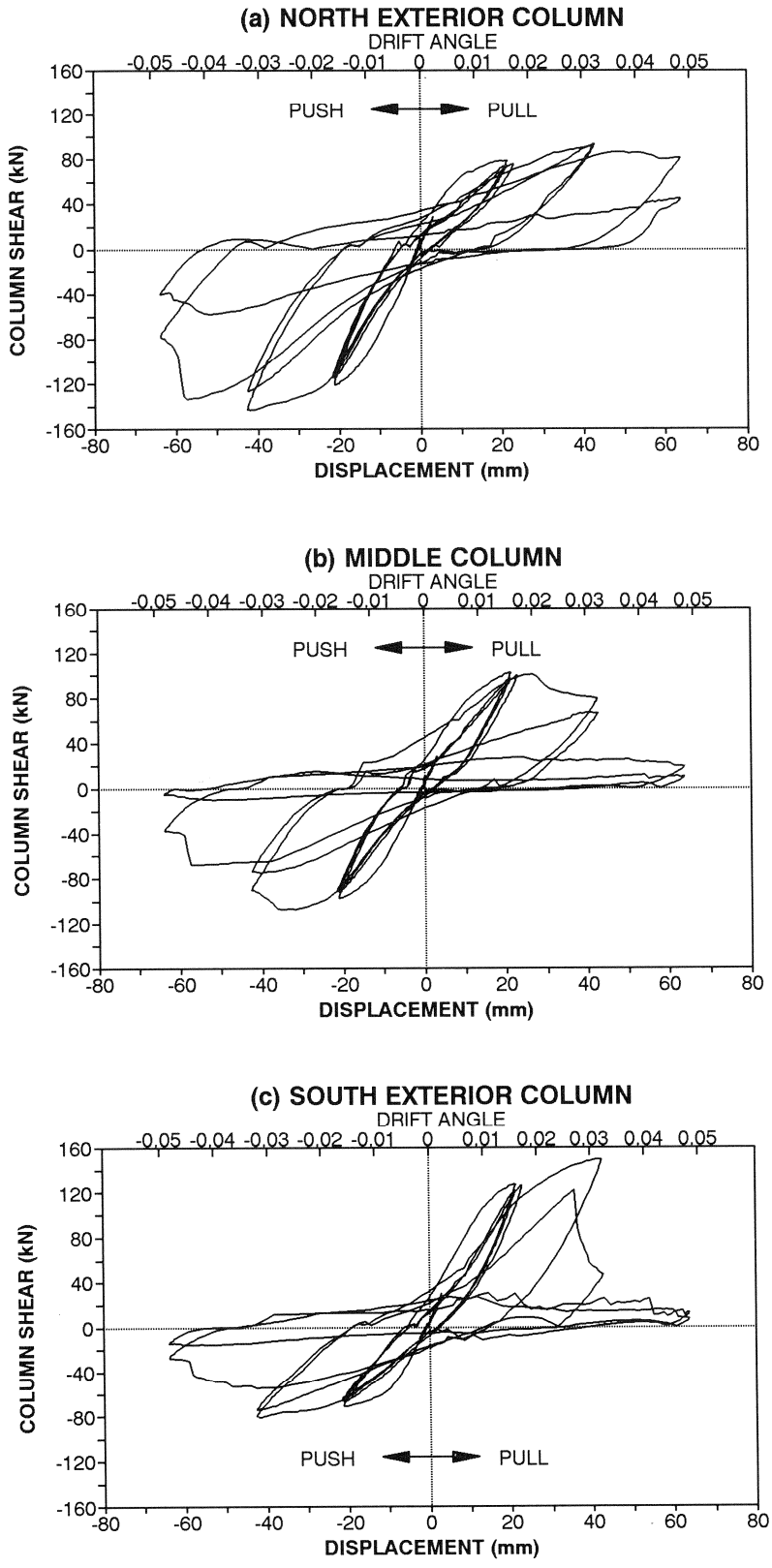

Figure 4-8. Hysteretic behavior of individual columns of retrofitted model pier.

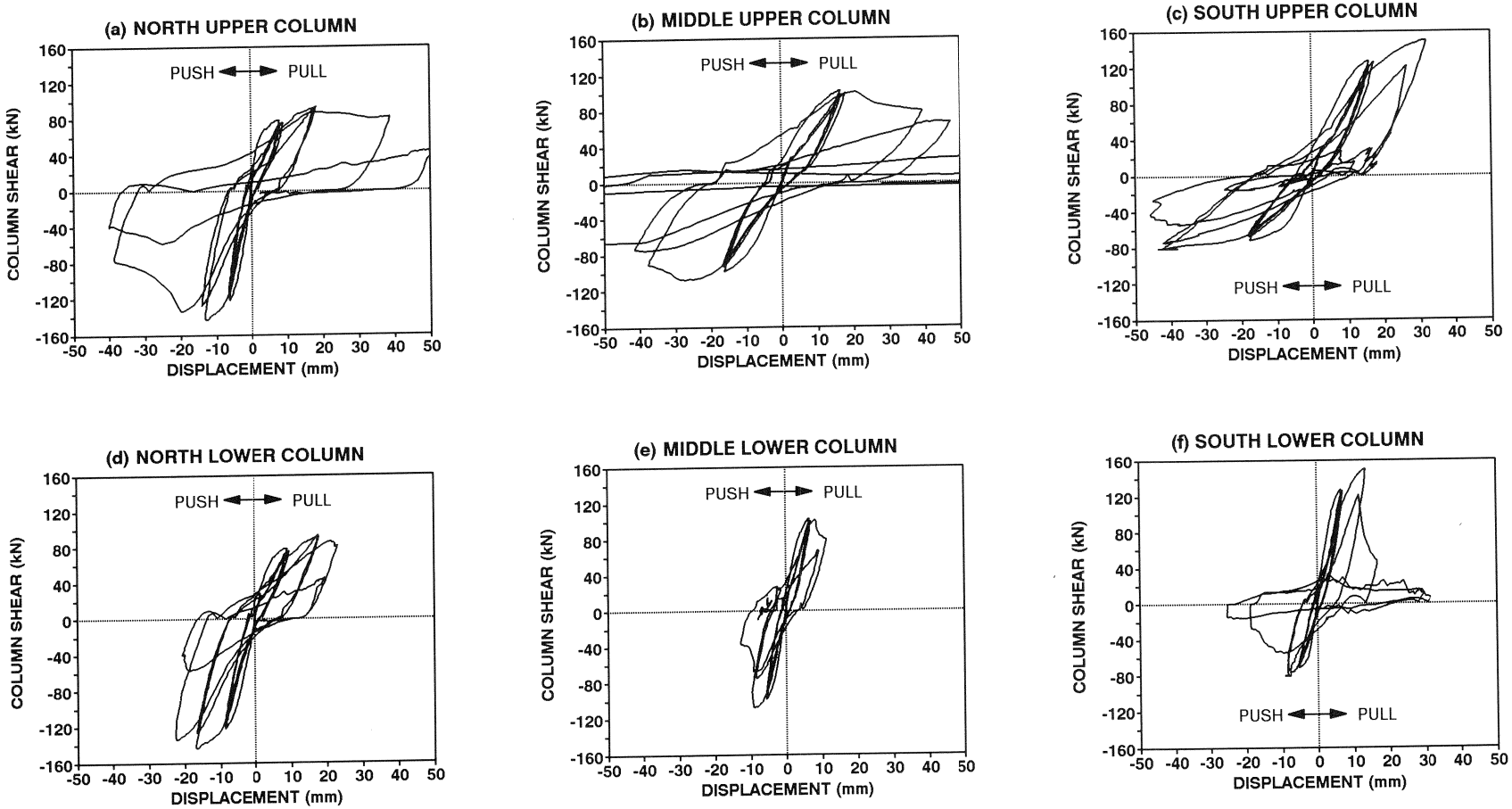

Figure 4-9. Hysteretic performance of column halves of retrofitted model pier.

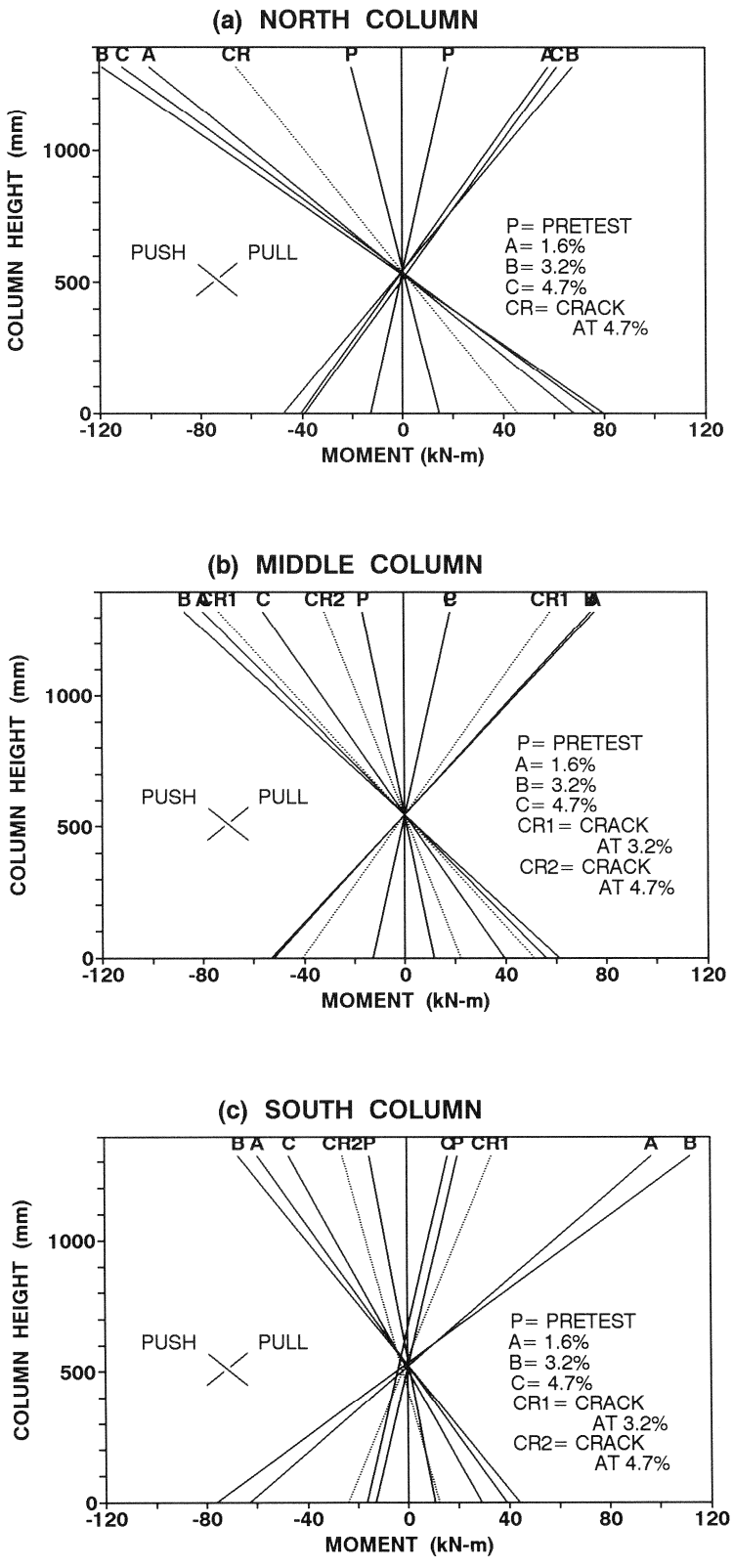

Figure 4-10. Column moment profiles of retrofitted model pier.

Figure 4-7 also plots a lower bound strength capacity based on shear resistance provided by the transverse hoops alone. This is given by the equation *(Ang, et al., 1989)*:

$$V_s = \frac{\pi}{2} A_{sh} f_{sh} \frac{D'}{s} \cot\theta \qquad \textbf{(4-1)}$$

where A_{sh} = section area of a hoop, f_{sh} = tensile stress in a hoop, D' = center-to-center diameter of the transverse hoop steel, θ = angle of diagonal crack measured from the column longitudinal axis, and s = hoop spacing. In equation (4-1) it should be noted that the factor $\pi/2$ accounts for the shape of the circular hoop reinforcement in the shear resistance mechanism. For the computation of V_s used herein, the actual angles of diagonal cracks $\theta = 26°$ measured from the experiment have been applied to equation (4-1). It was assumed that the contribution of concrete in shear resistance was zero at the stage of widely opened cracking as shown in figure 4-6.

4.5.3 Column Curvatures

Figure 4-11 presents the column shear versus curvature relationships for the retrofitted model pier in the neighborhood of the column ends. The figures show that most of the inelasticity was concentrated at the end 150 mm of the columns.

4.5.4 Column Axial Load-Moment Interaction

Figure 4-12 shows schematically the effect of eccentrically located load cells on the column end moments and the curvature distribution along the column height. Thus, column end moments were determined from the load cells by the equations:

$$M_{top} = -M_c + VL_1 \qquad \textbf{(4-2)}$$

$$M_{bot} = M_c + VL_2 \qquad \textbf{(4-3)}$$

where M_c = measured column moment at load cell, M_{top}= column top end moment, M_{bot}= column bottom end moment, V= measured shear force at load cell, L_1= distance between center

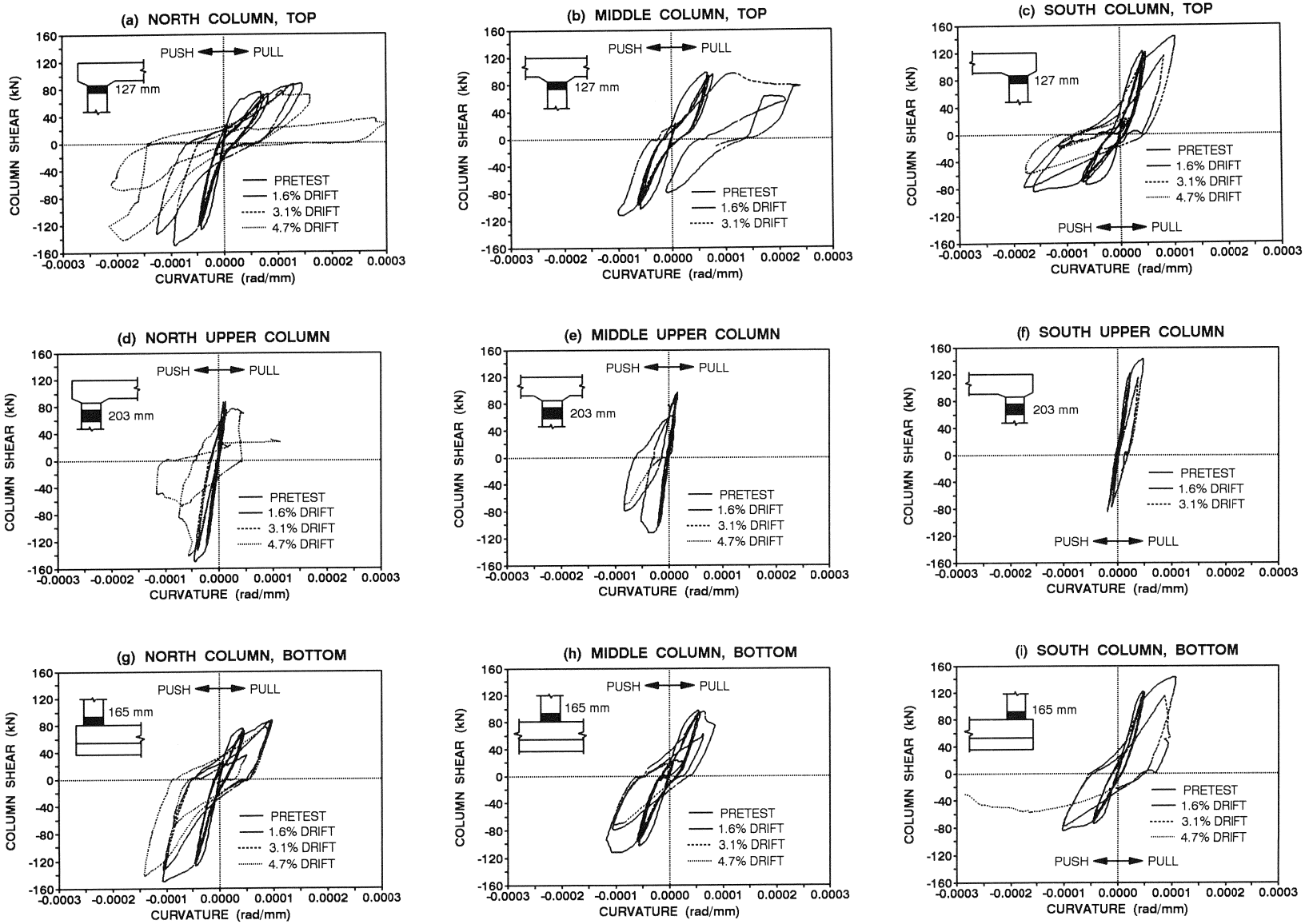

Figure 4-11. Column shear-curvature relationship of retrofitted model pier.

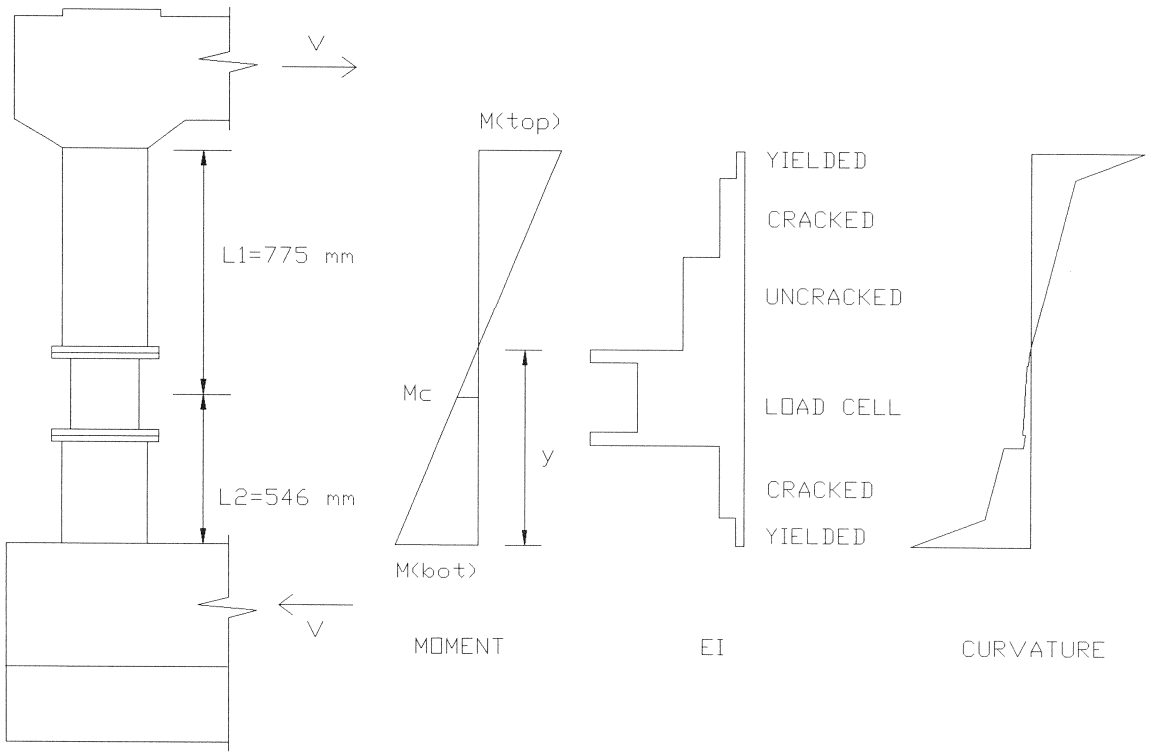

Figure 4-12. Effect of load cells on column moment and curvature.

of load cell and column top end, and L_2= distance between center of load cell and column bottom end. Moment profiles along the column height for various drift amplitudes are presented in figure 4-10.

Figure 4-13 presents the axial load-moment interaction diagrams for each of the column ends of the retrofitted model pier bent. The interaction curves have been computed in accordance with the usual ACI 318 assumptions *(1995)*, that is, the reinforcing steel behaves elasto-plastically and the concrete strain at the extreme compression fiber is 0.003.

These interaction diagrams clearly show the change in axial load in the exterior columns with axial load in the interior column remaining constant throughout the experiment. It is evident from figure 4-13 that the nominal ultimate strength has been exceeded on several occasions, principally due to the strain hardening of the longitudinal reinforcement as well as some extreme confinement effects provided by the concrete surrounding the critical section in the column ends (the cap and foundation beams). This overstrength capacity is particularly pronounced for the exterior columns when the joint is subjected to closing moments. From figure 4-13 it is evident that under closing moments, the nominal ultimate strength is exceeded by approximately 40% at the cap beam level.

4.5.5 Strains in Column Reinforcement

Figure 4-14 presents a series of extreme column reinforcement strains at various locations along the column height. The position of each gauge level is described in figures 4-4 and 4-14 with a level number in a parenthesis. It is noted that some strain gauges were inactive due to the excessive elongation in the previous testing on the pre-retrofitted model pier. The strain plots are limited to amplitude of ± 0.005 due to the way in which the strain gauges were calibrated in the data acquisition system. The yield strain of ± 0.00247 for Grade 60 #3 steel was determined experimentally.

In all cases during the elastic loading cycles, steel strain did not exceed about 40% of the

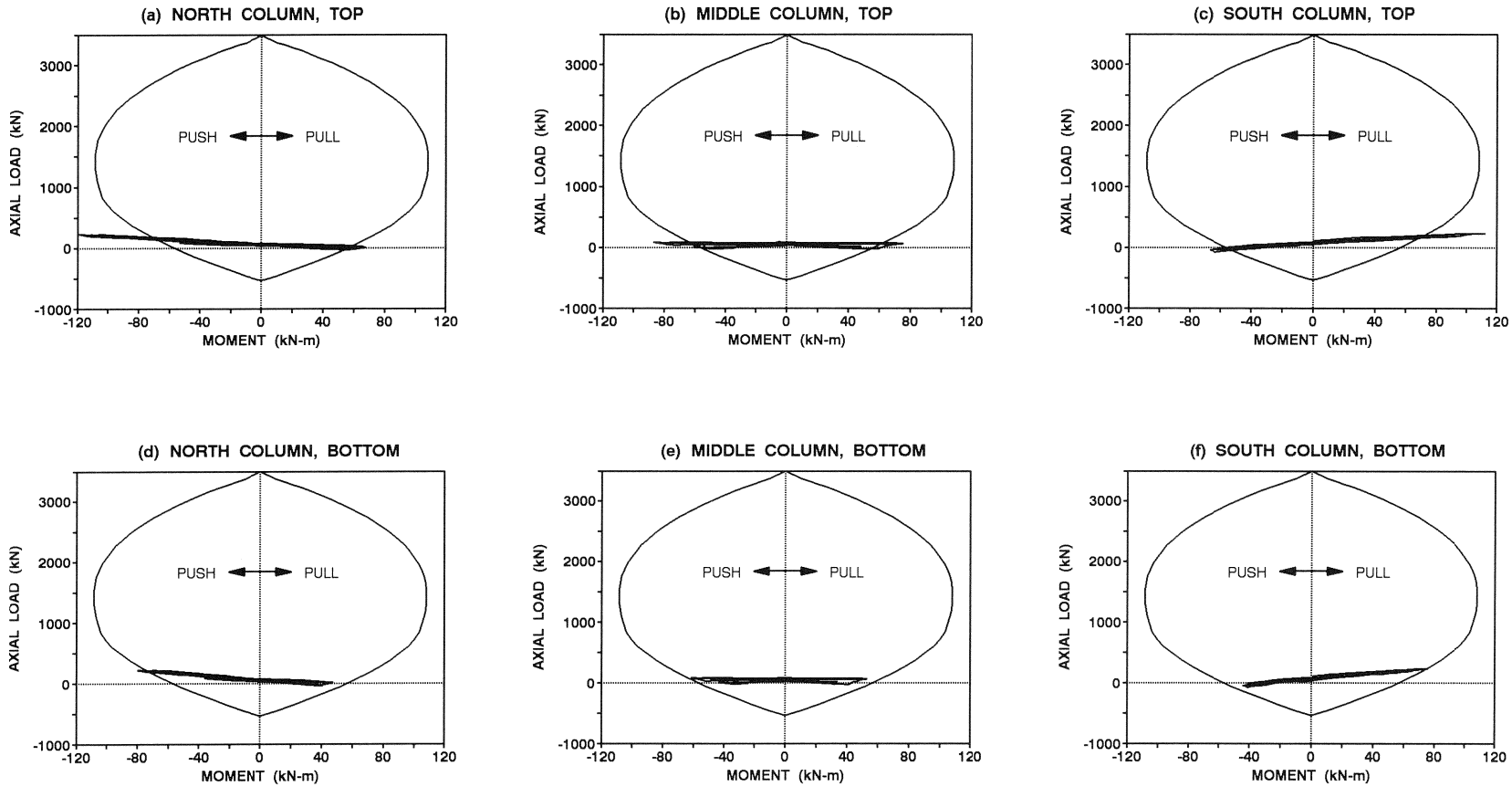

Figure 4-13. Column axial load-moment interaction of retrofitted model pier.

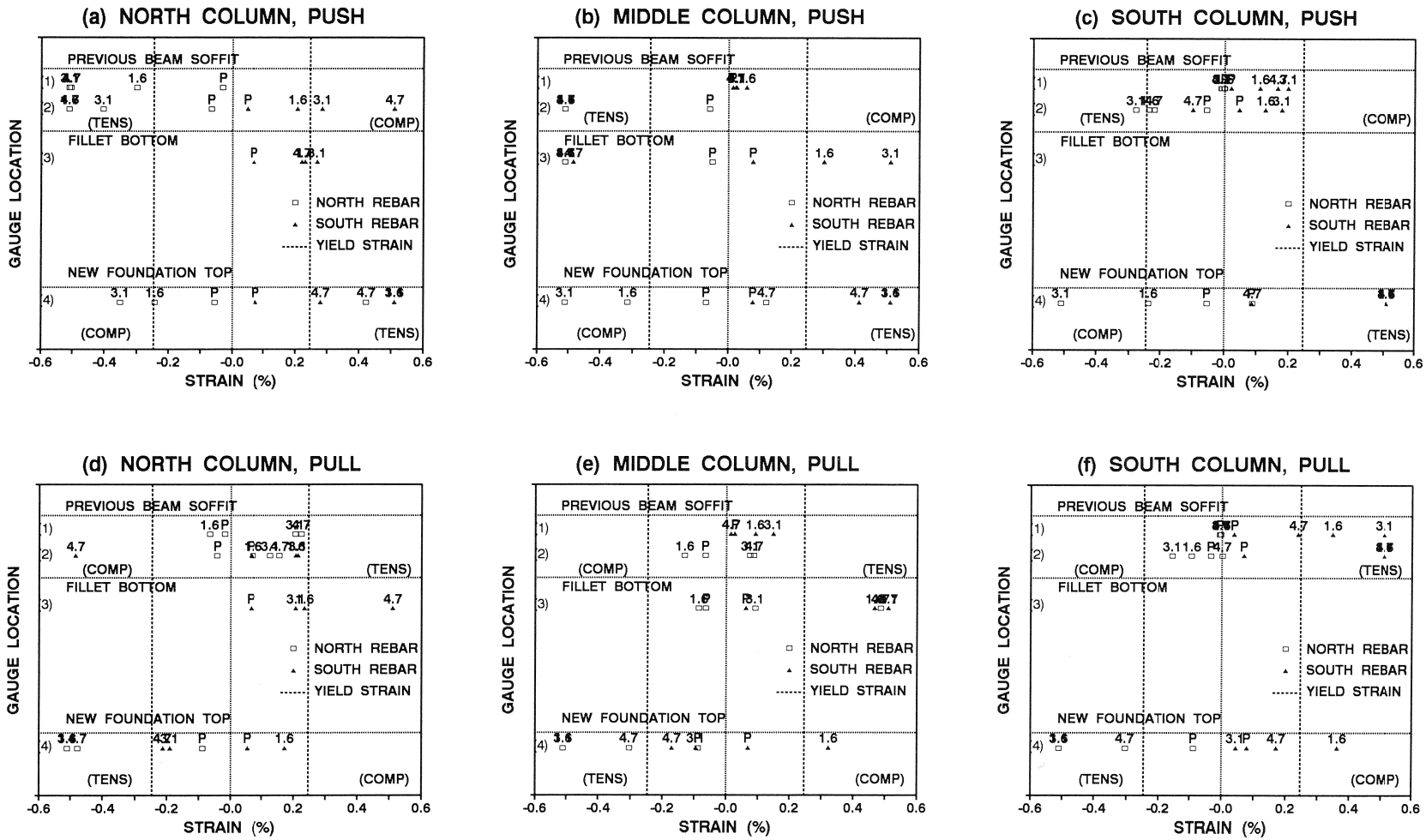

Figure 4-14. Longitudinal reinforcement strains in retrofitted model pier.

yield strain. During the inelastic cycles, it is evident that all the steel yielded in tension or compression with the exception of the middle column level (1) gauge. That gauge appeared to be faulty. It is noted that the strength loss in column shear capacity affected the longitudinal steel strains at 3.1% and 4.7% drift amplitudes in which some steel strains showed a decrease in amplitude or change of signs. In most cases, there was not so significant compression yielding.

4.5.6 Energy Absorption

The energy absorption capacity of the retrofitted model pier calculated by equation (2-10) is presented in figure 4-15 for unit loading cycles and cumulative drift, respectively. It is noted by comparison with figure 2-19 that the maximum energy dissipation per cycle in the retrofitted model pier is initially higher than that in the pre-retrofitted model pier. However, the energy absorption capacity is rapidly decreased due to the corner-to-corner diagonal shear cracks in column halves which prevailed after the second cycle of 3.1% drift amplitude.

4.6 Alternative Retrofit of Column Lap-Splice Zones

The previous subsections demonstrated that the retrofitted pier finally failed due to inadequate column shear capacity. This was largely due to the reduction in the clear column height and a corresponding increase in shear demand at flexural overstrength. An alternative method of retrofitting the pier is to reduce the column shear demand by providing pin-ended columns, or at least columns with a limited moment capacity at one end. One way of providing such a retrofit is to adjust the behavior of the base of the columns in the lap-splice zone. Such an alternative retrofit method is proposed as shown in figure 4-16 by cutting the existing longitudinal rebars in potential hinge or lap splice regions and then casting a reinforced concrete collar around the column. The column will then rock on the surface of the foundation when subjected to lateral loading. The study of the proposed improvement with rocking column base is left for future research.

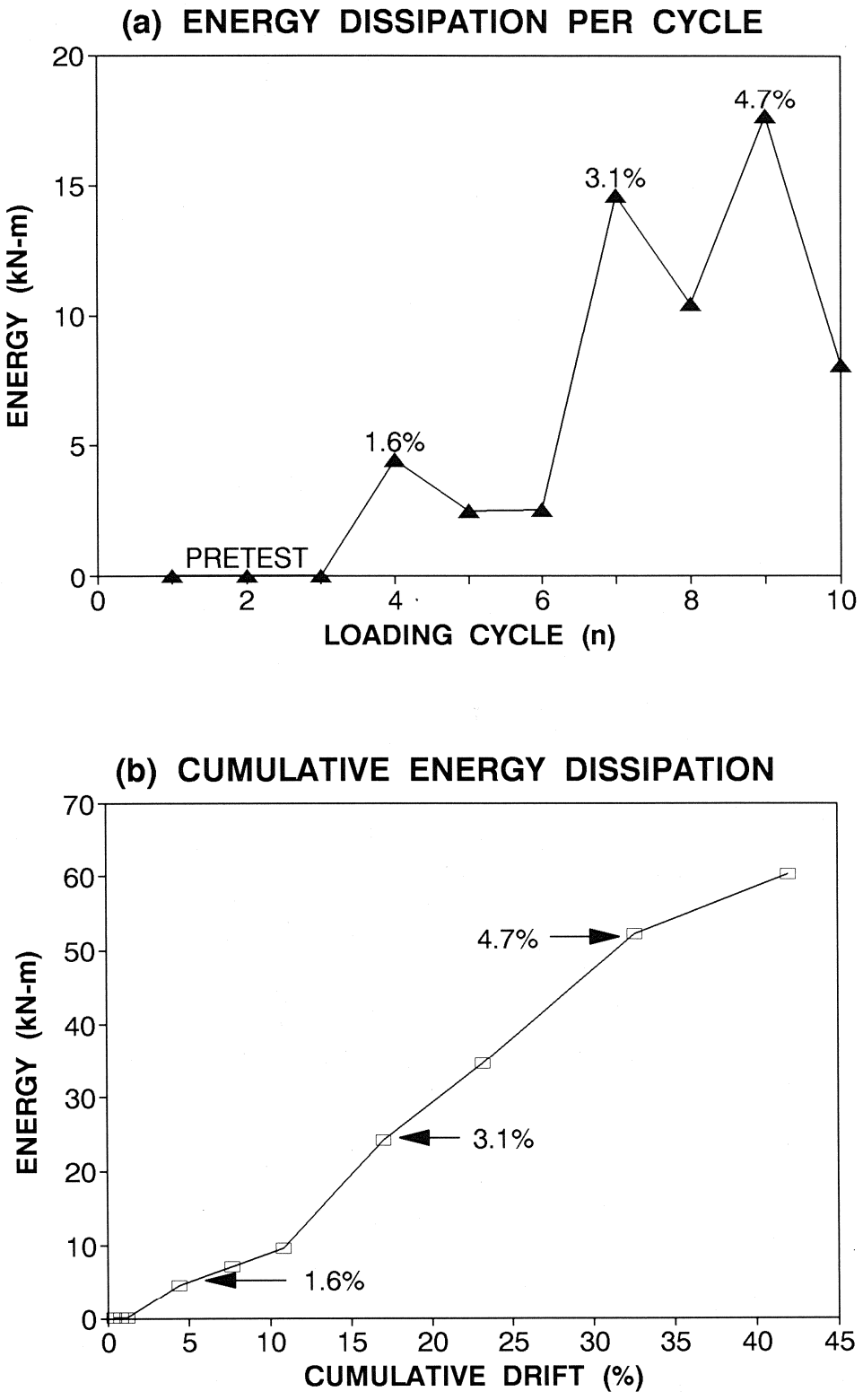

Figure 4-15. Energy absorption capacity of retrofitted model pier.

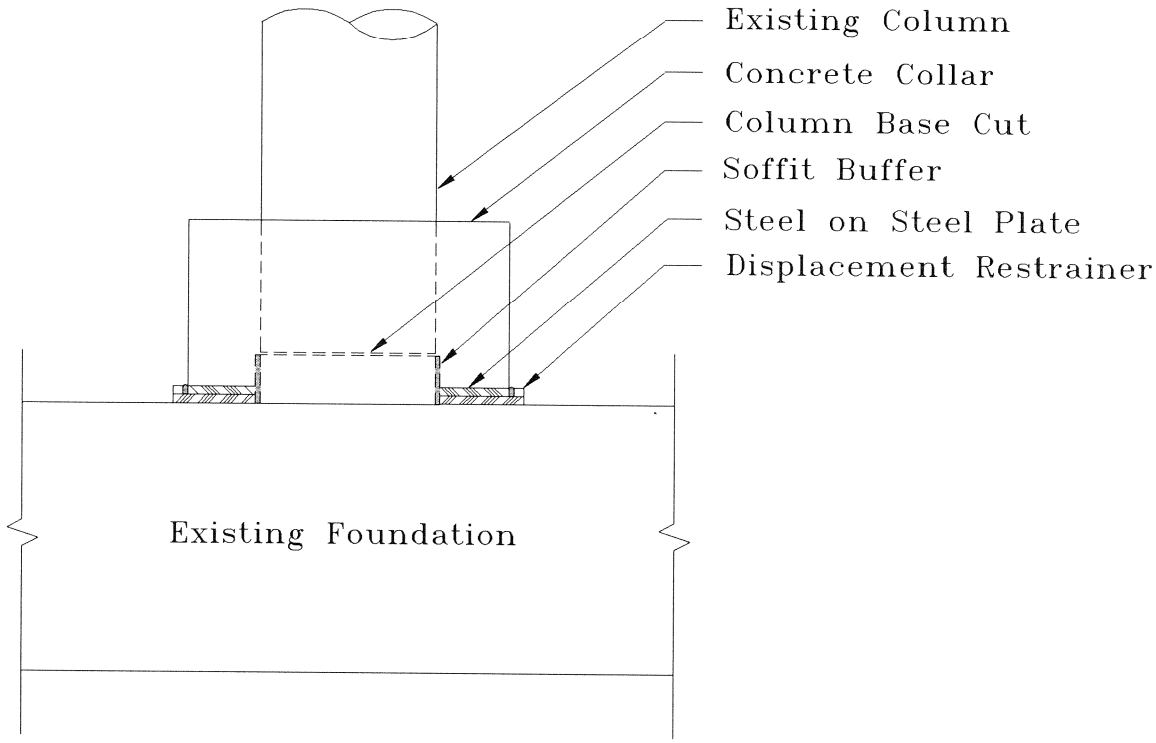

Figure 4-16. Alternative retrofit using rocking column base.

SECTION 5
A COMPARATIVE EVALUATION OF THE EXPERIMENTAL RESULTS

5.1 Performance of Model Pier Before and After Retrofit

5.1.1 Force-Displacement Relationship

The hysteretic performance of the model pier before and after retrofit is presented in figure 5-1. It is observed from the laboratory experiment that the retrofit is capable of changing the failure mode. The increase in strength is due to:

1. The shorter clear height of the columns,
2. The improved anchorage of column longitudinal reinforcement, and
3. The improved beam-column joint shear capacity.

These improvements also place a higher shear demand on the columns. Improvement in anchorage and joint shear capacity is evident when comparing the observed mechanism types that formed before and after retrofit, as shown in figure 5-1. The maximum force response of the pre-retrofitted model pier is close to the nominal flexural mechanism capacity while the retrofitted model pier shows some 10% overstrength due to flexural reinforcement strain-hardening which can be attained only when anchorage and joint shear capacity are sufficient. It is of interest to note that in both cases the maximum lateral load was attained at a plastic drift of 2%.

The presence of the column load cells prompted the retrofitted model pier columns to prematurely fail in shear. This was visually clear from the failure mode of columns which showed the concrete columns were badly diagonally cracked either above or below the load cells. The existing flexural cracks through the column height due to the previous experiment on the pre-retrofitted model pier together with the presence of the load cells possibly led to premature failure of columns in shear. Therefore, it is considered necessary to evaluate the proposed retrofit strategy in order to assess the reliability of seismic behavior.

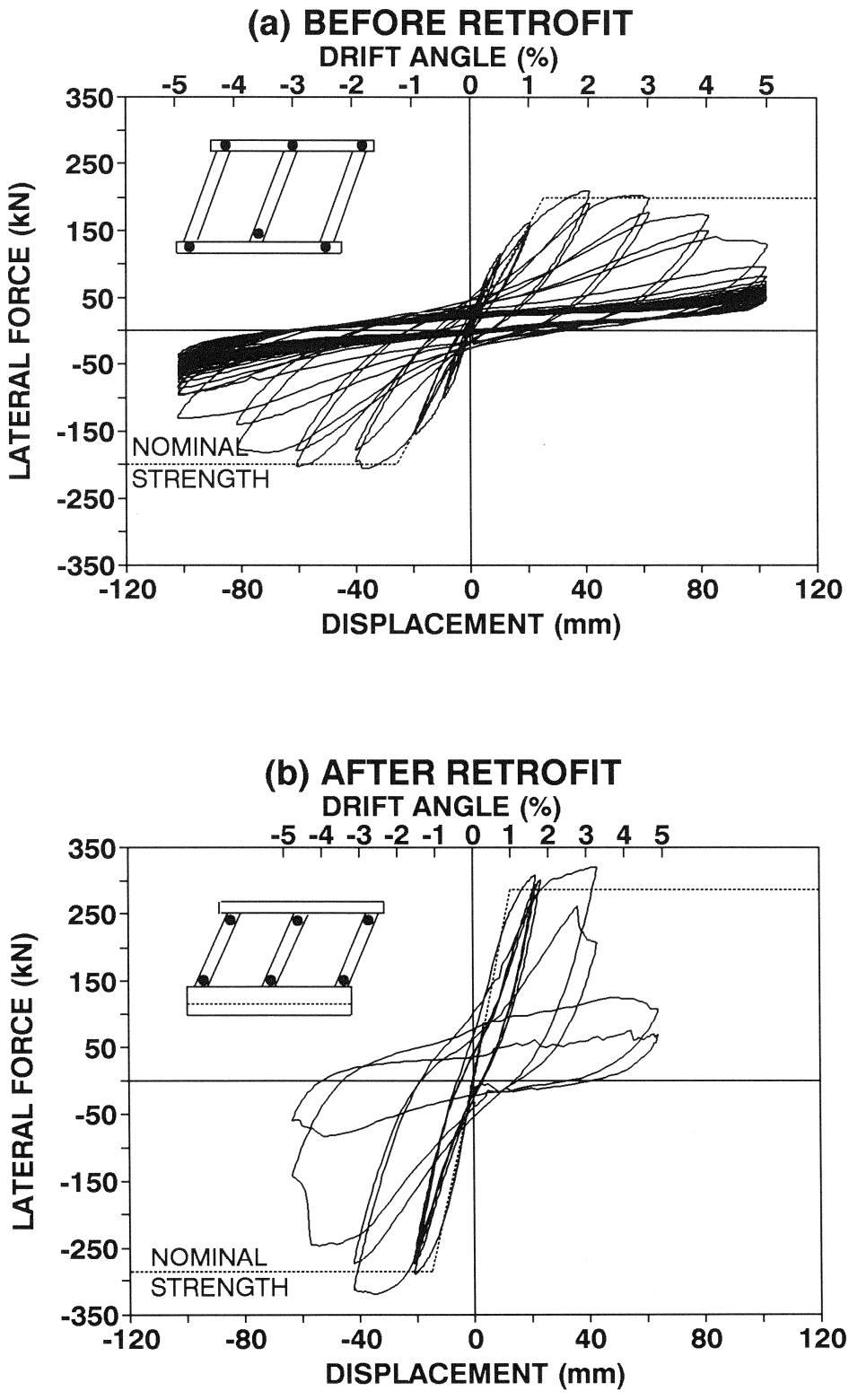

Figure 5-1. Hysteretic performance of model pier.

5.1.2 Energy Absorption Capacity

The cumulative energy absorbed by an elasto-perfectly plastic (EPP) system is defined by the area of parallelogram in the hysteretic loop as shown in figure 5-2, that is,

$$E_{EPP} = \left(F_n^+ + F_n^-\right)\Sigma\Delta_p = \left(F_n + F_n^-\right)h_c\Sigma\theta_p \qquad \textbf{(5-1)}$$

where $\left(F_n^+ + F_n^-\right)$= sum of nominal mechanism strengths of the system in the forward and reverse direction, $\Sigma\Delta_p = \Sigma\left(\Delta_p^+ + \Delta_p^-\right)$= cumulative plastic drift, h_c= column clear height, and $\Sigma\theta_p = \Sigma\left(\theta_p^+ + \theta_p^-\right)$= cumulative plastic drift angle. It is noted that for the symmetrical system $\left(F_n^+ + F_n^-\right)$ can be expressed as $2F_n$ where F_n= average nominal mechanism strength. Thus the elasto-perfectly plastic energy absorbed over n cycles of loading at an equi-amplitude plastic drift angle is

$$E_{EPP} = 4nF_nh_c\theta_p \qquad \textbf{(5-2)}$$

If the concept of energy absorption efficiency is now introduced whereby a system dissipating energy at the same rate as an EPP system, then the efficiency rate η is 100%, thus

$$\eta = 1 = \frac{E_{EPP}}{2F_nh_c\Sigma\theta_p} \qquad \textbf{(5-3)}$$

This is shown as a straight line with a slope of 1.0 in figure 5-3 where energy is normalized by dividing by $\left(F_n^+ + F_n^-\right)h_c$.

By considering the experimental results in a similar fashion, it is possible to determine the system efficiency with respect to the standard EPP system, thus

$$\eta = \frac{E_{expt}}{E_{EPP}} = \frac{\Sigma E_{cycle}}{2F_nh_c\Sigma\theta_p} \qquad \textbf{(5-4)}$$

where E_{cycle} is the energy dissipated per cycle and defined by equation (2-10). Experimental results of the cumulative energy absorption capacity normalized by $\left(F_n^+ + F_n^-\right)h_c$ are also plotted against cumulative plastic drift in figure 5-3. It is noted that the energy absorption capacity of reinforced concrete is usually deteriorated due to the imperfect nature of materials such as

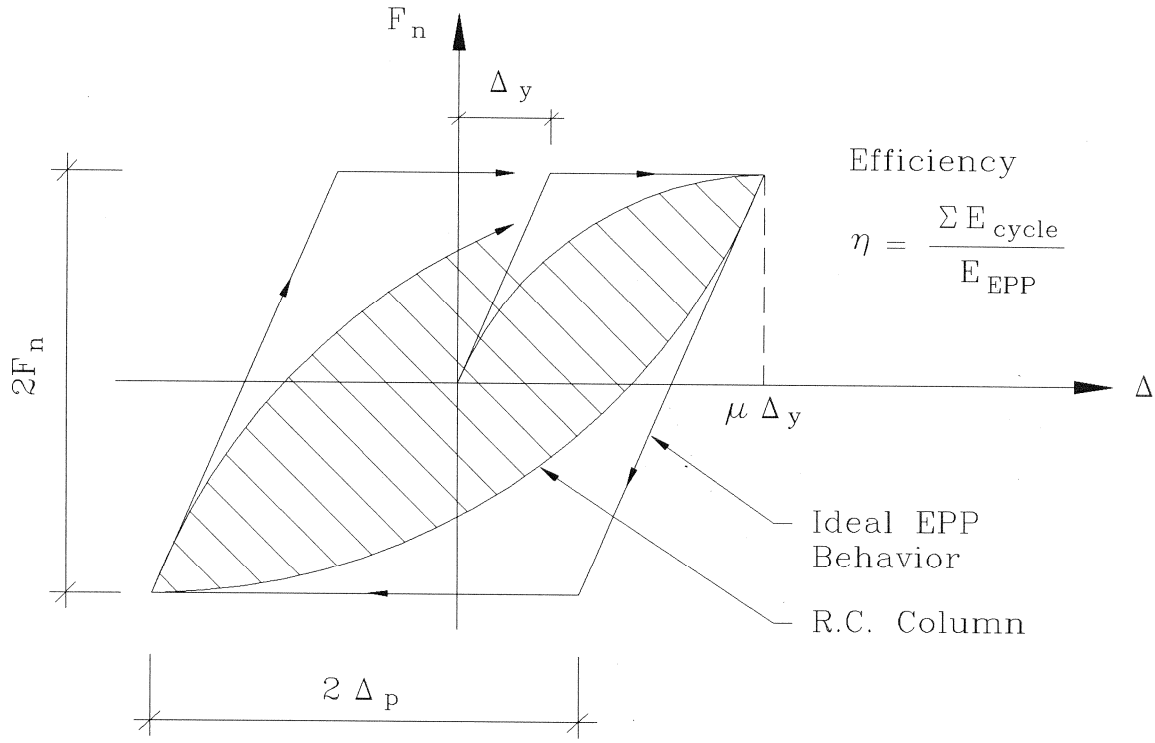

Figure 5-2. Definition of energy absorption efficiency.

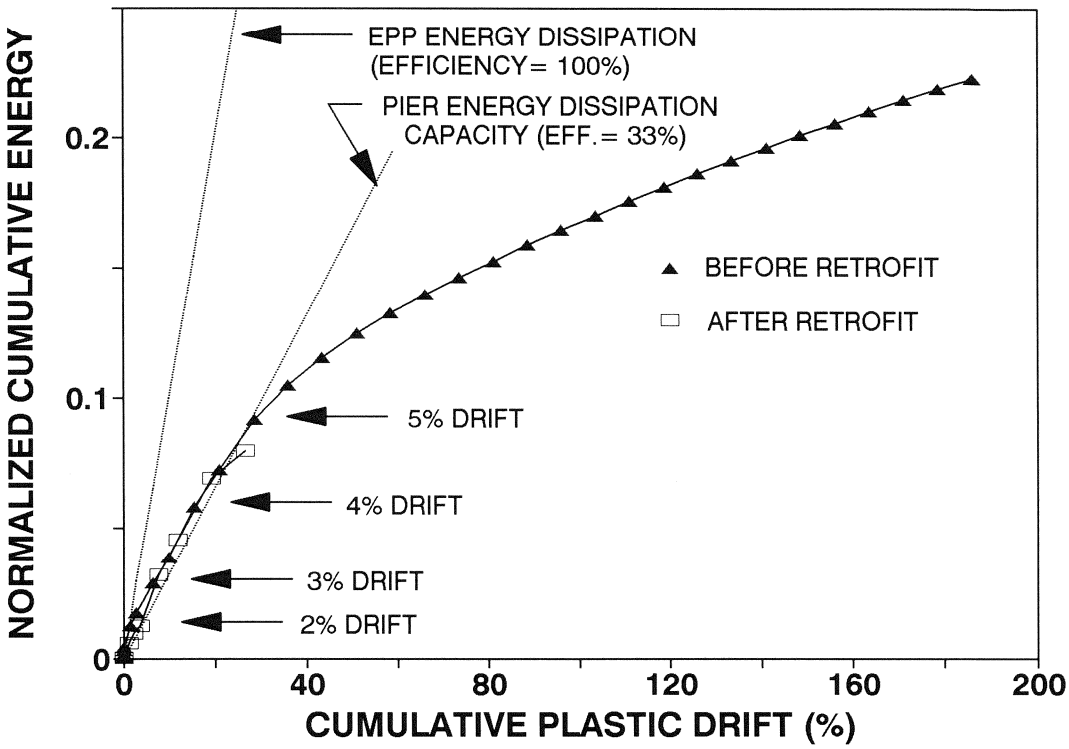

Figure 5-3. Energy absorption capacity of model pier.

concrete damage and bond/anchorage failure as shown with hatched part in figure 5-2.

Up to 25% cumulative plastic drift, the model pier before and after retrofit possessed an energy absorption efficiency of about 33% EPP. Here 25% was the threshold of the usefulness limit which is defined as the cumulative plastic drift at which the strength drops to about $0.8F_n$ due to inelastic cyclic loading. It is also noted that the post-retrofitted model pier showed early failure in column shear at the cumulative plastic drift of 27%.

5.1.3 Analytical Modeling

The computer program UB-COLA developed recently by Chang and Mander *(1994)* was used to simulate the experimentally obtained force-displacement hysteretic performance. UB-COLA has the following special features in analyzing reinforced concrete beam-columns:

1. Fiber elements are used to analyze the non-linear moment-curvature and force-displacement behavior under dynamic cyclic lateral loading.
2. A cyclic inelastic strut-tie (CIST) model is used to assess inelastic shear deformations.
3. Column base flexibility due to adjoining cap beam or foundation rotation is considered.
4. Low cycle fatigue of the longitudinal reinforcement, fracture of transverse hoops, and buckling of the longitudinal reinforcement can be predicted.
5. Shear failure due to crushing of the concrete strut can be predicted.

One half of the interior column with the average column axial load was used in the analysis on the basis that the contra-flexure point is located at mid-height of the column and the column represents the average of three columns of the model pier. These assumptions were necessary due to the present limitation of UB-COLA in analyzing a single column at a time.

The experimental and theoretical force-displacement relationship is presented in figures 5-4 and 5-5 up to 3% drift for pre-retrofitted and post-retrofitted model pier, respectively. Following this drift level, failure took place outside the column in joint before retrofit and

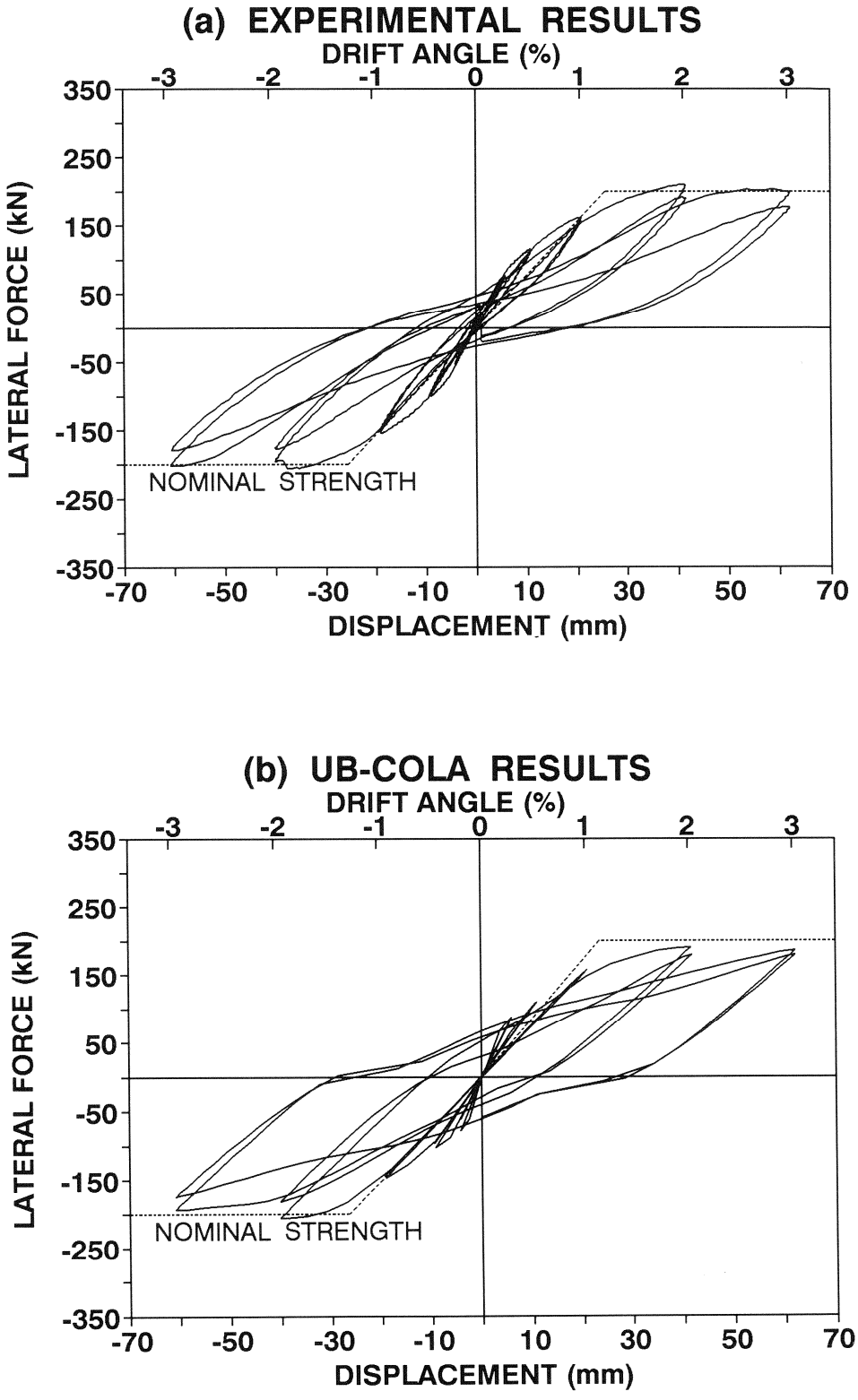

Figure 5-4. Experimental and analytical performance of model pier before retrofit.

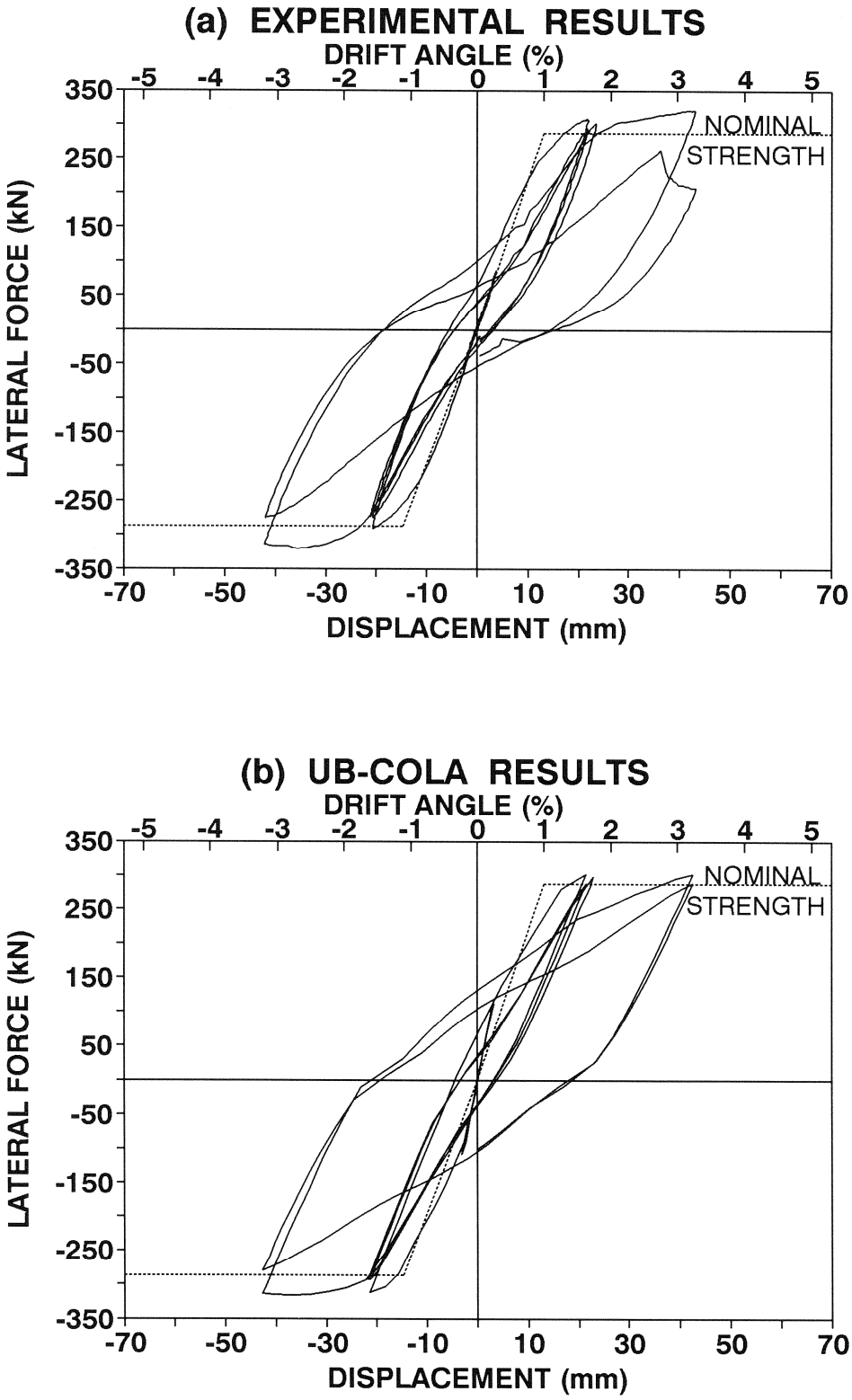

Figure 5-5. Experimental and analytical performance of model pier after retrofit.

premature column shear failure took place in the model after retrofit. As the behavior prior to the 3% drift amplitude was dominated by column flexure, the program UB-COLA is particularly suitable for simulating the force-displacement behavior. Column input data for UB-COLA analysis is summarized in table 5-1 for the model pier before and after retrofit. Good agreement with the experimental results is shown in the response before and after retrofit. One exception is the second cycle at the 42 mm displacement amplitude after retrofit. This is due to incipient failure with the opening of wide shear cracks resulting in the sudden drop in load between displacement + 35 mm to + 40 mm, as shown in figure 5-5(a).

Table 5-1. Model column input data for UB-COLA analysis.

Description	Parameters	Before Retrofit	After Retrofit
Concrete	Unconfined (f'_c), MPa	53	59[a]
	Confined (f'_{cc}), MPa	60	75[a]
	Tension (f'_t), MPa	6	6
Steel	f_y (ten, comp), MPa	474, 474	474, 474
	f_{su} (ten, comp), MPa	750, 750	750, 750
	ε_{sh} (ten, comp)	0.011, 0.011	0.005[b], 0.005[b]
	E_{sh} (ten, comp), MPa	3300, 4200	3300, 4200
	ε_{su} (ten, comp)	0.12, 0.12	0.12, 0.12
	Hoop f_y, MPa	268	268
Section	Diameter, mm	279	279
	Pitch Diameter, mm	229	229
	Number of Bars	16	16
	Bar Diameter, mm	10	10
	Hoop Diameter, mm	4.8	4.8
	Hoop Spacing, mm	102	102
Geometry	Shear Span, mm	927	660
	Hinge Length, mm	400	660[b]
	Yield Penetration, mm	180	300[b]
	Axial Load, kN	-47	-59
	Base Flexibility, $N^{-1}mm^{-1}$	$1.0x10^{-11}$	$4.5x10^{-12}$, [c]
Shear	Lever Arm (jd), mm	224	224
	Unconfined b_w, mm	59	59
	Confined b_w, mm	198	198

[a]Confinement effect due to concrete fillet and strong beam at column ends is assumed.
[b]Plastic deformation of steel due to pre-retrofitted model test is assumed.
[c]Stiffening effect due to strong foundation beam is assumed.

5.2 Performance of Prototype Cap Beam-Column Subassemblage Before and After Retrofit

A cap beam-column subassemblage was retrieved from the Niagara Parkway bridge pier and tested in the laboratory. The damaged knee joint was retrofitted and tested again. The detailed procedure of retrieval, laboratory experiment and retrofit construction is described in the work of Mander, et al. *(1996)*. This section presents a brief review of their experimental and analytical work.

5.2.1 Force-Displacement Relationship

The lateral force versus displacement relationship for the prototype pier subassemblage before and after retrofit is shown in figure 5-6. In spite of non-seismically designed transverse reinforcement details (12.7 mm dia hoops at 305 mm centers, i.e., #4 at 12"), the pre-retrofitted specimen behaved in a ductile manner. The column strength gradually decreased after 4% drift amplitude in the response of the pre-retrofitted specimen which was attributed to the partial loss of concrete resistance in shear as well as the loss of anchorage of the longitudinal column bars.

It is observed from figure 5-6 that the column strength in the pull (joint closing) direction increased after retrofit due to the shorter clear column height. However, no significant increase in strength can be detected in the push (joint opening) direction. This is due to the imperfect repair of the previously damaged anchorage of the column longitudinal reinforcement. Although the overall force-deformation behavior before and after retrofit appears similar, it should be noted that the failure modes were quite different. Prior to retrofit, the energy absorption was made within the joint core due to bond-slip of the column longitudinal reinforcement as well as shear deformation. After retrofit, the failure mode was moved to column flexure-shear failure.

5.2.2 Energy Absorption Capacity

The experimentally observed energy absorption capacity of the prototype pier subassemblage before and after retrofit in terms of the cumulative plastic drift angle is presented

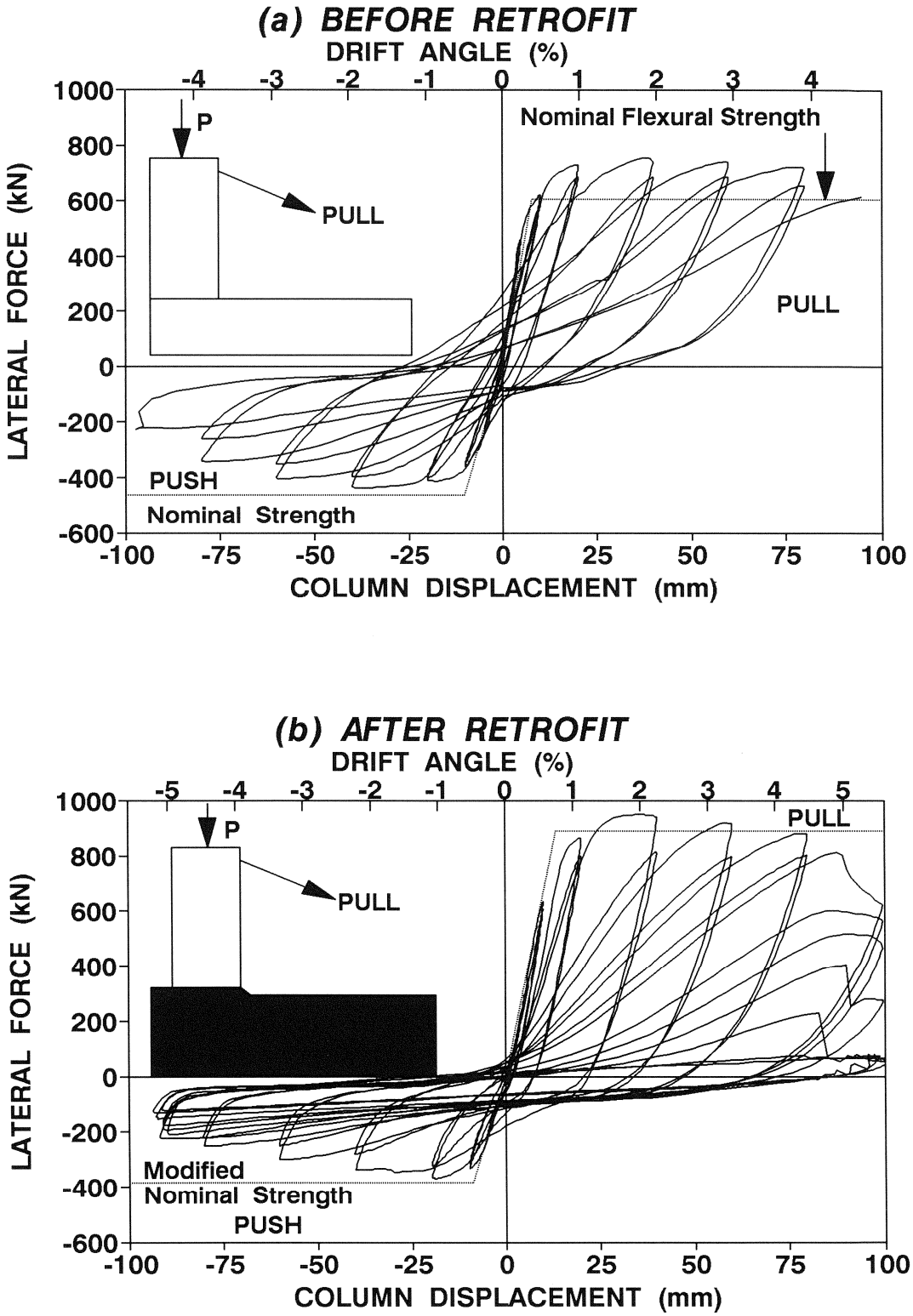

Figure 5-6. Hysteretic performance of prototype subassemblage.

in figure 5-7. The cumulative energy was normalized using the same procedure described in Section 5.1.2 and compared with the cumulative energy absorption capacity of the EPP system. Up to 25% cumulative plastic drift, the pre-retrofitted prototype subassemblage shows the efficiency rate of about 23% while the post-retrofitted prototype subassemblage gives about 30% efficiency relative to the EPP system.

5.2.3 Analytical Modeling

The experimental and theoretical force-displacement relationship is presented in figures 5-8 and 5-9 up to 4% drift angle for the pre-retrofitted prototype subassemblage and 3.3% for the post-retrofitted prototype subassemblage, respectively. Following these drift levels, similar to the model pier, failure took place in the joint core before retrofit and column flexure-shear failure took place in the prototype subassemblage after retrofit.

It is noted that the force inclination on the pier subassemblage specimen during the laboratory test and the inherent behavioral characteristics of the knee joint resulted in different forward and reverse strengths in the response as shown in figure 5-6. These variables cannot be accounted for with the current version of UB-COLA. Therefore, the difference in experimental response was overcome by taking the averages of absolute forces for positive and negative halves of the cycles. The resultant half loops are presented for comparison in figure 5-8 for the pre-retrofitted prototype subassemblage and in figure 5-9 for the post-retrofitted prototype subassemblage. Column input data for UB-COLA analysis is summarized in table 5-2. Reasonable agreement is shown between experimental and theoretical response before and after retrofit.

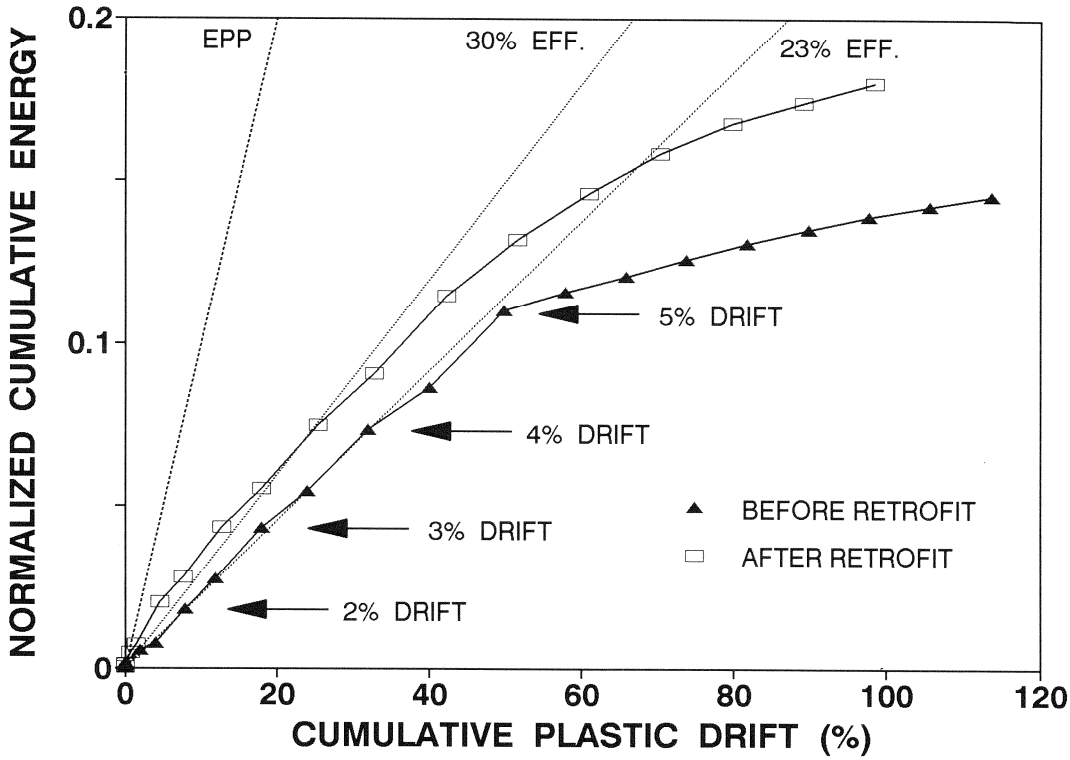

Figure 5-7. Energy absorption capacity of prototype cap beam-column subassemblage.

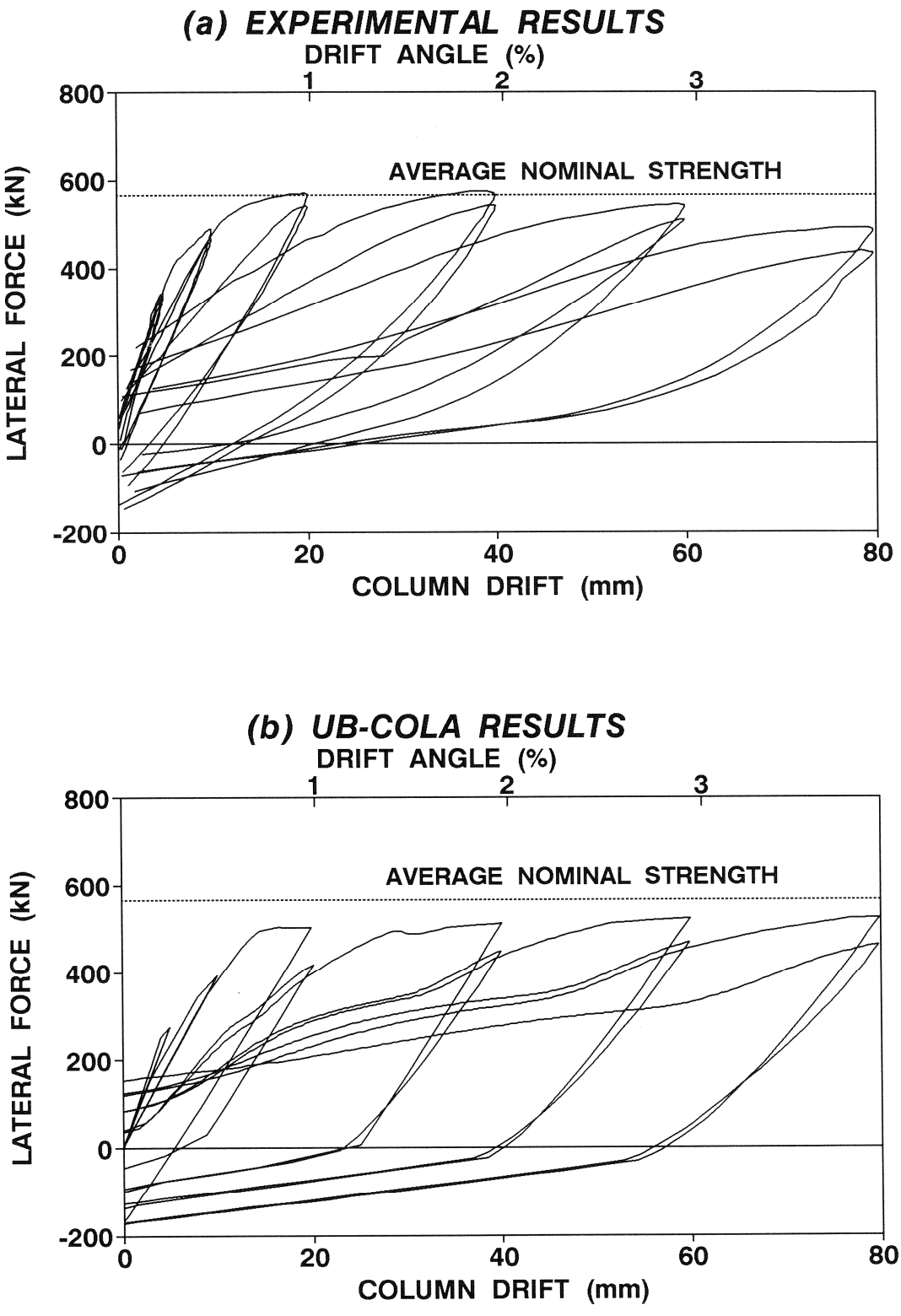

Figure 5-8. Hysteretic performance of prototype subassemblage before retrofit.

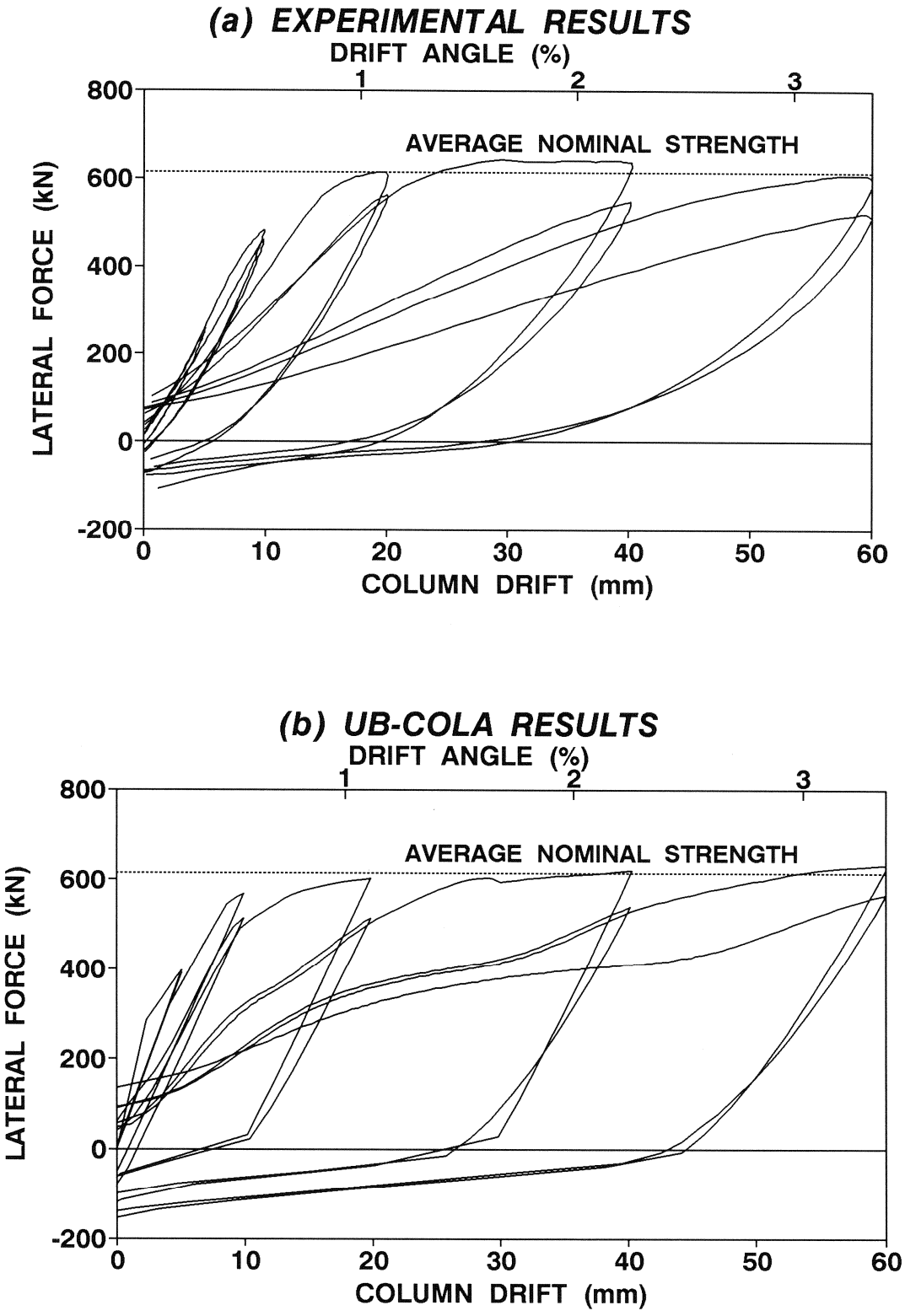

Figure 5-9. Hysteretic performance of prototype subassemblage after retrofit.

Table 5-2. Prototype column input data for UB-COLA analysis.

Description	Parameters	Before Retrofit	After Retrofit
Concrete	Unconfined (f'_c), MPa	45	45
	Confined (f'_{cc}), MPa	48	48
	Tension (f'_t), MPa	3.5	3.5
Steel	f_y (ten, comp), MPa	269, 304	269, 304
	f_{su} (ten, comp), MPa	421, 421	421, 421
	ε_{sh} (ten, comp)	0.018, 0.018	0.005[a], 0.005[a]
	E_{sh} (ten, comp), MPa	3300, 4200	3300, 4200
	ε_{su} (ten, comp)	0.19, 0.19	0.19, 0.19
	Hoop f_y, MPa	476	476
Section	Diameter, mm	838	838
	Pitch Diameter, mm	683	683
	Number of Bars	16	16
	Bar Diameter, mm	29	29
	Hoop Diameter, mm	12.7	12.7
	Hoop Spacing, mm	305	305
Geometry	Shear Span, mm	2045	1791
	Hinge Length, mm	838	1790[a]
	Yield Penetration, mm	0	0
	Axial Load, kN	-343	-343
	Base Flexibility, $N^{-1}mm^{-1}$	1.2×10^{-12}	3.4×10^{-13}, [b]
Shear	Lever Arm (jd), mm	683	683
	Unconfined b_w, mm	81	81
	Confined b_w, mm	603	603

[a]Plastic deformation of steel due to pre-retrofitted model test is assumed.
[b]Stiffening effect due to strong cap beam is assumed.

5.3 Model versus Prototype Performance

When comparing the behavior of the scaled model pier with that of the prototype cap beam-column subassemblage, it should be noted that even though the scaled model was carefully designed considering stress and strain similitude, some differences still remained such as material strengths and geometrical dimensions. These shortcomings may be partially overcome by normalizing the prototype and model behavior with respect to the nominal flexural strength F_n so that a direct comparison can be made. Figures 5-10 and 5-11 present the comparison of hysteretic performance of the pre- and post-retrofitted specimens, respectively. For the prototype cap beam-column subassemblage, the average of absolute normalized forces for positive and negative halves of the cycles are again used. Therefore, plots in figures 5-10 and 5-11 are the normalization of response in figures 5-8 and 5-9 for prototype subassemblage. It can be said that there is a considerable resemblance in the shapes of the loops with exception of the initial stiffness. The prototype specimen shows a higher initial stiffness both before and after retrofit. This may be due to the effect of experimental setup where the model pier had a more flexible foundation beam which was not modeled at all in the prototype subassemblage.

Comparison of energy absorption capacity of the model pier and prototype subassemblage in figure 5-12 shows the higher efficiency with respect to the EPP system for the model pier before and after retrofit. However, the response of pre-retrofitted model pier is shown up to 27% cumulative plastic drift angle due to premature failure in column shear.

5.4 Summary and Conclusions

1. The current retrofit results in a higher column shear demand due to the shorter clear height. The seismic retrofit functions favorably for the anchorage, beam-column joints, cap beam and foundation behavior. However, the presence of the load cells at the mid-height of the columns apparently adversely affected the shear resistance of the retrofitted model pier by inhibiting the formation of the usual corner-to-corner crack over the entire height of the column.

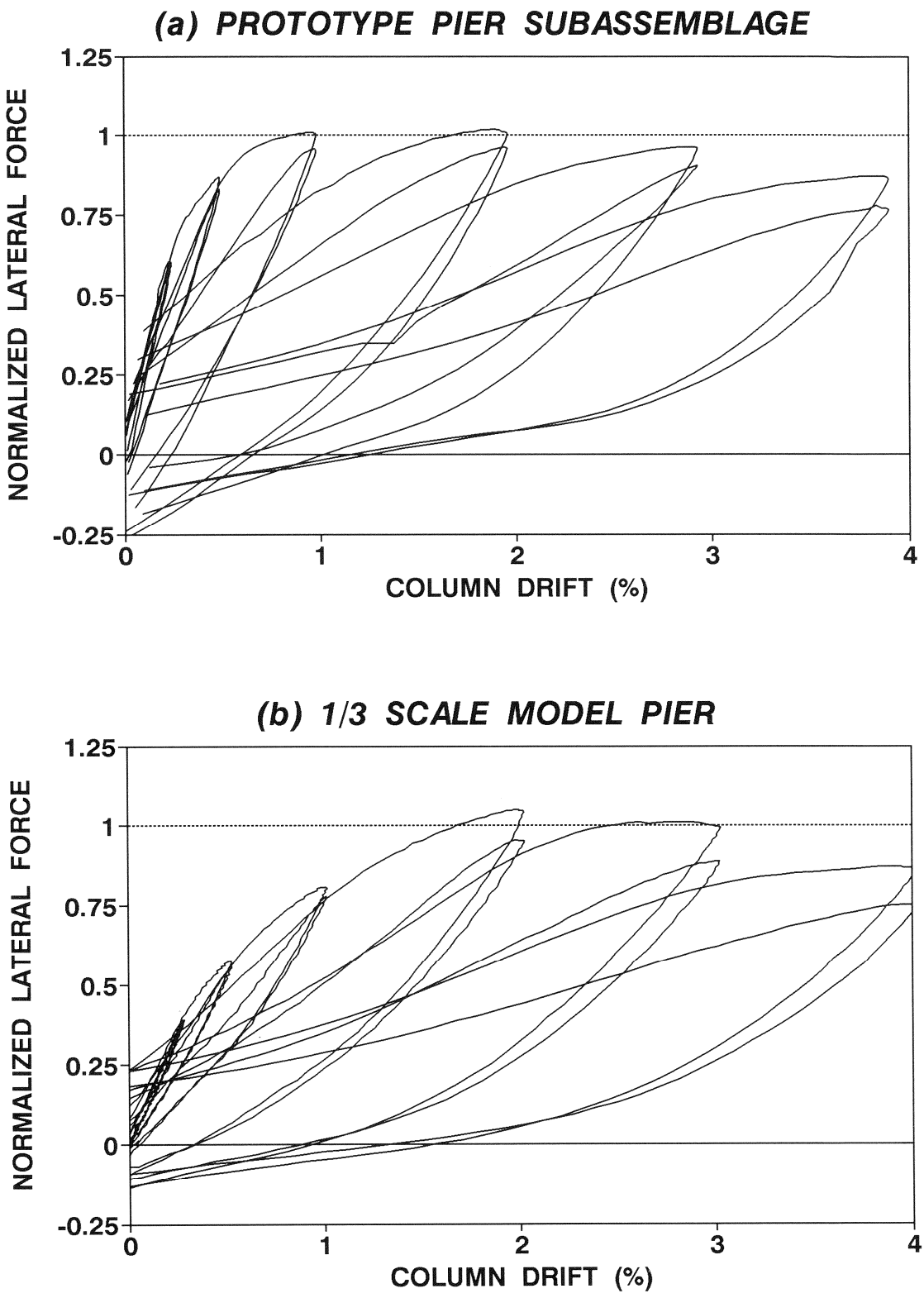

Figure 5-10. Comparison of experimental performance of pre-retrofitted specimens.

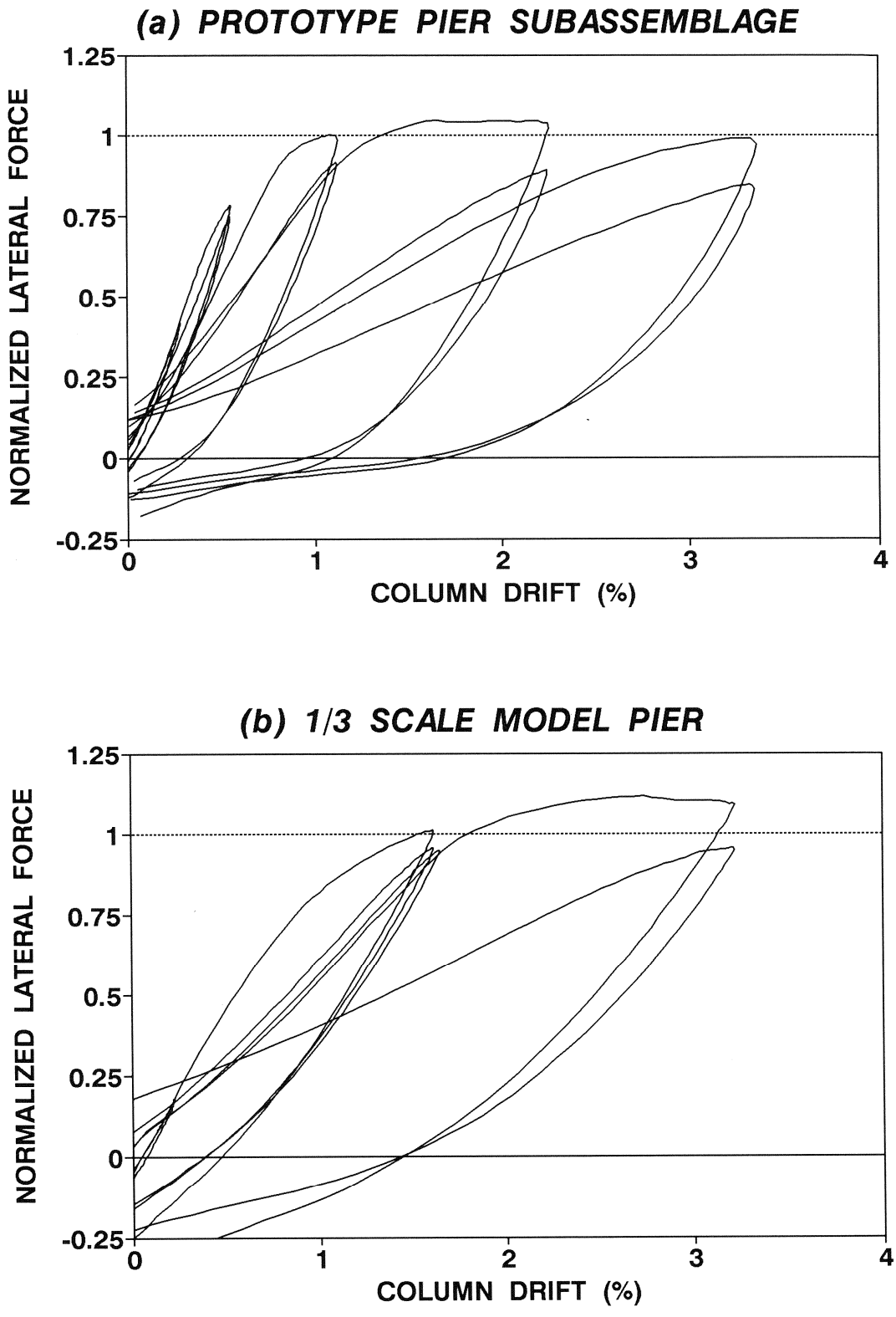

Figure 5-11. Comparison of experimental performance of post-retrofitted specimens.

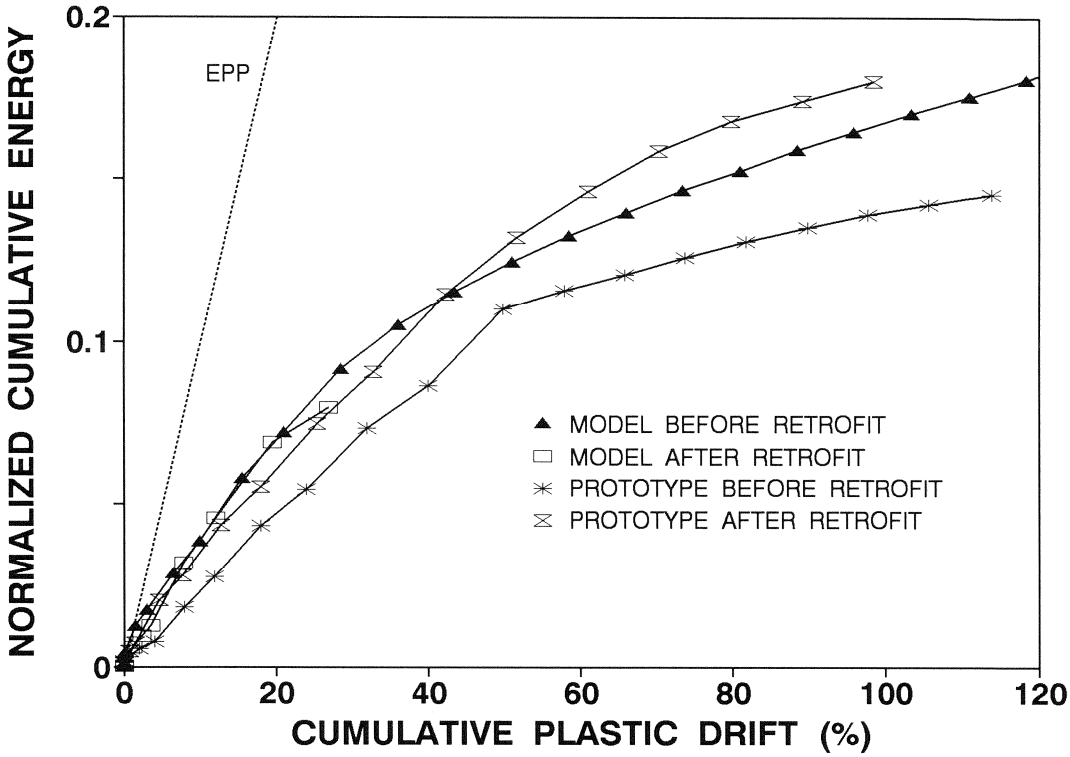

Figure 5-12. Comparison of energy absorption capacity of specimens.

2. The study of energy absorption capacity shows that about 33% efficiency relative to the EPP system for the pre- and post-retrofitted model pier was reached up to the usefulness limit in strength while 23% and 30% efficiencies were reached for the prototype subassemblage before and after retrofit, respectively.

3. The computer column analysis program UB-COLA *(Chang and Mander, 1994)* predicts a reasonably good agreement between the analytical and the experimental results, even though the current version has several shortcomings.

4. Experimental observations present similar failure mechanism patterns for the model pier and prototype cap beam-column subassemblage before and after retrofit. The specimen before retrofit was initially governed by flexure and at large displacement amplitude by joint shear leading to the bond/anchorage failure of column longitudinal reinforcement. The specimen after retrofit was governed by flexure-shear failure mode.

5. Even though the retrofitted model pier showed an apparent premature failure in column shear, the inelastic displacement capacity is substantial and would translate to 125 mm in prototype terms. Given the inherently stiff nature of the entire prototype pier with a natural frequency of about 10 Hz, it is expected that this displacement capability should be ample to resist any maximum credible earthquake.

SECTION 6
EVALUATION OF THE MODEL PIER BEFORE AND AFTER RETROFIT

6.1 Introduction

The behavior of the model pier, both before and after retrofitting, is evaluated using the two methods recommended in the recently published FHWA Seismic Retrofitting Manual for Highway Bridges *(Buckle and Friedland, 1995)*. These evaluation methods are presently used by practicing engineers. The first is based on the ATC 6-2 Capacity/Demand (C/D) ratio method which was first developed from 1970's research, while the second is the equivalent lateral force (push-over) method developed by Priestley, et al. *(1992)* from research in the late 80's and early 90's. The term *pre-retrofitted* is used for the original model pier described in Section 2, and the terms *retrofitted* and *post-retrofitted* for the rehabilitated model pier described in Section 4.

6.2 Evaluation by Capacity/Demand Ratio Method: ATC 6-2 Approach

This Capacity/Demand (C/D) evaluation method was first developed by the Applied Technology Council and reported as part of project ATC 6-2 *(1983)*. The methodology was later published as a recommended evaluation procedure by FHWA *(1983)*, and more recently as one possible method of evaluation in the revised FHWA Retrofitting Manual *(Buckle and Friedland, 1995)*. In this evaluation procedure, elastic moment demands at column ends and footings are first compared to the nominal ultimate moment capacities. Then, based on these elastic C/D ratios (nominal ultimate moment capacity with respect to the elastic moment demand), modified C/D ratios are calculated for anchorage and the splice in the column longitudinal reinforcement, transverse confinement for the plastic hinge region and column shear.

The elastic moment demands at column ends and footings were calculated for this study by the single-mode spectral analysis, since the Niagara Parkway bridge was relatively regular and had two simply supported spans. To account for the directional uncertainty of the earthquake in the analysis, a combination of seismic forces resulting from orthogonal loading on the bridge is

used: i) 100% of the absolute value of analysis results in the longitudinal direction plus 30% of the absolute value of analysis results in the transverse direction; or ii) 100% of the absolute value of analysis results in the transverse direction plus 30% of the absolute value of analysis results in the longitudinal direction, whichever is greater.

The slab-on-girder bridge with friction-free existing steel bearings can be represented by SDOF simple mass and spring in assessment of the natural period of the structure on the assumption that the footing is well founded. Thus, the natural period T is determined by

$$T = 2\pi\sqrt{\frac{W}{gK}} = 2\pi\sqrt{\frac{\theta_y h_c}{gC_n(c)}} \qquad \textbf{(6-1)}$$

where W= tributary weight of superstructure plus half of pier weight, g= gravitational acceleration, K= pier stiffness, θ_y= yield drift, h_c= column height, and $C_n(c)$= V/W= nominal base shear coefficient.

The corresponding base shear coefficient demand $C(d)$ for AASHTO response spectra *(1992)* is calculated by the lesser of

$$C(d) = \frac{1.2AS}{T^{2/3}} \qquad \textbf{(6-2a)}$$

$$C(d) = 2.5A \qquad \textbf{(6-2b)}$$

$$C(d) = (1 + 10T)AS \qquad \textbf{(6-2c)}$$

where A= peak ground acceleration (PGA) coefficient, and S= site coefficient for the soil characteristics.

With $\theta_y = 0.0125\ rad.$, $h_c = 1854\ mm$, $g = 9.81\ m/s^2$ and $C_n(c) = 1.42$, the calculated natural period of the pre-retrofitted model pier is $T = 0.25\ s$. For the post-retrofitted model pier $T = 0.18\ s$ with the values of $\theta_y = 0.01\ rad.$, $h_c = 1321\ mm$ and $C_n(c) = 1.62$. The base shear coefficient

demand for both the pre-retrofitted and the post-retrofitted model pier is then 2.5*A* with the foundation on rock. Therefore, a combination of orthogonal elastic seismic forces gives the base shear coefficient demand of 3.25*A*.

6.2.1 Moment C/D Ratio

The elastic moment demand in the model pier for the given elastic base shear demand is determined by a static analysis (portal frame method) assuming that 30% of base shear is resisted by the exterior column and 40% by the interior column. The nominal ultimate moment capacity is calculated using the usual assumptions of ACI 318 *(1995)* and applied to each column in the flexural mechanism analysis. A set of moment C/D ratios in terms of the peak ground acceleration coefficient ***A*** for columns and footings for the model pier before and after retrofit is presented in table 6-1. It is noticeable that capacities of columns and footings in flexure have been improved significantly by retrofitting. This also gives an improved margin of safety against the development of undesirable mechanisms. The moment C/D ratios predict that the interior column is the most vulnerable in flexure. Experimental results also indicated that the interior column was the only column having a plastic hinge form for the pre-retrofitted model pier.

Table 6-1. ATC 6-2 based moment C/D ratios for columns (r_{ec}) and footings (r_{ef}).

Component and Location	Before Retrofit			After retrofit		
	M_n (kN-m)	Demand (kN-m)	r_{ec} or r_{ef}	M_n (kN-m)	Demand (kN-m)	r_{ec} or r_{ef}
Windward Ext Col	51	128A	0.40/A	52	113A	0.46/A
Interior Column	63	170A	**0.37/A**	64	151A	**0.42/A**
Leeward Ext Col	72	128A	0.56/A	74	113A	0.65/A
Footing Ext End	53	128A	0.41/A	123	113A	1.09/A
Footing Int End	73	85A	0.86/A	151	76A	1.99/A

A= Peak Ground Acceleration Coefficient.
Note: Boldface is for critical cases.

6.2.2 Anchorage of Longitudinal Reinforcement

The C/D ratio for anchorage of longitudinal reinforcement r_{ca} is determined by taking the ratio of the provided (capacity) effective anchorage length $l_a(c)$ to the required (demand) effective anchorage length $l_a(d)$. It is then used to modify the elastic C/D ratios r_{ec} and r_{ef}.

The required anchorage length demand for a straight anchorage is given by

$$l_a(d) = \frac{0.083\, k_s\, d_b}{(1 + 2.5\, c/d_b + k_{tr})\sqrt{f'_c}} \geq 30 d_b \quad (mm) \qquad \textbf{(6-3a)}$$

and for anchorages with 90° standard hooks,

$$l_a(d) = 1.661\, k_m\, d_b \left(\frac{f_y}{\sqrt{f'_c}} \right) > 15 d_b \quad (mm) \qquad \textbf{(6-3b)}$$

where d_b = nominal bar diameter (mm), c = lesser of the clear cover over the bar or half the clear spacing between adjacent bars (mm), f'_c = concrete compression strength (MPa), $k_m = 0.7$ for #11 bars or smaller when side cover (normal to plane of the hook) is not less than 63 mm and cover on the bar extension beyond the hook is not less than 50 mm, $k_m = 1.0$ for all other cases, f_y = reinforcement yield strength (MPa), and k_s and k_{tr} are given by

$$k_s = \frac{f_y - 75.8}{33.1} \quad (MPa)$$

$$k_{tr} = \frac{A_{tr}(c)\, f_{yt}}{4.14\, s\, d_b} \leq 2.5 \quad (MPa)$$

where $A_{tr}(c)$ = area of transverse reinforcement normal to potential splitting cracks, f_{yt} = yield stress of transverse reinforcement (MPa), and s = spacing of transverse reinforcement.

If the provided effective development length is insufficient, $l_a(c) < l_a(d)$, then the C/D ratio for anchorage of longitudinal reinforcement is given by

$$r_{ca} = \frac{l_a(c)}{l_a(d)} r_{ec} \qquad \textbf{(6-4)}$$

This equation reflects the fact that the ultimate capacity of the steel cannot be developed with the insufficient anchorage length.

If the provided effective development length is sufficient, $l_a(c) \geq l_a(d)$, then the C/D ratio for anchorage of longitudinal reinforcement is calculated by:

$$r_{ca} = \mu r_{ef} \leq 1.0 \qquad \textbf{(6-5)}$$

where μ = ductility indicator. The value of ductility indicator may lie between 1.0 and 1.5 depending on the presence of the top layer of foundation flexural reinforcement and the type of anchorage. When adequate anchorage is provided in a cap beam, the C/D ratio for the anchorage is taken as 1.0 no matter what the cap beam strength is.

The provided anchorage lengths of #3 (10 mm diameter) longitudinal reinforcement before retrofitting were 254 mm in straight and 203 mm with 90° hook at cap beam and footing, respectively. The required anchorage lengths are calculated as 286 mm and 143 mm at cap beam and footing, respectively. After retrofit, the foundation top was raised up by 381 mm and the spliced part of longitudinal reinforcement is considered as straight anchorage. Thus the provided straight anchorage lengths of longitudinal reinforcement after retrofit became 406 mm and 381 mm at cap beam and footing, respectively. The required anchorage lengths are calculated as 149 mm and 213 mm at cap beam and footing, respectively. The C/D ratios for anchorage of column longitudinal reinforcement are presented in table 6-2. It is evident that there is insufficient anchorage of the column flexural reinforcement into the cap beam before retrofit. This would suggest vulnerability to an anchorage failure after a flexural mechanism has formed. This failure was observed in the laboratory experiment of the pre-retrofitted model pier bent. However, the ATC 6-2 method gives no indication of the level of ductility reduction due to such an anchorage failure.

Table 6-2. ATC 6-2 based C/D ratio for anchorage of column reinforcement.

Component and Location	Before Retrofit		After Retrofit	
	$l_a(c)/l_a(d)$	r_{ca}	$l_a(c)/l_a(d)$	r_{ca}
Column at Cap Beam	**0.89**	$0.89r_{ec}$	2.72	1.0
Column at Footing	1.42	1.0	1.79	$1.5r_{ef}$

r_{ca}= Anchorage C/D ratio for column reinforcement.
r_{ec}= Column moment C/D ratio.
r_{ef}= Footing moment C/D ratio.
Note: Boldface is for the critical case.

6.2.3 Splices in Longitudinal Reinforcement

The seismic C/D ratio for splices in longitudinal reinforcement r_{cs} is determined from the ratio of the provided (capacity) cross-sectional area of transverse hoops $A_{tr}(c)$ to the required (demand) minimum area of transverse reinforcement $A_{tr}(d)$.

The required minimum area of transverse reinforcement is given by

$$A_{tr}(d) = \frac{s f_y}{l_s f_{yt}} A_b \qquad \textbf{(6-6)}$$

where s= transverse hoop spacing, l_s= splice length, f_y= yield stress of the longitudinal steel, f_{yt}= yield stress of the transverse steel, and A_b = area of a spliced bar. It is assumed that the splice is adequate when

$$l_s \geq 154\, d_b / \sqrt{f'_c\ (MPa)}\ \ (mm);$$
$$A_{tr}(c) \geq A_{tr}(d);\ \text{and}$$
$$s \leq 150\, mm.$$

The C/D ratio with the adequate splice is calculated by

$$r_{cs} = \frac{A_{tr}(c)}{A_{tr}(d)} r_{ec} \leq 2\, r_{ec} \qquad \textbf{(6-7)}$$

The code notes that the extra splice length by itself does not significantly improve the inelastic response of splices.

The C/D ratio for splices with a inadequate splice length is then calculated by

$$r_{cs} = \frac{A_{tr}(c)}{A_{tr}(d)} \left[\frac{\left(\frac{150}{s}\right) l_s}{\left(\frac{154}{\sqrt{f'_c\,(MPa)}}\right) d_b} \right] r_{ec} \leq \frac{A_{tr}(c)}{A_{tr}(d)} r_{ec} \qquad \textbf{(6-8)}$$

where the ratio $150/s$ should not be taken larger than 1 and $154/\sqrt{f'_c\,(MPa)}$ should not be taken less than 30.

The longitudinal rebars were spliced at the bottom of columns by 381 mm and the calculated minimum area of transverse reinforcement is $A_{tr}(d) = 33\ mm^2$ while $A_{tr}(c) = 18\ mm^2$ was provided for the pre-retrofitted model pier. The determined C/D ratio for splices in column longitudinal reinforcement is $r_{cs} = 0.54 r_{ec}$. Though the lower C/D ratio predicts a failure in splices, no splice failure was observed from the laboratory experiment. In the retrofitted model pier, the spliced part was embedded in the new foundation beam.

6.2.4 Column Shear

The initial shear resistance $V_i(c)$ with assumed 45° diagonal shear crack adopted from ACI *(1989)* is given by

$$V_i(c) = V_c + V_s = 0.167 \sqrt{f'_c\,(MPa)}\, b_c\, d + A_v f_{yh} \frac{d}{s} \qquad \textbf{(6-9)}$$

where b_c = column width, A_v = area of shear reinforcement, f_{yh} = yield strength of a transverse hoop, d = effective depth = $0.8D$ (D = column diameter), and s = center-to-center spacing of a

transverse hoops. The final shear resistance $V_f(c)$ with assumption of $V_c = 0$ when the axial stress is less than $0.1f'_c$ is given by

$$V_f(c) = V_s = A_v f_{yh} \frac{d}{s} \qquad \textbf{(6-10)}$$

The shear demand due to plastic mechanism overstrength is calculated as $V_u(d) = 1.3\,\Sigma M_u / L_c$, where ΣM_u = sum of nominal moments at top and bottom of a column and L_c = clear height of a column. The maximum elastic shear force demand $V_e(d)$ is calculated by the single-mode spectral analysis.

The C/D ratio for column shear r_{cv} is determined by

$$r_{cv} = \frac{V_i(c)}{V_e(d)} \le r_{ec} \quad for\ V_i(c) < V_u(d) \qquad \textbf{(6-11a)}$$

$$r_{cv} = \mu\, r_{ec} \quad for\ V_i(c) \ge V_u(d) \qquad \textbf{(6-11b)}$$

where μ = ductility indicator. Equation (6-11a) is used when columns are insufficient to withstand the maximum shear force due to plastic hinges at column ends. Such columns may suffer a brittle shear failure prior to formation of a plastic mechanism. Equation (6-11b) is used when the initial shear resistance of a column is sufficient to withstand the maximum shear force due to a plastic mechanism. The ductility indicator depends on the amount of flexural yielding and is determined by

$$\mu = 2 + \left(0.75 \frac{L_c}{b_c}\right) \frac{V_i(c) - V_u(d)}{V_i(c) - V_f(c)} \quad for\ V_f(c) < V_u(d) \qquad \textbf{(6-12a)}$$

$$\mu = 2 + 0.75 \frac{L_c}{b_c} \quad for\ V_f(c) \ge V_u(d) \qquad \textbf{(6-12b)}$$

where L_c = column height and $L_c / b_c \le 4$. It is assumed that the initial shear capacity $V_i(c)$ is maintained up to $\mu = 2$ and the final shear capacity $V_f(c)$ is effective at $\mu \ge 5$, and linear interpolation of shear capacity is made between them.

For the model pier, the theoretical initial and final shear capacities for each column are $V_i(c) = 100kN$ and $V_f(c) = 22kN$, respectively. Plots for overall model pier shear capacity and demand before and after retrofit are presented in figure 6-1 and compared to the experimental results. This graph shows an average of absolute values of experimental maximum and minimum force and displacement responses at each cycle. The sum of theoretical column shear capacities and demands are also plotted. The calculated C/D ratios for column shear are presented in table 6-3. Since $V_i(c) < V_u(d)$ in the leeward exterior column of the pre-retrofitted model pier, a brittle shear failure is predicted in the column. However, brittle shear failure was not observed in the pre-retrofitted model pier column because a joint shear failure at the knee joint kept the column from forming a flexural mechanism. The ductility factor of the overall model pier due to column shear before retrofit is calculated as $\mu = 2.85$ using the sum of shear capacities and demands for all columns. For the post-retrofitted model pier, all columns are theoretically susceptible to brittle shear failure at a displacement ductility factor of $\mu < 1$. However, experimental results show that the column shear capacity was maintained up to a ductility factor of $\mu = 3$. Clearly the ATC 6-2 evaluation approach is overly conservative in the analysis of column shear.

Table 6-3. ATC 6-2 based C/D ratios for column shear (r_{cv}).

Component and Location	$V_i(c)$ (kN)	$V_f(c)$ (kN)	$V_u(d)$ (kN)	$V_e(d)$ (kN)	μ	r_{cv}
Before Retrofit						
Windward Ext Col	100	21.7	71.2	137.5A	3.83	$3.83r_{ec}$
Interior Column	100	21.7	87.7	183.3A	2.78	$2.78r_{ec}$
Leeward Ext Col	100	21.7	**101.0**	137.5A	< 1	$1.0r_{ec}$
After Retrofit						
Windward Ext Col	100	21.7	**101.9**	171.6A	< 1	$1.0r_{ec}$
Interior Column	100	21.7	**125.5**	228.8A	< 1	$1.0r_{ec}$
Leeward Ext Col	100	21.7	**146.4**	171.6A	< 1	0.58/A

r_{ec}= Column moment C/D ratio.
Note: Numbers in boldface are for critical cases.

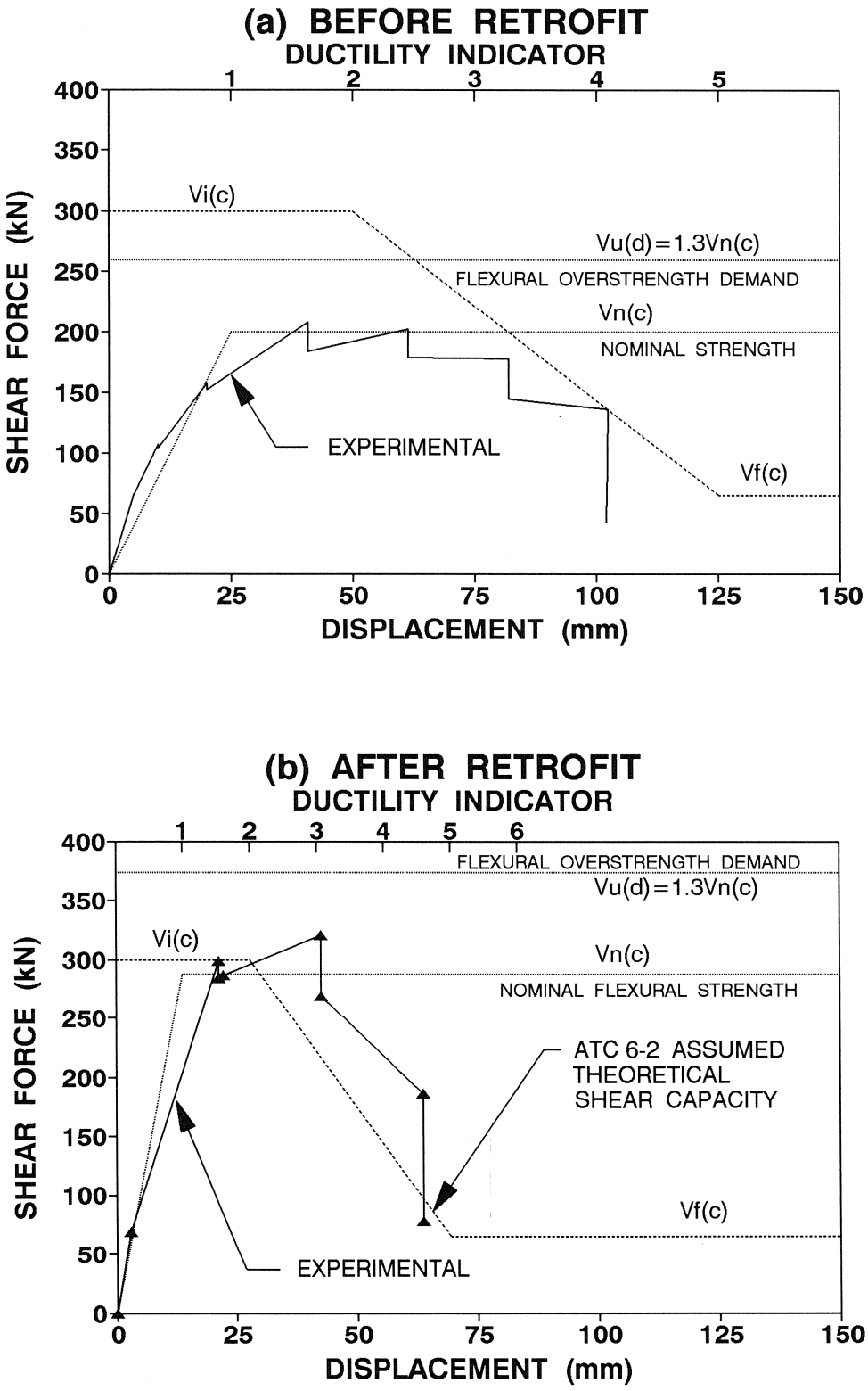

Figure 6-1. Overall shear strength of model pier based on ATC 6-2 recommendations.

6.2.5 Transverse Confinement Reinforcement

The New Zealand concrete code *(NZS 3101, 1982)* requires the maximum spacing of transverse steel for adequate concrete confinement to be the lesser of $6d_b$ or $0.2b_{min}$. This requirement enables columns to dependably withstand cyclic loading corresponding to a displacement ductility factor of $\mu \geq 6$. ATC 6-2 adopted the NZS 3101 equations for evaluating confinement for columns that violate these confinement requirements. The ductility indicator should be adjusted by the following equation

$$\mu = 2 + 4\left(\frac{k_1 + k_2}{2}\right)k_3 \qquad \textbf{(6-13)}$$

where

$$k_1 = \frac{\rho(c)}{\rho(d)\left(0.5 + \dfrac{1.25P_c}{f'_c A_g}\right)} \leq 1$$

$$k_2 = 6d_b/s \leq 1 \quad or \quad 0.2b_{min}/s \leq 1, \quad \textit{whichever is smaller}$$

for well anchored transverse bars,

$$k_3 = 1$$

for poorly anchored transverse bars,

$$k_3 = 1 \quad (\mu \leq 2)$$
$$k_3 = -0.25\mu + 1 \quad (2 \leq \mu \leq 4)$$
$$k_3 = 0 \quad (\mu \geq 4)$$

where $\rho(c)$= volumetric ratio of existing transverse reinforcement, $\rho(d)$= required volumetric ratio of transverse reinforcement given by the AASHTO specification, P_c= axial compression load on the column, f'_c= concrete compressive strength, A_g= column gross section area, s= spacing of transverse steel, d_b= column longitudinal bar diameter, and b_{min}= minimum width of column cross section. Since equation (6-13) and the parameter k_3 are inter-related, the ductility indicator needs to be calculated by iteration.

The C/D ratio for transverse confinement r_{cc} is thus given by

$$r_{cc} = \mu r_{ec} \quad \textbf{(6-14)}$$

For the model pier columns before and after retrofit, confinement was not adequate. Equation (6-13) gives the adjusted ductility indicator as $\mu = 2.5$. This gives the transverse confinement C/D ratio $r_{cc} = 2.5 r_{ec}$ for both the pre-retrofitted and the post-retrofitted model piers.

6.2.6 Summary of ATC 6-2 Method

The calculated ATC 6-2 based C/D ratios are summarized in table 6-4. The predictive C/D equations in this table are also plotted in figure 6-2 and compared with results inferred from the experimental observations. For the overall model pier, the average of three columns is taken as a representative value. The predicted column shear C/D ratio for the pre-retrofitted model pier is conservatively close to the experimentally observed one, but the post-retrofitted model pier column shear C/D ratio was not well predicted. However, the closeness for the pre-retrofitted model pier is misleading because the specimen behavior was not limited by column shear. This method predicts that shear strength and transverse confinement of the pre-retrofitted model pier

Table 6-4. Summary of ATC 6-2 based evaluation results.

Description		Before Retrofit	After Retrofit
Elastic Limit, r_{ec}		0.44/A	0.50/A
Column Shear, r_{cv}		$2.85r_{ec}$= 1.25/A[b]	$1.0r_{ec}$= **0.51/A**[c]
Ductile-Flexure, r_{cc}		$2.5r_{ec}$= **1.10/A**	$2.5r_{ec}$= 1.28/A
Experimental, r_{exp}[a]		$3.0r_{ec}$= 1.32/A	$3.0r_{ec}$= 1.53/A
Failure Modes	ATC Predicted	Column Confinement	Brittle Column Shear
	Observed	Joint Shear/Anchorage	Ductile Column Shear

[a]Based on experimentally observed displacement ductility factor.
[b]$V_i(c) > V_u(d)$.
[c]$V_i(c) < V_u(d)$ that implies a possible brittle shear failure.
Note: Boldface case governs.

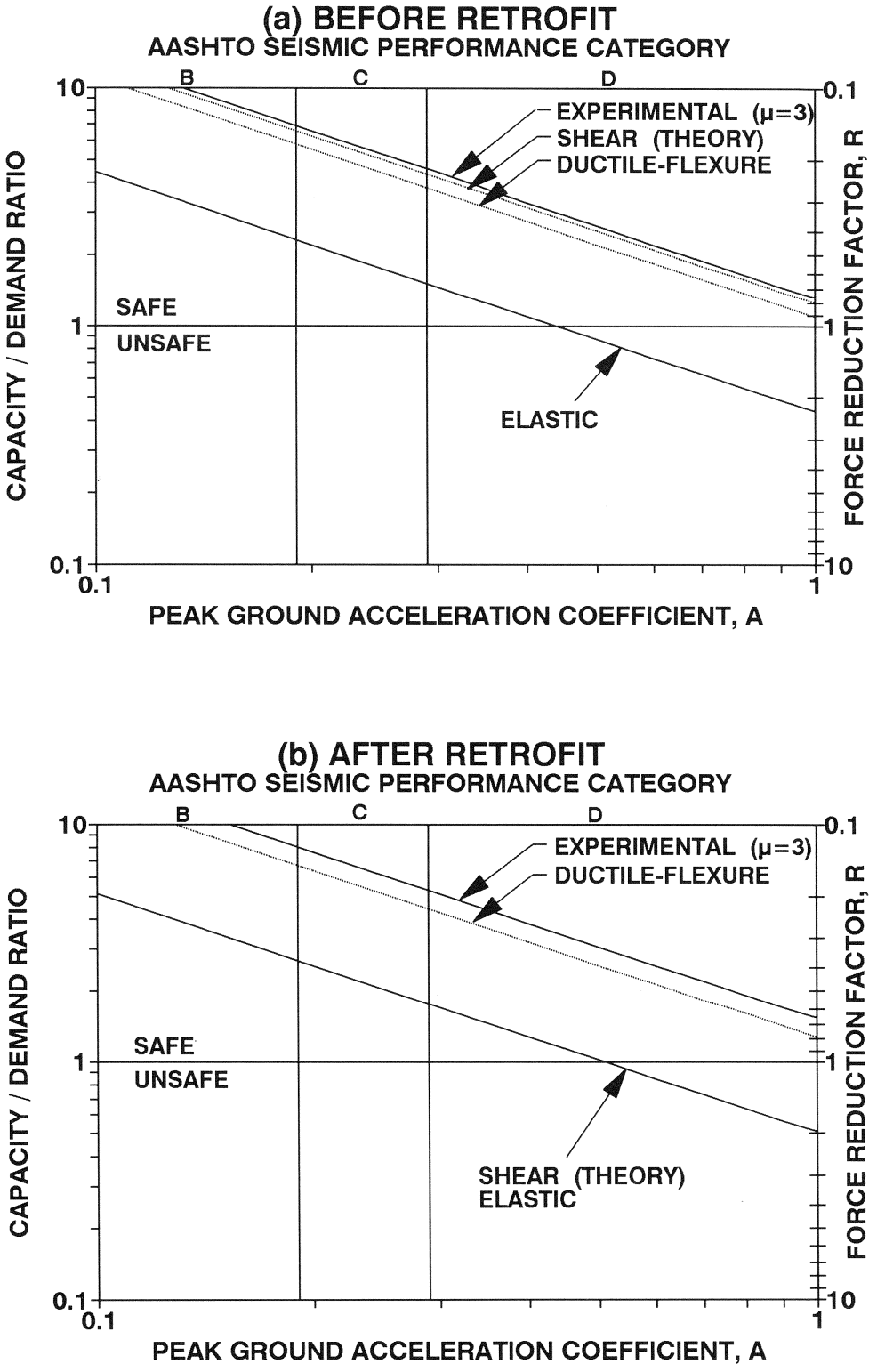

Figure 6-2. ATC 6-2 based C/D ratios for model pier.

can sustain the credible earthquake (PGA ≈ 1.2 g). However, this prediction is made on the assumption that beam-column joints have sufficient strength which in reality was not the case. The threshold of PGA for the onset of inelastic behavior is predicted as 0.44 g and 0.50 g for the pre-retrofitted and the post-retrofitted model pier, respectively.

6.3 Evaluation by Equivalent Lateral Strength Method

The equivalent lateral strength method of evaluation sometimes referred as the "push-over" method was first proposed by Priestley, et al. *(1992)* and is the second method recommended in the FHWA Retrofitting Manual *(Buckle and Friedland, 1995)*. This is recommended as an alternative approach to the ATC 6-2 based C/D ratio method described previously. The report points out two uncertainties in the ATC 6-2 based evaluation method: i) the assumed elastic response is of doubtful validity ; and ii) the force reduction factors may be a very poor indicator of member ductility demand. As a consequence, in this alternative evaluation procedure, a simple inelastic frame by frame push-over method is considered. An incremental collapse mechanism approach is applied to a frame (pier bent) to identify the critical elements and define the load-deformation curve for the frame (push-over analysis). Assessment of ductility capacity, integrity of lap splices, anchorage of reinforcement, and shear capacity of connections between members are considered.

6.3.1 Flexural Ductility

The flexural ductility capacity of a pier member can be calculated by considering a simple vertical cantilever element shown in figure 6-3. Assuming a linear elastic curvature distribution over the length l (from the point of maximum moment to the contraflexure point), then the yield displacement Δ_y and yield drift θ_y are given by

$$\Delta_y = \frac{\phi_y l^2}{3} \qquad \textbf{(6-15a)}$$

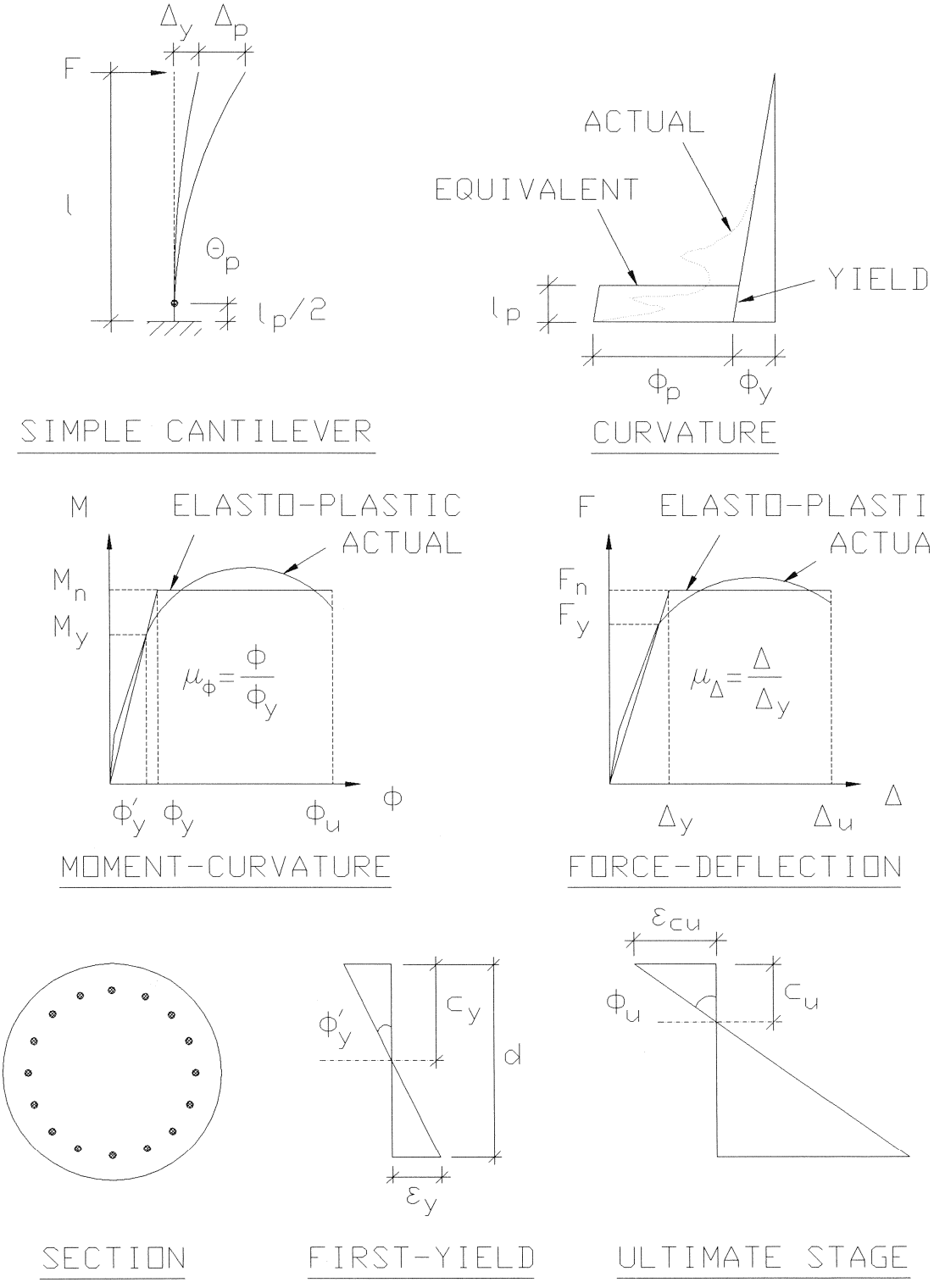

Figure 6-3. Calculation of flexural ductility using a simple cantilever column.

$$\theta_y = \frac{\Delta_y}{l} = \frac{\phi_y l}{3} \qquad \textbf{(6-15b)}$$

where ϕ_y= yield curvature.

If it is assumed that plastic curvature ϕ_p is constant over the length of an equivalent plastic hinge l_p, then the plastic hinge rotation θ_p and plastic displacement Δ_p at the cantilever tip can be calculated by

$$\theta_p = \phi_p l_p \qquad \textbf{(6-16a)}$$

$$\Delta_p = \theta_p (l - l_p/2) \qquad \textbf{(6-16b)}$$

where $l_p = 0.08l + \chi d_b$ ($\chi = 6$ for grade 40 rebar and 9 for grade 60 rebar and d_b= diameter of longitudinal reinforcement). Then the displacement ductility factor μ_Δ and the critical section curvature ductility factor μ_ϕ are obtained by

$$\mu_\Delta = 1 + \frac{\Delta_p}{\Delta_y} \qquad \textbf{(6-17a)}$$

$$\mu_\phi = 1 + \frac{\phi_p}{\phi_y} \qquad \textbf{(6-17b)}$$

where both μ_Δ and μ_ϕ are based on an elasto-plastic approximation of the force-deformation relationship. The equivalent elasto-plastic yield curvature ϕ_y is extrapolated from the curvature at first yield

$$\phi_y = \frac{M_n}{M_y}\phi'_y \qquad \textbf{(6-18)}$$

in which M_n= nominal moment capacity, M_y= first yield moment and the curvature at first yield is given by $\phi'_y = \varepsilon_y/(d - c_y)$ where ε_y= yield strain of the longitudinal reinforcement, d= effective depth of the member and c_y= neutral axis depth (from extreme compression fiber) at first yield. An ultimate compression strain of $\varepsilon_{cu} = 0.005$ is recommended for unconfined concrete.

The calculated ductility factors of the model pier columns before and after retrofit are presented in table 6-5. Since the columns were not retrofitted, ductility factors before and after retrofit are close. There is a difference in yield drift values between the experiment and theory. The experimentally determined yield drift is 1.25 % and 1 % for the pre- and post-retrofitted model pier, respectively. The difference is due to the cap beam and foundation flexibility.

Table 6-5. Flexural ductility factors of the model pier columns.

Component	Columns Before Retrofit			Columns After Retrofit		
	Windward	Interior	Leeward	Windward	Interior	Leeward
M_y[a] (kN-m)	33.9	44.8	55.3	34.6	46.3	57.7
M_n (kN-m)	50.8	62.5	72.2	51.7	63.7	74.3
l (mm)	927	927	927	660	660	660
l_p (mm)	160	160	160	140	140	140
ϕ'_y[b]D[c]	0.0035	0.0037	0.004	0.0035	0.0038	0.004
$\phi_y D$	0.0052	0.0052	0.0052	0.0052	0.0052	0.0052
$\phi_u D$	0.026	0.021	0.018	0.0256	0.0206	0.0174
μ_ϕ	5.0	4.04	3.46	4.92	3.96	3.35
θ_y (%)	0.572	0.575	0.572	0.411	0.407	0.407
θ_p (%)	1.2	0.909	**0.734**	1.0	0.771	**0.612**
Δ_y (mm)	5.3	5.3	5.3	2.7	2.7	2.7
Δ_p (mm)	10.2	7.7	6.2	5.9	4.6	3.6
Δ_u (mm)	15.5	13.0	11.5	8.6	7.3	6.3
μ_Δ	2.92	2.44	**2.17**	3.17	2.69	**2.34**

[a]Moment at first yield.
[b]Curvature at first yield.
[c]D= column diameter= 279 mm.
Note: Boldface is for critical cases.

The force-deformation plots based on a push-over analysis performed using the static options in the computer program DRAIN-2DX *(Prakash, et al., 1992a,b)* for the model pier bent before and after retrofit are presented in figure 6-4. For the push-over analysis an effective moment of inertia needs to be used which accounts for cracking in the members. This is primarily a function of the level of axial load or prestress. Based on a rational analysis of the elastic moment-curvature behavior, the effective flexural rigidities, used subsequently in the non-linear push-over analysis, were computed as follows:

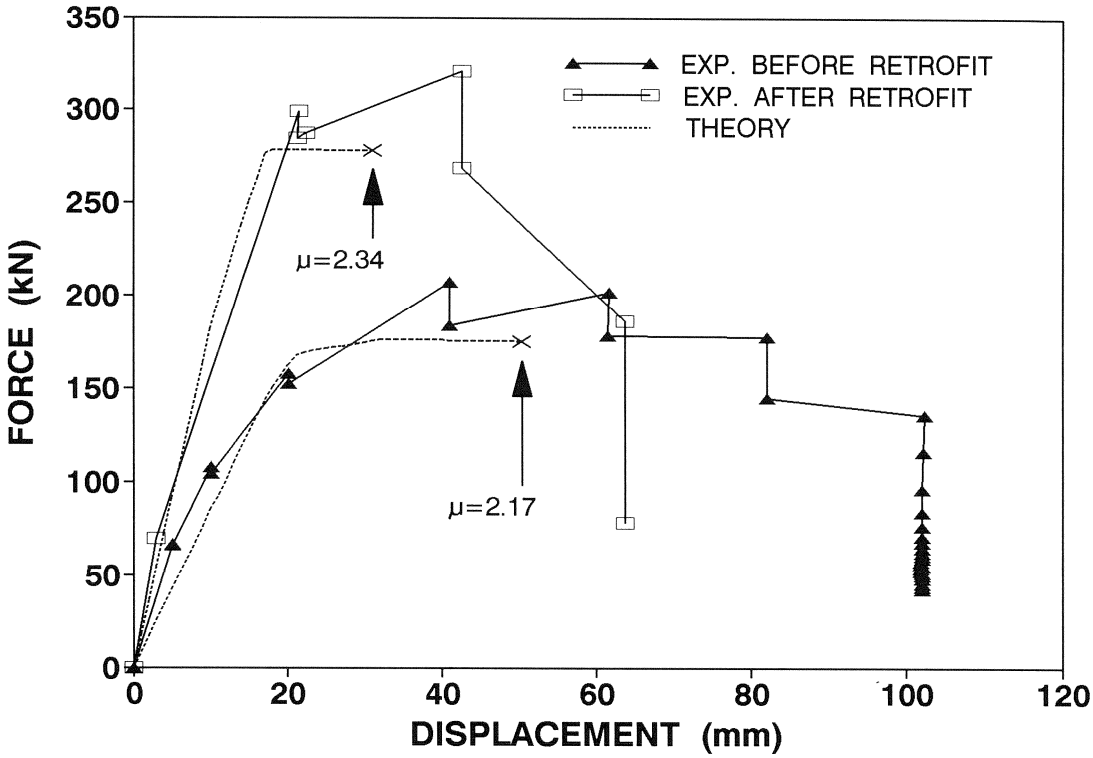

Figure 6-4. Push-over analysis for model pier.

$$\frac{EI_{eff}}{EI_g} = \frac{M_y' L^2}{3EI_g \Delta_y'} \qquad \textbf{(6-19)}$$

in which M_y'= moment at first yield of the longitudinal steel (or first crushing of column concrete at high axial load level), EI_g= gross section rigidity based on concrete alone, $L = M/V$ is shear span, and Δ_y'= displacement at first yield given by the first moment of area of the curvature diagram, that is,

$$\Delta_y = \int_0^L x\, \phi(x)\, dx \qquad \textbf{(6-20)}$$

For the present study, the following results were obtained and used in the non-linear push-over analysis:

Columns: $EI_{eff} = 0.15\, EI_g$ before retrofit and $0.10\, EI_g$ after retrofit;
Cap beams: $EI_{eff} = 0.32\, EI_g$ before retrofit and $0.10\, EI_g$ after retrofit; and
Foundation: $EI_{eff} = 0.32\, EI_g$ before and after retrofit.

The displacement ductility factor μ_Δ of the model pier before and after retrofit in the figure indicates the limit state and is defined as a member ductility at which the member first reaches its critical plastic hinge rotation capacity before any other members. Since the plastic hinge rotation capacity of the leeward column is the smallest one in table 6-5, the corresponding displacement ductility factor was used for the whole model pier before and after retrofit. In calculation of the force-displacement relationship, it is assumed that anchorage and splice in reinforcement, shear strength of members, and joint shear are sufficient to generate the maximum flexural strength in members.

6.3.2 Flexural Strength - Splices and Anchorages

6.3.2.1 Splices at Column Base

Refer to rebar type 6 in figure 6-5 for location. The minimum length of inadequately confined spliced bars for a circular column section can be calculated using the concrete tensile force on the assumed rupture surface at failure, thus,

$$l_{s_{\min}} = \frac{A_b f_s}{f_t \left[\frac{\pi D'}{2n} + 2(d_b + c) \right]} \qquad \textbf{(6-21)}$$

where A_b= spliced bar sectional area, f_s= column steel stress depending on the mechanism, f_t= concrete tensile strength= $0.33\sqrt{f'_c\,(MPa)}$, D'= pitch diameter of the hoop, n= number of spliced bars, d_b= bar diameter, c= concrete cover, and f'_c= concrete compressive strength. If $f_s > f_y$, the bar can develop its yield strength and the initial ideal flexural strength of the column may be developed. To prevent bond failure at high ductilities, $f_s = 1.5 f_y$ should be used. For a circular column with transverse hoops of cross sectional area A_h at spacing s, the effective confining stress f_l is given by

$$f_l = \frac{400 A_h}{D' s} \quad (MPa) \qquad \textbf{(6-22)}$$

where dilation strain $\varepsilon_d = 0.001$ and $E_s = 200\,GPa$ are recommended. Using the effective confining stress, the minimum length of adequately confined lap spliced column bars for a circular column section to prevent bond failure at high ductilities is given by the greater of

$$l_{s_{\min}} = \frac{1.5 A_b f_y}{1.4 f_l \left[\frac{\pi D'}{2n} + 2(d_b + c) \right]} \qquad \textbf{(6-23a)}$$

and

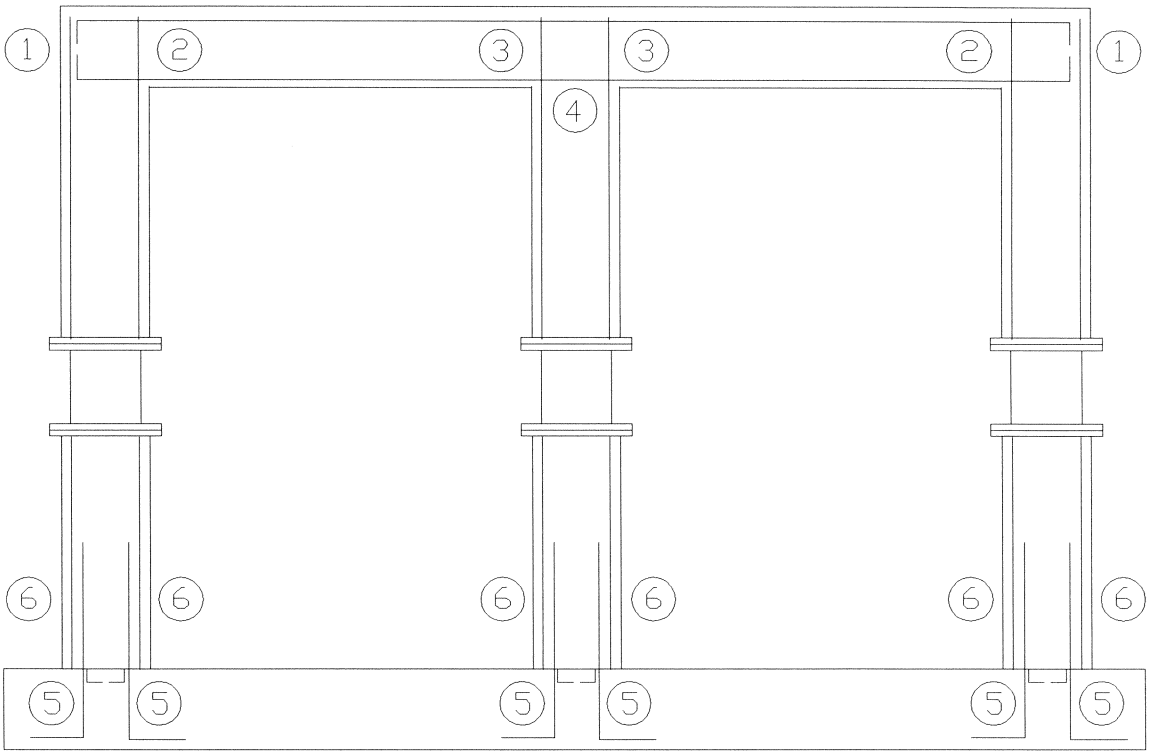

Figure 6-5. Location of spliced and anchored column steel bars of model pier.

$$l_{s_{\min}} = \frac{0.25\, d_b f_y}{\sqrt{f'_c\ (MPa)}} \qquad \textbf{(6-23b)}$$

where f_y = spliced bar yield strength.

For the pre-retrofitted model pier, column rebars were spliced at the bottom with dowels embedded into the foundation with 90° hook at the column base. Applying the appropriate values to equation (6-21) with $f_s = 1.5 f_y$, the required minimum lap length is $l_{s_{\min}} = 278\ mm$. However, this value may not be reliable, because attainment of full tensile strength cannot be expected from widely cracked unconfined concrete at large ductility. The effective confining stress with a 4.8 mm diameter transverse hoop is calculated as $f_l = 0.323\ MPa$ giving the required minimum lap length of $l_{s_{\min}} = 1538\ mm$ using equation (6-23) with appropriate values. As $l_{s_{provided}} = 381\ mm$, failure in lap splices is expected. However, it was observed from the laboratory experiment that no splices failed. This discrepancy is due to the column size effect built into equation (6-23) so that the required minimum lap length may be over-estimated for the scale model. Lap splice problems for the post-retrofitted model pier were avoided by casting the new foundation beam.

6.3.2.2 Straight Anchorage of Column Rebars at Outside of the Knee Joint

Refer to rebar type 1 in figure 6-5 for location. The adequacy of the straight anchorage at the outside of the knee joint depends on the type of flexural mechanism and presence of confinement. The required minimum anchorage length is determined by the following equations:

1. Weak column / strong beam:

   without confinement: equation (6-21) with $f_s = 1.5 f_y$.

   with confinement: equations (6-23a) and (6-23b) substituting $l_{a_{\min}}$ for $l_{s_{\min}}$.

2. Strong column / weak beam:

   without confinement:

$$l_{a_{\min}} = \frac{A_b f_y}{f_t \left[\frac{\pi D'}{2n} + 2 (d_b + c) \right]} \qquad \textbf{(6-24a)}$$

with confinement:

$$l_{a_{\min}} = \frac{A_b f_y}{1.4 f_l \left[\frac{\pi D'}{2n} + 2(d_b + c) \right]} \qquad \textbf{(6-24b)}$$

6.3.2.3 Straight Anchorage of Column Rebars at Inside of the Knee Joint

Refer to rebar 2 type in figure 6-5 for location.

1. Weak column / strong beam:
   The required minimum anchorage is calculated by equation (6-23b), substituting $l_{a_{\min}}$ for $l_{s_{\min}}$.

2. Strong column / weak beam:
   The minimum anchorage without additional confinement from the transverse reinforcement is given by

$$l_{a_{\min}} = \frac{A_b f_y}{f_t s} \qquad \textbf{(6-25)}$$

where s = center to center spacing of the bars.

6.3.2.4 Straight Anchorage of Column Rebars at T-Joint

Refer to rebar type 3 in figure 6-5 for location. Anchorages in this category may be checked with the equations for the straight anchorage of column rebars at inside of the knee joint.

6.3.2.5 Straight Anchorage of Beam Bottom Rebars at Joints

Refer to rebar type 4 in figure 6-5 for location.

1. Weak column / strong beam under opening moment:
   The minimum development length is calculated by equation (6-25).

2. Strong column / weak beam:
   The development length is checked with equation (6-23b).

6.3.2.6 Bent-out Anchorage of Column Rebars at Foundation

Refer to rebar type 5 in figure 6-5 for location. The bent-out anchorage is normally considered adequate. However, the practice of bending the column bars out may produce an undesirable situation in transferring moment between column and footing. It is thus recommended that such L-shaped anchorages face in toward the joint and not outward.

6.3.2.7 Model Pier Anchorage Evaluation Results

The required minimum anchorage of column steel at the knee joint and the T-joint in cap beam is compared to the provided anchorage in table 6-6. For the post-retrofitted model pier, the effective confining stress of $f_l = 4.0 MPa$ due to cap beam prestressing was used to calculate the

Table 6-6. Column reinforcement anchorage evaluation results.

Anchorage Location	Before Retrofit (mm)		After Retrofit (mm)	
	$(l_a)_{min}$	$(l_a)_{provided}$	$(l_a)_{min}$	$(l_a)_{provided}$
Outside of Knee Joint	187	254	125	406
Inside of Knee Joint	**303**	254	150	406
At T-Joint	**303**	254	150	406

Note: Boldface is for critical cases.

required minimum anchorage. The column rebar anchorage at foundation before and after retrofit is considered adequate, since the standard hook with 90° was provided for the pre-retrofitted model pier and anchorage length of 381 mm with $f_l = 2.5\,MPa$ due to confining steel at the new foundation level was provided for the post-retrofitted model pier. The comparison shows that all column rebars have insufficient anchorage except the bars at outside of the knee joint for the pre-retrofitted model pier. This is due to the equations suggested by *(Priestley, et al., 1992)* in which the postulated fracture surface for outside of the knee joint is larger than that for inside of the knee joint. Accordingly, the anchorage demand for outside of the knee joint becomes smaller than that for inside of the knee joint. It was observed from the laboratory experiment for the pre-retrofitted model pier that anchorages at cap beam/column joints loosened as the displacement ductility increased due to insufficient joint bond strength and confinement. Cap beam bottom bars were anchored with hooks at the knee joints and continued over the column at the T-joint. Therefore, it is considered not necessary to check the adequacy of anchorage for those bars.

6.3.3 Column Shear Strength

This evaluation procedure for column shear strength is based on the recent version of Priestley et al. *(1994)*. The column shear demand V_{if} is defined as a shear force at the maximum flexural response and expressed as

$$V_{if} = (M_t + M_b)/l \qquad \textbf{(6-26)}$$

where M_t = flexural strength at column top, M_b = flexural strength at column base and l = column clear height.

The column shear strength is given by

$$V_n = V_c + V_t + V_p \qquad \textbf{(6-27a)}$$

and

$$V_c = 0.8 A_g k \sqrt{f'_c \ (MPa)} \qquad \textbf{(6-27b)}$$

$$V_t = \frac{\pi}{2} A_{sh} f_{yh} \frac{D'}{s} \cot 30° \qquad \textbf{(6-27c)}$$

$$V_p = P \tan \alpha \qquad \textbf{(6-27d)}$$

where V_c= shear carried by concrete, V_t= shear carried by truss mechanism, V_p= shear carried by axial compression, k= coefficient of concrete shear strength, and $\tan\alpha \approx D'/l$ for double curvature column.

The concrete shear strength coefficient k for uni-directionally applied lateral load is determined by the shear ductility μ_s in which shear failure is expected. The coefficient k is taken as 0.29 for brittle shear failure ($\mu_s \leq 2$), 0.1 for ductile shear failure ($\mu_s \geq 4$), and linear interpolation is made in between them. The shear ductility μ_s is determined by comparing the shear demand V_{if} to the brittle shear strength V_{ni} and the ductile shear strength V_{nd} as follows:

$$\mu_s \leq 1 \quad (V_{if} \geq V_{ni}) \qquad \textbf{(6-28a)}$$

$$\mu_s = \mu_f \quad (V_{if} \leq V_{nd}) \qquad \textbf{(6-28b)}$$

$$\mu_s = 2 + 2\left(\frac{V_{ni} - V_{if}}{V_{ni} - V_{nd}}\right) \quad (V_{nd} \leq V_{if} \leq V_{ni}) \qquad \textbf{(6-28c)}$$

where μ_f= flexural ductility.

The calculated column shear demand, capacity and ductility for each column of the model pier before and after retrofit are summarized in table 6-7. Comparative plots for the overall model pier column shear strength and demand along with experimental results are also presented in figure 6-6. It is noted from the table and the figure that the displacement ductility factor due to column shear seems to be more appropriately predicted than in the ATC 6-2 based results. Shear failure is not predicted in any ductility level for the pre-retrofitted model pier, while it is

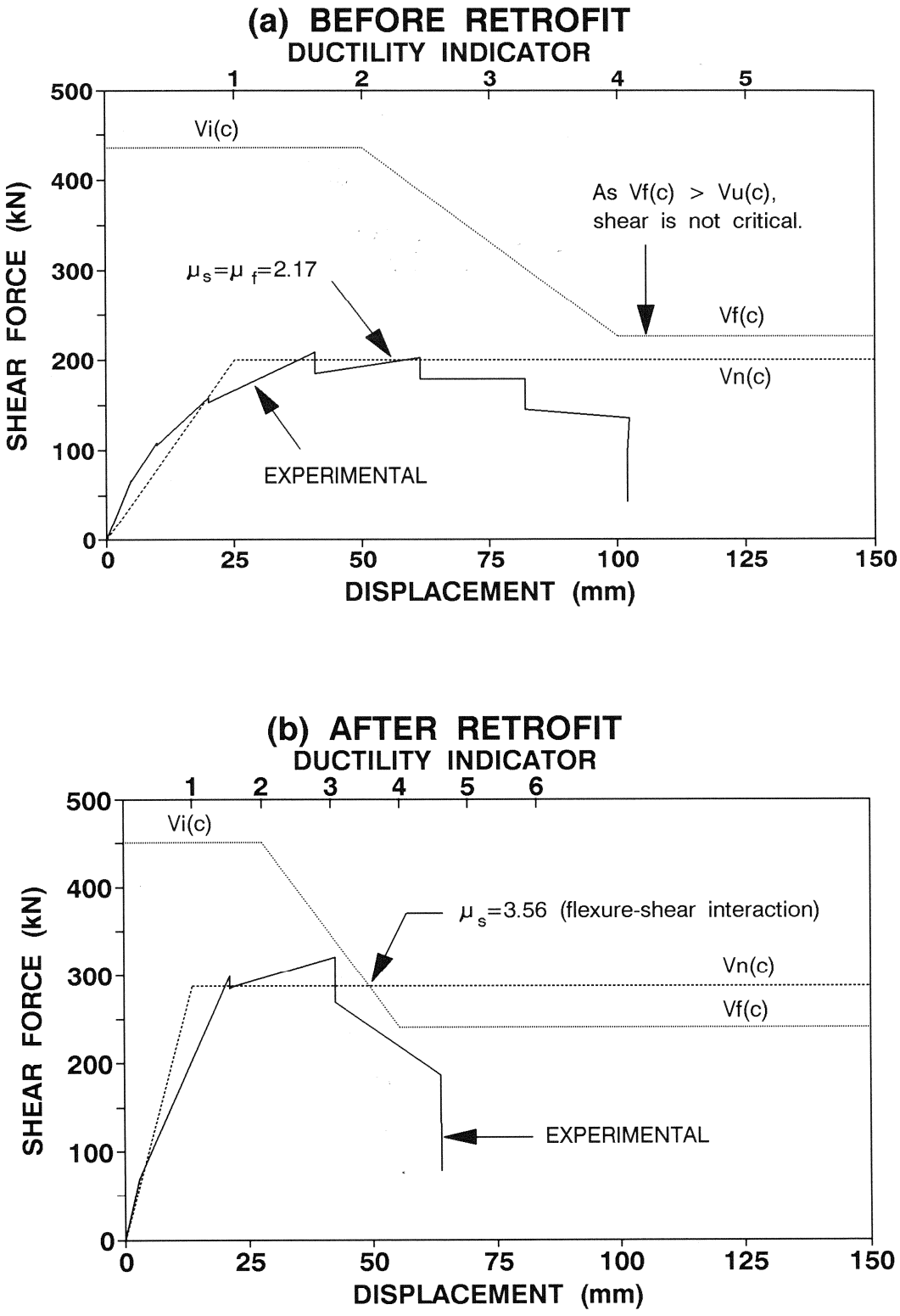

Figure 6-6. Column shear strength after Priestley, et al. (1994).

Table 6-7. Model pier column shear capacities and demands.

Component	Columns Before Retrofit			Columns After Retrofit		
	Windward	Interior	Leeward	Windward	Interior	Leeward
V_{ni} (kN)	130.3	145.3	160.3	127.7	150.3	173.1
V_{nd} (kN)	60.2	75.2	90.2	57.6	80.2	103
V_{if} (kN)	54.7	67.4	77.8	78.2	96.4	112.5
μ_s	2.92[a]	2.44[a]	**2.17**[a]	**3.4**	3.5	3.7

[a]Flexural displacement ductility factor μ_f is used for μ_s.
Note: Boldface is for critical cases.

predicted at the displacement ductility of $\mu_s = 3.56$ for the overall post-retrofitted model pier using sum of shear capacities and demands of all columns.

6.3.4 Joint Shear Strength

Joint shear force demands due to interaction between elements are calculated from equilibrium consideration at joint boundaries. For positive (opening) moment at knee joints shown in figure 6-7(a), the joint shear forces are

$$V_{jh} = C_B \qquad \textbf{(6-29a)}$$

$$V_{jv} = C_C = V_{jh} h_b / h_c \qquad \textbf{(6-29b)}$$

where V_{jh}= horizontal joint shear, C_B= flexural compression force in cap beam due to the moment, V_{jv}= vertical joint shear, C_C= flexural compression force in column due to the moment, h_b= overall depth of cap beam, and h_c= overall depth of column.

For negative (closing) moment at knee joints shown in figure 6-7(b), the joint shear forces are

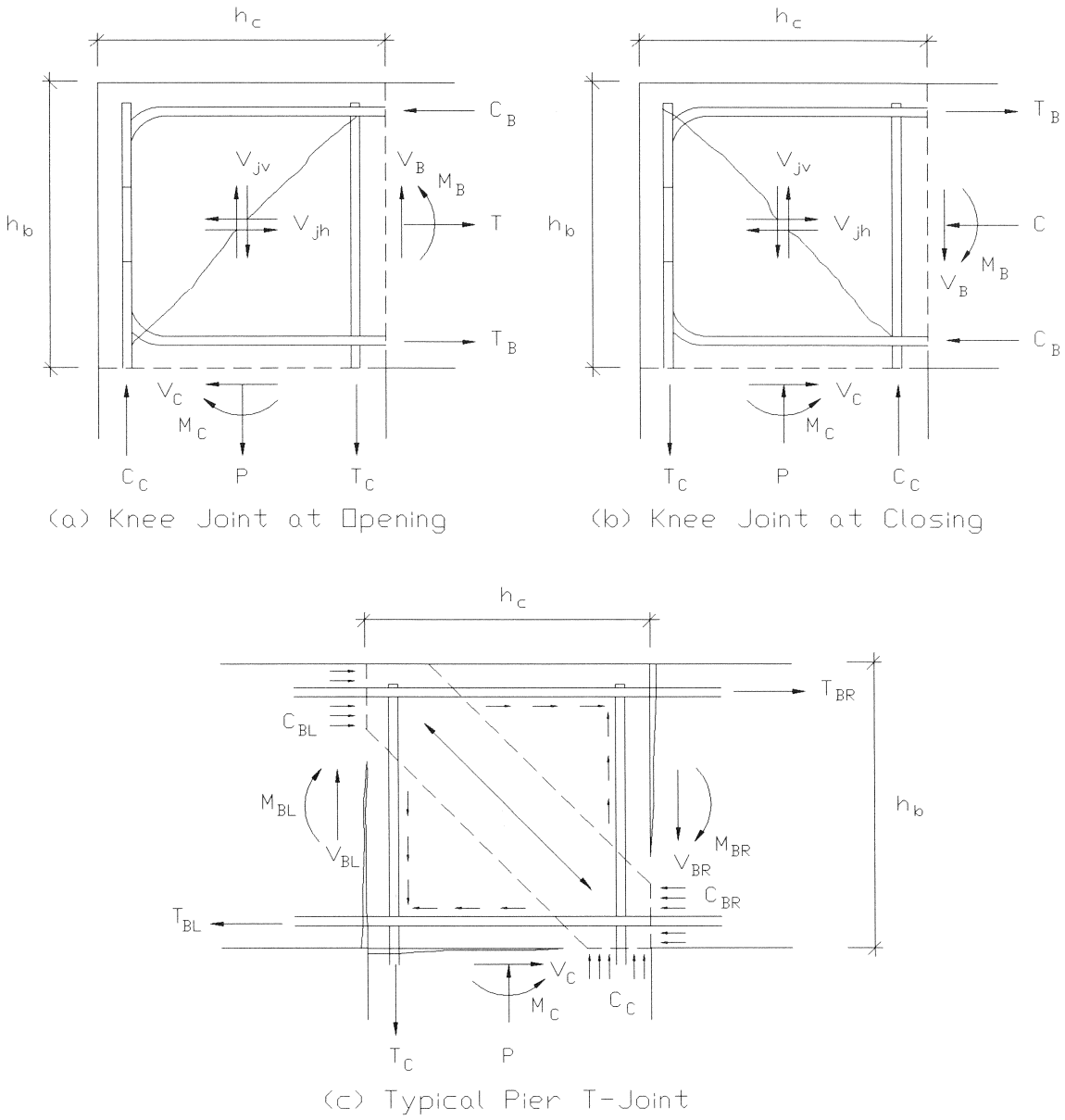

Figure 6-7. Force equilibrium at joints after Priestley, et al. *(1992)*.

$$V_{jh} = T_B = C_B - C \tag{6-30a}$$

$$V_{jv} = T_C = C_C - P = V_{jh} h_b / h_c \tag{6-30b}$$

where T_B= flexural tension force in cap beam due to the moment, C= compression force in cap beam due to the seismic overturning moment, T_C= flexural tension force in column due to the moment, and P= axial load due to gravity and earthquake.

The horizontal joint shear force at T-joints shown in figure 6-7(c) is given by

$$V_{jh} = T_{BR} + C_{BL} = \frac{1}{jd}(M_{BR} + M_{BL}) \tag{6-31}$$

where T_{BR}= flexural tension force at right hand side of the joint due to the moment, C_{BL}= flexural compression force at the left hand side of the joint due to the moment, $jd = 0.75 h_b$, M_{BR}= moment at the right hand side of the joint, and M_{BL}= moment at the left hand side of the joint. The vertical joint shear force of T-joint is also given by equation (6-29b).

The joint shear stress is then calculated by

$$v_{jh} = \frac{V_{jh}}{h_c b} \tag{6-32}$$

where b= joint width. The principal tensile stress demand f_t at joints due to the member flexure is then determined by

$$f_t = \sqrt{\left(\frac{f_a}{2}\right)^2 + v_{cj}^2} - \left(\frac{f_a}{2}\right) \tag{6-33}$$

The calculated principal joint stresses at joints for the model pier before and after retrofit are summarized in table 6-8.

Table 6-8. Principal stresses at joints of the model pier.

Component & Location	Before Retrofit				After Retrofit			
	f'_c (MPa)	f_a[a] (MPa)	v_{cj} (MPa)	$\frac{f_t}{\sqrt{f'_c}}$	f'_c (MPa)	f_a[a] (MPa)	v_{cj} (MPa)	$\frac{f_t}{\sqrt{f'_c}}$
Windward Col/Cap Beam	73.1	-0.77	1.86	0.27	61.4	-0.92	1.98	0.21
Windward Col/Footing	56.6	-0.77	2.59	0.4	29.7	-0.92	1.14	0.22
Interior Column/Cap Beam	73.1	0.54	3.35	0.37	61.4	0.75	2.5	0.07
Interior Column/Footing	56.6	0.54	3.24	0.4	29.7	0.75	1.44	NA[b]
Leeward Col/Cap Beam	73.1	1.85	1.84	0.13	61.4	2.44	3.42	0.04
Leeward Col/Footing	56.6	1.85	2.59	0.24	29.7	2.44	1.97	NA[b]

[a]Positive f_a is axial stress in compression.
[b]No tensile stress is generated.

The joint shear failure model proposed by *(Priestley, et al., 1992)* indicates three limiting conditions as shown in figure 6-8.

1. Elastic Joint: $f_t < 0.29\sqrt{f'_c(MPa)}$

In this class of joint, a flexural plastic hinge develops adjacent to the joint, and joint failure will not affect the displacement ductility as it remains uncracked. The displacement ductility factor μ_{joint} due to the joint shear is then $\mu_{joint} = \mu_f$, where μ_f= displacement ductility factor due to flexure.

2. Semi-Brittle Joint: $0.29\sqrt{f'_c(MPa)} \le f_t \le 0.42\sqrt{f'_c(MPa)}$

In this joint, diagonal tensile cracking occurs at a force level less than that required to develop the flexural strength in an adjacent member. Concrete tension strength in the principal stress direction at the joint degrades to zero at a member displacement of approximately three times that at the onset of diagonal cracking, which is taken to occur at $f_t = 0.29\sqrt{f'_c(MPa)}$. Even if a flexural plastic hinge forms in a member with a corresponding principal tensile stress range, initial ductile response occurs but the same falling branch will occur. This is due to the degradation of joint performance resulting from strain penetration from yielding bars into the joint region. The corresponding displacement ductility factor due to the joint shear is calculated by

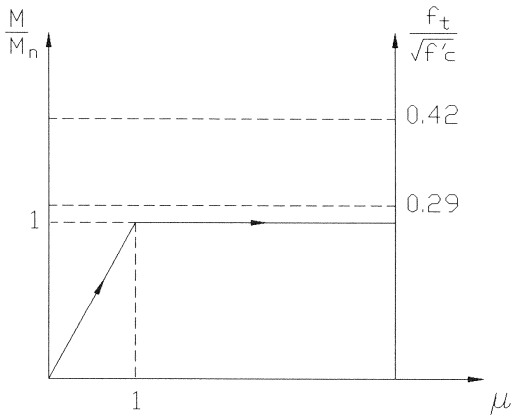

(a) Elastic Joint

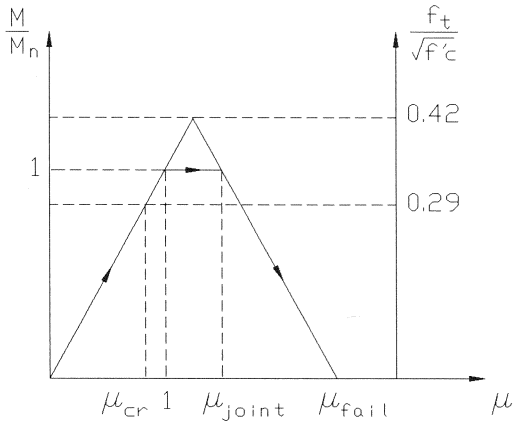

(b) Semi-brittle Joint

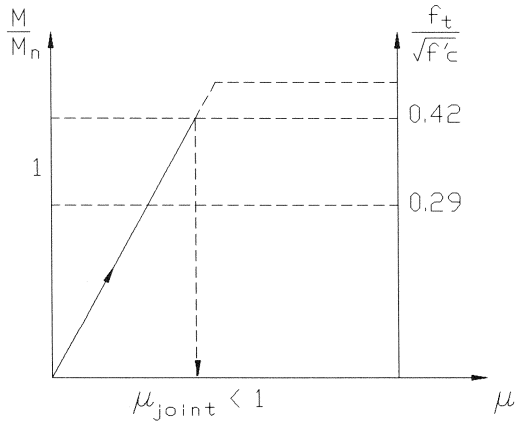

(c) Brittle Joint

Figure 6-8. Joint shear failure model after Priestley, et al. *(1992)*.

$$\mu_{joint} = \mu_{fail} - 1 = 3\mu_{cr} - 1 \qquad \textbf{(6-34a)}$$

where

$$\mu_{cr} = 0.29\frac{\sqrt{f'_c\,(MPa)}}{f_t} \qquad \textbf{(6-34b)}$$

$$\mu_{fail} = 3\mu_{cr} = 0.87\frac{\sqrt{f'_c\,(MPa)}}{f_t} \qquad \textbf{(6-34c)}$$

in which μ_{cr}= displacement ductility factor at cracking, μ_{fail}= displacement ductility factor at joint shear failure, and f_t= concrete tensile stress demand. It is noted from the equation (6-34) that the displacement ductility factor μ_{joint} due to joint shear force is bounded by $1 \le \mu_{joint} \le 2$.

*3. **Brittle Joint:** $f_t > 0.42\sqrt{f'_c\,(MPa)}$*

Even though the failure model in this category has not been suggested yet, it may not be farfetched to qualitatively expect the resultant behavior based on the above mentioned semi-brittle joint behavior. In this brittle system, it is expected that joint shear failure occurs at a force level less than that required to develop a plastic hinge in an adjacent member. The joint principal tension strength will be suddenly lost at a ductility less than 1.

The total joint shear strength is the sum of the contribution of the principal tensile strength of concrete and the contribution of any joint shear steel, and is given by

$$V_{jh} = v_{cj} b h_c + A_{jh} f_y \quad \textit{for horizontal shear} \qquad \textbf{(6-35a)}$$

$$V_{jv} = v_{cj} b h_b + A_{jv} f_y \quad \textit{for vertical shear} \qquad \textbf{(6-35b)}$$

where $v_{cj} = \sqrt{f_t(f_t - f_a)}$. When $\mu > \mu_{fail}$, the joint concrete shear strength v_{cj} should be considered to be zero.

The experimentally observed critical principal tensile stress due to joint shear is

$f_t = 0.4\sqrt{f'_c(MPa)}$ for the pre-retrofitted model pier. The corresponding displacement ductility factor due to joint shear strength is then $\mu_{joint} = 1.18$. All joints of the post-retrofitted model pier are classified as elastic, and therefore, the displacement ductility applicable to columns governs.

6.3.5 Ductility-Based C/D Estimation

The lateral strength method is extended using the relationship between response reduction factor and displacement ductility factor to evaluate a series of ductility based C/D ratios in terms of PGA. The ATC 6-2 based column moment C/D ratio r_{ec} is used for this evaluation procedure.

From the strength V_f and displacement ductility μ_Δ of the critical collapse mechanism, the equivalent elastic lateral strength V_E can be determined:

$$V_E = RV_f \tag{6-36}$$

where R is a force reduction factor given by

$$R = 1 + 0.67(\mu_\Delta - 1)\frac{T}{T_o} \le \mu_\Delta \tag{6-37}$$

in which T= elastic fundamental period of the structure, and T_o= period corresponding to AASHTO peak spectral response for the given site (T_o= 0.4 s is assumed for stiff soil or rock).

Equation (6-36) can be rewritten by dividing by the structural weight:

$$C(d) = RC_n(c) \tag{6-38}$$

The ductility dependent response reduction factor R_μ is defined by replacing the force reduction factor R such that

$$R_\mu = \frac{C(d)}{C_n(c)} = \frac{1}{r_{ec}} \tag{6-39}$$

Then, the displacement ductility demand $\mu(d)$ can be determined by the inverse form of equation (6-37) substituting R_μ for R

$$\mu(d) = 1 + 1.5(R_\mu - 1)\frac{T_o}{T} \geq R_\mu \qquad \textbf{(6-40)}$$

in which $T_o = 0.4$ sec. The ductility based C/D ratio r_μ is defined as

$$r_\mu = \frac{\mu(c)}{\mu(d)} \qquad \textbf{(6-41)}$$

where $\mu(c)$ is the displacement ductility factor corresponding to the concrete ultimate compression strain of $\varepsilon_{cu} = 0.005$.

The C/D ratios in this procedure in terms of PGA are plotted in figure 6-9. The flexural C/D ratio predicts conservatively the pre-retrofitted model pier response compared to the experimental observation. The C/D ratio for the joint shear failure provides the lower bound response of the pre-retrofitted model pier. The threshold PGA for the brittle joint shear failure is predicted as $A = 0.45\,g$ while experimental results give $A = 0.89\,g$. For the post-retrofitted model pier, the column shear strength and the flexure model provide the upper ($A = 0.98\,g$) and lower ($A = 0.71\,g$) limits, respectively, close to the experimentally observed response ($A = 0.89\,g$). The lateral strength method gives more conservative interpretation in C/D ratios at the site of AASHTO seismic performance category *D* than the ATC 6-2 based method with the exception of prediction of the column shear response for the post-retrofitted model pier.

6.4 Summary and Discussion of the Evaluation Methods

The results of discussed evaluation methods (ATC 6-2 and Equivalent Lateral Strength) are summarized in table 6-9 in terms of PGA for the safety threshold. Based on the experimental observations and the theoretical evaluation results, the following conclusions are drawn:

1. Evaluation by the ATC 6-2 based C/D ratio method is really useful only to indicate the onset of inelastic response. This method predicts a ductile shear behavior ($\mu = 2.85$) for the pre-retrofitted model pier and a brittle shear behavior ($\mu < 1$) for the post-retrofitted model pier. However, even though the experimentally observed ductility is favorably matched to the

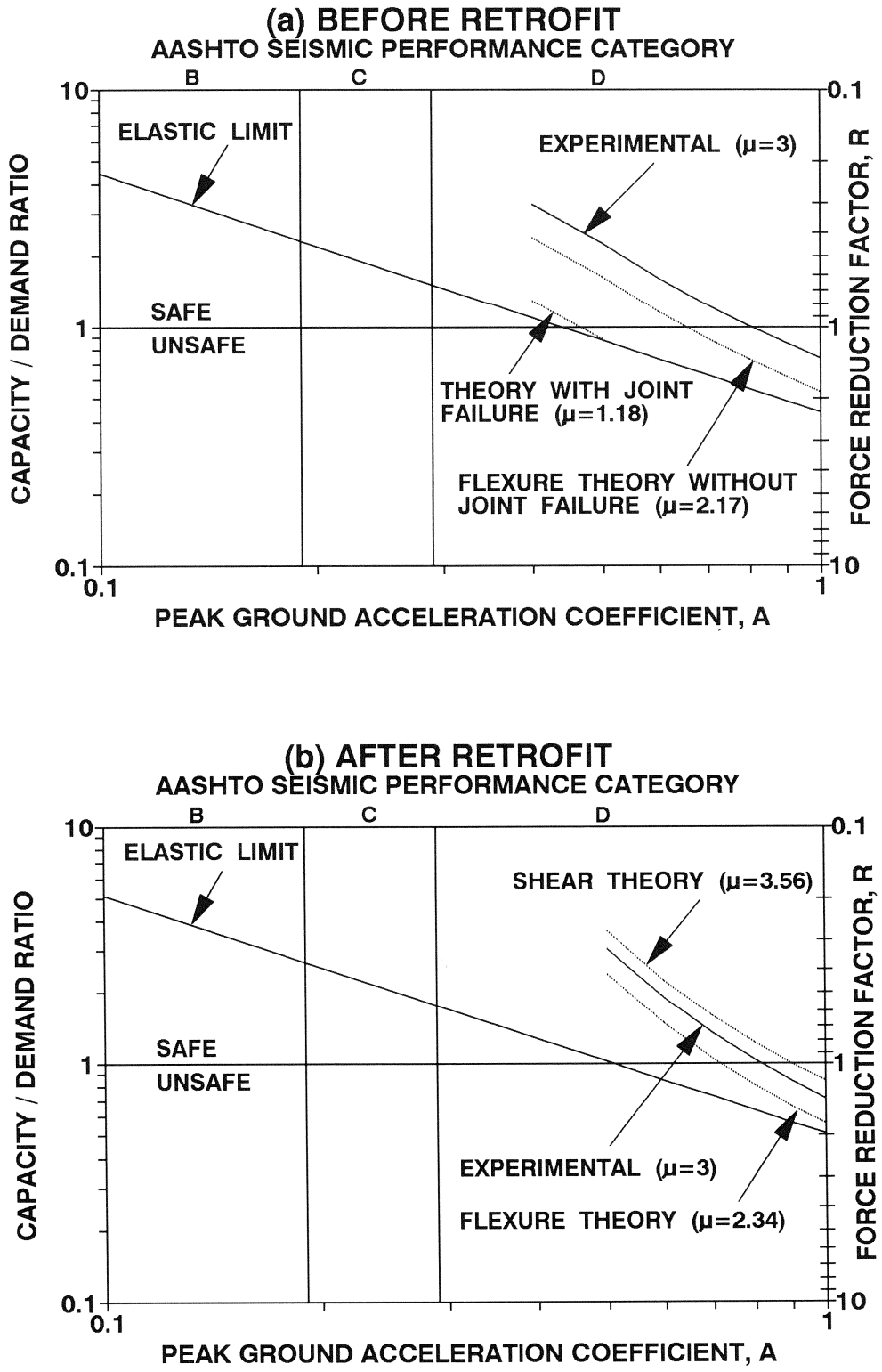

Figure 6-9. Ductility based C/D ratios for model pier.

Table 6-9. Summary of the PGA's at failure for the considered evaluation methods.

Evaluation Method	Before Retrofit (g)	After Retrofit (g)
ATC 6-2 Evaluation	1.1[a]	0.52[b]
Ductility Based Evaluation	0.45[c]	0.71[a]

[a]Ductile-flexure mode.
[b]Column shear mode.
[c]Joint shear mode after Priestley, et al. *(1992)*.

prediction for the pre-retrofitted model pier, the experiment resulted in a joint shear/anchorage failure mode. The experimentally observed failure mode for the post-retrofitted model pier was a ductile shear failure ($\mu > 1$). It is noted from table 6-9 that the theoretically predicted safety threshold by this method are 1.1g (ductile-flexure mode) and 0.52g (column shear mode).

2. Ductility-based evaluation by the equivalent lateral strength (push-over) method of analysis considers flexural ductility, lap splices and anchorage zones as well as the shear capacity of connections and members. When compared with test results, this method predicted anchorage and joint shear strength quite well. Also, the overall column shear capacity seemed to be adequately predicted both before and after retrofit. It is noted from table 6-9 that the theoretical safety thresholds are 0.45g (joint shear mode) and 0.71g (ductile-flexure mode) for the model pier before and after retrofit.

SECTION 7
CONCLUSIONS AND RECOMMENDATIONS FOR FUTURE RESEARCH

7.1 Conclusions

This study has investigated both experimentally and analytically the strength, deformation and energy dissipation behavior of an existing non-seismically designed bridge pier bent model before and after retrofit. From this study the following conclusions are drawn:

1. The experimental study on a 1/3 scale model reinforced concrete bridge pier, typical of existing frame pier bents in the central and eastern United States, showed some vulnerability in resisting simulated seismic lateral loading due to lack of strength in the beam-column joint connections, bond/anchorage of column longitudinal reinforcement, and transverse confinement in potential plastic hinge zones. The experimental performance, however, was better than that projected by the existing state-of-the-art seismic evaluation techniques.

2. Using *Capacity Analysis and Redesign* techniques developed in this study it was possible to retrofit frame type pier bents and eliminate undesirable failure mechanisms such as joint shear and anchorage. This redesign philosophy was validated through the experiment on the retrofitted pier model. Careful consideration of column overstrength shear demand is required to avoid premature loss in the ductility capability due to inadequate shear capacity.

3. Laboratory experimental results on the companion prototype pier cap beam-column subassemblage *(Mander, et al., 1996)* showed similar results to those observed in the present study on the scale model pier bent both before and after retrofit. The combined joint shear and bond/anchorage failure mode dominated the response of the pre-retrofitted specimen while column flexure-shear failure mode governed the behavior of the post-retrofitted specimen. It is noted that retrofit changed the failure mode.

4. The ATC 6-2 based C/D ratio method in evaluation of the model pier bent is only useful

to indicate the onset of inelastic response. The equivalent lateral strength method evaluates the model pier more rationally for the flexural ductility, lap splice and anchorage, ductility based column shear capacity, and joint shear strength. However, cyclic loading effects are not considered explicitly and thus the duration effects of earthquake excitations are not accounted for.

5. This research demonstrates that using rational guidelines, it is possible to suppress undesirable failure modes such as joint shear failure in the cap beam and anchorage failure in the foundation. Designers should be warned that such retrofits shorten the clear height of the columns and hence increase the shear demand, potentially leading to a shear brittle condition. In this study such a shear-critical condition was deliberately induced to study the efficacy of the apparently conflicting FHWA Retrofitting Manual *(Buckle and Friedland, 1994)* shear evaluation guidelines. Such deficiencies have been pointed out herein. In a follow-up report to this study, the improved shear evaluation methods will be proposed and validated, in part, by the experiments discussed herein.

7.2 Recommendations for Future Research

The following items are recommended for further research to more rationally evaluate existing bridge pier bents and to suggest better retrofit if necessary:

1. Incorporation of soil-structure interaction effects into future experimental and analytical studies is desirable.

2. Proper modeling technique for column shear and joint shear behavior needs to be considered.

3. Consideration of the effect of superstructure stiffness and strength on the inelastic behavior of concrete pier bents is recommended. Of particular importance is the performance of bridges with continuous versus simply supported girders.

4. Study of the inelastic behavior of concrete pier bents in the longitudinal direction of the bridge is recommended.

5. Bi-axial flexural behavior of concrete pier bents for earthquake induced ground shaking from random direction should be considered.

6. Effect of high-strength concrete and reinforcement on behavior of members and connections is recommended to be considered.

7. Alternative methods for retrofitting concrete bridge pier bents can also be considered: rocking column base for lap-splice zone; infilled frame pier with masonry or concrete; and implementation of mechanical devices such as recentering damping devices.

8. Shear resisting mechanism of reinforced concrete members and interaction with flexure should be studied to improve shear evaluation methods.

SECTION 8
REFERENCES

_____ ACI (1970), *Models for Concrete Structures*, ACI Publication SP-24, American Concrete Institute, Detroit.

_____ ACI (1982), *Dynamic Modeling of Concrete Structures*, ACI Publication SP-73, American Concrete Institute, Detroit.

_____ AASHTO (1992), *Standard Specifications for Highway Bridges*, 15th ed., American Association of State Highway and Transportation Officials, Washington, D.C.

_____ AASHTO (1994), *AASHTO LRFD Bridge Design Specifications*, 1st ed., American Association of State Highway and Transportation Officials, Washington, D.C.

_____ ACI Committee 318 (1989), *Building Code Requirements for Reinforcement Concrete and Commentary*, ACI 318-89, American Concrete Institute, Detroit.

_____ ACI Committee 408 (1991), "Abstract of: State-of-the-Art-Report: Bond under Cyclic Loads", ACI Materials Journal, V. 88, No. 6, pp. 669-673, Nov.-Dec.

_____ ACI Committee 408 (1992), *State-of-the-Art-Report on Bond under Cyclic Loads*, ACI 408, American Concrete Institute.

Ang, B.G., Priestley, M.J.N, and Paulay, T. (1989), "Seismic Shear Strength of Circular Reinforced Concrete Columns", ACI Structural Journal, Title no. 86-S6, Jan.-Feb., pp. 45-59.

_____ ASTM (1984), "Standard Test Method for Flexural Strength of Concrete (Using Simple Beam with Third-Point Loading)", C78-84, *Annual Book of ASTM Standards*, American

Society for Testing and Materials, Philadelphia.

_____ ASTM (1990), "Standard Test Method for Splitting Tensile Strength of Cylindrical Concrete Specimens", C496-90, *Annual Book of ASTM Standards*, American Society for Testing and Materials, Philadelphia.

_____ ATC 6-2 (1983), *Seismic Retrofitting Guidelines for Highway Bridges*, Report ATC-6-2, Applied Technology Council, 1983. Also published by Federal Highway Administration as Report no. FHWA/RD-83/007.

Buckle, I.G. and Friedland, I.M. (1995), *Seismic Retrofitting Manual for Highway Bridges*, Federal Highway Administration Report no. FHWA-RD-94-052.

Buckle, I.G., Mayes, R.L., and Button, M.R. (1987), *Seismic Design and Retrofit Manual for Highway Bridges*, Prepared for Federal Highway Administration, Report No. FHWA-IP-87-6, Computech Engineering Services, Inc., Berkeley.

Chai, Y.H., Priestley, M.J.N, and Seible, F. (1991), "Seismic Retrofit of Circular Bridge Columns for Enhanced Flexural Performance", ACI Structural Journal, V. 88, No. 5, Sept.-Oct., pp.572-584.

Chang, G.A. and Mander, J.B. (1994), *Seismic Energy Based Fatigue Damage Analysis of Bridge Columns, Part I: Evaluation of Seismic Capacity*, Technical Report NCEER-94-0006, National Center for Earthquake Engineering Research, State University of New York at Buffalo, New York.

Eligehausen, R., Popov, E.P., and Bertero, V.V. (1983), *Local Bond Stress-Slip Relationships of Deformed Bars Under Generalized Excitations*, Report No. UCB/EERC 83-23, Earthquake Engineering Research Center, University of California at Berkeley, California.

_____ FHWA (1983), See ATC 6-2 (1983).

Housner, G.W. (1990), *Competing Against Time*, Report to Gov. G. Deukmejian, Governor's Board of Inquiry on 1989 Loma Prieta Earthquake, North Highlands, California.

Hungspreug, S. (1981), *Local Bond between A Steel Bar and Concrete Under High Intensity Cyclic Load*, Ph.D. Dissertation, Cornell University, Ithaca, New York.

Malvar, L.J. (1992), "Bond of Reinforcement Under Controlled Confinement", ACI Materials Journal, V. 89, No. 6, Nov.-Dec., pp. 593-601,

Mander, J.B., Priestley, M.J.N., and Park, R. (1984), *Seismic Design of Bridge Piers*, Research Report No. 84-2, University of Canterbury, New Zealand.

Mander, J.B., Waheed, S.M., and Chaudhary, M.T.A., Chen, S.S. (1993), *Seismic Performance of Shear-Critical Reinforced Concrete Bridge Piers*, Technical Report NCEER-93-0010, National Center for Earthquake Engineering Research, State University of New York at Buffalo, New York.

Mander, J.B., Mahmoodzadegan, B., Bhadra, S, and Chen, S.S. (1996), *Seismic Evaluation of A 30-Year Old Non-Ductile Highway Bridge Pier and Its Retrofit*, Technical Report NCEER-96-0008, National Center for Earthquake Engineering Research, State University of New York at Buffalo, New York.

Mayes, R.L. and Sharpe, R.L. (1981), *Seismic Design Guidelines for Highway Bridges: Earthquake Protection of Transportation Structures*, Federal Highway Administration Report no. FHWA-RD-81-081.

Nickerson, R.L. (1969), "Reinforced Concrete Bridges - Working Stress versus Ultimate Strength", ACI Publication SP-23, American Concrete Institute, Detroit, pp. 407-422.

Nilson, A.H. (1987), *Design of Prestressed Concrete*, 2nd edition, John Wiley & Sons, Inc., New York.

_____ NZS (1982), *Code of Practice for Design of Concrete Structures*, NZS 3101, Standards Association of New Zealand, Wellington.

Park, R. and Paulay, T. (1975), *Reinforced Concrete Structures*, John Wiley and Sons, Inc., New York.

Paulay, T. (1982), "Lapped Splices in Earthquake-Resisting Columns", ACI Journal Title No. 79-44, American Concrete Institute, Detroit, pp.458-469.

Paulay, T. and Priestley, M.J.N. (1992), *Seismic Design of Reinforced Concrete and Masonry Structures*, John Wiley and Sons, Inc., New York.

Prakash, V., Powell, G.H., and Filippou, F.C. (1992a), *DRAIN-2DX: Base Program User Guide*, Department of Civil Engineering, University of California at Berkeley, California.

Prakash, V., Powell, G.H., Campbell, S.D., and Filippou, F.C. (1992b), *DRAIN-2DX: Preliminary Element User Guide*, Department of Civil Engineering, University of California at Berkeley, California.

Priestley, M.J.N. and Seible, F., and Chai, Y.H. (1992), *Design Guidelines for Assessment Retrofit and Repair of Bridges for Seismic Performance*, Research Report SSRP-92/01, Dept. of Applied Mechanics and Engineering Sciences, University of California, San Diego.

Priestley, M.J.N., Verma, R., and Xiao, Y. (1994), "Seismic Shear Strength of Reinforced Concrete Columns", Journal of Structural Engineering, Vol. 120, No. 8, American Society of Civil Engineers, pp. 2310-2329, August.

_____ SEAOC (1988), *Recommended Lateral Force Requirements and Tentative Commentary*, 5th edition, Seismology Committee, Structural Engineers Association of California, San Francisco, California.

NATIONAL CENTER FOR EARTHQUAKE ENGINEERING RESEARCH
LIST OF TECHNICAL REPORTS

The National Center for Earthquake Engineering Research (NCEER) publishes technical reports on a variety of subjects related to earthquake engineering written by authors funded through NCEER. These reports are available from both NCEER Publications and the National Technical Information Service (NTIS). Requests for reports should be directed to NCEER Publications, National Center for Earthquake Engineering Research, State University of New York at Buffalo, Red Jacket Quadrangle, Buffalo, New York 14261. Reports can also be requested through NTIS, 5285 Port Royal Road, Springfield, Virginia 22161. NTIS accession numbers are shown in parenthesis, if available.

NCEER-87-0001 "First-Year Program in Research, Education and Technology Transfer," 3/5/87, (PB88-134275, A04, MF-A01).

NCEER-87-0002 "Experimental Evaluation of Instantaneous Optimal Algorithms for Structural Control," by R.C. Lin, T.T. Soong and A.M. Reinhorn, 4/20/87, (PB88-134341, A04, MF-A01).

NCEER-87-0003 "Experimentation Using the Earthquake Simulation Facilities at University at Buffalo," by A.M. Reinhorn and R.L. Ketter, to be published.

NCEER-87-0004 "The System Characteristics and Performance of a Shaking Table," by J.S. Hwang, K.C. Chang and G.C. Lee, 6/1/87, (PB88-134259, A03, MF-A01). This report is available only through NTIS (see address given above).

NCEER-87-0005 "A Finite Element Formulation for Nonlinear Viscoplastic Material Using a Q Model," by O. Gyebi and G. Dasgupta, 11/2/87, (PB88-213764, A08, MF-A01).

NCEER-87-0006 "Symbolic Manipulation Program (SMP) - Algebraic Codes for Two and Three Dimensional Finite Element Formulations," by X. Lee and G. Dasgupta, 11/9/87, (PB88-218522, A05, MF-A01).

NCEER-87-0007 "Instantaneous Optimal Control Laws for Tall Buildings Under Seismic Excitations," by J.N. Yang, A. Akbarpour and P. Ghaemmaghami, 6/10/87, (PB88-134333, A06, MF-A01). This report is only available through NTIS (see address given above).

NCEER-87-0008 "IDARC: Inelastic Damage Analysis of Reinforced Concrete Frame - Shear-Wall Structures," by Y.J. Park, A.M. Reinhorn and S.K. Kunnath, 7/20/87, (PB88-134325, A09, MF-A01). This report is only available through NTIS (see address given above).

NCEER-87-0009 "Liquefaction Potential for New York State: A Preliminary Report on Sites in Manhattan and Buffalo," by M. Budhu, V. Vijayakumar, R.F. Giese and L. Baumgras, 8/31/87, (PB88-163704, A03, MF-A01). This report is available only through NTIS (see address given above).

NCEER-87-0010 "Vertical and Torsional Vibration of Foundations in Inhomogeneous Media," by A.S. Veletsos and K.W. Dotson, 6/1/87, (PB88-134291, A03, MF-A01). This report is only available through NTIS (see address given above).

NCEER-87-0011 "Seismic Probabilistic Risk Assessment and Seismic Margins Studies for Nuclear Power Plants," by Howard H.M. Hwang, 6/15/87, (PB88-134267, A03, MF-A01). This report is only available through NTIS (see address given above).

NCEER-87-0012 "Parametric Studies of Frequency Response of Secondary Systems Under Ground-Acceleration Excitations," by Y. Yong and Y.K. Lin, 6/10/87, (PB88-134309, A03, MF-A01). This report is only available through NTIS (see address given above).

NCEER-87-0013 "Frequency Response of Secondary Systems Under Seismic Excitation," by J.A. HoLung, J. Cai and Y.K. Lin, 7/31/87, (PB88-134317, A05, MF-A01). This report is only available through NTIS (see address given above).

NCEER-87-0014 "Modelling Earthquake Ground Motions in Seismically Active Regions Using Parametric Time Series Methods," by G.W. Ellis and A.S. Cakmak, 8/25/87, (PB88-134283, A08, MF-A01). This report is only available through NTIS (see address given above).

NCEER-87-0015 "Detection and Assessment of Seismic Structural Damage," by E. DiPasquale and A.S. Cakmak, 8/25/87, (PB88-163712, A05, MF-A01). This report is only available through NTIS (see address given above).

NCEER-87-0016 "Pipeline Experiment at Parkfield, California," by J. Isenberg and E. Richardson, 9/15/87, (PB88-163720, A03, MF-A01). This report is available only through NTIS (see address given above).

NCEER-87-0017 "Digital Simulation of Seismic Ground Motion," by M. Shinozuka, G. Deodatis and T. Harada, 8/31/87, (PB88-155197, A04, MF-A01). This report is available only through NTIS (see address given above).

NCEER-87-0018 "Practical Considerations for Structural Control: System Uncertainty, System Time Delay and Truncation of Small Control Forces," J.N. Yang and A. Akbarpour, 8/10/87, (PB88-163738, A08, MF-A01). This report is only available through NTIS (see address given above).

NCEER-87-0019 "Modal Analysis of Nonclassically Damped Structural Systems Using Canonical Transformation," by J.N. Yang, S. Sarkani and F.X. Long, 9/27/87, (PB88-187851, A04, MF-A01).

NCEER-87-0020 "A Nonstationary Solution in Random Vibration Theory," by J.R. Red-Horse and P.D. Spanos, 11/3/87, (PB88-163746, A03, MF-A01).

NCEER-87-0021 "Horizontal Impedances for Radially Inhomogeneous Viscoelastic Soil Layers," by A.S. Veletsos and K.W. Dotson, 10/15/87, (PB88-150859, A04, MF-A01).

NCEER-87-0022 "Seismic Damage Assessment of Reinforced Concrete Members," by Y.S. Chung, C. Meyer and M. Shinozuka, 10/9/87, (PB88-150867, A05, MF-A01). This report is available only through NTIS (see address given above).

NCEER-87-0023 "Active Structural Control in Civil Engineering," by T.T. Soong, 11/11/87, (PB88-187778, A03, MF-A01).

NCEER-87-0024 "Vertical and Torsional Impedances for Radially Inhomogeneous Viscoelastic Soil Layers," by K.W. Dotson and A.S. Veletsos, 12/87, (PB88-187786, A03, MF-A01).

NCEER-87-0025 "Proceedings from the Symposium on Seismic Hazards, Ground Motions, Soil-Liquefaction and Engineering Practice in Eastern North America," October 20-22, 1987, edited by K.H. Jacob, 12/87, (PB88-188115, A23, MF-A01).

NCEER-87-0026 "Report on the Whittier-Narrows, California, Earthquake of October 1, 1987," by J. Pantelic and A. Reinhorn, 11/87, (PB88-187752, A03, MF-A01). This report is available only through NTIS (see address given above).

NCEER-87-0027 "Design of a Modular Program for Transient Nonlinear Analysis of Large 3-D Building Structures," by S. Srivastav and J.F. Abel, 12/30/87, (PB88-187950, A05, MF-A01). This report is only available through NTIS (see address given above).

NCEER-87-0028 "Second-Year Program in Research, Education and Technology Transfer," 3/8/88, (PB88-219480, A04, MF-A01).

NCEER-88-0001 "Workshop on Seismic Computer Analysis and Design of Buildings With Interactive Graphics," by W. McGuire, J.F. Abel and C.H. Conley, 1/18/88, (PB88-187760, A03, MF-A01). This report is only available through NTIS (see address given above).

NCEER-88-0002 "Optimal Control of Nonlinear Flexible Structures," by J.N. Yang, F.X. Long and D. Wong, 1/22/88, (PB88-213772, A06, MF-A01).

NCEER-88-0003 "Substructuring Techniques in the Time Domain for Primary-Secondary Structural Systems," by G.D. Manolis and G. Juhn, 2/10/88, (PB88-213780, A04, MF-A01).

NCEER-88-0004 "Iterative Seismic Analysis of Primary-Secondary Systems," by A. Singhal, L.D. Lutes and P.D. Spanos, 2/23/88, (PB88-213798, A04, MF-A01).

NCEER-88-0005 "Stochastic Finite Element Expansion for Random Media," by P.D. Spanos and R. Ghanem, 3/14/88, (PB88-213806, A03, MF-A01).

NCEER-88-0006 "Combining Structural Optimization and Structural Control," by F.Y. Cheng and C.P. Pantelides, 1/10/88, (PB88-213814, A05, MF-A01).

NCEER-88-0007 "Seismic Performance Assessment of Code-Designed Structures," by H.H-M. Hwang, J-W. Jaw and H-J. Shau, 3/20/88, (PB88-219423, A04, MF-A01). This report is only available through NTIS (see address given above).

NCEER-88-0008 "Reliability Analysis of Code-Designed Structures Under Natural Hazards," by H.H-M. Hwang, H. Ushiba and M. Shinozuka, 2/29/88, (PB88-229471, A07, MF-A01). This report is only available through NTIS (see address given above).

NCEER-88-0009 "Seismic Fragility Analysis of Shear Wall Structures," by J-W Jaw and H.H-M. Hwang, 4/30/88, (PB89-102867, A04, MF-A01).

NCEER-88-0010 "Base Isolation of a Multi-Story Building Under a Harmonic Ground Motion - A Comparison of Performances of Various Systems," by F-G Fan, G. Ahmadi and I.G. Tadjbakhsh, 5/18/88, (PB89-122238, A06, MF-A01). This report is only available through NTIS (see address given above).

NCEER-88-0011 "Seismic Floor Response Spectra for a Combined System by Green's Functions," by F.M. Lavelle, L.A. Bergman and P.D. Spanos, 5/1/88, (PB89-102875, A03, MF-A01).

NCEER-88-0012 "A New Solution Technique for Randomly Excited Hysteretic Structures," by G.Q. Cai and Y.K. Lin, 5/16/88, (PB89-102883, A03, MF-A01).

NCEER-88-0013 "A Study of Radiation Damping and Soil-Structure Interaction Effects in the Centrifuge," by K. Weissman, supervised by J.H. Prevost, 5/24/88, (PB89-144703, A06, MF-A01).

NCEER-88-0014 "Parameter Identification and Implementation of a Kinematic Plasticity Model for Frictional Soils," by J.H. Prevost and D.V. Griffiths, to be published.

NCEER-88-0015 "Two- and Three- Dimensional Dynamic Finite Element Analyses of the Long Valley Dam," by D.V. Griffiths and J.H. Prevost, 6/17/88, (PB89-144711, A04, MF-A01).

NCEER-88-0016 "Damage Assessment of Reinforced Concrete Structures in Eastern United States," by A.M. Reinhorn, M.J. Seidel, S.K. Kunnath and Y.J. Park, 6/15/88, (PB89-122220, A04, MF-A01). This report is only available through NTIS (see address given above).

NCEER-88-0017 "Dynamic Compliance of Vertically Loaded Strip Foundations in Multilayered Viscoelastic Soils," by S. Ahmad and A.S.M. Israil, 6/17/88, (PB89-102891, A04, MF-A01).

NCEER-88-0018 "An Experimental Study of Seismic Structural Response With Added Viscoelastic Dampers," by R.C. Lin, Z. Liang, T.T. Soong and R.H. Zhang, 6/30/88, (PB89-122212, A05, MF-A01). This report is available only through NTIS (see address given above).

NCEER-88-0019 "Experimental Investigation of Primary - Secondary System Interaction," by G.D. Manolis, G. Juhn and A.M. Reinhorn, 5/27/88, (PB89-122204, A04, MF-A01).

NCEER-88-0020 "A Response Spectrum Approach For Analysis of Nonclassically Damped Structures," by J.N. Yang, S. Sarkani and F.X. Long, 4/22/88, (PB89-102909, A04, MF-A01).

NCEER-88-0021 "Seismic Interaction of Structures and Soils: Stochastic Approach," by A.S. Veletsos and A.M. Prasad, 7/21/88, (PB89-122196, A04, MF-A01). This report is only available through NTIS (see address given above).

NCEER-88-0022 "Identification of the Serviceability Limit State and Detection of Seismic Structural Damage," by E. DiPasquale and A.S. Cakmak, 6/15/88, (PB89-122188, A05, MF-A01). This report is available only through NTIS (see address given above).

NCEER-88-0023 "Multi-Hazard Risk Analysis: Case of a Simple Offshore Structure," by B.K. Bhartia and E.H. Vanmarcke, 7/21/88, (PB89-145213, A05, MF-A01).

NCEER-88-0024 "Automated Seismic Design of Reinforced Concrete Buildings," by Y.S. Chung, C. Meyer and M. Shinozuka, 7/5/88, (PB89-122170, A06, MF-A01). This report is available only through NTIS (see address given above).

NCEER-88-0025 "Experimental Study of Active Control of MDOF Structures Under Seismic Excitations," by L.L. Chung, R.C. Lin, T.T. Soong and A.M. Reinhorn, 7/10/88, (PB89-122600, A04, MF-A01).

NCEER-88-0026 "Earthquake Simulation Tests of a Low-Rise Metal Structure," by J.S. Hwang, K.C. Chang, G.C. Lee and R.L. Ketter, 8/1/88, (PB89-102917, A04, MF-A01).

NCEER-88-0027 "Systems Study of Urban Response and Reconstruction Due to Catastrophic Earthquakes," by F. Kozin and H.K. Zhou, 9/22/88, (PB90-162348, A04, MF-A01).

NCEER-88-0028 "Seismic Fragility Analysis of Plane Frame Structures," by H.H-M. Hwang and Y.K. Low, 7/31/88, (PB89-131445, A06, MF-A01).

NCEER-88-0029 "Response Analysis of Stochastic Structures," by A. Kardara, C. Bucher and M. Shinozuka, 9/22/88, (PB89-174429, A04, MF-A01).

NCEER-88-0030 "Nonnormal Accelerations Due to Yielding in a Primary Structure," by D.C.K. Chen and L.D. Lutes, 9/19/88, (PB89-131437, A04, MF-A01).

NCEER-88-0031 "Design Approaches for Soil-Structure Interaction," by A.S. Veletsos, A.M. Prasad and Y. Tang, 12/30/88, (PB89-174437, A03, MF-A01). This report is available only through NTIS (see address given above).

NCEER-88-0032 "A Re-evaluation of Design Spectra for Seismic Damage Control," by C.J. Turkstra and A.G. Tallin, 11/7/88, (PB89-145221, A05, MF-A01).

NCEER-88-0033 "The Behavior and Design of Noncontact Lap Splices Subjected to Repeated Inelastic Tensile Loading," by V.E. Sagan, P. Gergely and R.N. White, 12/8/88, (PB89-163737, A08, MF-A01).

NCEER-88-0034 "Seismic Response of Pile Foundations," by S.M. Mamoon, P.K. Banerjee and S. Ahmad, 11/1/88, (PB89-145239, A04, MF-A01).

NCEER-88-0035 "Modeling of R/C Building Structures With Flexible Floor Diaphragms (IDARC2)," by A.M. Reinhorn, S.K. Kunnath and N. Panahshahi, 9/7/88, (PB89-207153, A07, MF-A01).

NCEER-88-0036 "Solution of the Dam-Reservoir Interaction Problem Using a Combination of FEM, BEM with Particular Integrals, Modal Analysis, and Substructuring," by C-S. Tsai, G.C. Lee and R.L. Ketter, 12/31/88, (PB89-207146, A04, MF-A01).

NCEER-88-0037 "Optimal Placement of Actuators for Structural Control," by F.Y. Cheng and C.P. Pantelides, 8/15/88, (PB89-162846, A05, MF-A01).

NCEER-88-0038 "Teflon Bearings in Aseismic Base Isolation: Experimental Studies and Mathematical Modeling," by A. Mokha, M.C. Constantinou and A.M. Reinhorn, 12/5/88, (PB89-218457, A10, MF-A01). This report is available only through NTIS (see address given above).

NCEER-88-0039 "Seismic Behavior of Flat Slab High-Rise Buildings in the New York City Area," by P. Weidlinger and M. Ettouney, 10/15/88, (PB90-145681, A04, MF-A01).

NCEER-88-0040 "Evaluation of the Earthquake Resistance of Existing Buildings in New York City," by P. Weidlinger and M. Ettouney, 10/15/88, to be published.

NCEER-88-0041 "Small-Scale Modeling Techniques for Reinforced Concrete Structures Subjected to Seismic Loads," by W. Kim, A. El-Attar and R.N. White, 11/22/88, (PB89-189625, A05, MF-A01).

NCEER-88-0042 "Modeling Strong Ground Motion from Multiple Event Earthquakes," by G.W. Ellis and A.S. Cakmak, 10/15/88, (PB89-174445, A03, MF-A01).

NCEER-88-0043 "Nonstationary Models of Seismic Ground Acceleration," by M. Grigoriu, S.E. Ruiz and E. Rosenblueth, 7/15/88, (PB89-189617, A04, MF-A01).

NCEER-88-0044 "SARCF User's Guide: Seismic Analysis of Reinforced Concrete Frames," by Y.S. Chung, C. Meyer and M. Shinozuka, 11/9/88, (PB89-174452, A08, MF-A01).

NCEER-88-0045 "First Expert Panel Meeting on Disaster Research and Planning," edited by J. Pantelic and J. Stoyle, 9/15/88, (PB89-174460, A05, MF-A01). This report is only available through NTIS (see address given above).

NCEER-88-0046 "Preliminary Studies of the Effect of Degrading Infill Walls on the Nonlinear Seismic Response of Steel Frames," by C.Z. Chrysostomou, P. Gergely and J.F. Abel, 12/19/88, (PB89-208383, A05, MF-A01).

NCEER-88-0047 "Reinforced Concrete Frame Component Testing Facility - Design, Construction, Instrumentation and Operation," by S.P. Pessiki, C. Conley, T. Bond, P. Gergely and R.N. White, 12/16/88, (PB89-174478, A04, MF-A01).

NCEER-89-0001 "Effects of Protective Cushion and Soil Compliancy on the Response of Equipment Within a Seismically Excited Building," by J.A. HoLung, 2/16/89, (PB89-207179, A04, MF-A01).

NCEER-89-0002 "Statistical Evaluation of Response Modification Factors for Reinforced Concrete Structures," by H.H-M. Hwang and J-W. Jaw, 2/17/89, (PB89-207187, A05, MF-A01).

NCEER-89-0003 "Hysteretic Columns Under Random Excitation," by G-Q. Cai and Y.K. Lin, 1/9/89, (PB89-196513, A03, MF-A01).

NCEER-89-0004 "Experimental Study of `Elephant Foot Bulge' Instability of Thin-Walled Metal Tanks," by Z-H. Jia and R.L. Ketter, 2/22/89, (PB89-207195, A03, MF-A01).

NCEER-89-0005 "Experiment on Performance of Buried Pipelines Across San Andreas Fault," by J. Isenberg, E. Richardson and T.D. O'Rourke, 3/10/89, (PB89-218440, A04, MF-A01). This report is available only through NTIS (see address given above).

NCEER-89-0006 "A Knowledge-Based Approach to Structural Design of Earthquake-Resistant Buildings," by M. Subramani, P. Gergely, C.H. Conley, J.F. Abel and A.H. Zaghw, 1/15/89, (PB89-218465, A06, MF-A01).

NCEER-89-0007 "Liquefaction Hazards and Their Effects on Buried Pipelines," by T.D. O'Rourke and P.A. Lane, 2/1/89, (PB89-218481, A09, MF-A01).

NCEER-89-0008 "Fundamentals of System Identification in Structural Dynamics," by H. Imai, C-B. Yun, O. Maruyama and M. Shinozuka, 1/26/89, (PB89-207211, A04, MF-A01).

NCEER-89-0009 "Effects of the 1985 Michoacan Earthquake on Water Systems and Other Buried Lifelines in Mexico," by A.G. Ayala and M.J. O'Rourke, 3/8/89, (PB89-207229, A06, MF-A01).

NCEER-89-R010 "NCEER Bibliography of Earthquake Education Materials," by K.E.K. Ross, Second Revision, 9/1/89, (PB90-125352, A05, MF-A01). This report is replaced by NCEER-92-0018.

NCEER-89-0011 "Inelastic Three-Dimensional Response Analysis of Reinforced Concrete Building Structures (IDARC-3D), Part I - Modeling," by S.K. Kunnath and A.M. Reinhorn, 4/17/89, (PB90-114612, A07, MF-A01).

NCEER-89-0012 "Recommended Modifications to ATC-14," by C.D. Poland and J.O. Malley, 4/12/89, (PB90-108648, A15, MF-A01).

NCEER-89-0013 "Repair and Strengthening of Beam-to-Column Connections Subjected to Earthquake Loading," by M. Corazao and A.J. Durrani, 2/28/89, (PB90-109885, A06, MF-A01).

NCEER-89-0014 "Program EXKAL2 for Identification of Structural Dynamic Systems," by O. Maruyama, C-B. Yun, M. Hoshiya and M. Shinozuka, 5/19/89, (PB90-109877, A09, MF-A01).

NCEER-89-0015 "Response of Frames With Bolted Semi-Rigid Connections, Part I - Experimental Study and Analytical Predictions," by P.J. DiCorso, A.M. Reinhorn, J.R. Dickerson, J.B. Radziminski and W.L. Harper, 6/1/89, to be published.

NCEER-89-0016 "ARMA Monte Carlo Simulation in Probabilistic Structural Analysis," by P.D. Spanos and M.P. Mignolet, 7/10/89, (PB90-109893, A03, MF-A01).

NCEER-89-P017 "Preliminary Proceedings from the Conference on Disaster Preparedness - The Place of Earthquake Education in Our Schools," Edited by K.E.K. Ross, 6/23/89, (PB90-108606, A03, MF-A01).

NCEER-89-0017 "Proceedings from the Conference on Disaster Preparedness - The Place of Earthquake Education in Our Schools," Edited by K.E.K. Ross, 12/31/89, (PB90-207895, A012, MF-A02). This report is available only through NTIS (see address given above).

NCEER-89-0018 "Multidimensional Models of Hysteretic Material Behavior for Vibration Analysis of Shape Memory Energy Absorbing Devices, by E.J. Graesser and F.A. Cozzarelli, 6/7/89, (PB90-164146, A04, MF-A01).

NCEER-89-0019 "Nonlinear Dynamic Analysis of Three-Dimensional Base Isolated Structures (3D-BASIS)," by S. Nagarajaiah, A.M. Reinhorn and M.C. Constantinou, 8/3/89, (PB90-161936, A06, MF-A01). This report has been replaced by NCEER-93-0011.

NCEER-89-0020 "Structural Control Considering Time-Rate of Control Forces and Control Rate Constraints," by F.Y. Cheng and C.P. Pantelides, 8/3/89, (PB90-120445, A04, MF-A01).

NCEER-89-0021 "Subsurface Conditions of Memphis and Shelby County," by K.W. Ng, T-S. Chang and H-H.M. Hwang, 7/26/89, (PB90-120437, A03, MF-A01).

NCEER-89-0022 "Seismic Wave Propagation Effects on Straight Jointed Buried Pipelines," by K. Elhmadi and M.J. O'Rourke, 8/24/89, (PB90-162322, A10, MF-A02).

NCEER-89-0023 "Workshop on Serviceability Analysis of Water Delivery Systems," edited by M. Grigoriu, 3/6/89, (PB90-127424, A03, MF-A01).

NCEER-89-0024 "Shaking Table Study of a 1/5 Scale Steel Frame Composed of Tapered Members," by K.C. Chang, J.S. Hwang and G.C. Lee, 9/18/89, (PB90-160169, A04, MF-A01).

NCEER-89-0025 "DYNA1D: A Computer Program for Nonlinear Seismic Site Response Analysis - Technical Documentation," by Jean H. Prevost, 9/14/89, (PB90-161944, A07, MF-A01). This report is available only through NTIS (see address given above).

NCEER-89-0026 "1:4 Scale Model Studies of Active Tendon Systems and Active Mass Dampers for Aseismic Protection," by A.M. Reinhorn, T.T. Soong, R.C. Lin, Y.P. Yang, Y. Fukao, H. Abe and M. Nakai, 9/15/89, (PB90-173246, A10, MF-A02).

NCEER-89-0027 "Scattering of Waves by Inclusions in a Nonhomogeneous Elastic Half Space Solved by Boundary Element Methods," by P.K. Hadley, A. Askar and A.S. Cakmak, 6/15/89, (PB90-145699, A07, MF-A01).

NCEER-89-0028 "Statistical Evaluation of Deflection Amplification Factors for Reinforced Concrete Structures," by H.H.M. Hwang, J-W. Jaw and A.L. Ch'ng, 8/31/89, (PB90-164633, A05, MF-A01).

NCEER-89-0029 "Bedrock Accelerations in Memphis Area Due to Large New Madrid Earthquakes," by H.H.M. Hwang, C.H.S. Chen and G. Yu, 11/7/89, (PB90-162330, A04, MF-A01).

NCEER-89-0030 "Seismic Behavior and Response Sensitivity of Secondary Structural Systems," by Y.Q. Chen and T.T. Soong, 10/23/89, (PB90-164658, A08, MF-A01).

NCEER-89-0031 "Random Vibration and Reliability Analysis of Primary-Secondary Structural Systems," by Y. Ibrahim, M. Grigoriu and T.T. Soong, 11/10/89, (PB90-161951, A04, MF-A01).

NCEER-89-0032 "Proceedings from the Second U.S. - Japan Workshop on Liquefaction, Large Ground Deformation and Their Effects on Lifelines, September 26-29, 1989," Edited by T.D. O'Rourke and M. Hamada, 12/1/89, (PB90-209388, A22, MF-A03).

NCEER-89-0033 "Deterministic Model for Seismic Damage Evaluation of Reinforced Concrete Structures," by J.M. Bracci, A.M. Reinhorn, J.B. Mander and S.K. Kunnath, 9/27/89, (PB91-108803, A06, MF-A01).

NCEER-89-0034 "On the Relation Between Local and Global Damage Indices," by E. DiPasquale and A.S. Cakmak, 8/15/89, (PB90-173865, A05, MF-A01).

NCEER-89-0035 "Cyclic Undrained Behavior of Nonplastic and Low Plasticity Silts," by A.J. Walker and H.E. Stewart, 7/26/89, (PB90-183518, A10, MF-A01).

NCEER-89-0036 "Liquefaction Potential of Surficial Deposits in the City of Buffalo, New York," by M. Budhu, R. Giese and L. Baumgrass, 1/17/89, (PB90-208455, A04, MF-A01).

NCEER-89-0037 "A Deterministic Assessment of Effects of Ground Motion Incoherence," by A.S. Veletsos and Y. Tang, 7/15/89, (PB90-164294, A03, MF-A01).

NCEER-89-0038 "Workshop on Ground Motion Parameters for Seismic Hazard Mapping," July 17-18, 1989, edited by R.V. Whitman, 12/1/89, (PB90-173923, A04, MF-A01).

NCEER-89-0039 "Seismic Effects on Elevated Transit Lines of the New York City Transit Authority," by C.J. Costantino, C.A. Miller and E. Heymsfield, 12/26/89, (PB90-207887, A06, MF-A01).

NCEER-89-0040 "Centrifugal Modeling of Dynamic Soil-Structure Interaction," by K. Weissman, Supervised by J.H. Prevost, 5/10/89, (PB90-207879, A07, MF-A01).

NCEER-89-0041 "Linearized Identification of Buildings With Cores for Seismic Vulnerability Assessment," by I-K. Ho and A.E. Aktan, 11/1/89, (PB90-251943, A07, MF-A01).

NCEER-90-0001 "Geotechnical and Lifeline Aspects of the October 17, 1989 Loma Prieta Earthquake in San Francisco," by T.D. O'Rourke, H.E. Stewart, F.T. Blackburn and T.S. Dickerman, 1/90, (PB90-208596, A05, MF-A01).

NCEER-90-0002 "Nonnormal Secondary Response Due to Yielding in a Primary Structure," by D.C.K. Chen and L.D. Lutes, 2/28/90, (PB90-251976, A07, MF-A01).

NCEER-90-0003 "Earthquake Education Materials for Grades K-12," by K.E.K. Ross, 4/16/90, (PB91-251984, A05, MF-A05). This report has been replaced by NCEER-92-0018.

NCEER-90-0004 "Catalog of Strong Motion Stations in Eastern North America," by R.W. Busby, 4/3/90, (PB90-251984, A05, MF-A01).

NCEER-90-0005 "NCEER Strong-Motion Data Base: A User Manual for the GeoBase Release (Version 1.0 for the Sun3)," by P. Friberg and K. Jacob, 3/31/90 (PB90-258062, A04, MF-A01).

NCEER-90-0006 "Seismic Hazard Along a Crude Oil Pipeline in the Event of an 1811-1812 Type New Madrid Earthquake," by H.H.M. Hwang and C-H.S. Chen, 4/16/90, (PB90-258054, A04, MF-A01).

NCEER-90-0007 "Site-Specific Response Spectra for Memphis Sheahan Pumping Station," by H.H.M. Hwang and C.S. Lee, 5/15/90, (PB91-108811, A05, MF-A01).

NCEER-90-0008 "Pilot Study on Seismic Vulnerability of Crude Oil Transmission Systems," by T. Ariman, R. Dobry, M. Grigoriu, F. Kozin, M. O'Rourke, T. O'Rourke and M. Shinozuka, 5/25/90, (PB91-108837, A06, MF-A01).

NCEER-90-0009 "A Program to Generate Site Dependent Time Histories: EQGEN," by G.W. Ellis, M. Srinivasan and A.S. Cakmak, 1/30/90, (PB91-108829, A04, MF-A01).

NCEER-90-0010 "Active Isolation for Seismic Protection of Operating Rooms," by M.E. Talbott, Supervised by M. Shinozuka, 6/8/9, (PB91-110205, A05, MF-A01).

NCEER-90-0011 "Program LINEARID for Identification of Linear Structural Dynamic Systems," by C-B. Yun and M. Shinozuka, 6/25/90, (PB91-110312, A08, MF-A01).

NCEER-90-0012 "Two-Dimensional Two-Phase Elasto-Plastic Seismic Response of Earth Dams," by A.N. Yiagos, Supervised by J.H. Prevost, 6/20/90, (PB91-110197, A13, MF-A02).

NCEER-90-0013 "Secondary Systems in Base-Isolated Structures: Experimental Investigation, Stochastic Response and Stochastic Sensitivity," by G.D. Manolis, G. Juhn, M.C. Constantinou and A.M. Reinhorn, 7/1/90, (PB91-110320, A08, MF-A01).

NCEER-90-0014 "Seismic Behavior of Lightly-Reinforced Concrete Column and Beam-Column Joint Details," by S.P. Pessiki, C.H. Conley, P. Gergely and R.N. White, 8/22/90, (PB91-108795, A11, MF-A02).

NCEER-90-0015 "Two Hybrid Control Systems for Building Structures Under Strong Earthquakes," by J.N. Yang and A. Danielians, 6/29/90, (PB91-125393, A04, MF-A01).

NCEER-90-0016 "Instantaneous Optimal Control with Acceleration and Velocity Feedback," by J.N. Yang and Z. Li, 6/29/90, (PB91-125401, A03, MF-A01).

NCEER-90-0017 "Reconnaissance Report on the Northern Iran Earthquake of June 21, 1990," by M. Mehrain, 10/4/90, (PB91-125377, A03, MF-A01).

NCEER-90-0018 "Evaluation of Liquefaction Potential in Memphis and Shelby County," by T.S. Chang, P.S. Tang, C.S. Lee and H. Hwang, 8/10/90, (PB91-125427, A09, MF-A01).

NCEER-90-0019 "Experimental and Analytical Study of a Combined Sliding Disc Bearing and Helical Steel Spring Isolation System," by M.C. Constantinou, A.S. Mokha and A.M. Reinhorn, 10/4/90, (PB91-125385, A06, MF-A01). This report is available only through NTIS (see address given above).

NCEER-90-0020 "Experimental Study and Analytical Prediction of Earthquake Response of a Sliding Isolation System with a Spherical Surface," by A.S. Mokha, M.C. Constantinou and A.M. Reinhorn, 10/11/90, (PB91-125419, A05, MF-A01).

NCEER-90-0021 "Dynamic Interaction Factors for Floating Pile Groups," by G. Gazetas, K. Fan, A. Kaynia and E. Kausel, 9/10/90, (PB91-170381, A05, MF-A01).

NCEER-90-0022 "Evaluation of Seismic Damage Indices for Reinforced Concrete Structures," by S. Rodriguez-Gomez and A.S. Cakmak, 9/30/90, PB91-171322, A06, MF-A01).

NCEER-90-0023 "Study of Site Response at a Selected Memphis Site," by H. Desai, S. Ahmad, E.S. Gazetas and M.R. Oh, 10/11/90, (PB91-196857, A03, MF-A01).

NCEER-90-0024 "A User's Guide to Strongmo: Version 1.0 of NCEER's Strong-Motion Data Access Tool for PCs and Terminals," by P.A. Friberg and C.A.T. Susch, 11/15/90, (PB91-171272, A03, MF-A01).

NCEER-90-0025 "A Three-Dimensional Analytical Study of Spatial Variability of Seismic Ground Motions," by L-L. Hong and A.H.-S. Ang, 10/30/90, (PB91-170399, A09, MF-A01).

NCEER-90-0026 "MUMOID User's Guide - A Program for the Identification of Modal Parameters," by S. Rodriguez-Gomez and E. DiPasquale, 9/30/90, (PB91-171298, A04, MF-A01).

NCEER-90-0027 "SARCF-II User's Guide - Seismic Analysis of Reinforced Concrete Frames," by S. Rodriguez-Gomez, Y.S. Chung and C. Meyer, 9/30/90, (PB91-171280, A05, MF-A01).

NCEER-90-0028 "Viscous Dampers: Testing, Modeling and Application in Vibration and Seismic Isolation," by N. Makris and M.C. Constantinou, 12/20/90 (PB91-190561, A06, MF-A01).

NCEER-90-0029 "Soil Effects on Earthquake Ground Motions in the Memphis Area," by H. Hwang, C.S. Lee, K.W. Ng and T.S. Chang, 8/2/90, (PB91-190751, A05, MF-A01).

NCEER-91-0001 "Proceedings from the Third Japan-U.S. Workshop on Earthquake Resistant Design of Lifeline Facilities and Countermeasures for Soil Liquefaction, December 17-19, 1990," edited by T.D. O'Rourke and M. Hamada, 2/1/91, (PB91-179259, A99, MF-A04).

NCEER-91-0002 "Physical Space Solutions of Non-Proportionally Damped Systems," by M. Tong, Z. Liang and G.C. Lee, 1/15/91, (PB91-179242, A04, MF-A01).

NCEER-91-0003 "Seismic Response of Single Piles and Pile Groups," by K. Fan and G. Gazetas, 1/10/91, (PB92-174994, A04, MF-A01).

NCEER-91-0004 "Damping of Structures: Part 1 - Theory of Complex Damping," by Z. Liang and G. Lee, 10/10/91, (PB92-197235, A12, MF-A03).

NCEER-91-0005 "3D-BASIS - Nonlinear Dynamic Analysis of Three Dimensional Base Isolated Structures: Part II," by S. Nagarajaiah, A.M. Reinhorn and M.C. Constantinou, 2/28/91, (PB91-190553, A07, MF-A01). This report has been replaced by NCEER-93-0011.

NCEER-91-0006 "A Multidimensional Hysteretic Model for Plasticity Deforming Metals in Energy Absorbing Devices," by E.J. Graesser and F.A. Cozzarelli, 4/9/91, (PB92-108364, A04, MF-A01).

NCEER-91-0007 "A Framework for Customizable Knowledge-Based Expert Systems with an Application to a KBES for Evaluating the Seismic Resistance of Existing Buildings," by E.G. Ibarra-Anaya and S.J. Fenves, 4/9/91, (PB91-210930, A08, MF-A01).

NCEER-91-0008 "Nonlinear Analysis of Steel Frames with Semi-Rigid Connections Using the Capacity Spectrum Method," by G.G. Deierlein, S-H. Hsieh, Y-J. Shen and J.F. Abel, 7/2/91, (PB92-113828, A05, MF-A01).

NCEER-91-0009 "Earthquake Education Materials for Grades K-12," by K.E.K. Ross, 4/30/91, (PB91-212142, A06, MF-A01). This report has been replaced by NCEER-92-0018.

NCEER-91-0010 "Phase Wave Velocities and Displacement Phase Differences in a Harmonically Oscillating Pile," by N. Makris and G. Gazetas, 7/8/91, (PB92-108356, A04, MF-A01).

NCEER-91-0011 "Dynamic Characteristics of a Full-Size Five-Story Steel Structure and a 2/5 Scale Model," by K.C. Chang, G.C. Yao, G.C. Lee, D.S. Hao and Y.C. Yeh," 7/2/91, (PB93-116648, A06, MF-A02).

NCEER-91-0012 "Seismic Response of a 2/5 Scale Steel Structure with Added Viscoelastic Dampers," by K.C. Chang, T.T. Soong, S-T. Oh and M.L. Lai, 5/17/91, (PB92-110816, A05, MF-A01).

NCEER-91-0013 "Earthquake Response of Retaining Walls; Full-Scale Testing and Computational Modeling," by S. Alampalli and A-W.M. Elgamal, 6/20/91, to be published.

NCEER-91-0014 "3D-BASIS-M: Nonlinear Dynamic Analysis of Multiple Building Base Isolated Structures," by P.C. Tsopelas, S. Nagarajaiah, M.C. Constantinou and A.M. Reinhorn, 5/28/91, (PB92-113885, A09, MF-A02).

NCEER-91-0015 "Evaluation of SEAOC Design Requirements for Sliding Isolated Structures," by D. Theodossiou and M.C. Constantinou, 6/10/91, (PB92-114602, A11, MF-A03).

NCEER-91-0016 "Closed-Loop Modal Testing of a 27-Story Reinforced Concrete Flat Plate-Core Building," by H.R. Somaprasad, T. Toksoy, H. Yoshiyuki and A.E. Aktan, 7/15/91, (PB92-129980, A07, MF-A02).

NCEER-91-0017 "Shake Table Test of a 1/6 Scale Two-Story Lightly Reinforced Concrete Building," by A.G. El-Attar, R.N. White and P. Gergely, 2/28/91, (PB92-222447, A06, MF-A02).

NCEER-91-0018 "Shake Table Test of a 1/8 Scale Three-Story Lightly Reinforced Concrete Building," by A.G. El-Attar, R.N. White and P. Gergely, 2/28/91, (PB93-116630, A08, MF-A02).

NCEER-91-0019 "Transfer Functions for Rigid Rectangular Foundations," by A.S. Veletsos, A.M. Prasad and W.H. Wu, 7/31/91, to be published.

NCEER-91-0020 "Hybrid Control of Seismic-Excited Nonlinear and Inelastic Structural Systems," by J.N. Yang, Z. Li and A. Danielians, 8/1/91, (PB92-143171, A06, MF-A02).

NCEER-91-0021 "The NCEER-91 Earthquake Catalog: Improved Intensity-Based Magnitudes and Recurrence Relations for U.S. Earthquakes East of New Madrid," by L. Seeber and J.G. Armbruster, 8/28/91, (PB92-176742, A06, MF-A02).

NCEER-91-0022 "Proceedings from the Implementation of Earthquake Planning and Education in Schools: The Need for Change - The Roles of the Changemakers," by K.E.K. Ross and F. Winslow, 7/23/91, (PB92-129998, A12, MF-A03).

NCEER-91-0023 "A Study of Reliability-Based Criteria for Seismic Design of Reinforced Concrete Frame Buildings," by H.H.M. Hwang and H-M. Hsu, 8/10/91, (PB92-140235, A09, MF-A02).

NCEER-91-0024 "Experimental Verification of a Number of Structural System Identification Algorithms," by R.G. Ghanem, H. Gavin and M. Shinozuka, 9/18/91, (PB92-176577, A18, MF-A04).

NCEER-91-0025 "Probabilistic Evaluation of Liquefaction Potential," by H.H.M. Hwang and C.S. Lee," 11/25/91, (PB92-143429, A05, MF-A01).

NCEER-91-0026 "Instantaneous Optimal Control for Linear, Nonlinear and Hysteretic Structures - Stable Controllers," by J.N. Yang and Z. Li, 11/15/91, (PB92-163807, A04, MF-A01).

NCEER-91-0027 "Experimental and Theoretical Study of a Sliding Isolation System for Bridges," by M.C. Constantinou, A. Kartoum, A.M. Reinhorn and P. Bradford, 11/15/91, (PB92-176973, A10, MF-A03).

NCEER-92-0001 "Case Studies of Liquefaction and Lifeline Performance During Past Earthquakes, Volume 1: Japanese Case Studies," Edited by M. Hamada and T. O'Rourke, 2/17/92, (PB92-197243, A18, MF-A04).

NCEER-92-0002 "Case Studies of Liquefaction and Lifeline Performance During Past Earthquakes, Volume 2: United States Case Studies," Edited by T. O'Rourke and M. Hamada, 2/17/92, (PB92-197250, A20, MF-A04).

NCEER-92-0003 "Issues in Earthquake Education," Edited by K. Ross, 2/3/92, (PB92-222389, A07, MF-A02).

NCEER-92-0004 "Proceedings from the First U.S. - Japan Workshop on Earthquake Protective Systems for Bridges," Edited by I.G. Buckle, 2/4/92, (PB94-142239, A99, MF-A06).

NCEER-92-0005 "Seismic Ground Motion from a Haskell-Type Source in a Multiple-Layered Half-Space," A.P. Theoharis, G. Deodatis and M. Shinozuka, 1/2/92, to be published.

NCEER-92-0006 "Proceedings from the Site Effects Workshop," Edited by R. Whitman, 2/29/92, (PB92-197201, A04, MF-A01).

NCEER-92-0007 "Engineering Evaluation of Permanent Ground Deformations Due to Seismically-Induced Liquefaction," by M.H. Baziar, R. Dobry and A-W.M. Elgamal, 3/24/92, (PB92-222421, A13, MF-A03).

NCEER-92-0008 "A Procedure for the Seismic Evaluation of Buildings in the Central and Eastern United States," by C.D. Poland and J.O. Malley, 4/2/92, (PB92-222439, A20, MF-A04).

NCEER-92-0009 "Experimental and Analytical Study of a Hybrid Isolation System Using Friction Controllable Sliding Bearings," by M.Q. Feng, S. Fujii and M. Shinozuka, 5/15/92, (PB93-150282, A06, MF-A02).

NCEER-92-0010 "Seismic Resistance of Slab-Column Connections in Existing Non-Ductile Flat-Plate Buildings," by A.J. Durrani and Y. Du, 5/18/92, (PB93-116812, A06, MF-A02).

NCEER-92-0011 "The Hysteretic and Dynamic Behavior of Brick Masonry Walls Upgraded by Ferrocement Coatings Under Cyclic Loading and Strong Simulated Ground Motion," by H. Lee and S.P. Prawel, 5/11/92, to be published.

NCEER-92-0012 "Study of Wire Rope Systems for Seismic Protection of Equipment in Buildings," by G.F. Demetriades, M.C. Constantinou and A.M. Reinhorn, 5/20/92, (PB93-116655, A08, MF-A02).

NCEER-92-0013 "Shape Memory Structural Dampers: Material Properties, Design and Seismic Testing," by P.R. Witting and F.A. Cozzarelli, 5/26/92, (PB93-116663, A05, MF-A01).

NCEER-92-0014 "Longitudinal Permanent Ground Deformation Effects on Buried Continuous Pipelines," by M.J. O'Rourke, and C. Nordberg, 6/15/92, (PB93-116671, A08, MF-A02).

NCEER-92-0015 "A Simulation Method for Stationary Gaussian Random Functions Based on the Sampling Theorem," by M. Grigoriu and S. Balopoulou, 6/11/92, (PB93-127496, A05, MF-A01).

NCEER-92-0016 "Gravity-Load-Designed Reinforced Concrete Buildings: Seismic Evaluation of Existing Construction and Detailing Strategies for Improved Seismic Resistance," by G.W. Hoffmann, S.K. Kunnath, A.M. Reinhorn and J.B. Mander, 7/15/92, (PB94-142007, A08, MF-A02).

NCEER-92-0017 "Observations on Water System and Pipeline Performance in the Limón Area of Costa Rica Due to the April 22, 1991 Earthquake," by M. O'Rourke and D. Ballantyne, 6/30/92, (PB93-126811, A06, MF-A02).

NCEER-92-0018 "Fourth Edition of Earthquake Education Materials for Grades K-12," Edited by K.E.K. Ross, 8/10/92, (PB93-114023, A07, MF-A02).

NCEER-92-0019 "Proceedings from the Fourth Japan-U.S. Workshop on Earthquake Resistant Design of Lifeline Facilities and Countermeasures for Soil Liquefaction," Edited by M. Hamada and T.D. O'Rourke, 8/12/92, (PB93-163939, A99, MF-E11).

NCEER-92-0020 "Active Bracing System: A Full Scale Implementation of Active Control," by A.M. Reinhorn, T.T. Soong, R.C. Lin, M.A. Riley, Y.P. Wang, S. Aizawa and M. Higashino, 8/14/92, (PB93-127512, A06, MF-A02).

NCEER-92-0021 "Empirical Analysis of Horizontal Ground Displacement Generated by Liquefaction-Induced Lateral Spreads," by S.F. Bartlett and T.L. Youd, 8/17/92, (PB93-188241, A06, MF-A02).

NCEER-92-0022 "IDARC Version 3.0: Inelastic Damage Analysis of Reinforced Concrete Structures," by S.K. Kunnath, A.M. Reinhorn and R.F. Lobo, 8/31/92, (PB93-227502, A07, MF-A02).

NCEER-92-0023 "A Semi-Empirical Analysis of Strong-Motion Peaks in Terms of Seismic Source, Propagation Path and Local Site Conditions, by M. Kamiyama, M.J. O'Rourke and R. Flores-Berrones, 9/9/92, (PB93-150266, A08, MF-A02).

NCEER-92-0024 "Seismic Behavior of Reinforced Concrete Frame Structures with Nonductile Details, Part I: Summary of Experimental Findings of Full Scale Beam-Column Joint Tests," by A. Beres, R.N. White and P. Gergely, 9/30/92, (PB93-227783, A05, MF-A01).

NCEER-92-0025 "Experimental Results of Repaired and Retrofitted Beam-Column Joint Tests in Lightly Reinforced Concrete Frame Buildings," by A. Beres, S. El-Borgi, R.N. White and P. Gergely, 10/29/92, (PB93-227791, A05, MF-A01).

NCEER-92-0026 "A Generalization of Optimal Control Theory: Linear and Nonlinear Structures," by J.N. Yang, Z. Li and S. Vongchavalitkul, 11/2/92, (PB93-188621, A05, MF-A01).

NCEER-92-0027 "Seismic Resistance of Reinforced Concrete Frame Structures Designed Only for Gravity Loads: Part I - Design and Properties of a One-Third Scale Model Structure," by J.M. Bracci, A.M. Reinhorn and J.B. Mander, 12/1/92, (PB94-104502, A08, MF-A02).

NCEER-92-0028 "Seismic Resistance of Reinforced Concrete Frame Structures Designed Only for Gravity Loads: Part II - Experimental Performance of Subassemblages," by L.E. Aycardi, J.B. Mander and A.M. Reinhorn, 12/1/92, (PB94-104510, A08, MF-A02).

NCEER-92-0029 "Seismic Resistance of Reinforced Concrete Frame Structures Designed Only for Gravity Loads: Part III - Experimental Performance and Analytical Study of a Structural Model," by J.M. Bracci, A.M. Reinhorn and J.B. Mander, 12/1/92, (PB93-227528, A09, MF-A01).

NCEER-92-0030 "Evaluation of Seismic Retrofit of Reinforced Concrete Frame Structures: Part I - Experimental Performance of Retrofitted Subassemblages," by D. Choudhuri, J.B. Mander and A.M. Reinhorn, 12/8/92, (PB93-198307, A07, MF-A02).

NCEER-92-0031 "Evaluation of Seismic Retrofit of Reinforced Concrete Frame Structures: Part II - Experimental Performance and Analytical Study of a Retrofitted Structural Model," by J.M. Bracci, A.M. Reinhorn and J.B. Mander, 12/8/92, (PB93-198315, A09, MF-A03).

NCEER-92-0032 "Experimental and Analytical Investigation of Seismic Response of Structures with Supplemental Fluid Viscous Dampers," by M.C. Constantinou and M.D. Symans, 12/21/92, (PB93-191435, A10, MF-A03).

NCEER-92-0033 "Reconnaissance Report on the Cairo, Egypt Earthquake of October 12, 1992," by M. Khater, 12/23/92, (PB93-188621, A03, MF-A01).

NCEER-92-0034 "Low-Level Dynamic Characteristics of Four Tall Flat-Plate Buildings in New York City," by H. Gavin, S. Yuan, J. Grossman, E. Pekelis and K. Jacob, 12/28/92, (PB93-188217, A07, MF-A02).

NCEER-93-0001 "An Experimental Study on the Seismic Performance of Brick-Infilled Steel Frames With and Without Retrofit," by J.B. Mander, B. Nair, K. Wojtkowski and J. Ma, 1/29/93, (PB93-227510, A07, MF-A02).

NCEER-93-0002 "Social Accounting for Disaster Preparedness and Recovery Planning," by S. Cole, E. Pantoja and V. Razak, 2/22/93, (PB94-142114, A12, MF-A03).

NCEER-93-0003 "Assessment of 1991 NEHRP Provisions for Nonstructural Components and Recommended Revisions," by T.T. Soong, G. Chen, Z. Wu, R-H. Zhang and M. Grigoriu, 3/1/93, (PB93-188639, A06, MF-A02).

NCEER-93-0004 "Evaluation of Static and Response Spectrum Analysis Procedures of SEAOC/UBC for Seismic Isolated Structures," by C.W. Winters and M.C. Constantinou, 3/23/93, (PB93-198299, A10, MF-A03).

NCEER-93-0005 "Earthquakes in the Northeast - Are We Ignoring the Hazard? A Workshop on Earthquake Science and Safety for Educators," edited by K.E.K. Ross, 4/2/93, (PB94-103066, A09, MF-A02).

NCEER-93-0006 "Inelastic Response of Reinforced Concrete Structures with Viscoelastic Braces," by R.F. Lobo, J.M. Bracci, K.L. Shen, A.M. Reinhorn and T.T. Soong, 4/5/93, (PB93-227486, A05, MF-A02).

NCEER-93-0007 "Seismic Testing of Installation Methods for Computers and Data Processing Equipment," by K. Kosar, T.T. Soong, K.L. Shen, J.A. HoLung and Y.K. Lin, 4/12/93, (PB93-198299, A07, MF-A02).

NCEER-93-0008 "Retrofit of Reinforced Concrete Frames Using Added Dampers," by A. Reinhorn, M. Constantinou and C. Li, to be published.

NCEER-93-0009 "Seismic Behavior and Design Guidelines for Steel Frame Structures with Added Viscoelastic Dampers," by K.C. Chang, M.L. Lai, T.T. Soong, D.S. Hao and Y.C. Yeh, 5/1/93, (PB94-141959, A07, MF-A02).

NCEER-93-0010 "Seismic Performance of Shear-Critical Reinforced Concrete Bridge Piers," by J.B. Mander, S.M. Waheed, M.T.A. Chaudhary and S.S. Chen, 5/12/93, (PB93-227494, A08, MF-A02).

NCEER-93-0011 "3D-BASIS-TABS: Computer Program for Nonlinear Dynamic Analysis of Three Dimensional Base Isolated Structures," by S. Nagarajaiah, C. Li, A.M. Reinhorn and M.C. Constantinou, 8/2/93, (PB94-141819, A09, MF-A02).

NCEER-93-0012 "Effects of Hydrocarbon Spills from an Oil Pipeline Break on Ground Water," by O.J. Helweg and H.H.M. Hwang, 8/3/93, (PB94-141942, A06, MF-A02).

NCEER-93-0013 "Simplified Procedures for Seismic Design of Nonstructural Components and Assessment of Current Code Provisions," by M.P. Singh, L.E. Suarez, E.E. Matheu and G.O. Maldonado, 8/4/93, (PB94-141827, A09, MF-A02).

NCEER-93-0014 "An Energy Approach to Seismic Analysis and Design of Secondary Systems," by G. Chen and T.T. Soong, 8/6/93, (PB94-142767, A11, MF-A03).

NCEER-93-0015 "Proceedings from School Sites: Becoming Prepared for Earthquakes - Commemorating the Third Anniversary of the Loma Prieta Earthquake," Edited by F.E. Winslow and K.E.K. Ross, 8/16/93, (PB94-154275, A16, MF-A02).

NCEER-93-0016 "Reconnaissance Report of Damage to Historic Monuments in Cairo, Egypt Following the October 12, 1992 Dahshur Earthquake," by D. Sykora, D. Look, G. Croci, E. Karaesmen and E. Karaesmen, 8/19/93, (PB94-142221, A08, MF-A02).

NCEER-93-0017 "The Island of Guam Earthquake of August 8, 1993," by S.W. Swan and S.K. Harris, 9/30/93, (PB94-141843, A04, MF-A01).

NCEER-93-0018 "Engineering Aspects of the October 12, 1992 Egyptian Earthquake," by A.W. Elgamal, M. Amer, K. Adalier and A. Abul-Fadl, 10/7/93, (PB94-141983, A05, MF-A01).

NCEER-93-0019 "Development of an Earthquake Motion Simulator and its Application in Dynamic Centrifuge Testing," by I. Krstelj, Supervised by J.H. Prevost, 10/23/93, (PB94-181773, A-10, MF-A03).

NCEER-93-0020 "NCEER-Taisei Corporation Research Program on Sliding Seismic Isolation Systems for Bridges: Experimental and Analytical Study of a Friction Pendulum System (FPS)," by M.C. Constantinou, P. Tsopelas, Y-S. Kim and S. Okamoto, 11/1/93, (PB94-142775, A08, MF-A02).

NCEER-93-0021 "Finite Element Modeling of Elastomeric Seismic Isolation Bearings," by L.J. Billings, Supervised by R. Shepherd, 11/8/93, to be published.

NCEER-93-0022 "Seismic Vulnerability of Equipment in Critical Facilities: Life-Safety and Operational Consequences," by K. Porter, G.S. Johnson, M.M. Zadeh, C. Scawthorn and S. Eder, 11/24/93, (PB94-181765, A16, MF-A03).

NCEER-93-0023 "Hokkaido Nansei-oki, Japan Earthquake of July 12, 1993, by P.I. Yanev and C.R. Scawthorn, 12/23/93, (PB94-181500, A07, MF-A01).

NCEER-94-0001 "An Evaluation of Seismic Serviceability of Water Supply Networks with Application to the San Francisco Auxiliary Water Supply System," by I. Markov, Supervised by M. Grigoriu and T. O'Rourke, 1/21/94, (PB94-204013, A07, MF-A02).

NCEER-94-0002 "NCEER-Taisei Corporation Research Program on Sliding Seismic Isolation Systems for Bridges: Experimental and Analytical Study of Systems Consisting of Sliding Bearings, Rubber Restoring Force Devices and Fluid Dampers," Volumes I and II, by P. Tsopelas, S. Okamoto, M.C. Constantinou, D. Ozaki and S. Fujii, 2/4/94, (PB94-181740, A09, MF-A02 and PB94-181757, A12, MF-A03).

NCEER-94-0003 "A Markov Model for Local and Global Damage Indices in Seismic Analysis," by S. Rahman and M. Grigoriu, 2/18/94, (PB94-206000, A12, MF-A03).

NCEER-94-0004 "Proceedings from the NCEER Workshop on Seismic Response of Masonry Infills," edited by D.P. Abrams, 3/1/94, (PB94-180783, A07, MF-A02).

NCEER-94-0005 "The Northridge, California Earthquake of January 17, 1994: General Reconnaissance Report," edited by J.D. Goltz, 3/11/94, (PB193943, A10, MF-A03).

NCEER-94-0006 "Seismic Energy Based Fatigue Damage Analysis of Bridge Columns: Part I - Evaluation of Seismic Capacity," by G.A. Chang and J.B. Mander, 3/14/94, (PB94-219185, A11, MF-A03).

NCEER-94-0007 "Seismic Isolation of Multi-Story Frame Structures Using Spherical Sliding Isolation Systems," by T.M. Al-Hussaini, V.A. Zayas and M.C. Constantinou, 3/17/94, (PB193745, A09, MF-A02).

NCEER-94-0008 "The Northridge, California Earthquake of January 17, 1994: Performance of Highway Bridges," edited by I.G. Buckle, 3/24/94, (PB94-193851, A06, MF-A02).

NCEER-94-0009 "Proceedings of the Third U.S.-Japan Workshop on Earthquake Protective Systems for Bridges," edited by I.G. Buckle and I. Friedland, 3/31/94, (PB94-195815, A99, MF-A06).

NCEER-94-0010 "3D-BASIS-ME: Computer Program for Nonlinear Dynamic Analysis of Seismically Isolated Single and Multiple Structures and Liquid Storage Tanks," by P.C. Tsopelas, M.C. Constantinou and A.M. Reinhorn, 4/12/94, (PB94-204922, A09, MF-A02).

NCEER-94-0011 "The Northridge, California Earthquake of January 17, 1994: Performance of Gas Transmission Pipelines," by T.D. O'Rourke and M.C. Palmer, 5/16/94, (PB94-204989, A05, MF-A01).

NCEER-94-0012 "Feasibility Study of Replacement Procedures and Earthquake Performance Related to Gas Transmission Pipelines," by T.D. O'Rourke and M.C. Palmer, 5/25/94, (PB94-206638, A09, MF-A02).

NCEER-94-0013 "Seismic Energy Based Fatigue Damage Analysis of Bridge Columns: Part II - Evaluation of Seismic Demand," by G.A. Chang and J.B. Mander, 6/1/94, (PB95-18106, A08, MF-A02).

NCEER-94-0014 "NCEER-Taisei Corporation Research Program on Sliding Seismic Isolation Systems for Bridges: Experimental and Analytical Study of a System Consisting of Sliding Bearings and Fluid Restoring Force/Damping Devices," by P. Tsopelas and M.C. Constantinou, 6/13/94, (PB94-219144, A10, MF-A03).

NCEER-94-0015 "Generation of Hazard-Consistent Fragility Curves for Seismic Loss Estimation Studies," by H. Hwang and J-R. Huo, 6/14/94, (PB95-181996, A09, MF-A02).

NCEER-94-0016 "Seismic Study of Building Frames with Added Energy-Absorbing Devices," by W.S. Pong, C.S. Tsai and G.C. Lee, 6/20/94, (PB94-219136, A10, A03).

NCEER-94-0017 "Sliding Mode Control for Seismic-Excited Linear and Nonlinear Civil Engineering Structures," by J. Yang, J. Wu, A. Agrawal and Z. Li, 6/21/94, (PB95-138483, A06, MF-A02).

NCEER-94-0018 "3D-BASIS-TABS Version 2.0: Computer Program for Nonlinear Dynamic Analysis of Three Dimensional Base Isolated Structures," by A.M. Reinhorn, S. Nagarajaiah, M.C. Constantinou, P. Tsopelas and R. Li, 6/22/94, (PB95-182176, A08, MF-A02).

NCEER-94-0019 "Proceedings of the International Workshop on Civil Infrastructure Systems: Application of Intelligent Systems and Advanced Materials on Bridge Systems," Edited by G.C. Lee and K.C. Chang, 7/18/94, (PB95-252474, A20, MF-A04).

NCEER-94-0020 "Study of Seismic Isolation Systems for Computer Floors," by V. Lambrou and M.C. Constantinou, 7/19/94, (PB95-138533, A10, MF-A03).

NCEER-94-0021 "Proceedings of the U.S.-Italian Workshop on Guidelines for Seismic Evaluation and Rehabilitation of Unreinforced Masonry Buildings," Edited by D.P. Abrams and G.M. Calvi, 7/20/94, (PB95-138749, A13, MF-A03).

NCEER-94-0022 "NCEER-Taisei Corporation Research Program on Sliding Seismic Isolation Systems for Bridges: Experimental and Analytical Study of a System Consisting of Lubricated PTFE Sliding Bearings and Mild Steel Dampers," by P. Tsopelas and M.C. Constantinou, 7/22/94, (PB95-182184, A08, MF-A02).

NCEER-94-0023 "Development of Reliability-Based Design Criteria for Buildings Under Seismic Load," by Y.K. Wen, H. Hwang and M. Shinozuka, 8/1/94, (PB95-211934, A08, MF-A02).

NCEER-94-0024 "Experimental Verification of Acceleration Feedback Control Strategies for an Active Tendon System," by S.J. Dyke, B.F. Spencer, Jr., P. Quast, M.K. Sain, D.C. Kaspari, Jr. and T.T. Soong, 8/29/94, (PB95-212320, A05, MF-A01).

NCEER-94-0025 "Seismic Retrofitting Manual for Highway Bridges," Edited by I.G. Buckle and I.F. Friedland, to be published.

NCEER-94-0026 "Proceedings from the Fifth U.S.-Japan Workshop on Earthquake Resistant Design of Lifeline Facilities and Countermeasures Against Soil Liquefaction," Edited by T.D. O'Rourke and M. Hamada, 11/7/94, (PB95-220802, A99, MF-E08).

NCEER-95-0001 "Experimental and Analytical Investigation of Seismic Retrofit of Structures with Supplemental Damping: Part 1 - Fluid Viscous Damping Devices," by A.M. Reinhorn, C. Li and M.C. Constantinou, 1/3/95, (PB95-266599, A09, MF-A02).

NCEER-95-0002 "Experimental and Analytical Study of Low-Cycle Fatigue Behavior of Semi-Rigid Top-And-Seat Angle Connections," by G. Pekcan, J.B. Mander and S.S. Chen, 1/5/95, (PB95-220042, A07, MF-A02).

NCEER-95-0003 "NCEER-ATC Joint Study on Fragility of Buildings," by T. Anagnos, C. Rojahn and A.S. Kiremidjian, 1/20/95, (PB95-220026, A06, MF-A02).

NCEER-95-0004 "Nonlinear Control Algorithms for Peak Response Reduction," by Z. Wu, T.T. Soong, V. Gattulli and R.C. Lin, 2/16/95, (PB95-220349, A05, MF-A01).

NCEER-95-0005 "Pipeline Replacement Feasibility Study: A Methodology for Minimizing Seismic and Corrosion Risks to Underground Natural Gas Pipelines," by R.T. Eguchi, H.A. Seligson and D.G. Honegger, 3/2/95, (PB95-252326, A06, MF-A02).

NCEER-95-0006 "Evaluation of Seismic Performance of an 11-Story Frame Building During the 1994 Northridge Earthquake," by F. Naeim, R. DiSulio, K. Benuska, A. Reinhorn and C. Li, to be published.

NCEER-95-0007 "Prioritization of Bridges for Seismic Retrofitting," by N. Basöz and A.S. Kiremidjian, 4/24/95, (PB95-252300, A08, MF-A02).

NCEER-95-0008 "Method for Developing Motion Damage Relationships for Reinforced Concrete Frames," by A. Singhal and A.S. Kiremidjian, 5/11/95, (PB95-266607, A06, MF-A02).

NCEER-95-0009 "Experimental and Analytical Investigation of Seismic Retrofit of Structures with Supplemental Damping: Part II - Friction Devices," by C. Li and A.M. Reinhorn, 7/6/95, (PB96-128087, A11, MF-A03).

NCEER-95-0010 "Experimental Performance and Analytical Study of a Non-Ductile Reinforced Concrete Frame Structure Retrofitted with Elastomeric Spring Dampers," by G. Pekcan, J.B. Mander and S.S. Chen, 7/14/95, (PB96-137161, A08, MF-A02).

NCEER-95-0011 "Development and Experimental Study of Semi-Active Fluid Damping Devices for Seismic Protection of Structures," by M.D. Symans and M.C. Constantinou, 8/3/95, (PB96-136940, A23, MF-A04).

NCEER-95-0012 "Real-Time Structural Parameter Modification (RSPM): Development of Innervated Structures," by Z. Liang, M. Tong and G.C. Lee, 4/11/95, (PB96-137153, A06, MF-A01).

NCEER-95-0013 "Experimental and Analytical Investigation of Seismic Retrofit of Structures with Supplemental Damping: Part III - Viscous Damping Walls," by A.M. Reinhorn and C. Li, 10/1/95.

NCEER-95-0014 "Seismic Fragility Analysis of Equipment and Structures in a Memphis Electric Substation," by J-R. Huo and H.H.M. Hwang, 8/10/95.

NCEER-95-0015 "The Hanshin-Awaji Earthquake of January 17, 1995: Performance of Lifelines," Edited by M. Shinozuka, 11/3/95, (PB96-176383, A15, MF-A03).

NCEER-95-0016 "Highway Culvert Performance During Earthquakes," by T.L. Youd and C.J. Beckman, 11/6/95, to be published.

NCEER-95-0017 "The Hanshin-Awaji Earthquake of January 17, 1995: Performance of Highway Bridges," Edited by I.G. Buckle, 12/1/95, to be published.

NCEER-95-0018 "Modeling of Masonry Infill Panels for Structural Analysis," by A.M. Reinhorn, A. Madan, R.E. Valles, Y. Reichmann and J.B. Mander, 12/8/95.

NCEER-95-0019 "Optimal Polynomial Control for Linear and Nonlinear Structures," by A.K. Agrawal and J.N. Yang, 12/11/95, (PB96-168737, A07, MF-A02).

NCEER-95-0020 "Retrofit of Non-Ductile Reinforced Concrete Frames Using Friction Dampers," by R.S. Rao, P. Gergely and R.N. White, 12/22/95.

NCEER-95-0021 "Parametric Results for Seismic Response of Pile-Supported Bridge Bents," by G. Mylonakis, A. Nikolaou and G. Gazetas, 12/22/95.

NCEER-95-0022 "Kinematic Bending Moments in Seismically Stressed Piles," by A. Nikolaou, G. Mylonakis and G. Gazetas, 12/23/95.

NCEER-96-0001 "Dynamic Behavior of Unreinforced Masonry Buildings with Flexible Diaphragms," by A.C. Costley and D.P. Abrams," to be published.

NCEER-96-0002 "State of the Art Review: Foundations and Retaining Structures," by I. Po Lam, to be published.

NCEER-96-0003 "Ductility of Rectangular Reinforced Concrete Bridge Columns with Moderate Confinement," by N. Wehbe, M. Saiidi, D. Sanders and B. Douglas, 5/24/96.

NCEER-96-0004 "Proceedings of the Long-Span Bridge Seismic Research Workshop," by I.G. Buckle and I.M. Friedland, to be published.

NCEER-96-0005 "Establish Representative Pier Types for Comprehensive Study: Eastern United States," by J. Kulicki and Z. Prucz, 5/28/96.

NCEER-96-0006 "Establish Representative Pier Types for Comprehensive Study: Western United States," by R. Imbsen, R.A. Schamber and T.A. Osterkamp, 5/28/96.

NCEER-96-0007 "Nonlinear Control Techniques for Dynamical Systems with Uncertain Parameters," by R.G. Ghanem and M.I. Bujakov, 5/27/96.

NCEER-96-0008 "Seismic Evaluation of a 30-Year Old Non-Ductile Highway Bridge Pier and Its Retrofit," by J.B. Mander, B. Mahmoodzadegan, S. Bhadra and S.S. Chen, 5/31/96.

NCEER-96-0009 "Seismic Performance of a Model Reinforced Concrete Bridge Pier Before and After Retrofit," by J.B. Mander, J.H. Kim and C.A. Ligozio, 5/31/96.

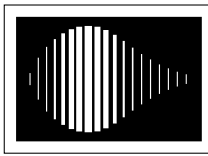

NATIONAL CENTER FOR EARTHQUAKE ENGINEERING RESEARCH

Headquartered at the State University of New York at Buffalo

State University of New York at Buffalo
Red Jacket Quadrangle
Buffalo, New York 14261
Telephone: 716/645-3391
FAX: 716/645-3399

ISSN 1088-3800